Tool Wear Monitoring in Turning Using Fused Data Sets of Calibrated Acoustic Emission and Vibration

A thesis submitted for the degree of Doctor of Philosophy in the Faculty of Technology

By

Asa Prateepasen

Brunel Centre of Manufacturing Metrology,
Brunel University, Cleveland Road, Uxbridge, Middlesex

January 2001

Acknowledgements

I would like to thank deeply my principal supervisor Dr. Y H J Au for his valuable comments, assistance and support to guide my work to a satisfactory conclusion.

I am pleased to have had the opportunity to work with INTErSECT Faraday Partnership Flagship Project, "Acoustic Emission Traceable Sensing and Signature Diagnostics (AESAD)". I acknowledge the help and useful discussions from all my AESAD colleagues, especially Professor Barry E. Jones.

I am especially grateful to Brian Shaw and his technical colleagues for their special kindness and professionalism, together with their expert advice on the experimental work.

I would like to thank my friend K.Pakorn for his comments in the area of data classification and signal processing. I am also grateful to Professor C. Clark for his suggestions.

I acknowledge the grant from Petroleum Authority of Thailand and King Mongkut's University of Technology Thonburi (KMUTT) for the level-two training courses on five Nondestructive Testing (NDT) methods in Canada and ASNT level-two on AE in USA in 1993. That was my first exposure to NDT, and the experience convinced me the need to pursue Ph.D. research in acoustic emission.

I am indebted to The Royal Thai Government for the scholarship to support my PhD research. I would also like to express my gratitude to KMUTT, the university that I have worked in, for allowing me to pursue this PhD work.

Finally my greatest debts are due to my deceased parents who had given me their love and support when they were alive. My special thanks go to my wife who has been waiting patiently for me back in Thailand throughout this period. I am most indebted to her for her love, understanding and encouragement. Her support has motivated me to work hard with single-mindedness.

Abstract

The main aim of this research is to develop an on-line tool wear condition monitoring intelligent system for single-point turning operations. This is to provide accurate and reliable information on the different states of tool wear. Calibrated acoustic emission and vibration techniques were implemented to monitor the progress of wear on carbide tool tips.

Previous research has shown that acoustic emission (AE) is sensitive to tool wear. However, AE, as a monitoring technique, is still not widely adopted by industry. This is because it is as yet impossible to achieve repeatable measurements of AE. The variability is due to inconsistent coupling of the sensor with structures and the fact that the tool structure may have different geometry and material property. Calibration is therefore required so that the extent of variability becomes quantifiable, and hence accounted for or removed altogether. Proper calibration needs a well-defined and repeatable AE source.

In this research, various artificial sources were reviewed in order to assess their suitability as an AE calibration source for the single-point machining process. Two artificial sources were selected for studying in detail. These are an air jet and a pulsed laser; the former produces continuous-type AE and the latter burst type AE. Since the air jet source has a power spectrum resembling closely the AE produced from single-point machining and since it is readily available in a machine shop, not to mention its relative safety compared to laser, an air-jet source is a more appealing choice.

The calibration procedure involves setting up an air jet at a fixed stand-off distance from the top rake of the tool tip, applying in sequence a set of increasing pressures and measuring the corresponding AE. It was found that the root-mean-square value of the AE obtained is linearly proportional to the pressure applied. Thus, irrespective of the layout of the sensor and AE source in a tool structure, AE can be expressed in terms of the common currency of 'pressure' using the calibration curve produced for

that particular layout. Tool wear stages can then be defined in terms of the 'pressure' levels.

In order to improve the robustness of the monitoring system, in addition to AE, vibration information is also used. In this case, the acceleration at the tool tip in the tangential and feed directions is measured. The coherence function between these two signals is then computed. The coherence is a function of the vibration frequency and has a value ranging from 0 to 1, corresponding to no correlation and full correlation respectively between the two acceleration signals. The coherence function method is an attempt to provide a solution, which is relatively insensitive to the dynamics and the process variables except tool wear.

Three features were identified to be sensitive to tool wear and they are; AErms, and the coherence function of the acceleration at natural frequency (2.5-5.5 kHz) of the tool holder and at high frequency end (18-25kHz) respectively. A belief network, based on Bayes' rule, was created providing fusion of data from AE and vibration for tool wear classification. The conditional probabilities required for the belief network to operate were established from examples. These examples were presented to the belief network as a file of cases. The file contains the three features mentioned earlier, together with cutting conditions and the tool wear states. Half of the data in this file was used for training while the other half was used for testing the network. The performance of the network gave an overall classification error rate of 1.6 % with the WD acoustic emission sensor and an error rate of 4.9 % with the R30 acoustic emission sensor.

Forum Attended and Papers Published

A. Prateepasen, Acoustic Emission Traceable Sensing, "International Forum for 1999, Frontiers of Science and Measurement", (NPL, 21-25 June 1999), UK.

A. Prateepasen, Y. H. J. Au and B.E. Jones, Comparison of Artificial Acoustic Emission Sources as Calibration Sources for Tool Wear Monitoring in Single-Point Machining, "Proceedings of the 24th European Conference on Acoustic Emission Testing" (Senlis, 24-26. May 2000), CETIM, France, 2000. P.253-260
(Published in Journal of Acoustic Emission Vol 18, 2000. P 196-204)

A. Prateepasen, Y. H. J. Au, Acoustic Emission and Vibration for Tool Wear Monitoring in Single-Point Machining Using Belief network, "Doctoral Research Conference 2000", (Brunel, 14-15 September 2000), UK, 2000
(Accepted by "IEEE Instrumentation and Measurement Technology Conference" (Budapest 21-23 May 2001), Hungary, 2001.

A. Prateepasen, Y. H. J. Au and B.E. Jones, Calibration of Acoustic Emission for Tool Wear Monitoring, "XVI IMEKO World Congress" (Vienna 25-28. September 2000), Austria, 2000, Volume VI, P. 255-260.

A. Prateepasen, Y. H. J. Au and B.E. Jones, Transferability Validation of AE for Tool Wear Monitoring, "Eurosensor XV, 11th International Conference on Solid-State Sensors and Actuators" (Munich 10-14 June 2001), Germany, 2001. (Submitted)

Contents

Chapter 3:Tool Wear Measures and Preliminary Study of Artificial AE Sources

Chapter 4: Comparison of Artificial Acoustic Emission Sources as Calibration Sources

Chapter 1
Introduction

1.1 General introduction

Metal cutting is a metal removal process. There is a wide variety of cutting operations of which the three most widely used are turning, milling and drilling. In this research, flank wear in turning was studied. In turning, a single-point tool is used remove unwanted work material to produce a surface of revolution. The machine tool on which this is accomplished is called the lathe.

All cutting tools wear during machining and continue to do so until they come to the end of their tool life. The life of a tool refers to the productive time available for machining that will generate surface texture and work piece geometry accuracy of an acceptable quality. In each cutting operation, the choice of tool material and tool shape is based on not just cost but also on the wear and failure resistance of the tool. Most tools fail either by fracturing or by gradual wear. The two main types of gradual wear are flank wear and crater wear, both resulting from the effect of sliding friction. Flank wear occurs on the side face of the tool that rubs against the machined work surface and crater wear on the top face over which the chip slides.

Dan (1990) reported that tool failure contributed on average up to 6.8% of the down time of machining centres. Tool wear or failure may damage the tool holder, workpiece or machine leading to total disruption of the manufacturing system and may even cause injury to the machine.

In machining, whether a tool needs to be changed is decided either by a machine operator performing a visual inspection of the tool or by prediction based on its life expectancy. Visual inspection of the tool condition or machined finish requires a certain level of experience. The decision based on tool-life expectancy suggests the idea of a shortest life for a class of tools calculated from previous data. For a

particular machining condition, the tool manufacturer gives a recommended tool life for a certain insert. The practice of tool replacement based on fixed tool life may not be the most economical since a tool can be replaced prematurely or only after damage has been done. Consequently, besides the unnecessary wastage of some tools, frequent tool changes incur higher machine downtime, decreasing thereby the system productivity and increasing production costs.

In an increasingly competitive global market, manufacturing companies are put under pressure to achieve continual efficiency gains by reducing cost and improving product quality. Advances in manufacturing technology in the form of machining centres have facilitated these gains; but because of the high capital investment involved, machining centres need to be run at peak efficiency and therefore be maintained to be in perfect condition. Traditional maintenance policies, such as fixed-time preventive maintenance, not to mention 'run-to-failure', are unable to deliver the kind of maintenance required for these machining centres; condition monitoring appears to provide the only sensible alternative.

Investigations into sensitive methods of measuring tool life and assessing tool damage have been done for two main potential advantages. Cost can be reduced by implementing on-line tool failure detection; the fact that tool conditions can be correctly identified means that the number of scrapped items is minimised while product quality is improved.

Reliable on-line tool monitoring to provide information on the exact time of tool change is undoubtedly desirable. Various techniques for tool wear monitoring have been studied over the past few decades. However, most of them only work under strictly specified ranges of operating condition. The main reason is that the mechanism of tool wear is complex and depends on a host of factors, for example, the material properties of the cutting tool and workpiece, tool geometry and cutting conditions. Thus, data features extracted from a sensor may be incomplete and hence unlikely to give a unique interpretation of the tool condition. Multi-sensor data fusion is more likely to be the answer. Data fusion refers with the combination of data from multiple sensors into one coherent and consistent internal representation. The sensor

data sets may be of the same or different data types. In this research, both acoustic emission and acceleration sensors were used and the corresponding types of data are different. Together, they would provide a complementary view of the state of the cutting tool and the data features can be used to synthesise inferences that are impossible to make based on an individual sensor alone. In addition, since two accelerometers were used, producing competitive data sets about the same characteristics of the environment, they would reduce the uncertainty in the fused inference.

1.2 Acoustic emission and vibration for tool wear detection

Acoustic emission (AE) is the phenomenon of transient elastic waves produceded by rapid release of energy within a material [McIntire (1987)]. Minute displacements resulting from these waves as small as 10^{-14} metre can be detected. There is a great amount of research literature on AE and a sizeable proportion is on AE applied to tool wear monitoring with encouraging results reported. However, AE as a technique suffers from one fundamental problem: data obtained under apparently identical conditions is often non-repeatable. This fact makes knowledge transfer from one system to another very difficult. The main causes of the inconsistency problem are due to:

1) The interfacial coupling condition between the sensor and the tool.
2) The interfacial coupling condition between the tool tip insert and the tool holder.
3) The difference in the spatial locations of the AE source and the sensor and in the nature of the signal propagation path.

In this research, a study was attempted to minimise the effects on the measured data of the three causes mentioned above. An artificial source, the air jet, was used to calibrate the tool system.

As mentioned earlier, vibration signals were also used in conjunction with the AE signal for detecting tool wear. A coherence function was established between the two acceleration signals in the feed force and tangential force directions. By virtue of its definition, the coherence function can only assume a range of values from zero, and

when to one. The theory postulated is that when the two forces are completely uncorrelated, the coherence function is zero, and when the two forces are completely correlated, its value is unity. Values of the coherence function at around the natural frequency (5 kHz approximately) of the tool and at the high frequency range (18 – 25 kHz) were used to obtain inferences on the state of tool wear.

1.3 Aims of the project

This research is to develop an intelligent on-line tool wear condition monitoring system for single point turning operations using acoustic emission and vibration. There are three main aims, listed below:

1. To establish a methodology for calibrating the acoustic emission (AE) signal produced in single-point machining. This refers to the calibration of the whole tool system from the location of the source, through the signal propagating medium, to the AE sensor itself.
2. To provide accurate and reliable inferences on the stages of tool wear. The root-mean-square of AE and the vibration signals will be studied, and the data features extracted from these signals will be related to the flank wear on a carbide tool tip. Flank wear is used as the measure of the wear condition of the tool.
3. To design and test an expert system, also known as the belief network, to perform the necessary work of fusing data features from AE and acceleration and of making inferences on tool wear.

Calibration of AE systems allows different sensor data to be converted to a common reference, alleviating the variability caused by interfacial and structural variations. Research results in terms of calibrated AE are therefore readily transferable.

1.4 Objectives of the project

In order to achieve the aims of the project, the following tasks need to be performed:

(1) Reviewing up-to-date literature

Review of other researchers' findings and relevant theories (presented in Chapter 2) are conducted in order to:

- Understand the types of tool wear in metal cutting and the background theory of metal cutting.
- Understand the theories and techniques of AE and vibration, their advantages and disadvantages when applied to tool wear monitoring; find out the AE and vibration parameters which are sensitive to tool wear and select appropriate parameters to be used in this research.
- Study different AE calibration techniques and evaluate the strength and limitations of different artificial AE sources.
- Assess the performance of a small number of diagnostic systems and select one to provide the necessary data feature fusion of AE and vibration signals to draw inferences on the stage of tool wear.

(2) Studying available AE and vibration instruments and techniques

Preliminary tests are to be performed to identify the limitations of implementation. The different methods are to be investigated for measuring flank wear and for providing a record of the wear area. An air jet source and a pencil lead breakage source are to be investigated with regard to their possibility to be used as calibration sources. (This is presented in Chapter 3.)

(3) Selecting a suitable artificial AE source for tool wear monitoring

In order to calibrate a tool system, a repeatable artificial AE source is needed. Comparison of artificial AE sources is to be conducted based on the bandwidth, shape and size of the signal spectrum. A pulsed laser source and an air jet source are to be compared against AE obtained from machining. (This is presented in Chapter 4.)

(4) Establishing the methodology for calibrating a tool system using an air jet as the AE artificial source

The effect of clamping torque on the AE signal is to be studied. The clamping torque is the torque used to fasten a tool insert to its tool holder. Calibration curves of the air jet source are to be produced experimentally that relate the air jet pressure to the AE signal generated for two different transducers at two different locations. Results from the different set-ups are then compared. (This is presented in Chapter 4.)

(5) Proving the linearity of the tool system for AE transmission

The AE produced from machining is much stronger than that from the air jet. Experiments are to be performed in order to decide if AE from these two sources are similar and to verify that the tool system is linear. (This is presented in Chapter 5.)

(6) Determining the accuracy of system transferability

The AE signals from the two different sensors at different locations are to be converted to the equivalent pressure values. Machining at three different cutting conditions is to be performed in order to determine the degree of transferability of AE equivalent pressure values obtained form the two sensors using the Pearson correlation coefficient. (This is presented in Chapter 5.)

(7) Presenting the theory of the coherence function for tool wear detection

A linear mathematical model is to be developed to explain the relationship between flank wear and the coherence function. This function involves the two acceleration signals in the tangential and feed directions. Certain frequency bands of the coherence function are to be identified that are related to flank wear. (This is presented in Chapter 6.)

(8) Implementing an expert system to fuse AE and vibration data features for tool wear classification

Features are to be extracted from the AE and vibration data sets. These feature vectors are then used as inputs to a belief network to provide inferences on tool wear classification. (This is presented in Chapter 7.)

The aims and objectives of this research are summarised in the block diagram shown in Figure 1.

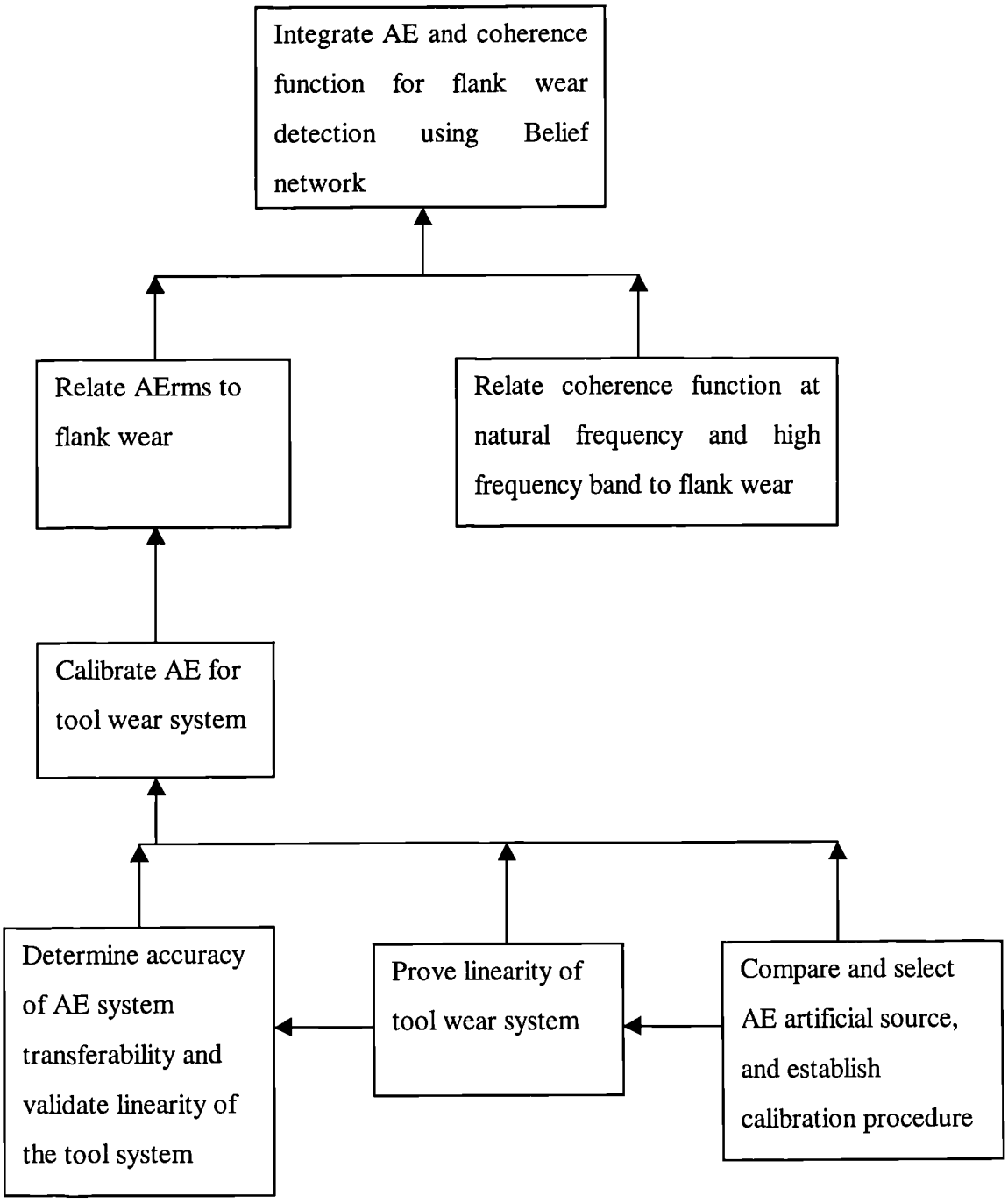

Figure 1. Diagram showing the main tasks of the research programme.

Chapter 2
Literature Review

In this chapter, the review of literature is divided in to 3 parts: wear in metal cutting, signal processing and classification techniques. In the first part, wear in metal cutting, the basic theories of metal cutting are presented along with a description of tool wear types and mechanisms. In the second part, signal processing, AE and vibration theories and their parameters are explained; previous research by other workers of AE and vibration in the area of tool wear monitoring are surveyed; and AE calibration and system calibration techniques to date are reviewed. In the third part, classification techniques, neural networks and belief networks are reviewed.

2.1 Wear in metal cutting

Turning is a process using a single point tool that removes unwanted material to produce a surface of revolution. The machine tool on which this is accomplished is called a lathe. The important variables of a cutting condition are the cutting speed, the feed and the depth of cut [Shaw (1984)].

2.1.1 Types of cutting tool wear mechanism

Shaw (1984) classified tool wear mechanisms into 3 types: adhesive or attrition wear, abrasive wear, and diffusion wear.

2.1.1.1 Adhesive wear or Attrition wear

Adhesive wear or attrition wear occurs mainly at low machining temperatures on the chip face of a tool. This mechanism often leads to the formation of a built-up edge on the cutting edge. Junctions between the chip and tool materials form strong bonds as part of the friction mechanism. If the bonds are stronger than the local strength of the material particle, small fragments of the tool material can be torn out and carried away on the underside of the chip or the new machined surface.

2.1.1.2 Abrasive wear

Abrasive wear is loss of tool material on the tool face. It occurs when hard particles in a chip rub with the tool rake face resulting in tool material being removed. Due to the great hardness of tungsten carbide, abrasive wear is much less likely to be a significant wear process with cemented carbides than with high speed steel.

2.1.1.3 Diffusion wear

Diffusion wear is the wear that occurs at high surface temperature.The chemical properties of the tool-material and the affinity of the tool-material to the work-piece material will decide the development of the diffusion wear mechanism. Hardness of the tool-material will not much effect the process. The metallurgical relationship between the materials will determine the amount of the wear mechanism. Some cutting tool materials are inert against most workpiece materials, while others have high affinity.

Tungsten carbide and steel have affinity towards each other leading to the diffusion wear mechanism developing. This results in the formation of a crater on the chip face of the insert. [Model Metal Cutting (1994)]

2.1.2 Types of tool failure

According to Shaw (1984), the sources of tool failure are all the above tool wear types plus the following three additions:

1) Fracture: that occurs more in brittle tools under interrupted cutting conditions.
2) Chipping: that is a small scale crumbling of the cutting edge.
3) Plastic deformation: that is caused by high temperature and high pressure on the cutting edge.

2.1.3 Types of tool wear and tool failure in carbide cutting tools

Many types of tool materials have been used such as high speed steel (HSS), tungsten carbide (WC), titanium carbide (TiC). The usefulness of each type of tool material is dependent on many factors such as the relative tool hardness, work material,

condition of machine and type of operation. In this research, the cemented-carbide, throw-away tool tip will be studied. Cemented carbide is a powder metallurgical product. These carbides are very hard and the main members of the family are tungsten carbide (WC), titanium carbide (TiC), tantalum carbide (TaC) and niobium carbide (NbC). The binder used is mostly cobalt (Co). Five main types of tool wear and tool failure are explained in the following sections.

2.1.3.1 Flank wear

Flank wear, shown as in Figure 2.1 is gradual wear caused by friction between the surface of the material being machined and the tool flank, mainly from the abrasive wear mechanism. Flank wear is sometimes called wear-land wear [Shaw (1984)]. It results in a loss of relief angle on the clearance face of the tool. The wear rate increases rapidly as the cutting speed is increased. Excessive flank wear often leads to poor surface texture, inaccuracy and increasing friction as the edge changes shape.

Figure 2.1. Flank wear of carbide tool [(Model Metal Cutting - A Practical Handbook, (1994)].

2.1.3.2 Crater wear

Crater wear, shown in Figure 2.2, is gradual wear on the tool face caused by the friction between the chip and tool face. Crater wear on the chip face can be due to

abrasive and diffusion wear. When cutting steel at high speed and feed, diffusion is predominant and a crater is formed on the rake face of the cutting tool. A characteristic form of crater wear is a hollow in the rake face some distance behind the cutting edge. The point of greatest depth usually occurs near the midpoint of the contact length since this is where the tool face temperature is normally maximum [Trent (1991)]. The volume available to be worn away before total destruction is much greater for crater wear than for wear-land wear. Excessive crater wear changes the geometry of the edge and can deteriorate chip formation, alter the cutting force direction and weaken the edge.

Under the very high speed and feed rate, crater wear is the type of wear that determines the life of a tool. But for economic cutting speed conditions, flank wear is usually the controlling factor.

Figure 2.2. Crater wear of carbide tool [Model Metal Cutting - A Practical Handbook, (1994)].

2.1.3.3 Deformation of nose radius

Deformation of the nose radius or plastic deformation under compressive stress is not a wear process since no material is removed from the tool. It takes place as a result of the combined high temperature and high pressure on the cutting edge. It is not usually

uniform along the tool edge but often starts at the nose of the tool. In high speed tool steel, forces and temperature may be increased locally and so the flow pattern in the work material is modified. These more severe conditions bring into play the accelerated wear processes which reduce tool life. In carbide tool steel when the cutting speed or feed are raised, the tool life is often limited by the deformation of the tool under compressive stress on the rake face. Carbide tools can withstand only limited deformation, even at elevated temperature, and cracks form leading to sudden fracture. Figure 2.3 shows such a crack in the rake face of a tool, this surface being stressed in tension as the edge is compressed.

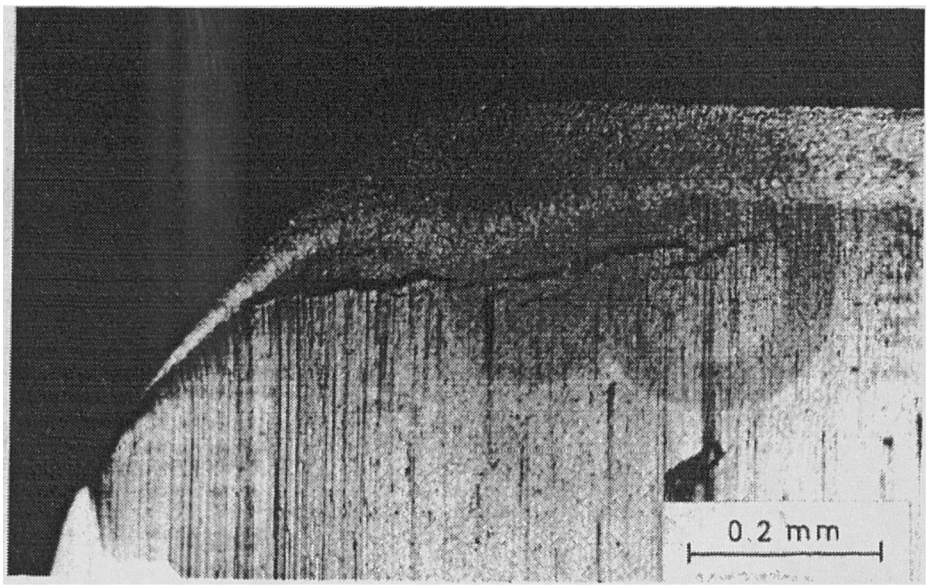

Figure 2.3. Crack across the nose of cemented carbide tool deformed during cutting [Trent (1991)].

2.1.3.4 Chipping

Chipping is the formation of fragments of the tool material of microscopic size, under conditions where a built-up edge is formed, resulting in fragments being torn from the tool edge. It is a slow wear mechanism with steel tools but may cause rapid wear on carbide tools. Fatigue, arising from cycles of loading and unloading during intermittent cutting, is a frequent cause of this wear type. Figure 2.4 shows the edge-chipping of a carbide tool after cutting steel at low speed with a built-up edge.

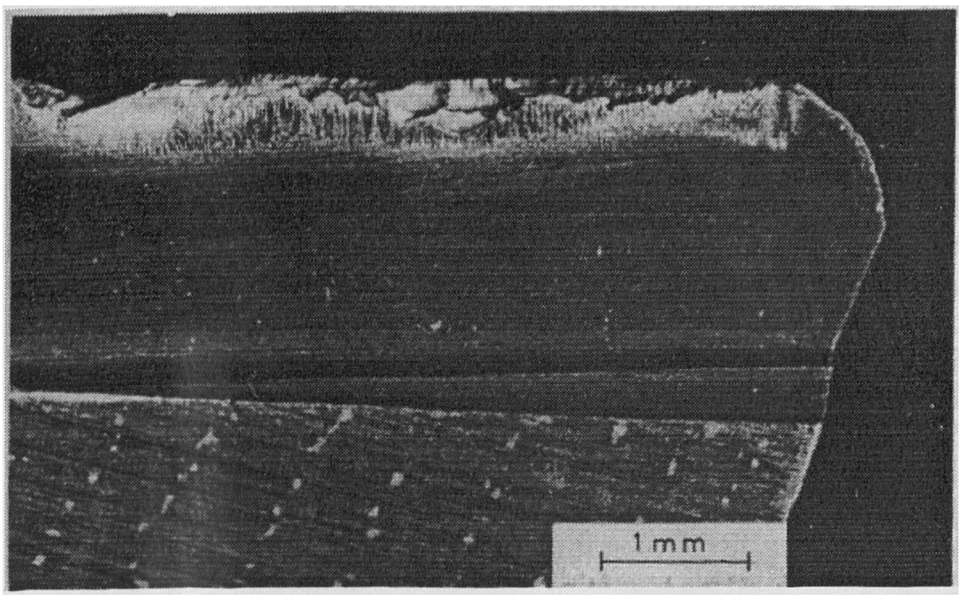

Figure 2.4. Edge chipping of carbide tool after cutting steel at low speed with a built-up edge [Trent (1991)].

2.1.3.5 Fracture

Fracture can be the catastrophic end of a cutting edge. It is rare for fracture on a part of the tool edge to occur while it is engaged in continuous cutting. More frequently the tool fractures on starting the cut, particularly if the tool edge comes up against a shoulder so the full feed is engaged suddenly. Interrupted cutting and operations such as milling are particularly severe and may involve fracture due to mechanical fatigue. Fracture may be initiated also by deformation of the tool, followed by crack formation.

2.1.4 Tool life

The end of a cutting tool's life corresponds to when the tool cannot be used properly in further cutting. The causes of the end of tool life are due to many types of tool wear and tool failure modes mentioned above. A common measure of tool life is the width of the flank wear and sometimes the dimensions of crater wear.

Figure 2.5 shows the features wear on a worn tool in turning operations. The ISO standard dealing with common criteria on tool life for sinter-carbide tools recommends:

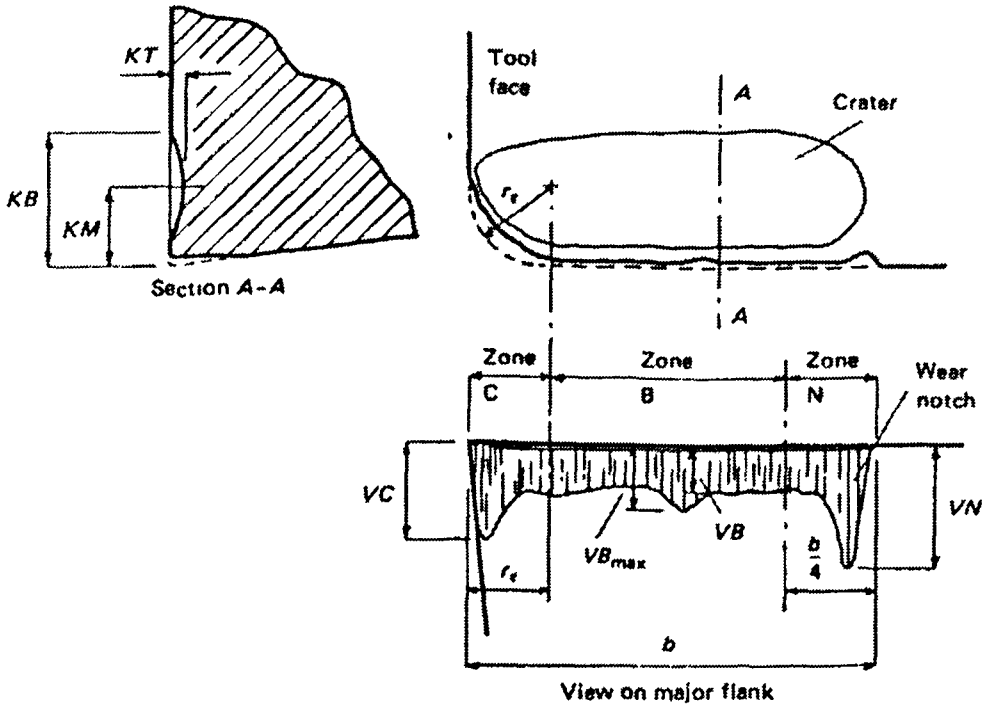

Figure 2.5. Some features of singer-point-tool wear in turning operation [Boothroyd (1983)].

1. Average flank wear (VB) = 0.3 mm, or
2. Maximum flank wear (VBmax) = 0.6 mm if the flank is irregularly worn or
3. Crater depth (KT) = 0.06 + 0.3 f, where f is the feed.

Taylor (1907) produced an empirical equation that related the tool life T, cutting speed V, feed t, and depth of cut b, as (Shaw 1984)

$$TV^{1/n} t^{1/m} b^{1/l} = c \qquad (2.1)$$

where ($n\langle m\langle l$) and n, m, l and c are constants for a given work and tool material and machining conditions other than the cutting speed, feed, depth of cut, cutting fluid, and tool geometry. The value of n changes for different material, being 0.1 and 0.2 for steel and tungsten carbide respectively.

2.2 Review of AE and its signal processing

Acoustic emission is a powerful technique for non-destructive testing and material evaluation. Older NDT techniques such as radiography, ultrasonic, eddy current detect geometric discontinuities by beaming some form of energy into the structure under test. Acoustic emission is different: it detects microscopic movement, not geometric discontinuities.

AE is a passive technique. The growing defect makes its own signal and the signal travels to the detecting sensors. The main benefits of AE compared to other NDT methods are that AE is a real time method and it is less intrusive. The discontinuities of defects can be detected by AE at an early stage when they are occurring or growing. AE techniques can be used as a warning system before the testing material is severely damaged. AE requires access only at sensors: on the other hand most other NDT techniques require access to all regions inspected.

Acoustic emissions, by definition, are transient elastic waves generated by the rapid release of energy from localised sources within a material [McIntire (1987)]. These elastic waves can be detected by microphones or transducers attached to the surface of the specimen. AE techniques have been used in many applications such as in material degradation, leak and flow, solidification, machining.

In order to detect AE events, a transducer is required to convert the very small surface displacement to a voltage. Displacements as small as 10^{-14} metre [(Course Handbook for SNT-TC-1A (1991)] can be detected by the use of the most sensitive sensors. The most common type of transducers are piezoelectric which are sensitive, easy to apply and cheap. A couplant is needed for good transmission, and is usually achieved by grease or ultrasonic couplants, together with some means of applying force to maintain contact.

There are two types of piezoelectric transducer: resonant transducers and broad-band transducers. The principal or resonant frequency of a piezoelectric element depends on its thickness. The piezoelectric element is unbacked or undamped in a resonant

transducer but a broad-band transducer has an element that is backed with an attenuating medium. The frequencies of most AE resonant transducers lie in the range of 100 kHz to 1 MHz. Resonant sensors are more sensitive than broadband types because of the gain provided by mechanical resonance. Broadband sensors are used when the object of interest is the frequency spectrum of AE but they do not have as high a sensitivity as resonant transducers. Because of the reliance on mechanical resonance, resonant sensors can be used to detect preferentially a frequency range which has been shown from previous experience to give a good indication of the AE changes. Alternatively, a broad-band sensor can be used and the required frequency selected by filters.

Elastic waves emitted from materials can be divided into 2 types based on their appearance: burst and continuous. A burst emission is a signal, oscillatory in shape, whose oscillations have a rapid increase in amplitude from an initial reference level (generally that of the background noise), followed by a decrease (general more gradual) to a value close to the initial level. A continuous emission is a qualitative term applied to acoustic emission when the bursts or pulses are not discernible. (A pulse is an acoustic emission signal that has a rapid increase in amplitude to its maximum value, followed by an immediate return.)

An AE burst in Figure 2.6 can be described by the parameters: event, ring down count, event energy, signal amplitude, duration and rise time.

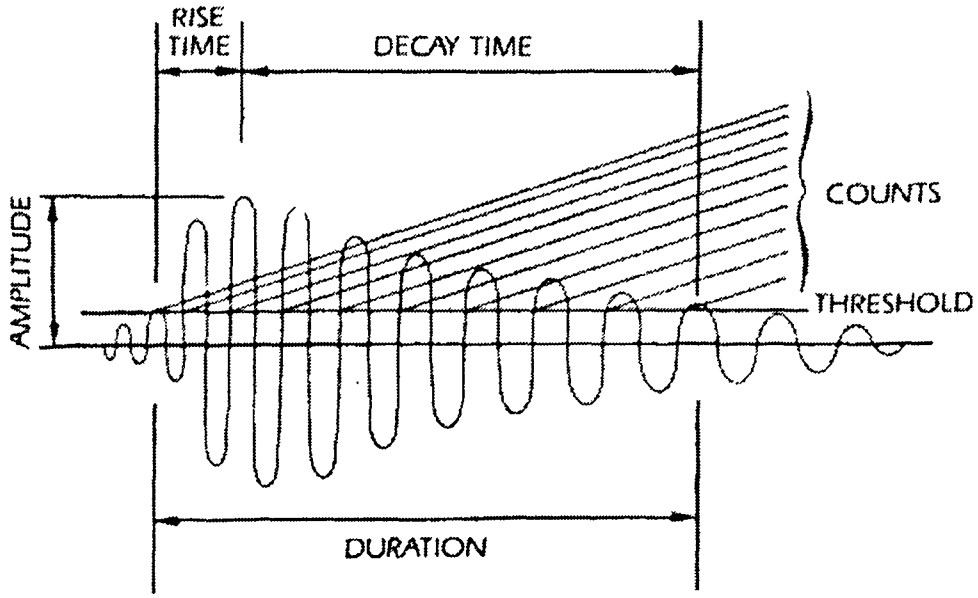

Figure 2.6. Definition of AE waveform parameters [Mclntire (1987)].

2.2.1 AE waveform parameters

1) Ring down count

Ring down count is the number of times a signal exceeds a pre-set threshold. This is a simple measure of the signal size, since larger signals typically give more counts. Electronically this is a very easy measurement, and it was the first to come into widespread use. By summing the counts from all the detected emissions, one has a convenient measure of the total emission from the specimen or structure. The number of counts (N) can be calculated by

$$N = \frac{\omega}{2\pi B} \ln \frac{V_0}{V_t} \tag{2.2}$$

where ω = angular frequency

B = decay constant(greater than 0)

V_0 = initial signal amplitude

V_t = threshold voltage of counter

2) AErms

AErms is the root mean squared value of the input signal. Since acoustic emission activity is attributed to the rapid release of energy in a material, the energy content of the acoustic emission signal can be related to this energy release. AErms can be defined as

$$V_{rms} = (\frac{1}{T}\int_0^T V^2(t)dt)^{\frac{1}{2}} \qquad (2.3)$$

where $V(t)$ = signal voltage function

T = period of time

3) Signal amplitude

Signal amplitude is the maximum value of amplitude of the received signal. This is an important parameter because it governs the detectability of the event (detection depends on the amplitude exceeding the pre-set threshold). Like counts, amplitude is a useful measure of the signal size; and it is the appropriate variable to use for attenuation measurements.

4) Duration

Duration is the time between the point at which the event first exceeds the threshold and the point at which the event goes below the threshold. This parameter is closely related to the ring down count, but it is used more for discrimination than for the measurement of emission quantities. For example, long duration events (several milliseconds) in composites are a valuable indicator of delamination. Signals from electromagnetic interference typically have very short durations, so the duration parameter can be used to filter them out.

5) Rise time

Rise time is the time between the point at which the event first exceeds the threshold and the point at which the amplitude reaches its peak value. This parameter is useful for source discrimination and signal filtering. It can be used to filter out signals from electromagnetic interference, which usually have very short rise times.

2.2.2 AE wave propagation

The AE waveform detected by a sensor is much more complex in form compared to the AE at source. It is shaped by the propagation effects between the source and sensor. The important factors of wave propagation for AE are wave modes and wave velocity, wave reflection and mode conversion, and attenuation.

2.2.2.1 Wave modes and wave velocity

There are 4 types of modes; compression (longitudinal), shear, surface (Rayleigh) and plate (Lamb). Each mode travels at the different speed depending on the material; and, for Lamb waves, the speed depends on the thickness of material as well. In an infinite medium, the longitudinal wave and the shear wave are the only two wave types that can exist. The Rayleigh wave exists in a semi-infinite medium and the Lamb wave mode in a finite plate. The velocity varies with frequency, a phenomenon known as velocity dispersion. The compression wave is the fastest. Shear and surface waves travel at approximately 60% and 50% respectively of that of the compression wave [Course Handbook for SNT-TC-1A (1991)]. The velocity of Lamb wave varies with frequency and the thickness of the medium.

2.2.2.2 Wave reflection and mode conversion

When a wave strikes an interface or boundary between two materials, the energy is partly reflected and party transmitted. The partition of energy between the transmitted and reflected waves depends on the angle of incidence and on a material property known as the acoustic impedance.

Mode conversion is the conversion of one wave mode into another. Mode conversion can occur only at an interface between two media.

2.2.2.3 Attenuation

Attenuation is the loss of amplitude with distance as the wave travels through a structure. The major causes of attenuation are:

(1) Geometric spreading of the waves by simple geometry and by loss in adjacent media. The amplitude falls off inversely with the distance in three-dimensional

media such as concrete blocks, and inversely with the square root of distance in two-dimensional media such as pressure vessel shells (LOCAN 320 User's Manual (1990)). This effect is dominant close to the source.

(2) Absorption or damping in the propagation media. The amplitude falls off exponentially with distance. Attention depends on material and on the operating frequency. The higher the frequency the higher the attenuation rate.

2.2.3 Sources of AE in metal cutting

Four different sources of AE, as shown in Figure 2.7, can be identified as [Teti and Dornfeld(1989)]:

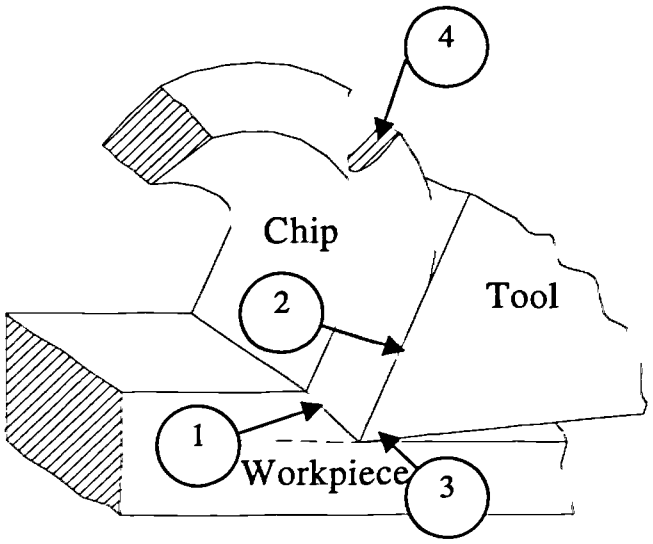

Figure 2.7. Four different sources of AE.

1) Plastic deformation on the shear plane formation (the primary deformation zone): -The plastic work of deformation occurs mainly by the movment of dislocations. A stress wave is produced in the material, which causes displacements on the surface of the material that can be picked up as AE.
2) Sliding friction and plastic deformation at the chip/tool interface (the secondary deformation zone): -When the friction stress on the tool face reaches a value equal to the shear flow stress of the chip material, flow occurs internally within the chip adjacent to the tool face. This flow produces AE.

3) Sliding friction at the tool flank/workpiece interface (the tertiary deformation zone) – Similar to what happens in (2), AE is also produced at the tool flank and workpiece interface.
4) Breakage of chips and their impact on the tool or workpiece.

Sources 1-3 generally release continuous type, whilst source 4 releases burst type acoustic emissions.

2.2.4 Models of AE for orthogonal machining

A simplified version of metal cutting is orthogonal, or two-dimension cutting, Orthogonal cutting is characterised by a single cutting edge, parallel to the work surface and perpendicular to the direction of the cutting velocity. Lathe cut-off is an example of orthogonal cutting in the single-point machining process. Although much practical work is three-dimensional cutting, the theory of metal cutting to date is still limited to orthogonal processes. The three force components acting on a single-point-cutting tool during oblique or three-dimensional cutting are shown in Figure 2.8

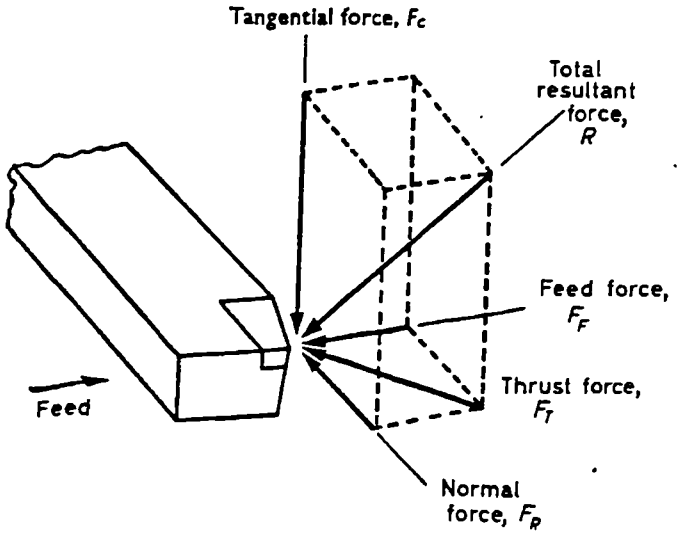

Figure 2.8. Three components of force acting on a single point cutting tool during oblique or 3-dimensional cutting [Boothroyd (1983)].

The forces acting on a cutting edge in an orthogonal cut were first studied by Ernst and Merchant and they are shown in Figure 2.9.

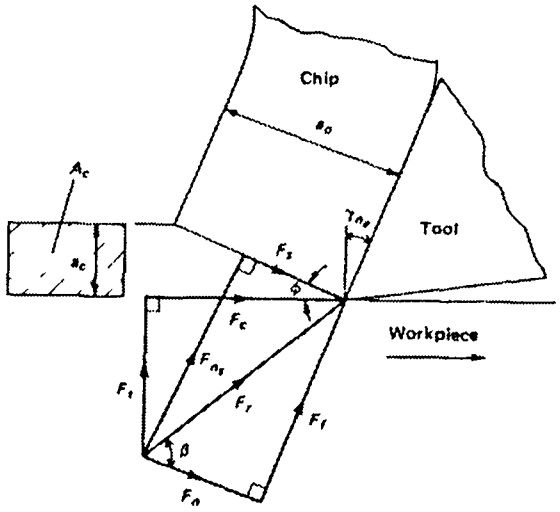

Figure 2.9. Force diagram for orthogonal cutting [Boothroyd (1983)].

In the above diagram, the following notations are used:

F_r	=	resultant tool force,
F_c	=	cutting force,
F_t	=	thrust force,
F_s	=	shear force on shear plane,
F_{n_s}	=	normal force on shear plane,
F_f	=	frictional force on tool face,
F_n	=	normal force on tool face,
ϕ	=	shear angle,
γ_{n_e}	=	working normal rake,
β	=	mean friction angle on tool face,
A_c	=	cross- sectional area of uncut chip,
a_c	=	undeformed chip thickness, and
a_0	=	chip thickness.

Previous investigations of AE in the metal cutting process have been restricted to the simplified two-dimensional case called orthogonal cutting. Asibu and Dornfeld (1981) proposed models of AE from machining based on the dependency of AE energy on the material properties such as flow stress, volume of material undergoing deformation, and strain rate. In the case of constant stress (σ) and strain rate ($\dot{\varepsilon}$), the work rate ($\dot{W}$) is given by:

$$\dot{W} = \sigma \dot{\varepsilon} v \tag{2.4}$$

where v is the volume of material being deformed.

Equation 2.4 shows that the energy rate of an emission signal is dependent on the rate of deformation (strain rate), and the volume of material involved in the deformation process.

Although there are four sources of AE in machining, the model focused on only the primary and secondary sources. The friction between the tool and flank face was minimised by using a fresh tool. The breakage of chips and their impact on the cutting tool or work piece can be minimised during continuous metal cutting by controlling and directing the chips away from the cutting area.

From the Ernst and Merchant model of orthogonal machining (Figure 2.9) the formula for the work rate in the primary zone (shear zone) can be expressed as:

$$\dot{W}_s = df\tau_k \frac{\cos\gamma_{n_e}}{\sin\phi\cos(\phi - \gamma_{n_e})} U \tag{2.5}$$

where d = depth of cut (width of chip)

f = uncut chip thickness

τ_k = average material shear strength

γ_{n_e} = working normal rake, rake angle

ϕ = shear angle

U = cutting velocity

the work rate in the sliding region ($\dot{W}_{c1}$) and the sticking region ($\dot{W}_{c2}$) of the secondary shear zone can be defined as:

$$\dot{W}_{c1} = \frac{1}{3}\tau_k d(l - l_1)U_c \tag{2.6}$$

$$\dot{W}_{c2} = \tau_k d l_1 U_c \tag{2.7}$$

where l = contact length between the chip and the tool rake face

l_1 = length from the tool edge to the end of the sliding zone on the tool rake face (sticking length)

$$U_c = \textit{chip velocity} = \sin\phi / \cos(\phi - \gamma_{n_e})U \tag{2.8}$$

Since

$$V_{rms}^2 = \dot{W}_s + \dot{W}_{c1} + \dot{W}_{c2}$$

From equations (2.5- 2.7) the relationship between the root-mean-square value of the voltage output V_{rms} from the AE sensor and the cutting parameters based on the Ernst and Merchant model is given by:

$$V_{rms} = C\{\tau_k dU[\frac{\cos\gamma_{n_e}}{\sin\phi\cos(\phi - \gamma_{n_e})} f + \frac{1}{3}(l + 2l_1)\frac{\sin\phi}{\cos(\phi - \gamma_{n_e})}\}^{0.5} \tag{2.9}$$

where C is the proportionality constant influenced by tool geometry, instrumentation gain.

2.2.5 Review of various techniques for tool wear detection

In the past two decades many researchers have investigated various techniques for tool condition monitoring. A great majority of them have focused on tool wear monitoring as determined by flank wear and crater wear, rather than plastic deformation, nose radius, chipping and micro fracture. Tool wear sensing can be classified into two major categories, direct and indirect methods [Dan and Mathew (1990)]. The direct method measures the actual tool wear, whilst the indirect method measures a parameter correlated with tool wear. The direct methods are described in the following five sections.

2.2.5.1 Optical measurement

Image analysis with a CCD camera has been used to measure flank wear on a single point cutting tool [Levi et al (1985)]. The flank wear could be seen clearly owing to the higher reflectivity of the worn area compared with the unworn surface. Sata et al (1979) proposed a system comprising a TV camera coupled to a pattern recognition technique to classify the morphology of tool failure. The morphology of wear was compared to the decision table, which had been established by a learning algorithm in advance. Laser light has also been used to illuminate the flank wear of a cutting tool (Jeon and Kim 1988). The image was converted into digital pixels which were then processed to determine the width of the wear land.

2.2.5.2 Wear particle and radioactivity

Uehara (1972) described a system for the detection of tool wear by scanning chips with an electron microprobe analyser. This technique is based on exciting a sample of wear and cutting debris by electron beams rays. The X-ray radiation emitted from them was collected and analysed to find the amount of wear by X-ray spectrometers. Tool wear can also be detected by using abraded radioactive wear particles. In a method reported by Cook (1980), a small amount of radioactive material was attached or implanted to the flank of the tool. The spot was checked at the end of each cutting cycle. If the spot disappeared, the tool would be considered to be worn.

2.2.5.3 Tool/work junction resistance

Uehara (1973) researched into a method relying on detecting resistance at the tool/work junction. A thin film conductor was bonded onto a tool flank. When the tool wears, parts of the conductor also wear. Consequently the resistance to current flow decreased indicating tool wear.

2.2.5.4 Changes in workpiece size

The dimension of a workpiece corresponds to the size of wear. Gomayel and Bregger (1986) used an electromagnetic sensor to measure the change of the diameter. The voltage output obtained from the electromagnetic sensor was directly related to the gap between the sensor and the workpiece, hence the extent of tool wear.

2.2.5.5 Tool/work distance

The distance between a tool holder (or tool post) and a workpiece decreases as the tool wears. The distance can be sensed by using an electronic feeler micrometer mounted on the tool holder or a stylus attached on the tool holder [Suzuki and Weinamann (1985)].

Indirect methods measure a parameter that is correlated with tool wear. They are presented in Sections 2.2.5.6 to 2.2.5.12.

2.2.5.6 Cutting forces

The three components of the cutting forces, which are the tangential force, the feed force and the normal force, were found to increase suddenly as a broken tool nose was jammed between the tool and the workpiece; they then consequently dropped to zero because of the gap between the tool and the workpiece as the broken part of the tool insert was released [Tlusty and Andrews (1983)]. By contrast Lan and Dornfeld (1984) observed that the tangential force decreased as an insert broke while the feed force might decrease or increase depending on the degree and type of microbreakage on the cutting edge. Dimla and Lister (2000) used a tool-post-dynamometer to generate cutting force data in the time domain and frequency domain. They proposed that as the tool wear reached catastrophic failure, amplitudes at certain frequencies correlated well with the dynamic force changes. Lee et al (1992) established the relationship between the dynamic tangential force and flank wear: the amplitude of the dynamic force increased with tool wear and then decreased just prior to the onset of tool failure. A personal computer was used to automate tool wear detection by setting up two criteria: the threshold value of the percentage drop of the dynamic tangential force from its maximum and the gradient of the curve of the dynamic force with time.

2.2.5.7 Sound

Flank wear on the tool can also be detected using the noise spectra resulting from the rubbing action of the tool and the workpiece. Sadat et al (1987) found that the noise

in the frequency range 2.75 – 3.5 kHz significantly increased from 9 to 24 dB as a sharp tool became worn.

2.2.5.8 Power/motor current

Liao (1974) investigated the relationship between the power or the current of the main drive motor of the spindle and the tool wear and tool breakage. He found that the motor current dropped and then subsequently recovered to a level before the drop as the tool broke. At the constant spindle speed of the cutting condition, the percentage increase of the motor current from the start to the end of the tool life was approximately constant when the same material was machined.

Constantinides and Bennett (1987) measured the spindle motor power from a vertical milling machine as well as the power spectral density. They concluded that the spectral energy fluctuations of the spindle motor power were linearly related it to the tool wear rate and that they were also affected by the cutting condition and tool geometry.

2.2.5.9 Cutting temperature

Colwell (1975), Turkovich and Kramer(1986), Lin (1995) and Radulescu and Kapoor (1994) attempted to measure the cutting tool temperature and related it to the tool wear. The temperature around the cutting tool edges was found to be related to the cutting tool wear and the friction between the chip and cutting tool.

2.2.5.10 Roughness of machined surface

The sharpness of the cutting edge affects the surface roughness of the workpiece. Takeyama et al (1976) observed that a slightest change of the cutting edge due to chipping or wear was detected using a pair of optical reflection systems.

2.2.5.11Acoustic emission

This is an important technique for tool condition monitoring and a detailed review will be given in Section 2.2.6.

2.2.5.12Vibration

This is another important area and details will be presented in Section 2.3.

2.2.6 Advantages and disadvantages of various methods

In summary, each method has its advantages and disadvantages. A disadvantage of the optical measurement is that it is an off-line method because measurement is possible only when the tool is not cutting. Not withstanding this, the method appears to be accurate and reliable. The radioactive method can be a health hazard: therefore good protection and safety is needed to minimise the effects of radiation on the shop floor. The method based on changing size suffers from the effects of thermal expansion of the workpiece and the movement of machine tools. The drawback of using cutting forces is that it is dependent upon the properties of the materials of the cutting tool and the workpiece and the variation of cutting conditions. The limitation of the method based on sound is that the ambient noise level on shop floor is often higher than the level detected from a worn tool.

Some of the methods proposed are on on-line direct methods, which are practically unachievable in a continuously moving system [Dimla et al (1997)]. Many researchers have attempted to use indirect methods and in order to improve sensitivity and reliability, multi sensor data fusion was used, where the loss of sensitivity in one sensor can be offset by another sensor. Dan and Mathew (1990) concluded that while many tool-failure monitoring techniques had been refined in laboratories, few of them were being used successfully in industry. There are still many problems with tool monitoring systems and the issues that need serious attention are the robustness, sensitivity and reliability. These involve research into multi sensor data fusion, multi sensor planning and multi sensor system architecture.

2.2.7 Review of AE techniques for tool wear detection

In the last two decades, many researchers investigated into the use of AE for tool wear and tool failure detection. The effectiveness was established of the acoustic emission based sensing methodologies for machine tool condition monitoring in machining under combination of feed rate, depth of cut and cutting velocity.

Acoustic emission from orthogonal metal cutting has been studied by many researchers experimentally to determine the influence of cutting parameters, and the rake angle of tool insert. AE in orthogonal cutting was analysed by Asibu and Dornfeld (1981), as described in section 2.2.4 of this Chapter, and a theory was proposed that related AE to the cutting conditions.

Heiple et al (1991) used AE to monitor single-point tool oblique machining in several materials. Results obtained showed that heat treatments, which increased the strength of 4340 steel, caused the amount of AE produced during machining to increase. Whilst heat treatments increased the strength of Ti-6Al-4V, the amount of AE produced during deformation decreased. If chip deformation was the main source of AE, then the AErms level of both materials should increase. Thus, they concluded that chip deformation is not the major source of AE, but that the sliding friction at the nose and the flank of a tool was the primary source of AE. Changes in the AE signal with tool wear were strongly material dependent. It was observed that AErms sharply increased with cutting speed for all materials, whilst the increase with feed was small and the pattern was similar for all materials, but the AErms produced, being sometimes strong and sometimes weak for different depth of cut, was strongly material dependent.

Chaung and Asibu (1985) identified the sources of AE originating from three zones: primary shear zone, free surface and tool- chip friction zone. They observed that the AE power changed with velocity more than with feed and depth of cut. AE power increased linearly with depth of cut but hardly with feed rate. The AE signal continuously increased with flank wear. Crater wear developed in two stages: first the formation of a built-up edge and then the formation of a crater. AE signal increased in the initial stage of crater wear and then decreased after a significant crater had occurred. It was observed that flank wear increased only friction without changing the other AE source mechanisms but crater wear changed the rake angle and hence the tool geometry. Thus in the initial stage, the rake angle increased but in the later stage the rake angle decreased.

Diei and Dornfeld (1987) addressed the quantitative aspect of the AE signal generated during the complete breakage of cutting tools by using a carbide insert in single and multitooth operations. The experiment showed that the amplitude of the AErms burst signal at the instant of tool fracture was much larger than the signal level associated with the engagement and disengagement of cutting in both turning and milling operations. They also observed that the peak value of the AErms was related to the fracture area.

Inasaki and Yunetsu (1981) used acoustic emission to detect flank wear and tool fracture in oblique single-point tool operations. They found that the amplitude of the acoustic emission during the cutting of carbon steels was hardly affected by the feed and depth of cut but influenced strongly by the cutting speed and the length of the flank wear. They suggested that tool fracture can be detected from the stepwise increase in the amplitude level as well as the occurrence of the burst type AE signal.

Iwata and Moriwaki (1977) studied the relationship between flank wear, on the one hand, and AE power signal, AE signal frequency and AE count, on the other, in oblique turning operations. They used a resonant transducer and band pass filter (100-400 kHz) chosen based on the results of a preliminary test. The amplitudes of the AErms voltage and of the power spectrum were found to increase within the range of initial tool wear and then levelled off. Frequency components of AE in these turning operations were found to be below than 400 kHz. Count rates showed three distinguished levels depending on the flank wear: low level for wear in 120-130 μm, intermediate level for wear in 130-150 μm, and high level for wear above 150 μm. The total count was found to be a good indication of tool wear: it remained almost negligibly small until the flank wear reached 120 to 140 μm and then increased linearly or quadratically, depending on the threshold.

Asibu and Dornfeld (1981) analysed a theoretical model that related the AErms to the parameters of an orthogonal cutting process. They validated the model by performing orthogonal cutting tests on tubular workpieces of 6061-T6 aluminium and SAE 1018 steel. The cutting speed was varied from 0.128 to 1.9 m/s and rake angle from 10 to

40 deg. The results showed that AErms increased as the cutting speed and the rake angle increased.

Morivaki (1980) observed that AE signals with large amplitudes were detected when tool chipping and fracture occurred with hard and brittle tool materials emitting larger amplitudes than those emitted from soft and ductile tool materials and that the magnitude of the amplitude was related to the cross-sectional area of the fracture surface and was relatively independent of the loading speed. Based on these observations, they proposed a tool monitoring and control system that would automatically stopped an NC lathe on the detection of tool failure.

Teti and Dornfeld (1981) compared the experimental results from difference research workers who used different AE systems and techniques. They summarised four sources of AE signal generated in metal cutting as 1) deformation in the shear zone, 2) deformation and sliding friction at the chip / tool interface, 3) sliding friction at the tool /workpiece interface and 4) the breaking of chips and their impact on the cutting tool. They revised their theoretical model for predicting AE energy from the orthogonal cutting process. Predicted AE energy from the model has limited accuracy compared to practical cutting conditions. These considerations include the microscopic variations of otherwise similar material used in machining tests as well as variations in instrumentation and signal transmission path with the experimental set-up. They concluded that, in oblique turning operations an SAE 1018 mild steel with carbide insert cutting tools, the AErms increased with cutting speed and decreased with rake angle. However, it remained practically constant with feed rate and depth of cut. The results were similar to carbon steel S45c with a P20 carbide tool.

Diniz et al (1992) monitored the changing workpiece surface roughness caused by tool wear using the AE signal in finishing turning of steel type 1045 with different cutting conditions. They found that the AErms and its standard deviation in the range of 200 to 300 kHz increased with tool wear and both were suitable to be used for monitoring the growth of surface roughness in finishing turning. The increase in tool wear and consequently in surface roughness only slightly increased the AErms in the high frequency band for all cutting conditions.

Bueno and Etxeberria (1993) showed that AErms had remarkable correspondence with tool wear rate for various materials: medium carbon steel, austenitic stainless steel and austempered ductile iron. AErms can be used to classify the machinability of materials. Materials with poor machinability gave higher AErms.

Capitany and Citi (1984) performed the experiments on turning and milling. In turning with a single point tool, the number of AE events increased with tool wear; milling with four cutting edges the frequency spectrum revealed distinct peaks at the spindle's rotation frequency and its harmonics. The AErms significantly increased with tool wear. The AE signal amplitude increased with feed rate and cutting speed.

Lan and Dornfeld (1984) used acoustic emission to detect tool breakage and chipping in turning together with the tangential and feed forces for comparison. They observed that a significant burst type AE signal was generated during tool fracture, the size of the burst being dependent on the tool fracture area. The tangential force dropped until the cutting tool re-engaged with the workpiece. The magnitude of this drop has a linear relationship with the fracture length. Chipping also generated an AE burst and it was difficult to distinguish between AE bursts related to chipping and noise signals due to metal chip impact effects. The result of chipping, the feed force level may increase or decrease depending on the degree and type of microbreakage.

Dalpiaz (1988) performed experiments in turning using cutting speed 80-250 m/min, feed rate 0.1-0.5 mm/rev and depth of cut 0.5 –3mm on material of type C 45 steel (AISI 1045) and C 40 steel. Results showed that for an unworn tool the AE amplitude increased and the kurtosis decreased with cutting speed and that both the amplitude and kurtosis were almost entirely independent of the feed rate and the depth of cut. They identified that chip breakage was the source of burst signal since the AE burst frequency was found to match the chip-breaking frequency.

Dimila and Lister (1997) reviewed the application of neural networks to tool condition monitoring. According to this survey, over 60% of the researchers used the multi-layer perceptron (MLP) neural network configuration which was trained via

back- propagation (BP). Some researchers used different MLP configurations to find the most appropriate number of hidden nodes required for optimum system performance. The majority of the papers surveyed referred to work using a single sensor. The cutting force and acoustic emission were the most widely researched sensor inputs. From the survey, superior performance of neural networks was achieved when data from multiple sensors were fused.

Leem et al (1995) fused data of acoustic emission and cutting force to provide on-line tool wear monitoring in turning processes. They used the unsupervised Kohonen's Feature Map procedure followed by an Input Feature Scaling algorithm. Seventy-four inputs were used which were made up of 32 frequency bands of AErms and Force spectrum, 4 statistics of amplitude of AErms and force signal, and 2 cutting conditions. Two hundred data samples were used. The best classification result for fresh and worn tool statuses was 94 %.

Lin and Ting (1996) monitored on-line drill wear using an MLP back-propagation algorithm. The inputs to the neural network were the mean values of thrust force and torque, spindle rotation speed, feed rate and drill diameter. Several configurations of neural networks were trained and all seemed satisfactory for tool wear estimation. However, they observed that neural networks trained with sample mode converged faster than with batch mode. Neural networks with two hidden layers learned faster and more accurately estimated tool wear than those with one hidden layer. Different training data sequence showed little difference in wear estimation. Neural networks trained with the learning rate of 0.7 gave more accurate tool wear estimate than did learning rate of 0.3. In this case the size of the neural network showed no significant effects on the accuracy of the tool wear estimates.

Waschkies et al (1994) monitored continuous types of AE signals in turning processes with a variety of work materials. Two types of AE burst signals, from the collision between the chip and the tool and from the chip breakage, were eliminated using a threshold. The AE parameters used for quantifying the continuous signals were the average signal level (ASL), AErms and Crest factor. Crest factor is the ratio between the maximum amplitude and ASL. The ASL can be defined as,

$$ASL = \frac{1}{T}\int_0^T |x(t)|dt$$

The results showed that a flank wear of 0.2 mm was clearly detectable by a doubling of the ASL. The microscopic fracture of the tool (tool edge chipping) can be detected after about 100 turned parts by an abrupt increase of Crest factor with nearly constant AErms. They concluded that tool wear monitoring solely based on the increase of ASL was not sufficient, since it did not detect all types of tool wear.

In summary, a variety of AE techniques have been studied for tool failure monitoring. It is in general agreed that tool failure can be detected by acoustic emission. The conclusions categorised in terms of AE parameters used for tool wear detection, effect of cutting condition on tool wear monitoring, frequency components and data classification for tool wear detection are as follows.

- **AE parameter used for tool wear detection**

The most commonly used AE parameter to detect tool wear is AErms [Diei and Dornfeld (1987), Iwata and Moriwaki (1977), Morivaki (1980), Bueno and Etxeberria (1993)]. Iwata and Moriwaki (1977) showed three distinct levels of count rates depending on the flank wear. Waschkies et al (1994) observed that a flank wear of 0.2 mm was clearly detectable by a doubling of the ASL. The microscopic fracture of the tool (tool edge chipping) can be detected after about 100 turned parts by an abrupt increase of Crest factor with nearly constant AErms.

- **Effects of cutting condition on tool wear monitoring**

Besides tool wear or breakage, cutting conditions influence the AE signal. AErms increases significantly with the cutting speed [Heiple et al (1991) , Chaung and Asibu (1985) , Inasaki and Yunetsu (1981) , Asibu and Dornfeld (1981) , Asibu and Dornfeld (1981), Teti and Dornfeld (1981), Capitany and Citi (14)] but is hardly affected by the depth of cut and feed rate [Inasaki and Yunetsu (1981)] or stays constant with feed rate [Teti and Dornfeld (1981)]. In contrast, Capitany and Citi (1984) reported that the AE signal amplitude increased with feed. Heiple et al (1991)

observed that AErms produced were sometimes strong and sometimes weak for different depths of cut but was strongly material dependent.

- **Frequency components**

Iwata and Moriwaki (1977) found that the frequency components of AE in turning operations were below 400 kHz. Diniz et al (1992) found that the AErms and its standard deviation in the range of 200 to 300 kHz increased with tool wear and were suitable to be used for monitoring the growth of surface roughness in finishing turning.

- **Data classification for tool wear detection**

Neural networks were used to diagnose the tool condition given the input data. More than 60 % of reported research used back-propagation techniques. To increase reliability and sensitivity, multi sensor data fusion was used with acoustic emission and cutting force sensor being the most common.

2.2.8 Advantages of AE for tool wear and failure detection

AE has some advantages over other indirect methods of tool wear and failure detection, and they are as follows:

1. The frequency range of the signal is far beyond that of the mechanical vibrations and noise and therefore they can be easily filtered to give a better signal-to-noise ratio. [Iwata and Morivaki (1977)].
2. The technology is non-intrusive because the transducer can simply be glued or attached by magnet to the system being monitored; there is no need to modify the existing system.
3. The transducer is simple and robust based on reliable piezoelectric technology.
4. Compared to other indirect methods, AE and tool force measurements are the most sensitive methods [Lee et al (1992)].

2.2.9 Limitation of AE for tool wear monitoring

One of the major problems in the application of AE techniques is the analysis and the interpretation of the emitted signals because of the randomness of AE process. An AE

signal is often nonperiodic, contains many frequencies and cannot be explicitly described by mathematical relationship. The waveform of the detected AE signals are dependent on the propagation media, the sensor response and the instrumentation settings.

In a turning process, AE sources generated at the edge of the insert propagated through the tool shank to the transducer. The AE arriving at the transducer has a waveform that has been modified by such mechanisms in the propagation medium as:

(1) reflection and mode conversion of waves at a boundary
(2) energy attenuation
(3) velocity dispersion
(4) geometry and material properties of tool holder
(5) coupling interfaces and
(6) the relative locations of the AE sources and receiving transducer.

These can cause the signal detected by the transducer to change its waveform considerably; such changes are difficult predict theoretically.

AE, as a monitoring technique, is still not widely adopted by industry. This is because it is as yet impossible to achieve repeatable measurements of AE. The variability is due to inconsistent coupling of the sensor and insert with structures. Modern machining uses indexable insert tools. An insert, clamped onto a tool-holder, is used to remove metal and when all its cutting edges are worn, a new insert is substituted. When monitoring tool wear using AE, the transmission characteristics of the tool between the tool tip and the sensor are exceedingly changeable. Not only is the sensed AE signal dependent on the geometry of the tool structure and the response characteristic of the sensor, it is also influenced by the subtle changes in the sensor and insert couplings with the tool holder, not to mention the effect of tool wear as observed by different researchers. As a result, AE data are hardly comparable between set-ups, making knowledge transfer very difficult, if not impossible. In order to utilise AE to monitor tool wear this problem needs to be solved.

To overcome the problem stated above, some form of calibration needs to be performed in order to establish the relationship between the AE measured by the sensor and the AE produced from a known reference source located on the tool tip.

2.2.10 AE transducer calibration versus system calibration.

The calibration of a sensor is the measurement of its voltage output into an established electrical load for a given input [McIntire (1987)]. Calibration results are usually expressed as a frequency response. The usefulness of the calibration frequency response is that it permits sensitivity comparison and the assurance of repeatability of the transducer. A sensor's response received from a test can be expressed as a frequency response. The calibration results or the frequency response obtained was related to known artificial AE sources and particular types of test block. The test block was a solid object for calibration of the sensor. Steel was normally chosen because it was expected that AE sensors would be used more on steel than any other material. Different types of media, having different acoustic impedance, will give different calibration.

The standard guideline E1106-86 (1992) provides a standard for primary calibration. The procedure involves the use of a step function source produced by breaking glass capillary tubing with the typical outside diameter of 0.2mm (0.1-0.3mm). The size of the cylindrical steel test block is 0.9m in diameter and 0.43 m tall. The source is at the centre of the top circular face of the steel block. The local transverse displacement due to AE propagation on the test block surface can be measured using a capacitive sensor at a location symmetrical to that of the sensor under test with respect to that of the source. The standard provides the absolute calibration of acoustic emission sensor. The transducer voltage response is determined at discrete frequency intervals of approximately 10 kHz up to 1 MHz. The unit of calibration is voltage per unit of free motion, for example, volts per metre.

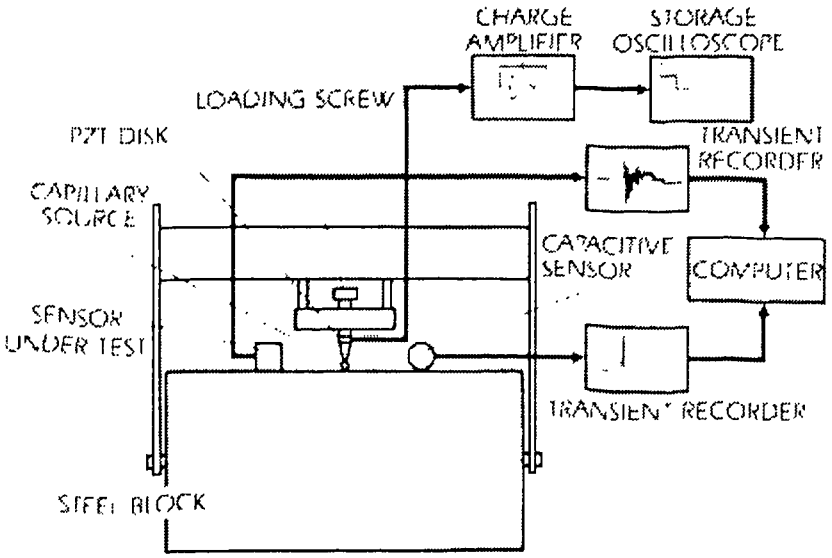

Figure 2.10. Diagram shows primary calibration [(McIntire (1987)].

Reciprocity calibration was provided by Nippon Steel Corporation [(McIntire (1987)] as a commercial service. The method used [Hatano et al (1976) and Hatano and Watanabe (1997)] requires three reversible AE transducers which are mounted on a common transfer medium. Three independent transmission/reception pairs are configurated through the transfer medium. If the transfer function of the medium from the source location to the receiver location is known, then from the purely electrical measurements of driving current in the source and output voltage at the receiver, the response functions of the transducers can be determined absolutely. The advantage of the reciprocity calibration technique is that it avoids the necessity of measuring or producing a known mechanical displacement or force.

The traditional approach for calibration and traceability of an AE sensor is inadequate and inappropriate for measuring in real applications. (Traceablility is the property of the result of a measurement or the value of a standard whereby it can be related to state references, usually national or international standards, through an unbroken chain of comparisons all having stated uncertainties [Charles (1998)]. System calibration is more useful than the calibration of AE transducers alone. The system calibration is the attempt to find the relationship between the value of a quantity indicated by a measuring instrument and the corresponding value from a reference standard and the relationship must be determined on the whole system and not only

on the transducer. In single-point turning the whole system comprises the tool insert, tool holder, insert/tool holder coupling, sensor/tool holder coupling, and sensor. It must be noted that when the layout of the source and sensor is changed, the system has to be calibrated again. The benefit of system calibration is that AE results obtained from different research can be compared; thus facilitate the ready transfer of knowledge.

2.2.11 Artificial sources for AE transducer calibration and AE system calibration

In order to calibrate an AE transducer or AE system, an artificial AE source is needed. Based on the wave shapes, artificial AE sources can be classified into three different categories [Hsu and Breckenridge (1981)] as:

1) **Noise** – produced from, for example, helium gas jet impact, fracture of silicon carbide particles, stress corrosion cracking and phase transformation in AU-47.5% Cd;
2) **Continuous waves** - generated by exciting piezoelectric, electro-magnetic and electro-static devices;
3) **Impulses** – arising from sparks, breakage of glass capillary, breakage of pencil lead, dropping of a steel ball on a hard surface to produce an impact, point-contact resistive heating and laser pulse heating.

In this research a pencil lead breakage, an air jet and a pulsed laser, were evaluated in reference to their suitability as a calibration source for single-point machining and tool wear monitoring. An review of each source is as presented below.

- **Gas jet**

Hsu and Breckenridge (1979) reported that McBridge and Hutchison (1976) and Bentley and Green (1976) directed a helium gas jet at the surface of a specimen to produce a continuous AE signal. In order to obtain a reproducible output, they suggested control parameters for helium gas jet sensor calibration listed in the table below:

Parameter	Value of parameter
Spectrum analysis band width	0.2 to 1.0 MHz
Pressure	145 ± 7 kPa (21 ± 1 psi)
Glass capillary tube	0.8 mm bore diameter by 90 mm long
Stand off distance	3.5 mm ± 0.1 mm
Bore angle	0° ± 1° with respect to surface normal

Table 2.1. Control parameter for Helium gas jet sensor calibration [Hsu and Breckenridge (1979)].

The American Society for Testing Materials (ASTM) (1994) issued a standard guide E976-94 for determining the reproducibility and checking for degradation of the AE sensor. The procedure is not capable of providing an absolute calibration of the sensor nor does it assure transferability of data sets between organisations. The standard recommended three artificial AE sources: an electrically driven ultrasonic sensor, a gas jet and an impulsive source produced by breaking a pencil lead. The specific purposes for checking sensors include: (1) checking the stability of its response with time; (2) checking the sensors for possible damage after accident or abuse; (3) comparing a number of sensors for use in a multichannel system to ensure that their response are adequately matched; and (4) checking the response after thermal cycling or exposure to a hostile environment.

The gas jet is one of the AE artificial sources suggested by the standard guide E976-94, and the gas are extra dry air, helium, etc. A pressure between 150 and 200 kPa (20 to 30 psi) is recommended for helium or extra dry air. The stand-off distance is 5 mm with the diameter of nozzle of 0.25 mm.

McBride and Hutchison (1978) used a helium gas jet to calibrate the AE system for measuring crack propagation in the vicinity of a notch. They showed that the helium gas jet produced a convenient and reproducible localised (point source) displacement spectrum over the frequency range 0.2-1MHz.

- **Pencil lead breakage**

Pencil lead breakage was recommended as an AE source by the standard guide E976-94. A repeatable acoustic wave can be generated by carefully breaking a pencil lead against the test block. The pencil source used was the 0.3 mm diameter lead (0.5-mm lead is also acceptable but produces a lager signal) The same length, between 2 and 3 mm are preferred, and the type of lead should be always controlled. The lead should always be broken at the same spot on the block with same angular orientation of the pencil.

Evans (1997) reviewed the use of different simulated AE sources for testing the diffuse field theory in structures. The various AE sources that were compared included glass capillary fracture, pencil lead breakage, ball impact and excitation of the conical piezoelectric transducer. He reported that variability of pencil lead breakage using 0.5-mm diameter 2H lead is ± 10 % peak amplitude. He selected the conical transducer for his diffuse field experiments because of its repeatability and ease of application.

Rangwala and Dornfeld.(1991) used pencil lead breakage test to normalise AE signal from single point machining. The experiment was to compare the corresponding AE from various inserts of different contact lengths (on top rake). Calibration was performed for the different set ups in order to compensate for the subtle changes in the shapes and sizes which could change the AE transmission characteristics for the tool material, and to account for changes due to slightly different coupling between the tool and sensor. The AE calibration source used was the fracturing of a 0.2 mm-diameter graphite lead at the tip of each tool the corresponding AErms measured. The normalising factors for all tools were calculated by dividing the AErms values form the lead-breakage test by the base value (at contact length = 0.75 mm). The AErms data for each tool from the cutting tests was then multiplied by these normalising factors.

- **Pulsed laser**

An Nd: YAG laser with optical fibre was used as an AE artificial sources [Aindow et al (1981), Hopko and Ume (1999), Scruby et al (1980) and Scruby et al (1981)]. Aindow et al (1980) used a source of low laser energy around 10 mJ. It was found that the pulsed laser can generate AE both in the thermoelastic and ablation ranges. He concluded that the laser energy as low as 3 mJ, without laser focusing is sufficient to generate AE in various metals.

Pulsed laser has been used to calibrate both an AE sensor and an AE system. Liebig et al (1998) used the pulsed laser to produce a surface wave to calibrate the piezoelectric sensor. The pulsed laser induced thermoelastic point source, which created a displacement measured by an interferometer with the output voltage from the piezoelectric sensor. The sensitivity of the sensor can be expressed in the absolute unit (V/nm) as a function of frequency.

Berlinskey et al (1991) used two artificial sources, a dropping ball and a pulsed laser, in the study of martensitic transformation in Fe- Ni. They established a qualitative linear relationship between the energy units of acoustic emission system and the known strain energy sources. The curve could then be used to determine the strain energy of naturally occurring sources during martensitic transformations.

2.2.12 Comparison of artificial AE sources

From the literature surveyed, it can be suggested that the more common artificial AE sources are:

- Pulsed laser,
- Dropping ball,
- Gas jet,
- Breaking pencil lead,
- Breaking glass capillary, and
- Electrically driven ultrasonic sensor

To qualify as an AE calibration source in tool wear monitoring, the source should possess similar characteristics (shape and bandwidth of frequency spectrum) to the AE sources produced in machining, and the important characteristic of reproducibility. Other considerations should include safety, cost and ease of use. Table 2.1 provides a comparison of different artificial AE sources in terms of convenience, cost and safety. Convenience refers to the ease with which the system can be set up and used. Cost includes both the set-up cost and the operating cost. Safety means the lack of hazard to operators, machines and the environment.

AE calibration sources	Convenience	Cost	Safety
Pulsed laser	√	x	x
Dropping ball	x	√	√
Gas jet	√	x*	√
Breaking pencil lead	√	√	√
Breaking glass capillary	√	√	√
Ultrasonic sensor	√	x	√

Table 2.2. Comparison of AE calibration sources.

*Cost of a gas jet can be reduced if air is used in place of the more expensive helium or hydrogen; air is readily available on the shop floor.

From Table 2.2 there are three sources that appear to score highly in terms of convenience, cost and safety. They are the breaking pencil lead, the breaking glass capillary and the air jet. Since both air jet and pencil lead breakage are cheap sources to use, readily available in machine shop, they were selected for studying as potentially suitable to tool wear system monitoring. Although the pulsed laser has the drawback in terms of cost and safety hazard, it has a dominant merit in that the energy at the incident point can be computed and related to the energy of the pulsed laser. Thus, using pulsed laser as a calibration source can readily invoke some unit of energy, which is the internationally accepted unit. Moreover, the pulsed laser source is more easily reproducible. Consequently, the research conducted by the author into AE calibration concerned the three artificial AE sources, namely, the pulsed laser,

breaking lead breakage and air jet. The investigation concerned the reproducibility of the sources, and the similarity of the sources to the real AE sources that they emulated. Details of this work are presented in Chapter 3 and Chapter 4.

2.3 Vibration signal processing

A system is vibrating if it is shaking or moving backwards and forwards in some way subjected to unsteady disturbances, generated by external or internal agencies. The amount and nature of vibration can be assessed using vibration monitoring which is a non-destructive technique. This technique has been used to monitor machines with rotating parts such as bearings or gears successfully. Thus, it is an important technique for condition monitoring.

2.3.1 Machine tool vibration

In this project, the cause of machine tool vibration generated by flank wear on tool tips was studied. However the flank wear is not the only source of machine tool vibration. Vibration can be categorised as free, forced and self-induced vibration. (Juneja and Sekhon)

2.3.1.1 Free vibration

Free vibration (or random or transient vibration) is normally induced by a shock (or impulsive) loading of the machine tool, for example, the tool striking a hard grain in the workpiece. Free vibration always decays, with time, and its rate of decay is dependent on the damping of the machine tool system.

2.3.1.2 Forced vibration

The system may be acted on by an external force, which is often of a repeated type that tends to maintain the oscillation. The motion of this system is a forced vibration. Forced vibration is usually caused by an out-of-balance force, such as produced by unbalanced rotating members, bearing imperfections or misalignments in a machine member, associated with a component integral with the machine tool. Forced vibration sometimes causes a relative oscillation between the tool and workpiece resulting in poor surface finish. Forced vibration in machine tools is also often caused by cyclic variations in the cutting forces. Such variations occur in side or face

milling, where the forcing frequency equals the product of the tool rotational frequency and the number of teeth on the tool.

2.3.1.3 Self-induced vibration

Vibration can occur in machining operations where cyclic variations in the cutting forces are not normally present such as in turning of plain cylindrical workpiece. It is called the self-induced (or self-excited) vibration in which the forces are generated by the machining process itself. The most important type of self-induced vibration is associated with a phenomenon called the regenerative effect. The regenerative effect occurs when a fluctuating force is created by the variation of uncut chip thickness (t). When the effective value of uncut chip thickness increases, the cutting force will be less. The reason is that the effective rake angle increases when t increases. If the energy produced by the fluctuating force is more than the loss of energy due to the damping of the system, then, vibration in the subsequent passes does not diminish. On the contrary, it may increase in magnitude.

2.3.2 Measures of vibration signal

Some of the simple measurements of vibration are explained below:

1) Peak value

A peak value, in Figure 2.11, is the peak amplitude of vibration. It reflects the maximum stress experienced by the vibrating part or the effectiveness of vibration isolation.

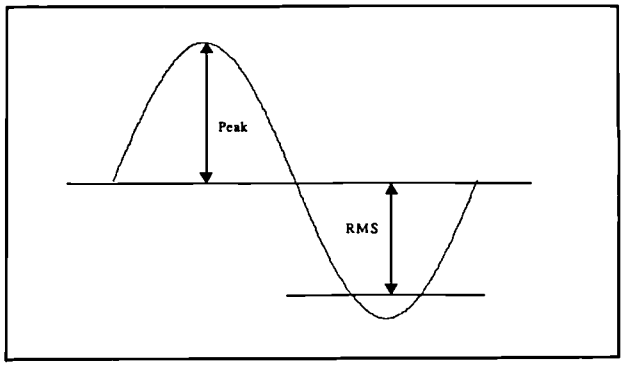

Figure 2.11. Peak and RMS value of vibration signal.

2) Mean value

The mean value of a vibration signal *x(t)* in time T is defined by

$$\bar{x} = \lim_{T\to\infty} \frac{1}{T} \int_0^T x\ (t)dt \tag{2.10}$$

The mean value is used to indicate the steady or static value of the vibration. Peak and the mean values are the two simplest quantities of the vibration measurement.

3) Mean square value

The mean square value is the power content of the vibration signal. For a signal *x(t)* the mean square value over time T is given by

$$\bar{x}^2 = \lim_{T\to\infty} \frac{1}{T} \int_0^T x^2(t)dt \tag{2.11}$$

4) Root mean square (RMS) value

The root mean square value, in Figure 2.11, is the simply the square root of the mean square value. It is written as

$$x_{rms} = \sqrt{\bar{x}^2} \tag{2.12}$$

5) Crest factor

Crest factor is the ratio of the peak value to the root-mean-square value. It has been applied to detect rotation imbalance or bearing problem successfully. Its value of between 2 and 6 refers to normal operation; whilst above 6 means that problems are developing.

2.3.3 Correlation techniques

Vibration signals that occur during tool wear are random processes. Various correlation techniques have been applied successfully for analysing random data. One of the correlation techniques, namely, the coherence function was utilised in this thesis. The correlation techniques are presented in this Section.

1) Autocorrelation function

The autocorrelation function $R_{xx}(\tau)$ of a quantity $x(t)$ is the average of the product of the quantity x at time t with the quantity x at time $(t+\tau)$. The autocorrelation can be defined as [Bendat(1986)].

$$R_{xx}(\tau) = \frac{1}{T}\int_0^T x(t)x(t+\tau)dt \tag{2.13}$$

The autocorrelation function is useful in identifying hidden periodicities, for example, the periodic signal buried in noise.

2) Cross correlation function

The cross correlation function $R_{xy}(\tau)$ of two quantities $x(t)$ and $y(t)$ is the average of the product of $x(t)$ at time t with $y(t)$ at time $(t+\tau)$. Similar to the autocorrelation function, the possible correlation or statistical dependence between two different random variables $x(t)$ and $y(t)$ is expressed by this function. The cross correlation is given as

$$R_{xy}(\tau) = \frac{1}{T}\int_0^T x(t)y(t+\tau)dt \tag{2.14}$$

The usefulness of the cross correlation function is for measuring time differences or time delay from one wave to another. This technique has been effectively used in acoustic emission testing in locating leak sites on pipes.

3) Cross-Correlation Coefficient Function

The Cross-Correlation Coefficient Function $\rho_{xy}(\tau)$ of two quantities $x(t)$ and $y(t)$ is the ratio of the cross-correlation $R_{xy}(\tau)$ to the square root of the product of the autocorrelation function of the two quantities at τ=0:

$$\rho_{xy}(\tau) = \frac{R_{xy}(\tau)}{\sqrt{R_{xx}(0)R_{yy}(0)}} \tag{2.15}$$

For all τ, the quantity $\rho_{xy}(\tau)$ satisfies $-1 \le \rho_{xy}(\tau) \le 1$

4) Autospectral density function

Autospectral density function, also known as the power spectral density function $G_{xx}(f)$, is defined for $0 \le f < \infty$ by

$$G_{xx}(f) = \frac{2}{T} E\left[\left| X_T(f) \right|^2 \right] \tag{2.16}$$

where $E[\,]$ is the ensemble average. The quantity $X_t(f)$ is the Fourier transform of $x(t)$ of length T.

5) Cross-spectral density function

Analogous to autospectral density function, cross-spectral density function $G_{xy}(f)$ is defined for $0 \le f < \infty$ by

$$G_{xy}(f) = \frac{2}{T} E\left[X_T^*(f) Y_T(f) \right] \tag{2.17}$$

where X_T^* is the complex conjugate of the finite Fourier transform $X_t(f)$ of $x(t)$. The quantity $Y_T(f)$ is the finite Fourier transform of $y(t)$.

6) Coherence function

The coherence function $\gamma_{xy}^2(f)$ of two quantities $x(t)$ and $y(t)$ is the ratio of the square of the absolute value of the cross-spectra density function to the product of the auto spectra density functions of the two quantities.

$$\gamma_{xy}{}^2(f) = \frac{\left| G_{xy}(f) \right|^2}{G_{xx}(f) G_{yy}(f)} \tag{2.18}$$

Or

$$\gamma_{xy}{}^2(f) = \frac{\left| S_{xy}(f) \right|^2}{S_{xx}(f) S_{yy}(f)} \tag{2.19}$$

where $G_{xx}(f)$ is the one-sided autospectral density function.

$S_{xx}(f)$ is the two-sided autospectral density function.

For all f, the quantity $\gamma_{xy}^2(f)$ satisfies $0 \le \gamma_{xy}{}^2(f) \le 1$

For stationary random data, the one-sided autospectral density function $G_{xx}(f)$ is twice the Fourier transform of the autocorrelation function $R_{xy}(\tau)$

$G_{xx}(f) = 2S_{xx}(f)$ when $f \geq 0$

This coherence function and the cross-correlation coefficient function are not Fourier transforms of each other.

The original use of coherence function is in the detection of noise in the input-output transfer or of non-linearity in the transfer function of a system. For example a constant parameter linear system with a single-input / single output is as shown in Figure 2.12, The system consists of a single input *x(t)* and an output *y(t)* with a frequency response function *H(f)*. The relation between one sided spectral density functions in the ideal case $G_{xx}(f)$, $G_{yy}(f)$ and $G_{xy}(f)$ is given by [Bendat (1986)]

$$G_{yy}(f) = |H(f)|^2 G_{xx}(f) \tag{2.20}$$

$$G_{xy}(f) = H(f) G_{xx}(f) \tag{2.21}$$

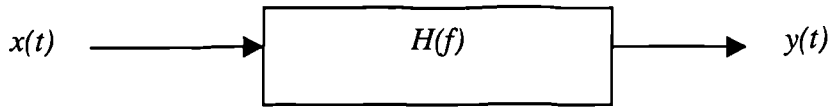

Figure 2.12. Single-input / single-out-put system.

Substituting Equations (2.20) and (2.21) in to Equation (2.18) to obtain

$$\gamma_{xy}^{\ 2}(f) = \frac{|H(f)|^2 G_{xx}^2(f)}{G_{xx}(f)|H(f)|^2 G_{xx}(f)} = 1 \tag{2.22}$$

if *x(t)* and *y(t)* are completely related. In other words, for the ideal case of a constant-parameter linear system with a single input and output, the coherence function will be unity. If *x(t)* and *y(t)* are completely unrelated, the coherence function will be zero. In actual practice, the coherence function is greater than zero but less than unity, one or more of three possible physical situations exist.

- Extraneous noise is present in the measurements.
- The system relating x(t) and y(t) is not linear.
- Y(t) is and output due to an input x(t) as well as to other inputs.

However the coherence function used in this research to establish correlation is between two signals that do not have an input-out put relation.

2.3.4 Vibration techniques for tool wear monitoring

Vibration is a technique that also has been widely used in detecting tool wear. Same as AE sensors, the vibration sensors can also be easily installed on a tool holder. In addition vibration sensors do not have the same stringent coupling requirement as for AE sensors although installation still needs to be properly done. In this research acceleration signals in both feed and tangent directions were investigated. It is proposed that vibration signals vary with tool failure in some frequency ranges. The use of coherence function was an attempt to provide a solution, which is relatively insensitive to the dynamics, and the process variables except tool wear. The approach using coherence function was first investigated by Dong (1987) who observed that the coherence in the frequency range up to 1.5 kHz followed a consistent trend.

Vibration signals have been found to vary with tool wear in some frequency ranges. Weller et al (1982) reported that the total amount of vibration energy in the frequency range of 4-8 kHz increased with flank wear in a wide range of feed, speed and depth of cut. Taglia et al (1976) observed that, the total power of the acceleration signal in the frequency range up to 2.5 kHz increased with wear up to 1.3-1.5 mm, and then fell rapidly back to the values found for little wear.

The coherence function of the accelerations of the tool in the tangential and feed directions was used as a method for tool wear detection by Au and Owen (1992) and Li et al (1997). Li et al (1997) used the coherence function for tool wear and chatter detection in the machining of a nickel-based supper alloy (Incronel 718). He found that as the tool wear progressed, the autospectra of the two accelerations and their coherence function would increase gradually in magnitude around the first natural

frequencies of the vibration of the shank. When the tool approached the severe wear stage, the peaks of the coherence function at the first natural frequencies increased rapidly to values close to unity.

Au and Owen (1992) studied the value of coherence function in the frequency range around the resonance region and observed that it fell with progressive tool wear. They also created a mathematical model to explain the relationship between the coherence function and tool wear. Owen and Au (1992) observed that the coherence function in the vicinity of the resonant frequency of the cutting tool was sensitive to tool wear. They used Principal Component Analysis to classify tool wear into two stages: good tool and worn tool for the three cutting conditions- roughing, semi-roughing and finishing. Clusters corresponding to the two different tool stages were clearly identifiable.

2.4 Classification techniques

There are a number of classification techniques that have been used for condition monitoring. The common ones are neural networks, expert systems and Bayes' rule. In this section, neural networks and Bayes' rule will be presented.

2.4.1 Neural networks

Complex phenomena occur in tool wear monitoring. Consequently the large amount of experimental data in a cutting process are difficult to analyse by humans. In the last decade, neural network has been applied to tool wear monitoring with some success. Of the different configurations, the three-layer feed forward perceptron network trained via back-propagation is the most common. A typical three-layered feed forward neural network is shown in Figure 2.13.

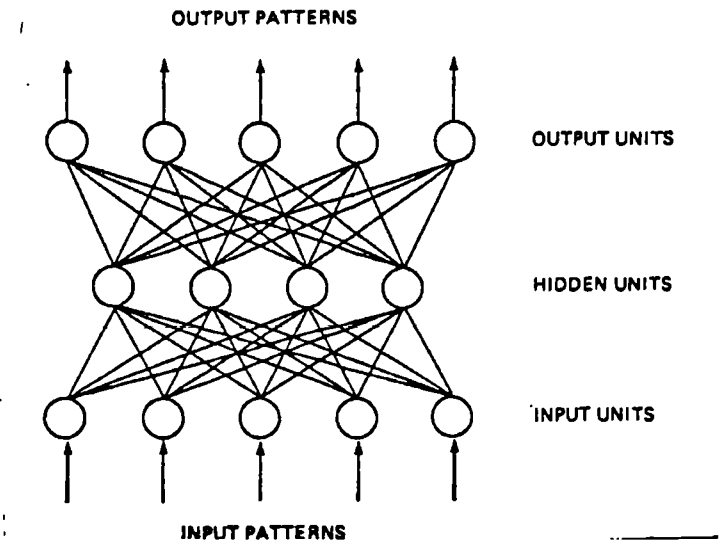

Figure. 2.13. A three-layered back-propagation network.

The bottom layer of units is the input layer. The units in this layer are the only units in the network that receive external input. The layer above is the hidden layer, which provides a processing connection to the layer above and below. The top layer is the output layer. The more neurons on a hidden layer, the more powerful is the network. Sometimes, very simple problems may be represented by a single layer of neurons.

The input of a neuron includes its bias and the sum of its weighted inputs. The output of a neuron depends on its transfer function. Many transfer functions can be used and the three most commonly used functions are Hard Limit (Step function), Linear and Log-Sigmoid.

The option of a transfer function with or without bias can be chosen. A bias can be a constant or allowed to change like the weights with an appropriate learning rule.

The backpropagation learning rule is used to train non-linear, multilayered networks to perform function approximation, pattern association, and pattern classification. It can be used to adjust the weights and biases of the networks in order to minimise the sum of squared error of the network. The sum of squared error is defined as

$$E = \frac{1}{2}\sum_{p=1}^{n}\sum_{i=1}^{m}(T_{pi} - O_{pi})^2 \qquad (2.23)$$

where m = the number of outputs in the output layer

n = the number of patterns

T_{pi} = the ith component of the desired output vector

O_{pi} = the calculated output of the ith neuron

The feature selection and the number of features are important for the accurate output. The input features must be given relative information and independent. The number of features must be large enough. However the more the number of features, the more training samples were needed. In practice, it should start with a small number of features and then the number is gradually increased.

To assess the performance of a neural network the following factors will be considered:

1. Sample mode or batch mode

If several input vectors are to be presented to a network, they may be presented one by one (sample mode) or in a batch (batch mode). Sample mode refers to a single input-output pattern set presented to the neural network. Batch mode occurs when all input-output pattern sets are presented to the neural network in a batch.

2. Training sequence

Training neural network with different training sequences makes a little difference in performance of neural networks.

3. The number of iteration to reach the acceptable value (target minimum error)

4. The number of hidden layers, and the number of neurons in each layer- Any reasonable function can be represented with a two-layer network: a sigmoid layer feeding a linear output layer.

5. Learning rate

Learning rate is measure of the rate of improvement of a backpropagation neural network during training. The training time can be decreased by the use of an adaptive learning step size as large as possible while keeping learning stable.

6. Transfer function

The output of a neuron is dependent on the type of transfer function.

2.4.2 Classification using Bayes' rule

In this thesis an expert system, named the belief network, was used to create diagrams and predict or classify the stages of tool wear. The belief network (also known as a Bayesian network or probabilistic causal network) captures beliefs between a set of variables which are relevant to some problem. The advantages of the belief network are its ease of use, user-friendly graphical interface and low cost. The belief network operates on the principle of "Bayes rule" and the "law of total probability of Bayes rule".

Before Bayes rule is presented, we shall provide an explanation of concepts such as "the probability of an event", "mutually exclusive or disjoint events" and "conditional probability".

- Probability of an Event

The probability of an event A is a measure of our belief that A will occur. One practical way to interpret this measurement is with the concept of relative frequency defined by

$$P(A) = \lim_{n \to \infty} \frac{Frequency}{n} \tag{2.24}$$

where P(A) is the probability of event A

Frequency is the number of times the event A has occurred.

n = the number of repetitions of the experiment

- Mutually Exclusive Events

If the two simple events A and B are mutually exclusive or disjoint (that is to say, when one event occurs, the other cannot), their probabilities must satisfy two conditions.

- Each probability must lie between 0 and 1.
- The sum of the probabilities for all simple events (an event that cannot be decomposed) in the sample space equals 1.
- $P(A \cap B) = 0$
- $P(A \cup B) = P(A) + P(B)$

2.4.2.1 Conditional probability

It is often necessary to consider the probability of the occurrence of an event A when additional information about the outcome of the experiment has been obtained from the occurrence of some other event B. This is called the conditional probability of A when B is given or has occurred. If P (B) > 0, then the conditional probability P(AlB) of A, given that B has occurred is defined to be

$$P(A \mid B) = \frac{P(A \cap B)}{P(B)} \tag{2.25}$$

2.4.2.2 Bayes' rule

Let $S_1, S_2 ..., S_k$ represent k mutually exclusive and exhaustive subpopulations with a prior probabilities $P(S_1)$, $P(S_2)$,..,$P(S_k)$. If an event A occurs, a posteriori probability of S_i given A is the conditional probability [Mendenhall et al (1999)]

$$P(S_i \mid A) = \frac{P(A \mid S_i)P(S_i)}{\sum_{j=1}^{k} P(A \mid S_j)P(S_j)} \tag{2.26}$$

for i = 1,2,....k

where

$P(S_i \mid A)$ = a posteriori probability of S_i given A

$P(A \mid S_i)$ = conditional probability of A given S_i

$P(S_i)$ = a priori probability of event S_i

2.4.2.3 Law of total probability of Bayes' rule

Given a set of events $S_1, S_2 ..., S_k$ that are mutually exclusive and exhaustive and an event A, the probability of the event A can be expressed as

$$P(A) = P(S_1)P(A \mid S_1) + P(S_2)P(A \mid S_2) + P(S_3)P(A \mid S_3) + ... + P(S_k)P(A \mid S_K) \tag{2.27}$$

where

$S_1, S_2, S_3 ..... S_k$ = a set of events.

P (A) = Probability of the event A.

To use the belief networks the conditional probability distribution of each variable given its neighbours or its parents need to be specified. In many applications these probabilities are allocated from experts. In the traditional statistical approach they are specified as parameters in the model and estimated by the maximum likelihood method [Gammerman (1995)]. In this research the conditional probability was learnt from the data contained in a file of cases.

Chapter 3
Tool Wear Measures and Preliminary Study of Artificial AE Sources

In this chapter, preliminary machining tests and their results were presented. Due to the fact that in tool wear monitoring, the AE and vibration parameters chosen have to be reliable, not just in the sense that they are sensitive to tool wear but also in the sense that they are repeatable given the same condition, consideration of the technical capability of the acoustic emission and vibration instruments is necessary. In addition, the machine tool chosen for the machining tests also needs to be considered. CNC program for machining on a Traub lathe is presented. In order to capture the nature of tool wear, a mould was produced of the tool cutting edge for the different stages of wear and a method, called the replica method, was used. This will be described in this Chapter. Finally, the artificial AE sources used to calibrate the tool system were investigated. The pencil lead breakage and the air jet noise sources were evaluated for their repeatability.

3.1 Objectives of preliminary test

The main objectives of the preliminary test are as follows:

1) To measure and eliminate the level of acoustic emission background noise released from the lathe and its surrounding.
2) To understand the use and the limitations of the equipment.
3) To select the proper time interval to record data and measure the progression of tool wear.
4) To choose the type of the tool insert, the workpiece material and the cutting conditions to perform the future test.
5) To find a method to measure accurately the size and progression of tool wear.

3.2 Set up of preliminary test

A precision Traubs CNC Lathe machine model TX 8F was used. The machining sequence was automatically controlled by a CNC program which is shown in Appendix A. From the allowable working volume of the lathe, the maximum size of the workpiece was selected to be 63.5mm in diameter by 150 mm in length. Tool inserts of type CG 4035 with chip breakers and of type GC 415 without chip breakers were used. They were mounted on a tool shank of type SDJCL 1616 H 11 (Sandvik Coromant). The workpiece material was either EN19 or EN24T.

The recommended cutting condition with cutting fluid by Sandvik Coromant [(Turning Tools-Metalworking Products (1998)] for EN24T (Hardness-Brinell between 275 to 350) with the CG 4035 tool insert is: the feed rate 0.1-0.4 mm/ rev and the cutting speed 170-110 m/min. The depth of cut and the feed rate also depend on the cutting condition. For example, for finishing cut, the feed rate is 0.1-0.3 mm/rev and the depth of cut is 0.5-2.0 mm.

Three cutting conditions (machining test 1-3) were selected in these preliminary tests with the specification as shown in Table 3.1 below.

	surface speed (m/min)	feed (mm/rev)	depth of cut (mm)
Machine test 1	150	0.1	0.3
Machine test 2	120	0.15	0.5
Machine test 3	120	0.2	1

Table 3.1. Three cutting conditions of preliminary tests.

3.3 Experimental equipment and specification of the tool tip and the tool holder

In this section, the experimental equipment, setting up and specification were presented. A schematic diagram of the experimental set up was as shown in Figure 3.1.

3.3.1 Detail of the tool tip and the tool holder

Carbide tool tips type GC 4035 DCMT 11 T3 04-UF (Sandvik Coromant Company) equivalent to ISO P 35 were used. It is chemical vapour deposition coated carbide (GC 4035) with a thick layer of Al_2O_3 on top of medium size of titanium carbides (TIC) or titanium nitrides (TIN). The geometry of the insert is: insert shape 55°, clearance angle 7°, rake angle 0°, cutting edge length 11 mm. and thickness 3.97 mm. The inserts were clamped on a left-hand tool holder (or tool shank) of type SDJCL 1616H11 (Sandvik Coromant Company). The clamping system consists of screw clamp from the top. The tool holder size is 16 mm x 16 mm x 100 mm.

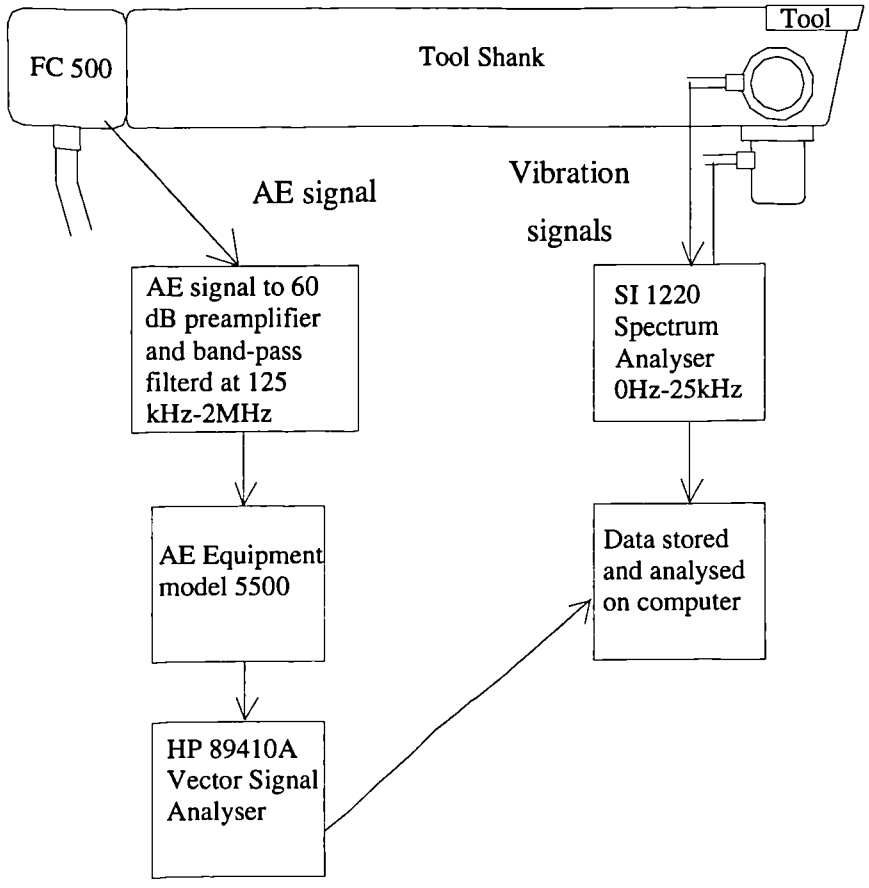

Figure 3.1. The experimental set-up.

3.3.2 AE equipment model 5500

An acoustic emission equipment, the AET 5500, was used. This provides the power to drive an AE preamplifier and transducer. A spectrum analyser was connected to

the AET 5500 to perform spectrum analysis on the input AE signal. The programming commands used to run the AET 5500 were given in Appendix B.

3.3.3 AE Transducer

A broad-band transducer model FC 500 (125 kHz - 2 MHz) was used. This transducer has a calibration curve (sensitivity vs. frequency) which is relatively smooth and flat, in the frequency band 100 kHz to 2 MHz. The placement of the transducer was carefully selected so that the transducer would receive consistent, strong and stable AE signals. It is also essential to hold the transducer securely in place for the duration of the test. The transducer was mounted at the end of the tool holder, 100 mm from the tool tip. Before attaching the transducer, the contacting surface at the end of the tool holder was ground flat. A Silicone Rubber Compound was used to provide the necessary transducer coupling and mounting.

3.3.4 AE filter and pre-amplifier

A pre-amplifier of 60-dB gain was connected to the AE transducer. The pre-amplifier is placed close to the transducer to amplify the signals. In order to reduce noise, from both mechanical sources and electro magnetic sources, a band pass filter of 125 kHz - 2 MHz was used inside the pre-amplifier.

3.3.5 Accelerometer

For the vibration measurement, two miniature accelerometers were used. Both were mounted close to the tool insert with one in the tangential force direction and the other in the feed force direction. These accelerometers were of type 303A03 driven by a PCB power supply unit. The frequency range of the accelerometer is 1 - 10,000 Hz (±5%) and 0.7 - 20,000 Hz (±10%). The accelerometers are designed for adhesive mounting. As the temperature could be very high during machining, glass-ceramic-disk insulators, measured 10-mm diameter by 1 mm thick, were inserted between the tool holder and accelerometers. The silicone rubber compound, which can withstand temperature up to 250°C, was used as a couplant at these interfaces. This compound was also used for the AE transducer mounting.

3.3.6 SI 1220 spectrum analyser

An SI 1220 multi-channel spectrum analyser, frequency range 0-25 kHz, was used to provide the signal analysis of the two vibration signals. The tangential acceleration signal was connected to channel 1 and the feed acceleration signal to channel 2.

The spectrum analyser was set up to show three results: Power spectra of the acceleration in the tangential and in the feed force directions and the coherence function between the tangential and the feed force direction. Details of the setting are given in Appendix C.

3.3.7 Hewlett Packard HP 89410A Vector Signal analyser

A two-channel Hewlett Packard HP 89410A Vector Signal Analyser was used to determine the frequency response of AE signal. This Vector Signal Analyser has a bandwidth of 0-10 MHz, which is much more powerful than SI 1220. In order to optimise the measurement resolution, measurement speed and display resolution, the analyser's functions such as resolution bandwidth, frequency span, main length and type of window must be considered (HP 89410A Operator's manual).

3.3.7.1 Resolution bandwidth

Resolution bandwidth is referred to as RBW. This function defines the analyser's frequency resolution. The maximum frequency resolution obtainable is actually determined by the resolution bandwidth. It may affect how fast the analyser makes a measurement. Usually, resolution bandwidth is adjusted automatically as the frequency span is adjusted. Manually selecting a narrow resolution bandwidth can slow down a measurement; on the other hand, selecting a resolution bandwidth that is too wide may not give adequate frequency resolution and can obscure spectral components that are close together.

3.3.7.2 Frequency span

The full-span available for HP 89401A is from 0Hz to 10 MHz. Measurement with spans that start at 0 Hz are often called baseband measurements.

3.3.7.3 Display resolution and frequency span

The number of displayable frequency points (also called number of points, lines or bins) of HP 89410 A, can be selected from 51 to 3201 points of resolution. For a given number of frequency points, narrower spans give finer frequency resolution, because the same number of frequency points represents a smaller range of frequencies. The display resolution can be defined as:

Display resolution = Frequency span/ (Number of frequency points-1)

Display resolution is different from frequency resolution. The frequency resolution bandwidth was determined by the resolution bandwidth. Selecting increasingly narrower spans will improve the display resolution until the point when the maximum resolution available is reached with the current resolution bandwidth setting.

3.3.7.4 Time record length

The time record length (T) depends upon the window bandwidth and the resolution bandwidth, (HP 89410A Operator's Manual) and it is given by

$$T = \frac{WBW}{RBW} \tag{3.1}$$

where:

WBW is the window bandwidth which is a constant depending on the window type; and

RBW is the resolution bandwidth.

However the maximum time record length (T_{max}) is limited by the number of frequency points,

$$T_{max} = \frac{(FP-1)}{span} \tag{3.2}$$

where:

FP is the number of frequency points.

The minimum time record length (T_{min}) is dependent on the window bandwidth to span ratio.

$$T_{\min} = \frac{WBW}{RBW\max} \tag{3.3}$$

where:

$$RWB_{\max} = .3 \times span \tag{3.4}$$

The reason that window is used in the time domain is to minimise the leakage problem. This problem arises because of the practical requirement that the observation of a signal must be by its very nature within a finite interval. The process of terminating the signal after a finite number of terms is equivalent to multiplying the signal by a window function. A window is a time-domain weighting function applied to the input signal and it can be seen as a filter used to compensate for the fact that most signals are not periodic within the input time record. Depending on the window shape, the ends of the input time record were attenuated accordingly. The net effect is a distortion of the spectrum. There is a spreading or leakage of the spectral components away from the correct frequency, resulting in an undesirable modification of the total spectrum.

3.3.7.5 Time record size

The time record size (TP), or the number of time points, can be defined as:

$$TP = SR \times T \tag{3.5}$$

where:

SR is the sample frequency rate.

The sample frequency rate was automatically determined by HP 89410 A and it is 2.56 times of the span (in baseband mode).

The details of calculating the parameters to set up the HP 89410A were presented in Appendix D. The parameter setting was given in Appendix E.

3.3.7.6 File format conversion

The measurement data from HP 89410A can be saved on a disk and the data file can then be converted to a PC-MATLAB file format by using the command "sdftoml /x". The usage of this command is as follows.

SDFTOML <sfile> <dfile> / x

where:

<sfile> is input standard format file

<dfile> is output PC-MATLAB file

x is output x axis data

If <dfile> is not specified, then a file named "SPECTRUM.MAT" will be created by default.

3.4 Microset Replica method

The degree of tool wear needs to be determined in tool wear monitoring. For machining with a tool insert, accurate measurement of tool wear can be achieved by removing the tool insert from the tool holder and then examining the cutting edges of the insert using various instruments. Often this action does not create a problem. But if one wants to use acoustic emission techniques for tool condition monitoring, the fact that the interface condition between the insert and tool holder has been disturbed can invalidate the monitoring techniques. A far better method will be one that does not upset the interface; in other words, the tool wear measurement is conducted with the tool insert in-situ.

The method used in this research is a two-part procedure and it is based on the idea of producing a replica of the region of the cutting edge. In the first step, a synthetic rubber compound, known under the trade name Microset, was used on the cutting edge to produce a mould. Microset can reproduce microscopic details the cutting edge to a micron and it cures within a short time typically around 7 minutes. Once the mould is formed, the second step of the procedure is ready to start. A liquid, known as Stycast 2057, is poured into the mould and with time it will solidify to give a replica of the cutting edge region of the insert.

Microset rubber material is supplied in two parts contained in a cartridge. To dispense microset rubber compound to the tool tip surface, the cartridge is fitted in a dispensing gun and the dispenser operated until the compound issues from both cartridge ports. According to the specification, it can record surface details which have dimensions significantly less than 1 micron. There appears to be no change in dimension during stripping of replicas but shrinkage of approximately 1.5% has been observed during the first twelve months of storage. There are 2 types of rubber compound, 101RF and 101RT; 101RF was selected because of the lower viscosity. The curing time is 7 minutes. However, owing to its low viscosity, a temporary plastic mould was built to contain the liquid microset during curing. The thickness of cured microset rubber has to be strong enough to retain the shape of the mould and it was chosen to be approximately 5 mm. The tool wear can be measured directly from the microset rubber mould using a two-dimensional optical toolmaker microscope.

Since the microset rubber is soft and flexible, only non-contacting measurement can be used. However a replica of the tool insert can be reproduced from the mould using a low viscosity and low shrinkage epoxy called Stycast 2057. With such a solid replica, contacting measurements can be carried out, for instance, to determine the surface roughness. The mixture used was formulated from thoroughly mixing 6 to 7 parts of Catalyst 9 by weight with 100 parts of STYCAST 2057. The curing time for this mixture is 8 hours at room temperature

To ascertain the accuracy of the STYCAST replicating the tool insert, four worn insert tools were subject to this treatment and characteristic dimensions were compared between the original and the replicas. These were the width between the opposite corners of the insert (A), the diameter of the hole (B) and the wear length (C) as shown in Figure 3.2. These dimensions were measured with a 2-dimensinal tool maker microscope.

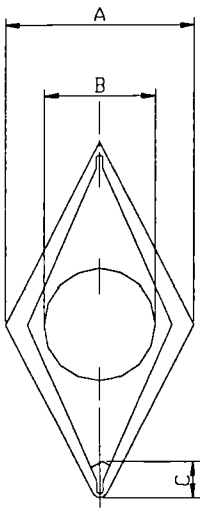

Figure 3.2. The length of tool tip to be measured.

The tool microscope has a table which can be driven by micrometers along two orthogonal axes. The amount of displacement in these two axes is digitally encoded and read into a personal computer using a program called "KSIMETRO", a listing of which is given in Appendix E. The object to be examined is placed on the table and the readings of various displacements provide the measurements needed. Results show that the length A of replica is 0.3 % smaller than that of the original. The hole diameter B of replication is bigger than the original by 0.3 %. The length C returns higher errors from, 1-5 %, because imperfect illumination on a black surface (black is colour of Stycast 2057) makes it difficult to locate the wear boundary accurately. Half of the STYCAST 2057 replica were found to have flaws in the form of internal and external bubbles, as well as crumpled edges.

3.5 Preliminary test procedure and results

The AErms power spectra displayed on the Hewlett Packard HP 89410A was set at 401points-display resolution. The resolution bandwidth was automatically selected by the equipment at 10 kHz. This resolution bandwidth corresponded to a time record length of 382 x 10^{-6} second. On the other hand if the instrument was set at 3201 points-display resolution, the time record length would be increased to 1.27 $\times$ 10^{-3} second, at the expense of longer processing time. Since record time length was short

and the AE signal was a rather changeable signal, a large number of samples was needed to make the averaged frequency spectra stable. The number of samples was chosen to be 250 by trial and error.

The averaged power spectra of acceleration in the tangential and the feed force directions and the coherence function were set at the maximum of 8 samples. The maximum number of samples used for calculating the average was limited by the machining cycle time and the processing time of spectrum analyser to produce a spectrum.

At first, the AE emission and vibration background noise were determined by running the Traub lathe idle under the designated rotating speed and feed. The AE noise spectrum obtained from HP89410A is shown in Figure 3.3. The vibration noise spectrum was not detectable except when the tool turret was indexing to a new position.

Two types of workpiece material EN19 and EN24T, and two types of tool inserts, GC4305 and GC415, were used for the machining tests. The AErms spectra obtained from different inserts and types of workpiece show a very similar shape. A typical AErms spectrum is shown in Figure 3.4. The tool insert without a chip breaker (GC415) produced long chips that could damage AE sensor cables and especially vibration sensor cables because they were mounted very close to the tool insert. Therefore, in order to avoid damaging the sensors or cables, the insert type GC4305 with a chip breaker was chosen to perform the subsequent tests. The EN24T work material was selected because of its greater hardness.

In the machining tests, workpieces of 63.5 mm initial diameter and 150 mm length were turned in successive passes until a minimum diameter of 27.5 to 29.0 mm was reached below which vibration of the workpiece would occur resulting in poor surface finish. The shape of the wear area was found to be the same as that shown in Figure 2.1 of Chapter 2. The maximum length of wear on the flank face was chosen as a measure of tool wear; this length is known as the flank wear height.

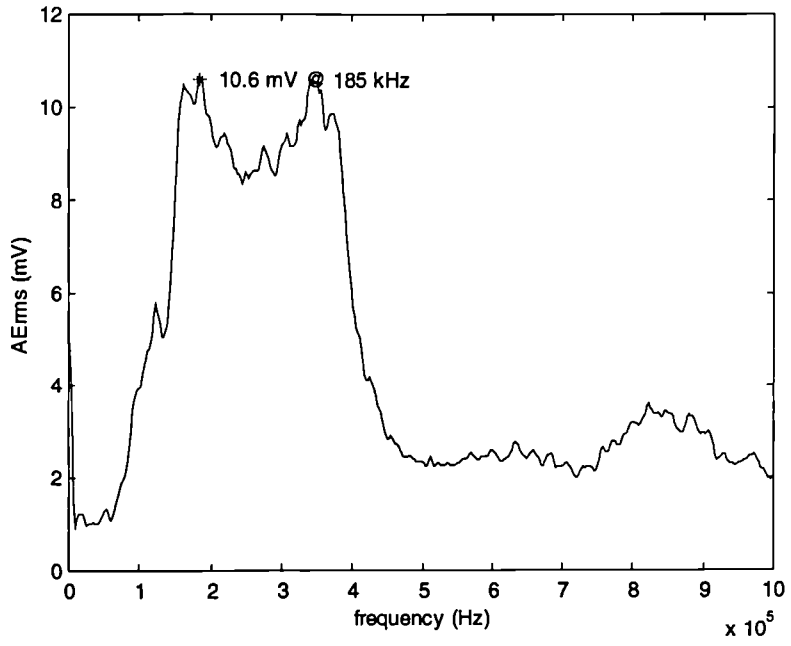

Figure 3.3. The AE background noise from machining.

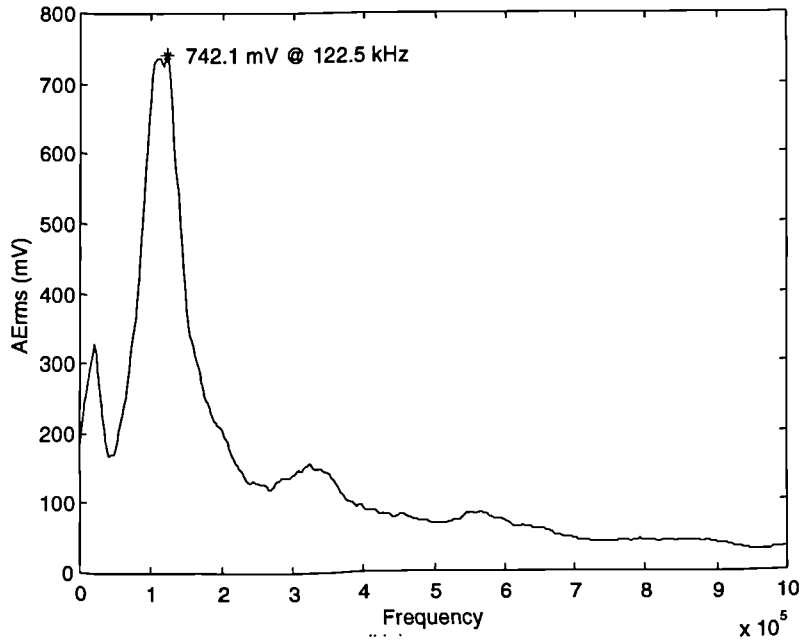

Figure 3.4. The typical AE spectrum obtained from machining process.

A microset rubber mould was made for every 2 full lengths (2x120 mm) of cut. The AE and vibration signals were recorded during the second full-length of machining. The recording started a few seconds after the engagement of the tool with the workpiece and stopped a few seconds before the end of cut was reached. This duration would allow 1000 samples to be taken for averaging when the bar diameter was 63.5 mm but only 250 samples when the bar diameter was 27 mm. The corresponding number of samples of the vibration spectra were 15 and 8 respectively.

The averaged AErms spectrum obtained from the HP80410A analyser was saved in a data file readable by the MATLAB application software. A MATLAB function was written to process this data file to compute the overall root-mean-squared value of the AE signal (in the frequency band of 0-1 MHz) from which the averaged AErms spectrum was generated.

A typical acceleration spectrum in the tangential and the feed directions and a typical coherence function obtained from the SI 1220 multi-channel spectrum analyser are shown in Figure 3.5. The relationship between tool wear and vibration was analysed. Different frequency ranges of the coherence function were chosen (for example 2.5 kHz to 5.5 kHz, 18 kHz to 22 kHz) and their averages were plotted against tool wear in the form of a scatter plot using AXUM 5, a graph plotting software package with signal processing capabilities. Some typical scatter plot are shown in Figure 6.17 to 6.19 of Chapter 6. It was evident that the coherence functions in some of the frequency bands appeared to be correlated with the progression of tool wear.

On the inspection of the tool tip after the preliminary test, it was found that the tool tip was worn back due to excessive rubbing with the workpiece. The worn area spread from the flank side to the top rake and it had a width of 1.7 mm. The flank wear was taken to be the standard by which the useful life of a tool insert was to be judged. For the type GC 4035 insert, the maximum allowable flank wear was 0.3 mm. The cause of this problem was that the cutting edge of the insert was cutting below the centre line of the workpiece.

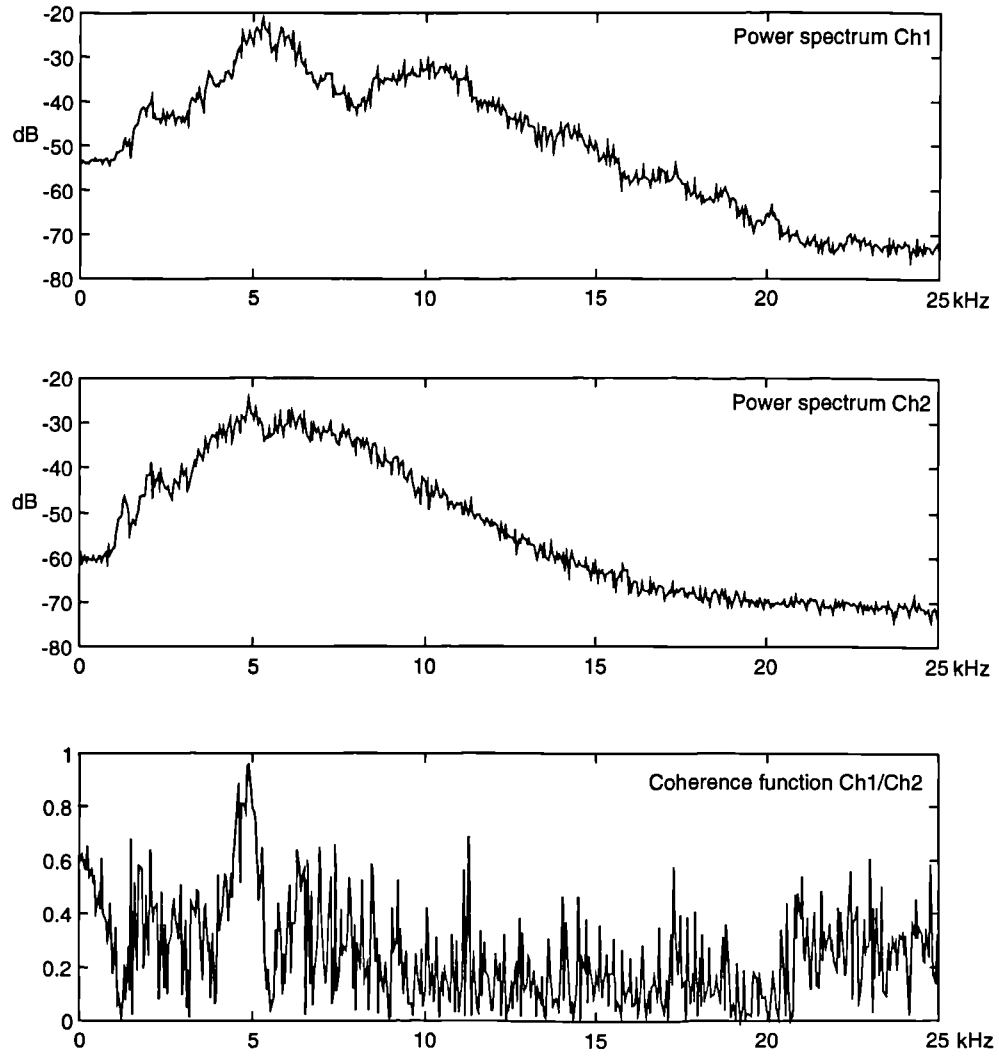

Figure 3.5. Typical vibration signal received from S 1220 spectrum analyser.

The problem was then rectified in subsequent tests by stacking the tool holder to the right height with metal shims.

The cutting conditions used in the preliminary tests are based on the recommendations from machining handbooks and the tests were very time-consuming. In order to keep the time for tool life machining tests to a reasonable length, higher cutting speeds and feed rates were chosen so as to speed up the tool wear. Accordingly, the following three machining conditions were chosen for subsequent tests:

- Roughing: cutting speed 150 m/s, feed rate 0.3 mm/rev and depth of cut 1mm.
- Semi-roughing: cutting speed 250 m/s, feed rate 0.25 mm/rev and depth of cut 0.75 mm.
- Finishing: cutting speed 300 m/s, feed rate 0.2 mm/rev and depth of cut 0.5 mm.

It is noted that the roughing condition agrees with the recommended practice whilst the other two have higher cutting speeds to accelerate flank wear development.

3.6 Preliminary test of Artificial AE sources

The objective is to find a suitable AE artificial source for the calibration of a tool system and for determining the effects on interface conditions on the AE detected. In the tool systems, there are two interfaces: 1) between the tool insert and the tool holder and 2) between the sensor and the tool holder. A suitable artificial AE source should be reproducible, inexpensive and easy to use. Three sources were chosen for investigation, namely, the pencil-lead breakage, the air jet and the laser pulse. In this Chapter, the preliminary test on the first two sources are reported whilst the last mentioned source will be discussed in Chapter 4.

3.6.1 Pencil-lead breakage source

In this test, an FAC 500 AE sensor was mounted with a silicone rubber compound in the middle of a 20-mm thick carbon steel plate measured 300 x 600 mm. The AE source was in the shape of a 0.5-mm pencil with a 2H-hardness pencil lead extending from the sleeve by 2.5 mm. The pencil lead was broken at the distance 100mm from the centre of the sensor. The angle between the pencil and the carbon steel plate was 30°. A 401-point AErms spectrum was recorded on the Hewlett Packard HP 89410A Spectrum analyser in the frequency range 0Hz -1 MHz.

The AErms spectra obtained from the fracture of pencil lead was repeatable. The resonance peak varied slightly from one spectrum to another. Skill is needed in producing a clean signal as the pencil sleeve may easily hit the steel plate.

3.6.2 Air jet source

An air jet was the second source to be investigated. The experimental set up was identical to the pencil-lead breakage test. A nozzle size measured 1.4-mm diameter was connected to a portable air compressor that could produce a pressure up to 10 bars. The nozzle was clamped in a stand clamp and the air jet was directed normally at the carbon steel plate at two different pressures of 1.5 and 4 bars. The stand-off distances were 4 and 16 mm and the distances between the centre of the sensor and the nozzle were 5 and 10 mm. AErms spectra of 401 points were recorded on the Hewlett Packard HP 89410A Vector signal and they spanned 0 to 1 MHz and averaged over 70 consecutive spectra.

The AErms spectra of the air jet appeared to vary less than those obtained from pencil lead breakage. The magnitude of the resonance peak was found to increase with the air pressure. The distance between the centre of the nozzle and the transducer did not affect the value of the resonance frequency but attenuate the height of the peak. The resonance peak varied with changes in the stand-off distance. The variability of AE spectra of the air jet was in part due to the lack of precision of the pressure regulator.

From the preliminary test, the air jet as an artificial AE source holds great promise. The pencil lead breakage is not as repeatable and requires skill for a clean signal to be produced. The air jet system is operator independent but it is necessary to develop the positioning jig to locate and control the position. The design of the air jet rig will be described in detail in Chapter 4.

3.7 Conclusions

The two-part procedure method based on the idea of producing a replica of the region of the cutting edge have been presented. In the first step, the synthetic microset rubber compound was used on the cutting edge to produce a mould. Then the Stycast 2057 is poured into the mould and with time, it will solidify to give a replica of the cutting edge region of the insert. Half of the STYCAST 2057 were found to have flaws in the form of internal and external bubbles, as well as crumpled.

The microset rubber compound (without STYCAST 2057) was chosen as the moulding material for obtaining a replica of the tool insert so that tool wear can be measured from it.

The AE emission and vibration background noise were determined by running the Traub lathe idle under the designated rotating speed and feed. The AE background noise was relatively low compared to the AE signal from machining. The vibration noise spectrum was not detectable except when the tool turret was indexing to a new position.

For acoustic emission, a large number of samples was needed to make the averaged frequency spectra stable. The number of samples was chosen to be 250. For vibration, the averaged power spectra of acceleration in the tangential and the feed force directions and the coherence function were set at the maximum of 8 samples. The maximum number of samples used for calculating the average was limited by the machining cycle time and the processing time of spectrum analyser to produce a spectrum.

MATLAB and AXUM5 application packages were used for data analysis. The AErms and the coherence functions in some frequency bands appear to have a good correlation with the progression of tool wear.

In order to avoid damaging the sensors or cables, the insert type GC4305 with a chip breaker was chosen for the subsequent tests. The EN24T work material was selected because of its greater hardness.

The cutting conditions used in the preliminary tests are based on the recommendations from machining handbooks and the tests were very time-consuming. In order to keep the time for tool life machining tests to a reasonable length, higher cutting speeds and feed rates were chosen so as to speed up the tool wear.

The AErms spectra of the air jet appeared to vary less than those obtained from pencil lead breakage. The air jet as an artificial AE source holds great promise. The pencil lead breakage is not as repeatable as the air jet and requires skill for a clean signal to be produced. The air jet system is operator independent but there is a need to develop a positioning jig to locate and control the position of the stand-off distances and the air-jet incident point.

Chapter 4

Comparison of Artificial Acoustic Emission Sources as Calibration Sources

In this chapter, two artificial AE sources, an air jet source and a pulsed laser source, were studied in order to assess their suitability as an AE calibration source for the single-point machining process. The effects on the AE were investigated of the clamping torque applied to the tool insert and a calibration procedure was suggested.

4.1 Introduction

Research into the use of acoustic emission (AE) for tool wear monitoring has established that there exists a definite relation between AE and tool wear. Attempts have been made to model the AE process in machining, but despite the fact that general trends could be predicted satisfactorily, the absolute values of AE produced in apparently identical machining processes could still differ markedly from one set-up to another.

The root cause of the problem is that the components that make up the AE transmission and measurement system as well as the interfaces between the components are highly variable. For single-point machining, typically, the components comprise an insert, a tool-holder and a sensor whereas the interfaces refer to those that occur between the tool insert and the tool-holder; and between the tool-holder and the sensor. Changes in either the components or the interfaces can produce a very different AE response. A striking example is the coupling between the insert and the tool-holder where, as will be reported in this chapter, an increase in the clamping torque on the insert results in a significant drop in the root-mean-square value of the AE signal (AErms). Consequently, AE results obtained from different research centres are not easy to compare making knowledge transfer at best difficult, if not impossible.

To achieve transferability of results and hence knowledge, some form of AE calibration is necessary. The process of calibration involves a measurement procedure carried out under specified conditions. Its objective is to establish the relationship between the value of a quantity as indicated by a measuring instrument and the corresponding value from a reference standard. When the result of the measurement can be ultimately related to a stated reference, such as a national or international standard, through an unbroken chain of comparisons all having stated uncertainties, then the measurement is said to be traceable to the standard.

It is important to note that the calibration of a sensor, as is conventionally done, in order to determine the AE at the sensing element of the sensor is not of much practical value. This is because one is often only interested in the character of AE at its source, for example, at the cutting edge in machining. What is immensely more useful is the calibration of the whole AE system with the location of the AE source known and the point of the sensor attachment decided. Understandably, once the layout of the source and sensor is changed, the system has to be calibrated again.

4.2 Artificial AE sources for tool wear monitoring

To qualify as an AE calibration source in tool wear monitoring, the source should possess similar characteristics to the AE sources produced in machining, in addition to the also important characteristic of reproducibility. Here, similarity suggests that the comparing sources have AErms-spectra that closely resemble each other in appearance.

The pulsed laser has been frequently used as an artificial AE source in the past two decades [56-59] for a number of reasons. Firstly, the laser source is broadband and highly reproducible because the pulse parameters can be clearly defined and tightly controlled. Secondly, the energy of a laser pulse is readily quantifiable once the electrical parameters that drive the laser are known. Thirdly, laser can be delivered to remote locations via optical fibres. However, a pulsed laser is not without its drawbacks: it is expensive, requires stringent safety consideration and produces low power, hence weak AE, when, by necessity, operated within the thermo-elastic range so as not to cause damage to the incident surface.

In many respects, an air jet source is similar to the helium jet source. The advantages of the air jet source are that it is non-contact, inexpensive, relatively safe, portable and readily available in a machine shop. The disadvantage is that the behaviour of an air jet in respect of the AE produced is affected by a host of environmental factors such as temperature and humidity.

4.3 Similarity Coefficient

An n-point RMS discrete AE-spectrum can be thought of as a vector u defining a point in the n-dimensional vector space. By analogy with vectors in the three-dimensional space, the length squared of u is the inner product of u with itself. Thus, the length of u can be computed from

$$|u| = \sqrt{u.u} = \sqrt{\sum_{k=1}^{n} u_k^2} \,. \tag{4.1}$$

This length is the same as the AErms of the signal from which the n-point discrete spectrum is derived. The vector $\boldsymbol{u}$ can be normalised by dividing its elements by the length of the vector. A normalised vector, denoted by $\overline{u}$, has a unit length.

Given two normalised vectors, $\overline{u}$ and $\overline{v}$, in the n-dimensional space, the included angle θ between them is related to the inner product of $\overline{u}$ and $\overline{v}$ as

$$\cos\theta = \overline{u}.\overline{v} \,. \tag{4.2}$$

If the two vectors are identical, then $cos\theta = 1$, whereas if they are orthogonal to each other, meaning that the projection of one vector on the other is zero, then $cos\theta = 0$. Since the value of $cos\theta$ suggests the degree of similarity between the two vectors, it is named the *similarity coefficient.*

4. 4 AE comparison of air jet, laser and machining

Three sets of tests were conducted to compare the shapes of the AErms-spectra obtained from single-point machining, the air jet and the pulsed laser. The repeatability of AErms-spectra from the air jet and pulsed laser sources was also assessed.

4.4.1 Machining tests

Machining tests were performed with the cutting process variables changing as follows:

- Surface cutting speeds from 80 to 150 m/min;
- Feed rates from 0.1 to 0.4 mm/rev; and
- Depths of cut from 0.3 to 1.0 mm.

The work-piece was made from EN24T (0.35-0.45 % carbon) and measured 63.5-mm in diameter by 150 mm in length. Tool inserts of type GC 4035 DCMT 11 T3 04 UF and a tool shank of type SDJCL 1616H 11 (Sandvik Coromant) were used. Details of the insert geometry are: cutting edge length 11mm, insert thickness 3.97mm, insert shape 55°, rake angle 0°, clearance angle 7° and nose radius 0.4 mm.

A broad band AE sensor (125 kHz – 2 MHz) was mounted at the end of the tool holder coupled with a silicone rubber compound. The preamplifier was total gain 80 dB with 125 kHz – 2 MHz built in filter. A Hewlett Packard HP 89410A Vector Signal Analyser was used to produce a 401-line AErms-spectrum with frequency from 0 to 1 MHz averaged over 70 consecutive spectra.

4.4.2 Air Jet Tests

From the preliminary results in Chapter 3, it was shown that the air jet source is a good repeatable source. Hence, the air jet equipment was redesigned to improve the repeatability by replacing parts with their high precision counterparts. A precision filter with a 5 μm filter cartridge was used instead. A precision pressure regulator with an operating range of 0.1 to 10 bar was connected to the precision filter. A new digital pressure gauge, with a reading range of 0 to 20 bars, was also added; its resolution is 0.01 bar.

As shown in the block diagram of Figure 4.1, air from an air supply passed through an air filter, a precision regulator, a precision pressure gauge, an on/off valve and a nozzle sequentially, emerging as an air jet.

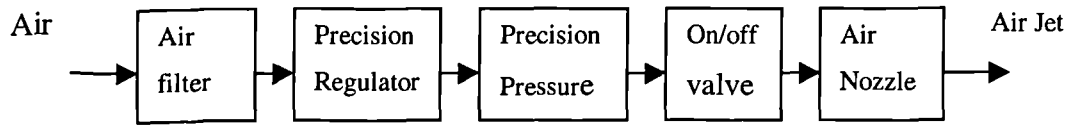

Figure 4.1. Block diagram of air flow in the jet equipment.

The air jet was directed normally at the top rake surface of the insert, 3 mm from the nose tip and equally distant from the leading and trailing edges of the insert. The location of the impact point is shown in Figure 4.2. The insert was clamped to the

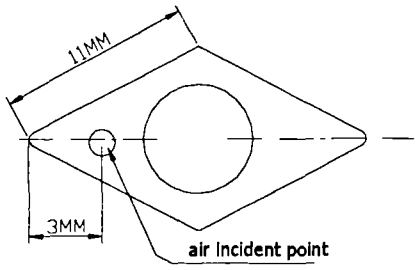

Figure 4.2 Location of the air incident point.

tool-holder with a clamping torque of 2 Nm and the tool holder was, in turn, held in a fixture. Both the stand-off distance from, and the location of the point of impact on, the rake face were controlled by micrometers. The positioning fixture is as shown in Figure 4.3. The measuring instruments and their settings were the same as those for the machining tests but the total gain is 60 dB. Two resolutions of the frequency spectrum were used, namely 401 and 3201 lines. The schematic diagram of the AE signal propagation path is shown in Figure 4.4

Tests were performed with two different sizes of nozzle diameters: 1.0 mm and 1.4 mm. The stand-off distance was varied from 2 to 16 mm, in increments of 2mm. The air jet pressure was varied between 1 and 5 bars, in increments of 1 bar.

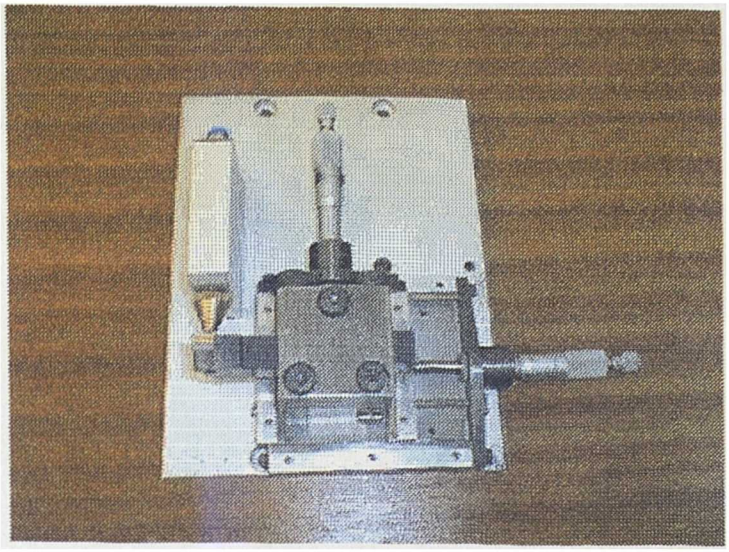

Figure 4.3. Positioning fixture of the air jet test.

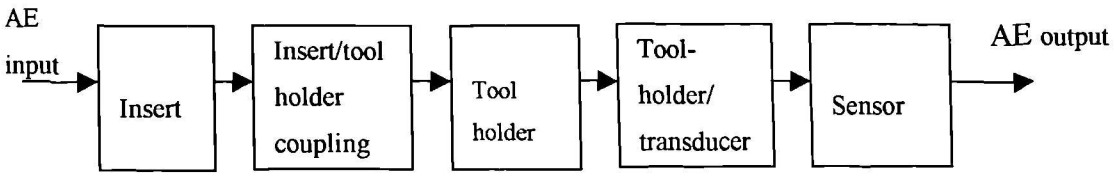

Figure 4.4. Schematic diagram showing the signal propagation path of AE in tool wear monitoring.

4.4.3 Pulsed Laser Test

A pulsed Nd: YAG laser system was used as the laser source. When using laser, it is important that the energy delivered to the surface does not cause too large thermal gradient in the surface, leading to rapid thermal expansion and hence damage to the insert. By trial and error, the energy level of 3 mJ was chosen. The energy of the laser was such chosen that it was insufficient to cause damage to the insert. The energy level of the laser was measured with a laser power meter, which registered the value of 3 mJ when the tip of the optical fibre was 2 mm away from the measuring matt black surface. The procedure and the set up of the measuring system were the same as those for the air jet tests excepting the spectrum resolution, which was 3201 lines.

4.5 Similarity of artificial and machining AE sources

All AErms-spectra from the machining tests have similar appearance with the average spectrum as shown in Figure 4.5.

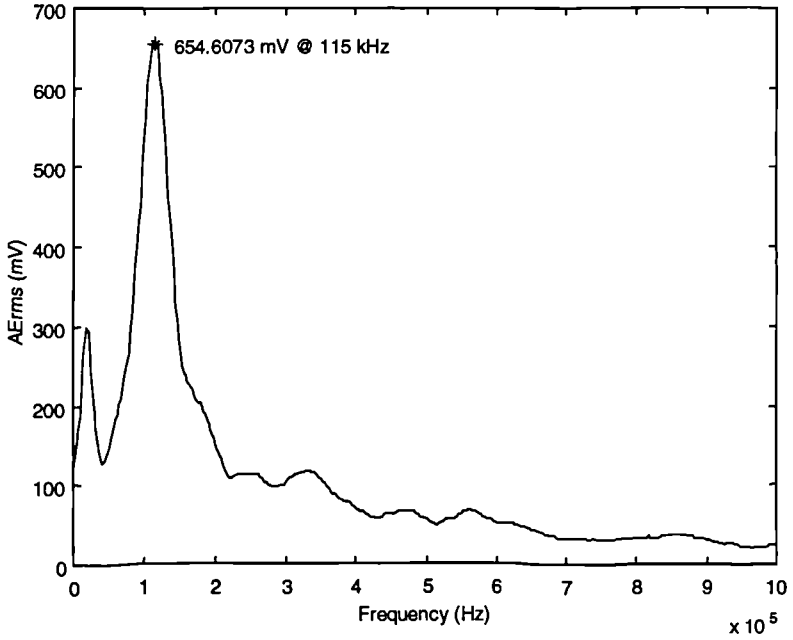

Figure 4.5. AErms-spectrum from machining EN24T with a GC 4035 insert.

Figures 4.6 and 4.7 show the typical AE time signals of the air jet and the pulsed laser. The air jet waveform is continuous whereas the pulsed laser is of burst type.

Figures 4.8 and 4.9 show the AErms-spectra for the two different artificial sources. It is evident that both the air jet and pulsed laser sources produced sufficient frequency bandwidth, 100 kHz –500 kHz, for tool wear monitoring purposes but the energy level of the pulsed-laser source is much lower.

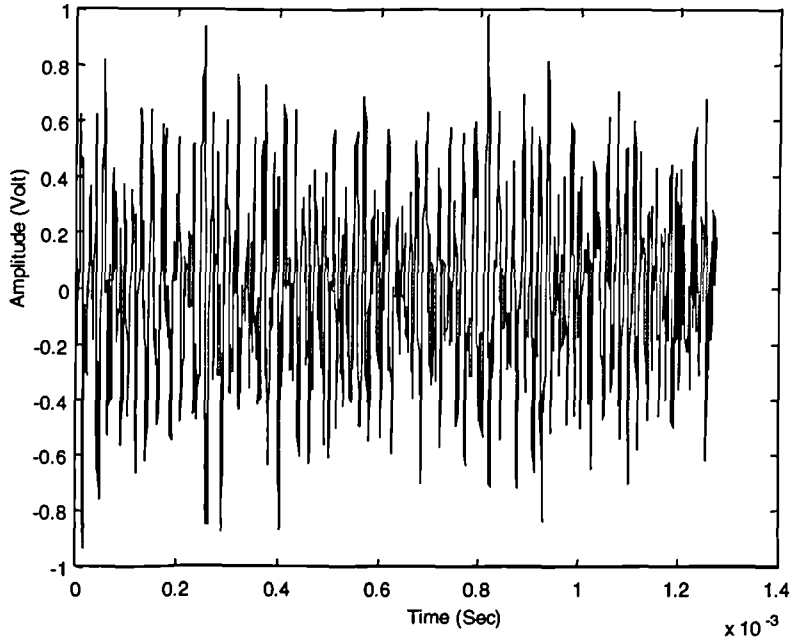

Figure 4.6. AE signal produced by air-jet.

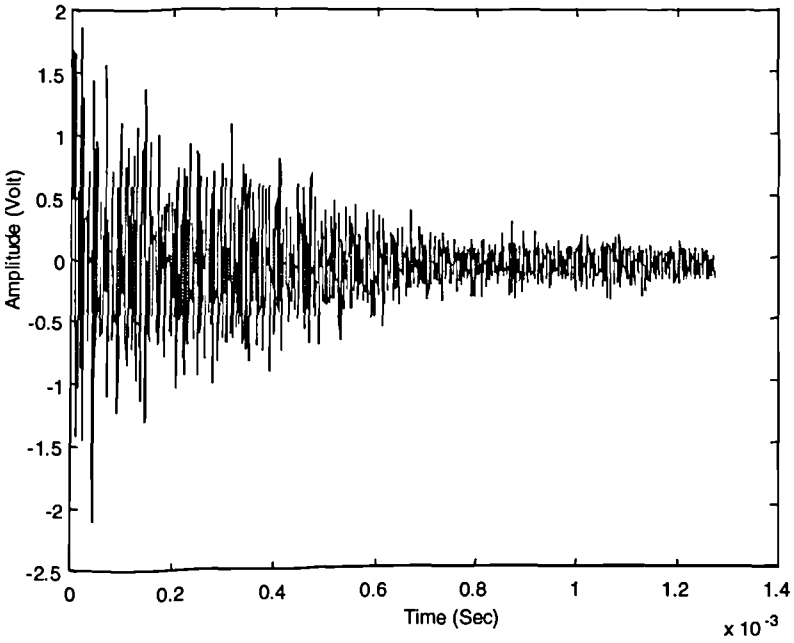

Figure 4.7. AE signal produced by laser.

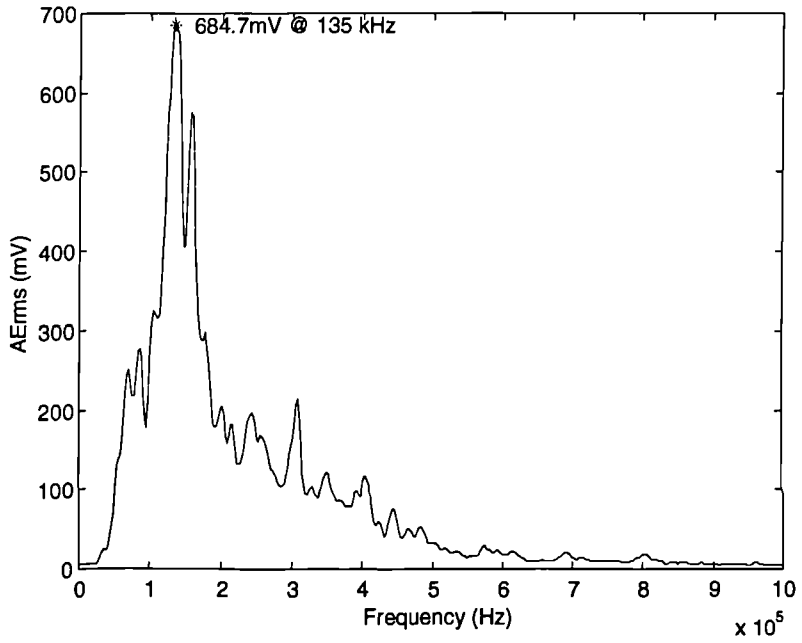

Figure 4.8. AErms spectrum of the air jet.

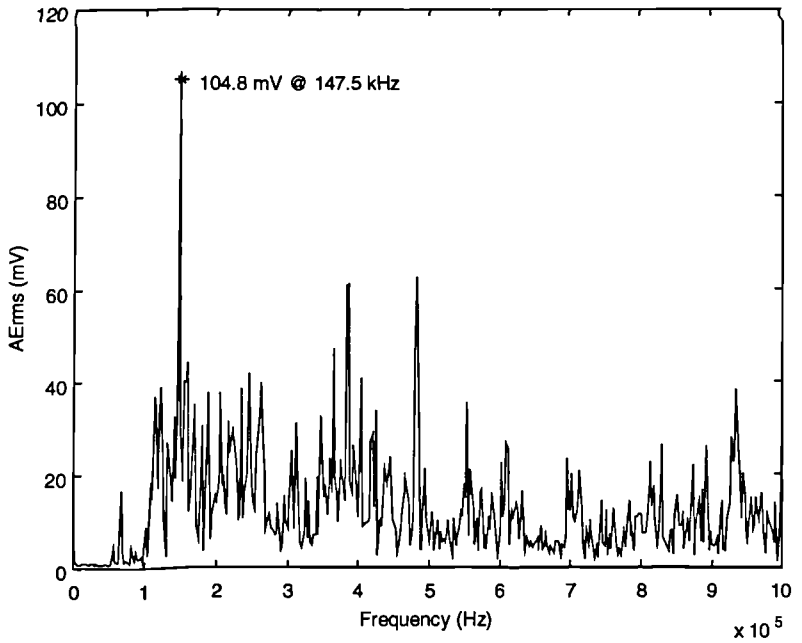

Figure 4.9. AErms spectrum of the pulsed laser.

Using the machining AErms-spectrum as the reference, its extent of similarity compared to the air-jet source and the pulsed-laser source, expressed in terms of the similarity coefficients as defined in Equation (4.2), are 0.86 and 0.56 respectively. This result is to be expected as is apparent from the AErms-spectra of Figures 4.5, 4.8 and 4.9.

The spectrum of the air jet pressure of 1, 3, 5 bars at the constant stand-off distances of 6mm are as shown in Figure 4.10. This diagram demonstrates the similarity of spectra shapes produced by the air jet at different pressures.

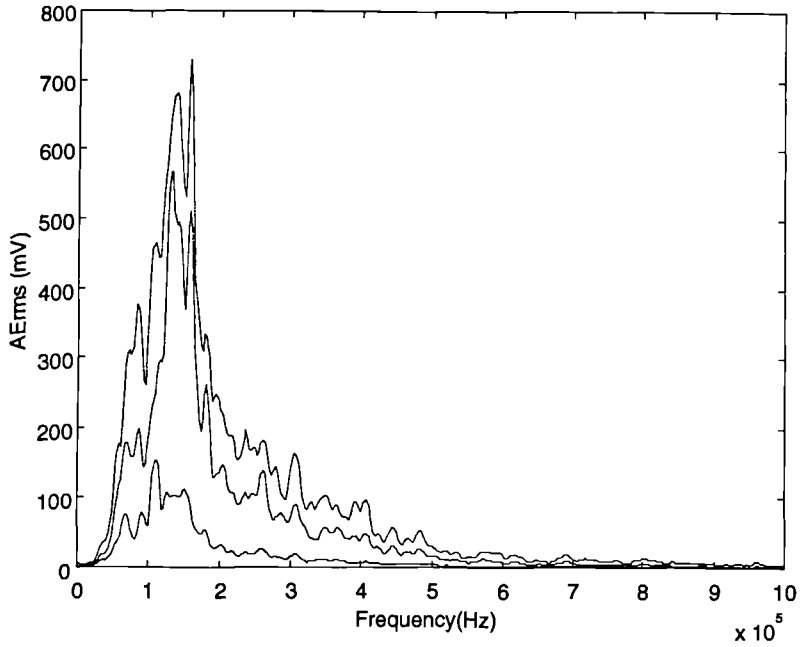

Figure 4.10. Spectrum of the air jet pressure of 1 bar (smallest peak), 3 bar (medium peak) and 5 bar (largest peak) at stand-off distance 6mm.

4.6 AE and air-jet pressure at different stand-off distances

Using Equation (4.1), the AErms value of the AE signal was calculated. For the air jet tests, the relationship was established between the AErms and the air-jet pressure at a stand-off distance from 2 to 16 mm, with bore diameters at the nozzle of 1 mm and 1.4 mm. Using the 1-mm diameter nozzle, the relation between AErms and the air-jet pressure for different stand-off distances are as shown in Figures 4.11 and 4.12. Relations between peak AErms amplitude and the air-jet pressure for different stand-off distances are as shown in Figures 4.13 and 4.14.

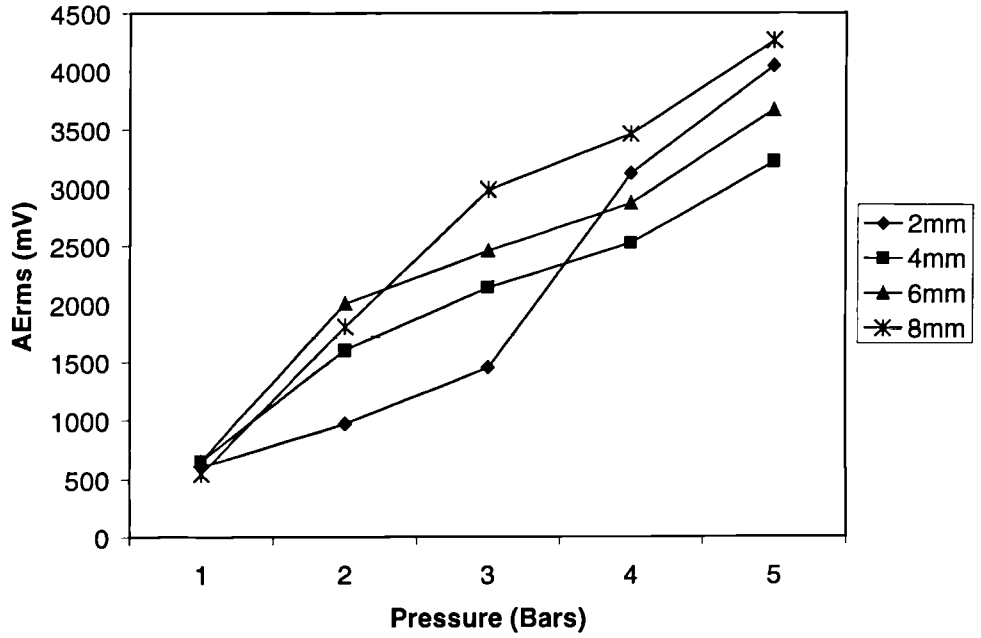

Figure 4.11. AErms of the air-jet at pressure, 1-5bars, and stand-off distances 2-8 mm.

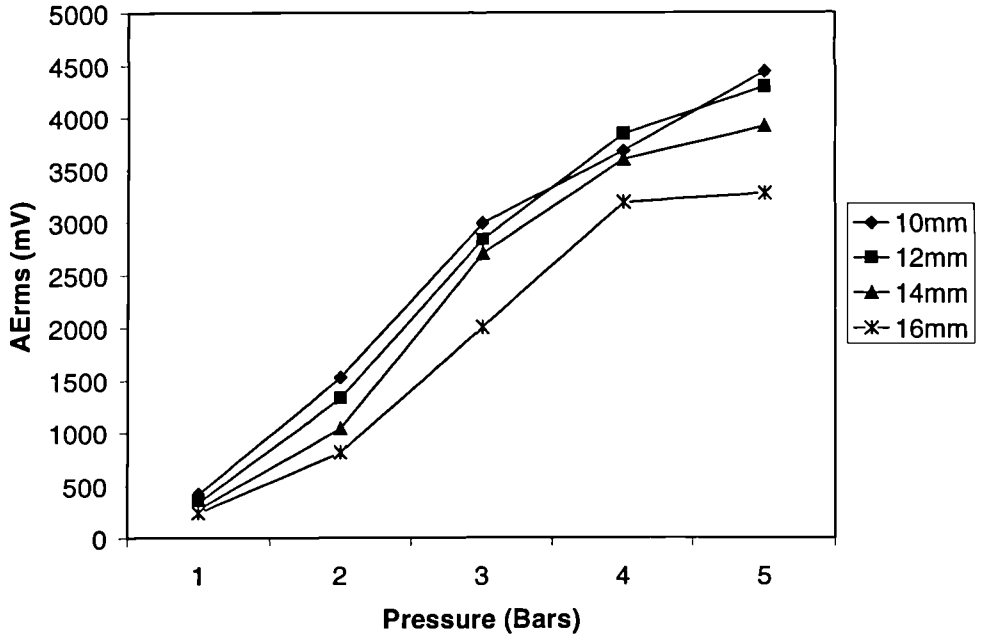

Figure 4.12. AErms of the air-jet at pressure, 1-5bars, and stand-off distances 10-16 mm.

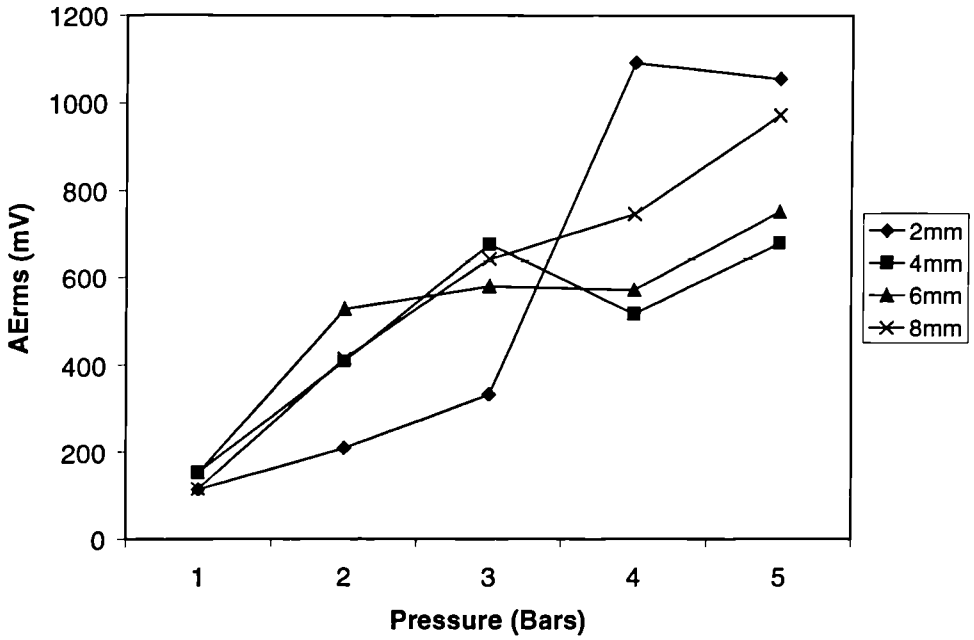

Figure 4.13. Peak AErms of the air-jet at pressure, 1-5bars, and stand-off distances 2-8 mm.

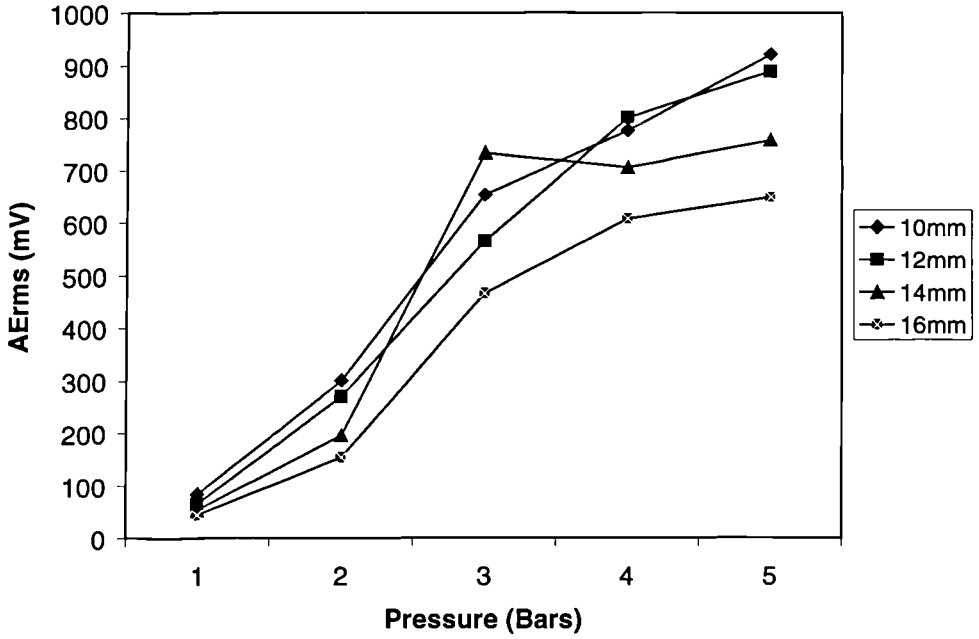

Figure 4.14. Peak AErms of the air-jet at pressure, 1-5bars, and stand-off distances 10-16 mm.

The shapes of the AErms-spectra at the two bore diameters were similar but the peak magnitude was higher for the bore diameter of 1.4 mm. On the other hand, the 1-mm diameter nozzle produced spectra that had lower variability. The variability of the AErms, defined as the ±1 standard deviation divided by the mean, was ± 2.26 %. Details of the variability of 1-mm diameter nozzle for different stand-off distances are as shown in Table 4.1 below.

Pressure (bar)	Variability of AErms at the stand-off distance (%)							
	2mm	4mm	6mm	8mm	10mm	12mm	14mm	16mm
1	1.90	2.50	1.44	1.45	2.61	2.06	1.86	5.24
2	1.14	1.78	2.33	1.33	3.38	2.97	1.81	2.58
3	1.84	2.48	1.87	2.03	2.67	4.59	1.97	1.88
4	3.75	2.03	1.89	2.13	1.20	1.61	2.06	2.02
5	1.71	1.59	2.85	1.88	2.12	1.84	1.97	2.32
mean	2.16	2.20	1.88	1.74	2.47	2.81	1.92	2.93

Table 4.1. Variability of AErms with the 1-mm diameter nozzle at different stand-off distances.

Other results which are of a similar nature to those just described are presented in Appendix G. Figures G1 and G2 in Appendix G. show the relation between AErms and the air-jet pressure for different stand-off distances but constant bore diameter of 1.4-mm. Peak AErms amplitude versus the air-jet pressure for different stand-off distances are shown in Figure G3 and G4. The variability of the 1.4-mm diameter nozzle at different stand-off distances is shown in Table G1 of Appendix G.

The variability of AErms at different frequency bandwidth, 0 Hz –1 MHz, 100 kHz-1 MHz, 100 kHz-400 kHz, 100 kHz-500 kHz and 20 kHz-500 kHz were also computed. All ranges provided similar variability. The variability at frequency range 0 Hz-1MHz was the lowest. The condition at the stand-off distance of 2 mm and pressure of 2 bars was chosen to show the variability of measurements. This condition showed the lowest variability amongst the set of combinations of tested stand-off distances and pressures.

Peak amplitude on the AErms-spectrum with 401-point resolution	=	± 5.05 %
Peak amplitude on the AErms-spectrum with 3201-point resolution	=	± 5.84 %
AErms from the AErms-spectrum with 401-point resolution	=	± 1.14 %
AErms from the AErms-spectrum with 3201-point resolution	=	± 1.27 %

For the pulsed laser tests, the variability of the measurements at the stand-off distance of 2mm and laser energy of 3 mJ are:

Peak amplitude on the AErms-spectrum with 3201-point resolution	=	±2.02%
AErms from the AErms-spectrum with 3201-point resolution	=	± 1.92 %

It is observed from these results that both artificial sources have similar variability. The AErms-spectra with 401 and 3201-point resolution also have close variability.

4.7 AE, air jet pressure and insert clamping torque

Air jet tests were conducted to study the effects of different sensor location and of different insert clamping torque on the AErms. The tool holder was held in the tool post instead of in the fixture. A new fixture was built to hold the nozzle and to locate the air incident point and the stand-off distance as in Figure 4.15. The air jet equipment and the experimental set-up were shown in Figure 4.16. Similar to the air-jet tests in Section 4.2, the air jet was positioned vertically above the top rake face of the insert 2-mm inwards from both the leading and trailing edges of the insert, at a stand-off distance of 5 mm. Three pairs of AE sensors were mounted with the first of each pair on the tool holder and the second on the tool post all held in position using a silicone rubber compound. These were all PAC sensors and the pairs were: WD and WD with response bandwidth of 100kHz-1MHz, UT1000 and UT1000 with response bandwidth of 60 kHz-1MHz, R30 (100 kHz-400 kHz) and R15 (50kHz-200kHz). The outputs of these sensors were amplified 60dB and band-pass filtered from 20kHz to 1MHz. The Hewlett Packard HP89410A Vector Signal Analyser was used to produce an AErms-spectrum with 401-point resolution averaged over 70 successive spectra. The insert was tightened to three levels of torque, namely 0.4 Nm, 1.2 Nm and 2.0 Nm. The air-jet pressure was varied between 3 and 8 bars in 1-bar increments.

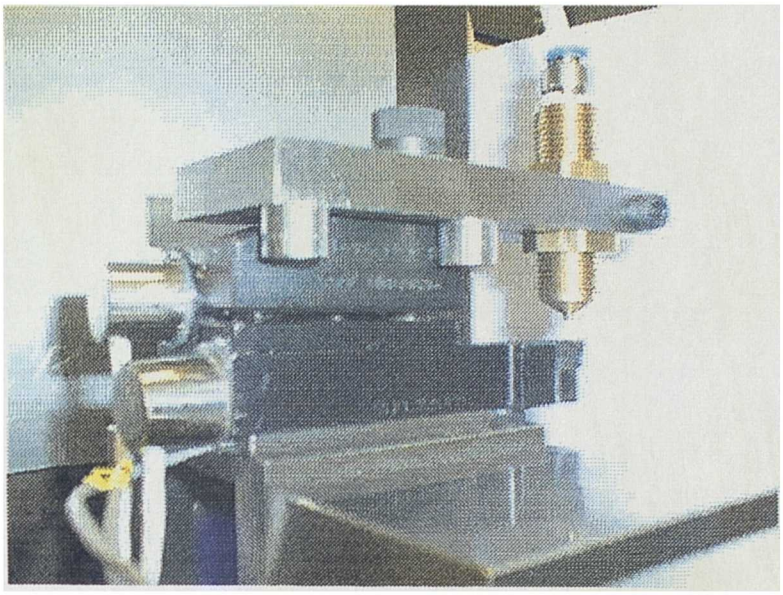

Figure 4.15. Air jet fixture to locate the air incident point and the stand-off distance.

Figure 4.16. Air jet equipment and experimental set-up.

Results showed that the AErms were linearly proportional to the air-jet pressure applied for all levels of clamping torque. The relation of AErms and the clamping

torque of each sensor pair at the torque value of 0.4, 1.2 and 2.0 Nm are shown in Figures 4.17, 4.18 and 4.19 respectively. It was also observed that the clamping torques 1.2 Nm and 2.0 Nm, produced AErms which were very close between each pair of sensors. The AErms was the highest at the torque value of 0.4 Nm but fell to a lower plateau value as the torque increased, therefore suggesting that the AErms was sensitive to the torque applied. AErms related to air jet pressure for the different sensors at the clamping torque of 2.0 Nm is shown in Figure 4.20.

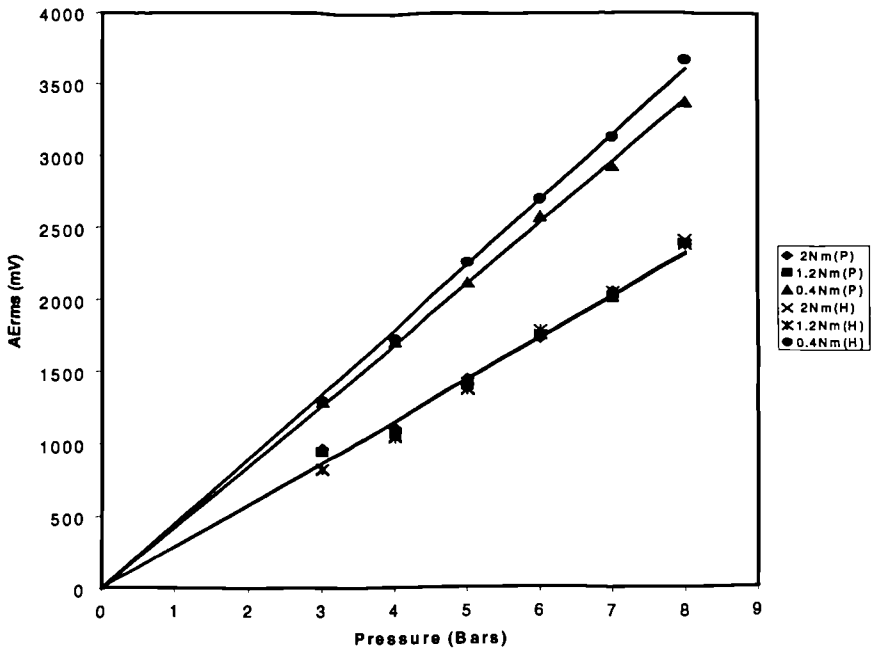

Figure 4.17. Graph of AErms and air jet pressure for the WD/WD sensor pair at the clamping torque values of 0.4, 1.2 and 2.0 Nm. ("P" and "H" refer to the tool post and the tool holder respectively)

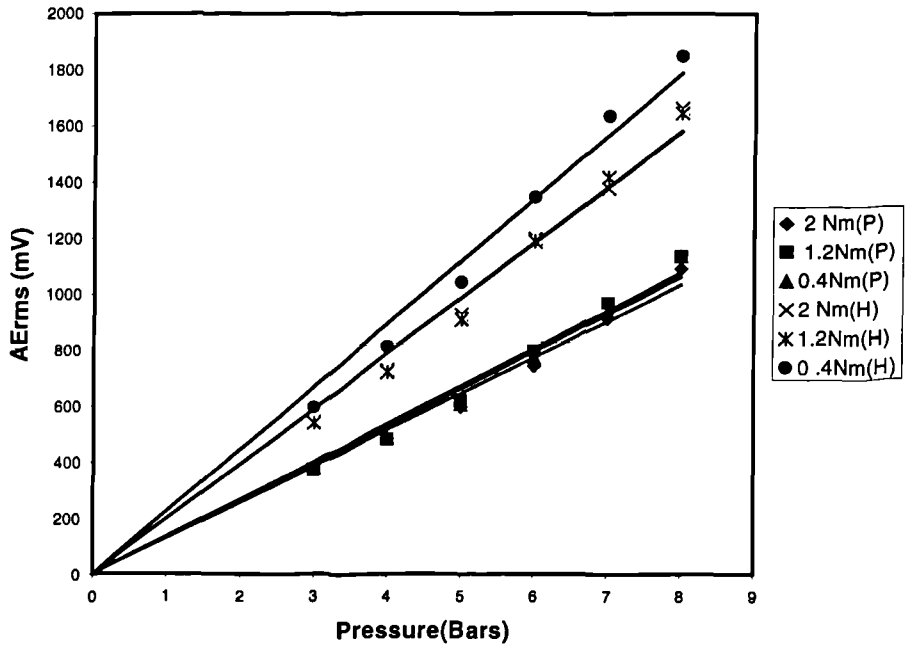

Figure 4.18. Graph of AErms and air jet pressure for the UT 1000/UT1000 sensor pair at the clamping torque values of 0.4, 1.2 and 2.0 Nm.

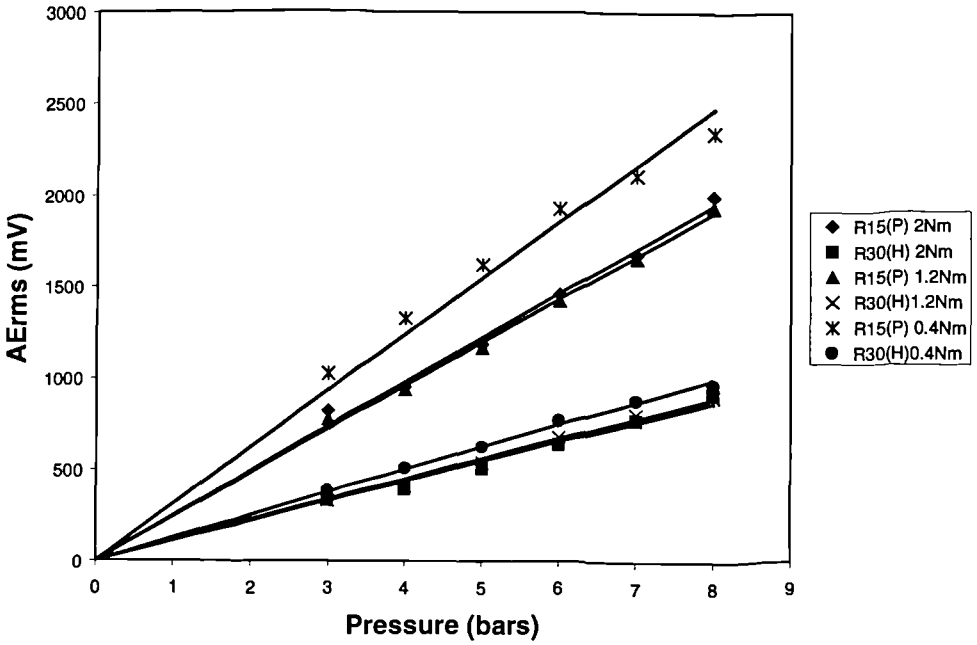

Figure 4.19 Graph of AErms and air jet pressure for the R30/R15 sensor pair at the clamping torque values of 0.4, 1.2 and 2.0 Nm .

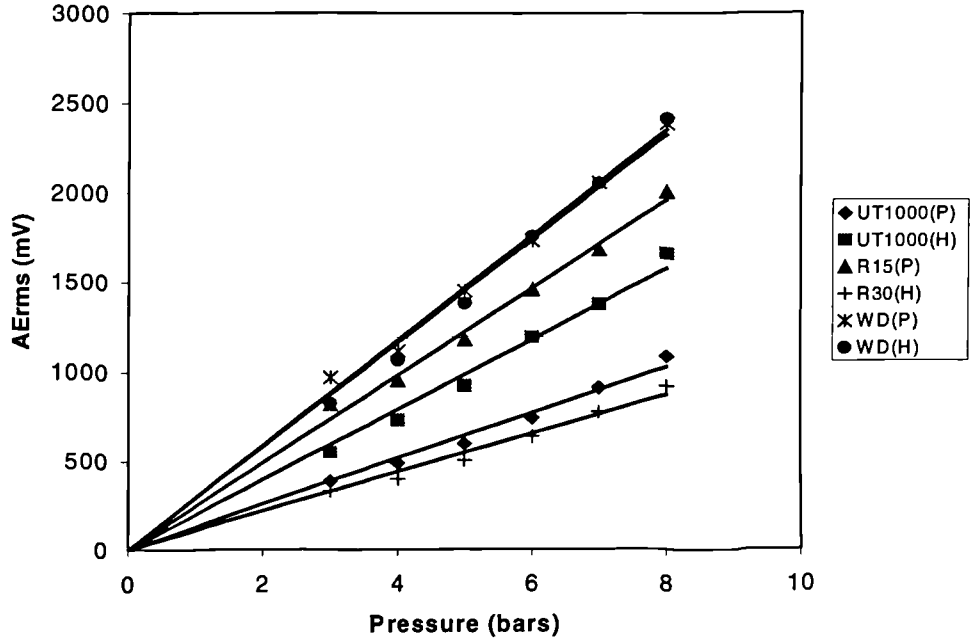

Figure 4.20. AErms related to air jet pressure for different sensors at the clamping torque of 2.0 Nm.

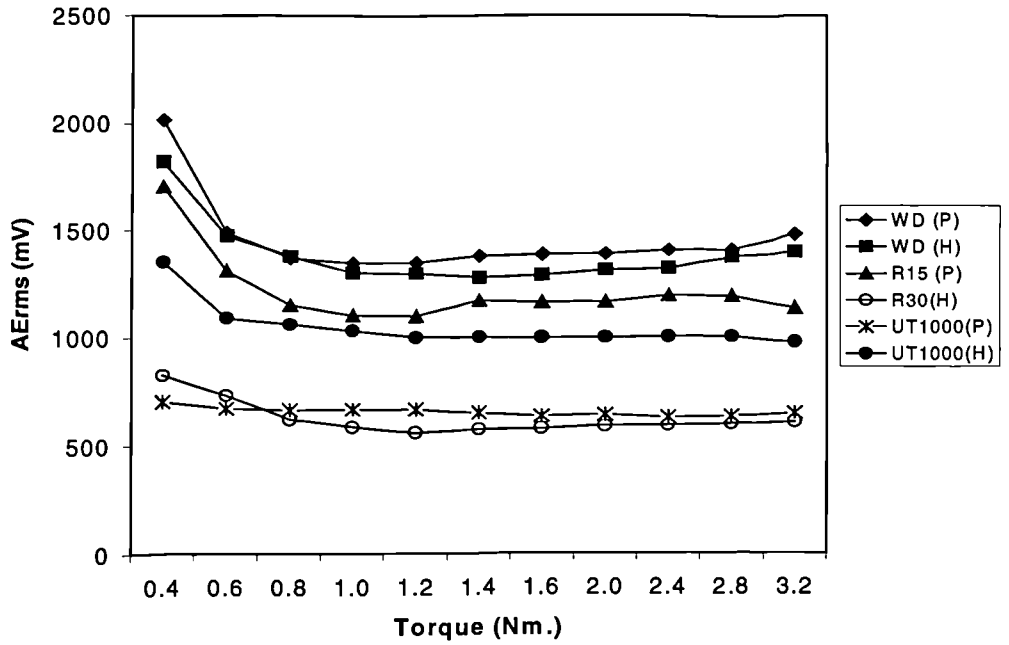

Figure 4.21. AErms related to clamping torque at constant pressure of 5 bars.

To study the relation between clamping torque and AErms, the air-jet pressure was fixed at 5 bars whilst the clamping torque was changed from 0.4 Nm to 3.2 Nm using an adjustable torque wrench. The results, as in Figure 4.21, show that the AErms decreases as the torque increases from 0.4 to1.2 Nm and then remains constant from 1.2 Nm to 3.2 Nm.

The ratios of AErms between the different pairs of sensors, one on the tool post and the other on the tool holder, were calculated for each value of clamping torque and they are as shown in Table 4.2 below:

Sensor pair	Mean of ratios	Standard Deviation of ratios	Variability (%)
WD/WD	1.049	0.031	2.984
UT1000/UT1000	0.630	0.038	6.093
R15/R30	1.949	0.084	4.303

Table 4.2 Variability of mean of ratios of each sensor pair with clamping torques from 0.4 Nm to 3.2 Nm.

By considering the means of ratios for a limited clamping torque range, from 1.2 Nm to 3.2 Nm, for the different pairs of sensors, Table 4.3, one could observe that the ratio mean varied less than when the full clamping torque range (0.4 Nm to 3.2 Nm) was considered.

Sensor pair	Mean of ratios	Standard Deviation of ratios	Variability (%)
WD/WD	1.056	0.019	1.836
UT1000/UT1000	0.646	0.016	2.470
R15/R30	1.978	0.056	2.809

Table 4.3 Variability of mean of ratios of each sensor pair with clamping torques from 1.2 Nm to 3.2 Nm.

4.8 Conclusions

The air jet equipment and fixture were developed. The nozzle diameter of 1.0 and 1.4 mm were compared. The 1.0 mm-nozzle was selected to evaluate with the pulsed laser as a calibration source for tool wear monitoring. In terms of the repeatability, the air jet and the pulsed-laser sources have similar variability. The similarity of the air jet and the pulsed-laser sources using the machining AErms-spectra as the reference are 0.86 and 0.56 respectively. Compared to the pulsed laser, the air jet is more suitable as an artificial calibration source for measuring systems used for machining study and tool wear monitoring. This is because the air jet source has an AErms- spectrum more similar to that observed in machining than the pulsed laser, is relative safe to use, is less expensive and is more readily available in a workshop.

The relation between the air jet pressure and AErms at different stand-off distances was established. For a fixed stand-off distance, the AErms of the air-jet increases linearly with the air-jet pressure.

The effect of the clamping torque applied to the insert on the AE signal was investigated. The clamping torque can affect the AErms if the torque value is low; but when the clamping torque exceeds 1.2 Nm, the AErms remains constant. (Above 1.2 Nm, the variability of the ratios of AErms between different pairs of sensors relatively decrease.) A safe clamping torque for the tool holder used in this research is around 2 Nm beyond which there is the risk of damaging the hexagonal head of the tightening screw.

In summary, a calibration procedure may be suggested as follows. With the insert clamping torque above 1.2 Nm, the AErms value obtained from a sensor can be converted into an air pressure value using the calibration graphs such as Figures 4.11 and 4.20. In this way, providing a set-up is calibrated using the air jet source under a prescribed condition, results obtained from different set-ups that have been calibrated in the same manner can be compared.

Chapter 5

Calibration of AE for Tool Wear Monitoring

5.1 Introduction

Results from Chapter 4 on the calibration procedure using an air jet as the artificial AE source presents evidence that the tool system (including the tool insert, tool holder, insert/tool holder coupling, sensor/tool holder coupling, and sensor) can be considered linear with respect to AE propagation. This chapter provides a proof that the AE produced from machining, which is much stronger than that of the air jet, is also linear. Then the calibration procedure for tool wear monitoring is utilised and an AErms value is converted into a common equivalent value based on the pressure of the air jet.

5.2 Comparison of shapes and sizes of AE

It was mentioned in Chapter 4 that the length of an n-point RMS discrete spectrum can be computed from

$$|u| = \sqrt{u.u} = \sqrt{\sum_{k=1}^{n} u_k^2} \qquad (5.1)$$

where $|u|$ = the length of an n-point RMS discrete spectrum

u_k = a point in the n-dimension vector space

This length $|u|$ gives the overall AErms of the AE signal.

The vector $\boldsymbol{u}$ can be normalised by dividing its elements by the length of the vector. Thus a normalised vector, denoted by $\bar{u}$, can be computed from

$$\bar{u} = u/|u|$$

Given two normalised vectors, $\bar{u}$ and $\bar{v}$, in the n-dimensional space, the included angle θ between them is related to the inner product of $\bar{u}$ and $\bar{v}$ as

$$\cos\theta = \bar{u}.\bar{v}. \qquad (5.2)$$

$cos\theta$ is named the similarity coefficient. When it is one the two unit vectors $\bar{u}$ and $\bar{v}$ point in the same direction. Which means that the two corresponding spectra have the same shape differing by a scale factor. When the similarity coefficient is zero, the two vectors $\bar{u}$ and $\bar{v}$ are orthogonal to each other, which suggests that the two corresponding spectra have nothing in common, or maximum dissimilarity.

Suppose there are m number of spectrum-vectors, u_1, u_2,..., u_m, to be compared, the individual lengths of these vectors can be computed by means of Equation (5.1) and the corresponding normalised vectors obtained, namely $\bar{u}_1$, $\bar{u}_2$, ..., $\bar{u}_m$. These normalised vectors, treated as column vectors, are then assembled into an n-by-m matrix A such that

$$A = (\bar{u}_1, \bar{u}_2, ..., \bar{u}_m). \tag{5.3}$$

The similarity coefficient matrix C, by virtue of Equation (5.2), is given by

$$C = A^T \cdot A \tag{5.4}$$

where the element c_{ij} in C is the similarity coefficient between the spectrum-vectors u_i and u_j. It is noted that the matrix C is a symmetric matrix.

Calibration involves comparison between a reference source and a given source. Whereas comparison in one dimension is relatively straightforward, comparison in n-dimensions is not so easily defined. The method suggested is to consider an AE signal from the perspective of its RMS spectrum and then proceed to make comparison with the reference RMS spectrum in respect of its size and shape. The size relates to the strength of the signal whilst the shape corresponds to the distribution of the energy in the relevant frequency range. The size of a signal can be represented by the overall AErms of its spectrum. When comparing two signals to decide if they are similar in shape, the similarity coefficient can be used.

5.3 Artificial AE air-jet source and air pressure

The air jet equipment was hung on the Traub lathe as shown in Figure 5.1. Figure 5.2 shows the tool holder which was clamped on the turret.

Figure 5.1. The air jet calibration rig on the Traub lathe.

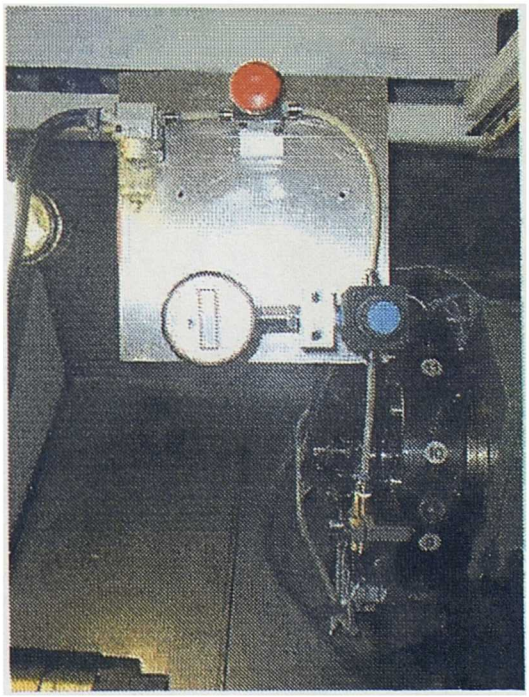

Figure 5.2 The tool holder clamped on the turret.

A nozzle with a 1.0-mm diameter bore was placed normal to the rake face of the tool insert at a fixed distance of 5 mm. The centre of the air stream was positioned 2 mm from both the leading and trailing edges of the insert. The insert was clamped to the tool holder with a tightening torque of 2 Nm. The air pressure was varied from 5 to 8 bars in increments of 0.5 bar.

A tool shank of type SDJCL 1616H 11 and carbide tool inserts of type CG 4035 DCMT 11 T3 04-UF (both from Sandvick Coromant) were used. The details of the insert geometry have been reported in Chapter 3 and were as follows: insert shape angle 55°, clearance angle 7°, rake angle 0°, cutting edge length 11 mm, thickness 3.97 mm and nose radius 0.4 mm.

Two AE sensors were mounted on the tool-holder: a WD sensor (PAC) at the end of the tool-holder and an R30 sensor (PAC) on the side as shown in Figure 5.3. Both signals were amplified by 40 dB at the pre-amplifiers fitted with a 100 kHz – 1 MHz band-pass filter. The AE signals detected at the two sensors were analysed in real time using a Hewlett Packard HP 89410A Vector Signal Analyser to produce a 401-line AErms spectrum spanning 0 to 1 MHz averaged over 70 consecutive spectra.

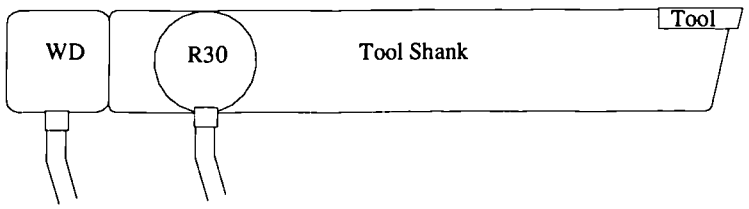

Figure 5.3. Two AE sensors (WD and R30) on the tool.

Typical AErms spectra of the air jet at the pressure of 5 bars obtained from the two sensors are shown in Figure 5.4. Their difference in shape is significantly due to the different frequency responses of the two sensors.

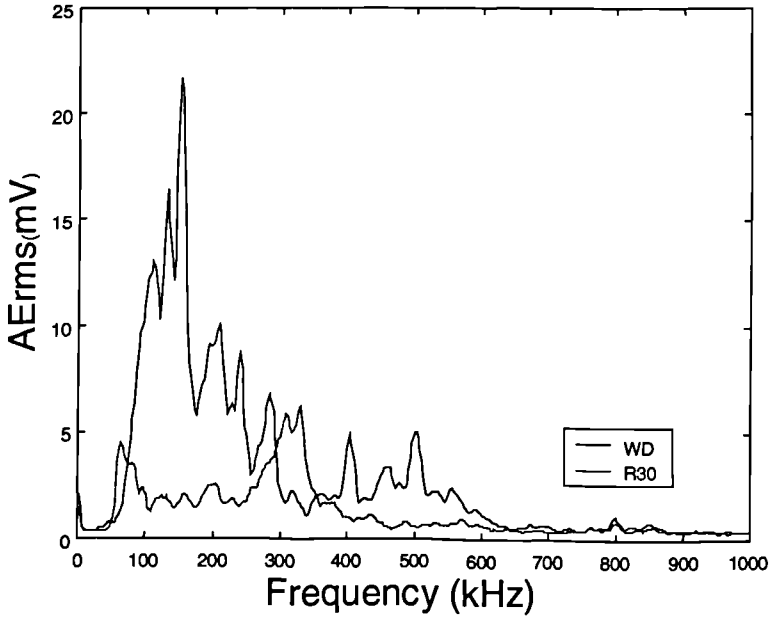

Figure 5.4. Response spectra of the two sensors, WD and R30, at the air jet pressure of 5 bars.

The AErms values of the air jet spectra obtained from pressures of 5 to 8 bars were computed using Equation (5.1). The results from both the WD and R30 sensors are plotted in Figure 5.5. It can be seen that the AErms and air pressure are linearly related and the gradients for the WD and R30 sensors are 19.658 and 7.552 mV/bar respectively. These values represent the sensitivity of the two sensing systems.

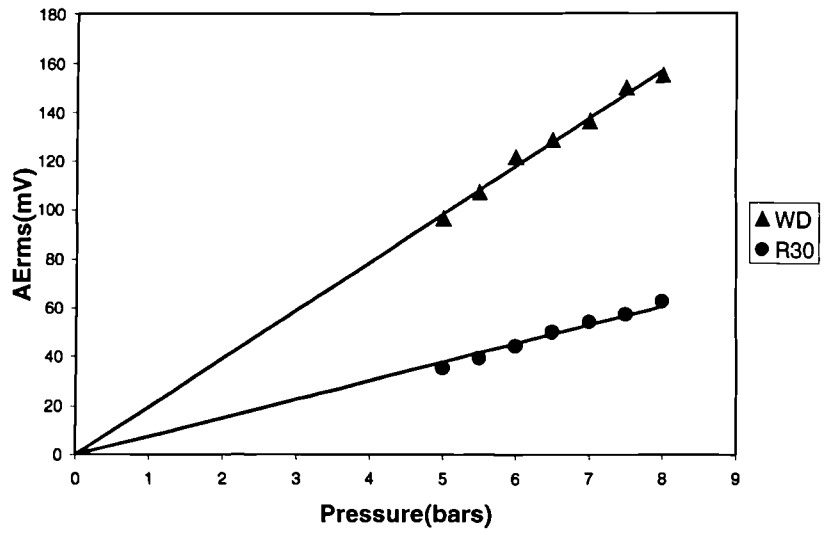

Figure 5.5. Relation between air-jet pressure and AErms.

The degree of likeness is computed using Equation (5.4), returning the similarity coefficient matrix C for the WD sensor as

Pressure(Bars)	5.0	5.5	6.0	6.5	7.0	7.5	8.0
5.0	1	0.997	0.995	0.992	0.991	0.987	0.984
5.5	0.997	1	0.996	0.993	0.994	0.992	0.988
6.0	0.995	0.996	1	0.996	0.997	0.993	0.993
6.5	0.992	0.993	0.996	1	0.994	0.992	0.994
7.0	0.991	0.994	0.997	0.994	1	0.995	0.996
7.5	0.987	0.992	0.993	0.992	0.995	1	0.996
8.0	0.984	0.988	0.993	0.994	0.996	0.996	1

Table 5.1. Similarity coefficient matrix for the WD sensor.

For the R30 sensor, the corresponding similarity coefficient matrix is given by

Pressure(Bars)	5.0	5.5	6.0	6.5	7.0	7.5	8.0
5.0	1	0.992	0.986	0.961	0.989	0.992	0.991
5.5	0.992	1	0.997	0.985	0.99	0.99	0.985
6.0	0.986	0.997	1	0.991	0.987	0.987	0.981
6.5	0.961	0.985	0.991	1	0.97	0.968	0.957
7.0	0.989	0.99	0.987	0.97	1	0.991	0.991
7.5	0.992	0.99	0.987	0.968	0.991	1	0.997
8.0	0.991	0.985	0.981	0.957	0.991	0.997	1

Table 5.2. Similarity coefficient matrix for the R30 sensor.

In these matrices, the rows and the columns represented the progressive pressure values of 5.0, 5.5, 6.0, 6.5, 7.0, 7.5 and 8.0 bars. It is evident from these matrices that the RMS spectra of a sensor are very similar to each other within this range of pressure as the coefficients are all very close to 1.

An RMS spectrum is simply the square root of the energy spectrum, also known as the spectral density function. In terms of the spectral density functions, the transfer characteristics from the air-jet input source to the output of the sensing instrument is governed by

$$G_y(f) = |H(f)|^2 \cdot G_x(f)$$

where the respective spectral density functions of the input and output are $G_x(f)$ and $G_y(f)$, and $H(f)$ is the frequency response function describing the dynamics of the signal transmission process which includes that of the tool and of the sensor. It should be noted that $G_x(f)$ denotes the AE produced at the tool tip as a result of the action of the air jet and not the air pressure itself.

Figure 5.6 shows the different signal propagation paths with common input for the two different layouts of the WD and R30 sensors denoted by the respective subscripts of 1 and 2.

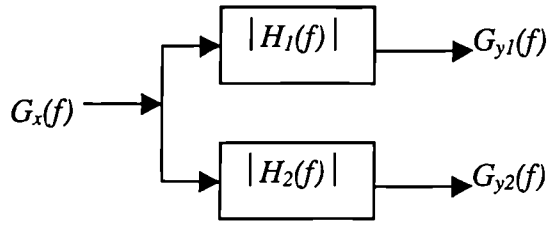

Figure 5.6. Different signal propagation paths with common input.

Since the same input $G_x(f)$ is used, their transfer Equations can be written as

$$G_{y1}(f) = |H_1(f)|^2 \cdot G_x(f) \tag{5.5}$$

and

$$G_{y2}(f) = |H_2(f)|^2 \cdot G_x(f) \tag{5.6}$$

Dividing Equation (5.5) by Equation (5.6) and with the fact that all quantities involved are functions of frequency f understood, we obtain

$$G_{y1}/G_{y2} = |H_1|^2 / |H_2|^2 \tag{5.7}$$

Figure 5.7 shows the ratio G_{y1}/G_{y2} for the range of air pressures from 5 to 8 bars with the curve of the mean ratio shown in bold solid line. The curves have been smoothed using the kernel smoothing technique.

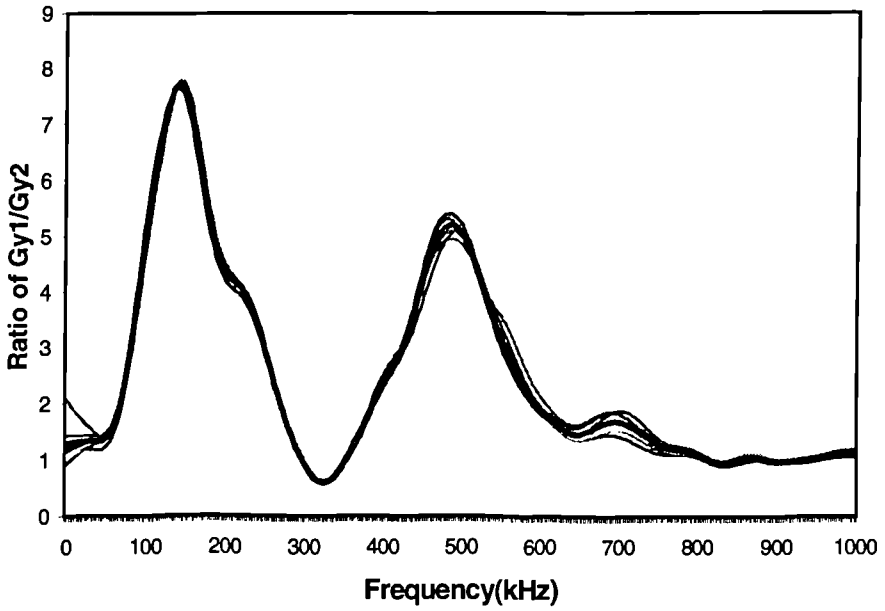

Figure 5.7. Ratio of G_{y1}/G_{y2} of air pressure from 5 to 8 bars in 0.5 bar increments; Mean ratio curve shown in bold solid line.

It is evident that all the curves are close to each other. According to Equation (5.7), this suggest that the ratio of the frequency response functions, corresponding to the different sensors layouts, remain the same at any pressure within 5 to 8 bars. There are only two possible inferences from this: 1) that $H_1(f)$ and $H_2(f)$ are not affected by the input states of the air pressure, or 2) that both $H_1(f)$ and $H_2(f)$ are affected equally by the input states such that the resulting ratio remain constant. The second possibility is highly improbable, as it means that the condition must be maintained at all frequencies, 0 to 1 MHz, across the spectrum.

Referring to either of Equation (5.5) or (5.6), since neither $G_{yi}(f)$ nor $H_i(f)$ $(i=1,2)$ changes its shape with pressure, so will $G_x(f)$ retain its own shape. Thus, the sensitivity values of 19.658 and 7.552 mV/bar for the respective WD and R30 sensors apply not just to the overall AErms of the total signal, but also to the individual spectral components too.

Whilst the theory presented proves adequate for AE signals produced by the air jet with 5- to 8-bars of pressure, the AE produced from machining is much stronger and

so the question of whether the calibration as described can be applied to the machining process needs to be answered.

5.4 AE from single-point machining

The instrumentation used for the machining tests was identical to that for the air-jet calibration except that the total gain of the sensor output was 34 dB instead of 40 dB. It was necessary to use a lower gain in order to avoid saturation of the signal.

Three sets of machining tests were conducted and their conditions are detailed in the following:

- Machining Test Set 1: Variable feed rates from 0.05 mm/rev to 0.4 mm/rev in increments of 0.05 mm/rev. Cutting speed and depth of cut were constant at 120 m/min and 0.75 mm respectively.
- Machining Test Set 2: Variable speeds from 80 m/min to 150 m/min in increments of 10 m/min. Feed rate and depth of cut were constant at 0.2 mm/rev and 0.75 mm respectively.
- Machining Test Set 3: Variable depths of cut from 0.3 mm to 1.0 mm in increments of 0.1 mm. Cutting speed and feed rate were constant at 120 mm/min and 0.2 mm/rev respectively.

As the preliminary test, the material of the workpiece, measured 63.5 mm in diameter and 150 mm in length, was EN24T with 0.35-0.45 % carbon. All tests were conducted on the Traub lathe.

The ratios of G_{y1}/G_{y2} for the three sets of machining tests were first obtained and then the mean ratio for each set was calculated. The mean ratios for the three different machining conditions and for the air jet calibration are shown in Figure 5.8.

It can be observed that these curves match each other very closely. The implication is that the frequency response functions $H_1(f)$ and $H_2(f)$ in Equations (5.5) and (5.6) are insensitive to the input states, whether they be caused by air-jet pressure or by machining.

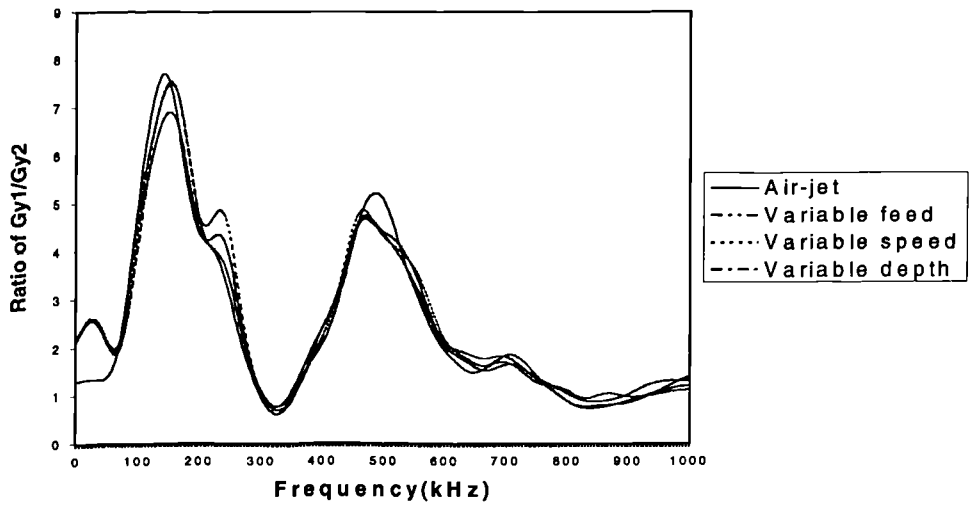

Figure 5.8. Mean ratios of G_{y1}/G_{y2} for the three sets of machining tests compared against the mean ratio curve from air-jet tests.

5.5 Calibration procedure

Based on the results presented, a simple calibration procedure for AE in machining studies is proposed. Using the air-jet artificial AE source set up under the conditions as stipulated in Section 5.3, the AErms output of a sensor is measured over the range of air pressures from 5 to 8 bars. The sensitivity is then calculated from the gradient of the straight line fitted to the data points similar to Figure 5.5. With the sensitivity value known for a given layout of the AE sensor, the sensor output can then be converted into the pressure unit in bars. This unit is the common currency, which forms the basis for comparison between results obtained with different sensor layouts or coupling conditions.

5.6 Air jet calibration for tool wear monitoring

With the same set-up as described in Section 5.3 for the air-jet calibration tests, further machining tests were performed with the conditions:

- Machining condition 1 (roughing): Cutting speed, depth of cut and feed rate were constant at 150 m/min, 1mm and 0.3 mm/rev respectively.
- Machining condition 2 (semi-roughing): Cutting speed, depth of cut and feed rate were constant at 250 m/min, 0.75mm and 0.25 mm/rev respectively.

- Machining condition 3 (finishing): Cutting speed, depth of cut and feed rate were constant at 300 m/min, 0.5mm and 0.2 mm/rev respectively.

Flank wear on the insert was measured every 2 cuts with a portable toolmaker microscope and the result was further confirmed by obtaining a mould of the tip of the insert using the replica method.

The AErms values of the air jet obtained from WD and R30 sensors were computed. The gradients of each test set for the three machining tests are shown in table below:

	Machining test # 1	Machining test # 2	Machining test # 3
	Gradient (mV/bars)	Gradient (mV/bars)	Gradient (mV/bars)
Sensor WD	18.847	18.470	18.891
Sensor R30	8.586	8.225	9.505

Table 5.3. Gradients of the three machining tests sets.

The AErms obtained from machining tool wear test of each cutting condition was shown in Figures 5.9, 5.10 and 5.11 respectively.

For all three cutting conditions the wear curves show that the flank wear increases approximately linearly with the cutting time as in Figures 5.9, 5.10 and 5.11. The rapid flank wear is apparent at the final stage. The final flank wear heights for the roughing, semi-roughing and finishing conditions before the on set of rapid wear are 0.34 mm at 38.9 min, 0.22 mm at 10.7 min and 0.28 mm at 19.9 min respectively.

For all three machining conditions, Figures 5.9, 5.10 and 5.11, the tool wear curves showed three stages of wear, namely the primary, secondary and tertiary stages. The primary stage was very short which happened within the first cut during which the wear rate was high. The secondary stage was relatively long and was marked by the slow wear rate throughout. The tertiary stage was the period of accelerated wear leading to cutting edge failure. The transition from one stage to the next was highlighted by the sudden change in the wear rate.

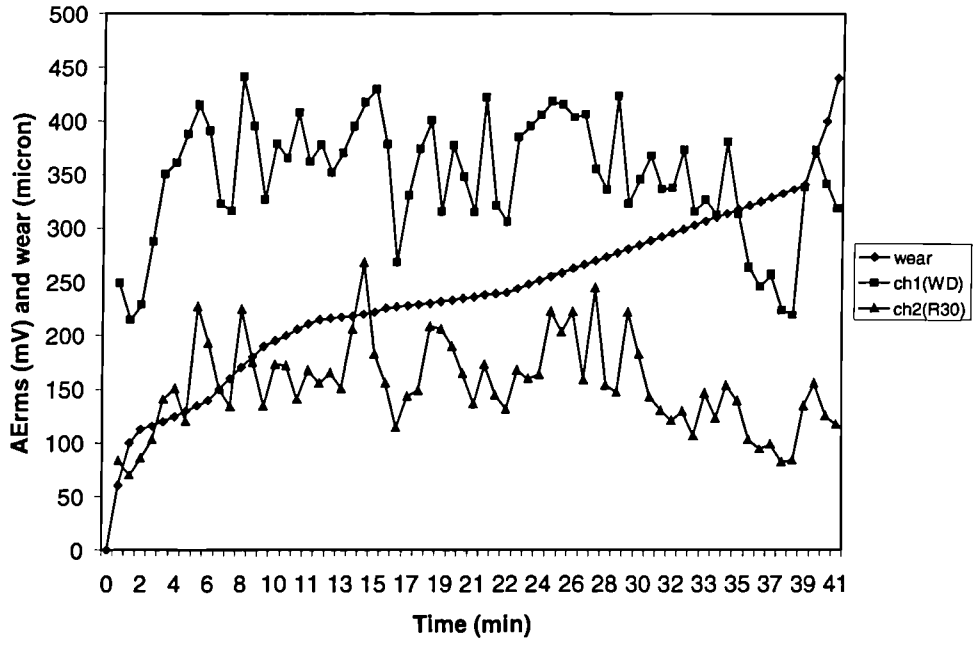

Figure 5.9. The AErms obtained from machining test at speed 150 m/min, depth of cut 1.0 mm and feed rate 0.3 mm/rev.

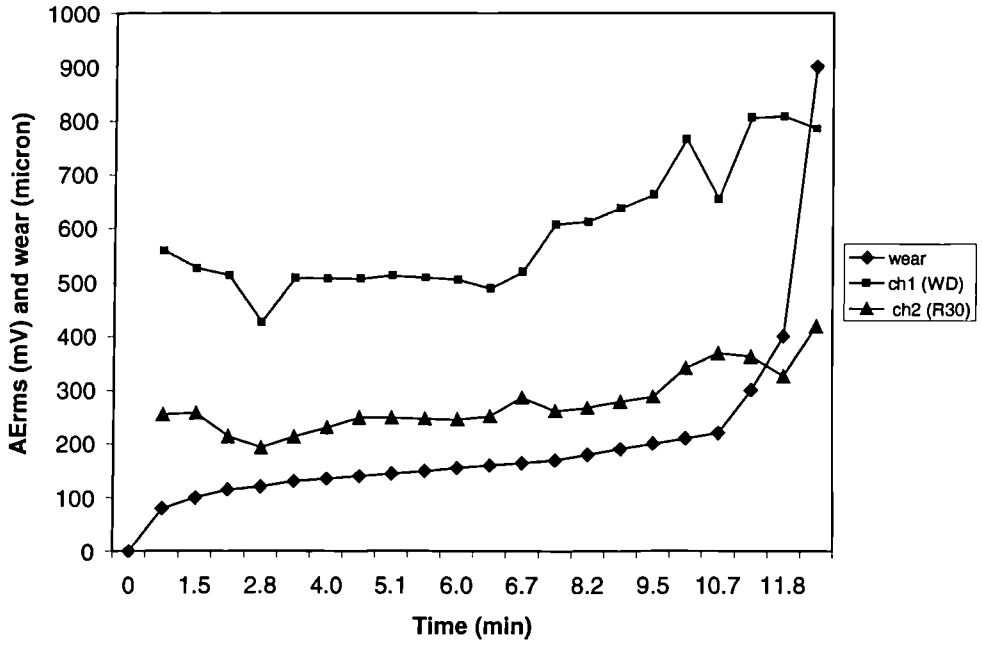

Figure 5.10. The AErms obtained from machining test at speed 250 m/min, depth of cut 0.75 mm and feed rate 0.25 mm/rev.

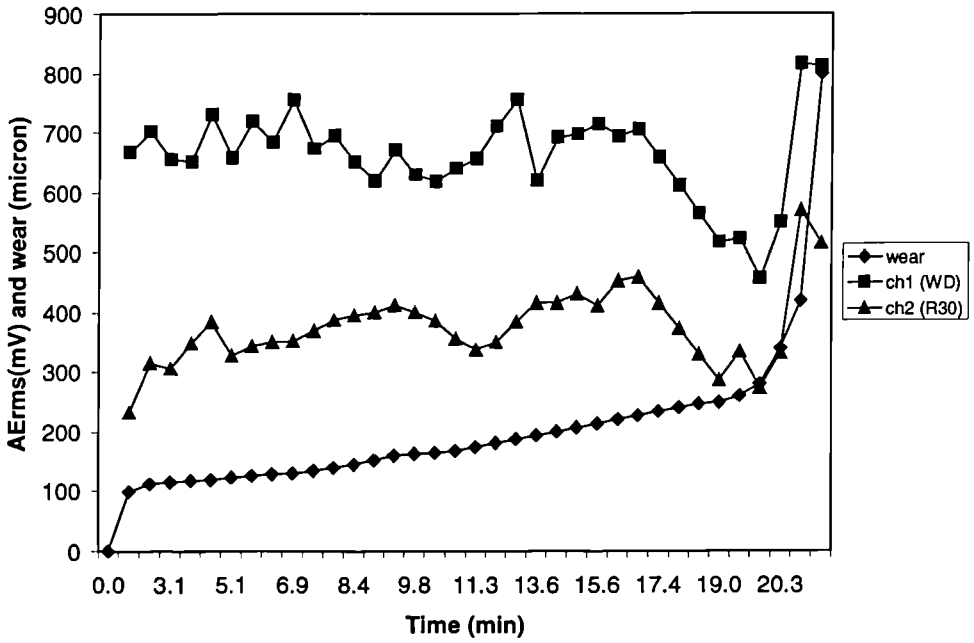

Figure 5.11. The AErms obtained from machining test at speed 300 m/min, depth of cut 0.5 mm and feed rate 0.2 mm/rev.

The fluctuation of AErms with tool wear was expected due to the combined action of flank wear and crater wear. According to Chaung and Asibu (1985) AErms increases with flank wear but increases with crater wear only in the initial stage and then decreases after significant crater wear has occurred.

5.7 Variability of *gradient of calibration curves*

The gradients of the calibration curves for the three inserts were compared in the reference of variability. They are the three calibration curves for the WD sensor (at the end of tool holder) the R30 sensor at the side of the tool holder and from the three cutting conditions as described in Section 5.6. All inserts were tightened with a 2.0-Nm clamping torque. The variability are shown in the Table 5.4 below: (The variability was based on ±1 standard deviation divided by the mean.)

Sensor	Cutting condition 1	Cutting condition 2	Cutting condition 3	average	S.D. of Gradient	Variability (%)
WD	18.847	18.470	18.891	18.736	0.231	1.235
R30	8.586	8.225	9.505	8.772	0.660	7.523
Ratio of WD/R30	2.195	2.240	1.988	2.141	0.134	6.277

Table 5.4. Variability of gradients of calibration curves.

The variability of the WD sensor mounted at the end of tool holder is 1.24%. The variability of the R30 sensor at the side of tool holder is 7.52 %. The variability of the ratio of the gradients WD to R30 is 6.28 %.

5.8 Equivalent pressure of machining for tool wear monitoring

The AErms values were converted into their equivalent pressure values using the gradients of the calibration curves. The equivalent pressure values with tool wear for each machining condition were shown in Figure 5.12, 5.13 and 5.14. The scatter plot of the equivalent pressure for all three cutting conditions are shown in Figure 5.15. The straight line in Figure 5.15 is line of equal pressure for both sensors. Ideally, points fall on this line if the conversion from AErms measured in volts to air pressure measured in bars are valid.

5.9 Relationship between AErms obtain from the two AE sensors

The variability of ratios of AErms obtained from each machining condition in Section 5.8 were carried out. The variability was based on ±1 standard deviation divided by the mean. Its deviation was compared to the mean ratios of the air jet (not the average ratios of machining). Because the ratio of the air jet is the gradient of the straight which passes through the origin of the graph. The variability of the ratios of roughing, semi-roughing and finishing are 18.65 %, 9.46 % and 17.04 % respectively.

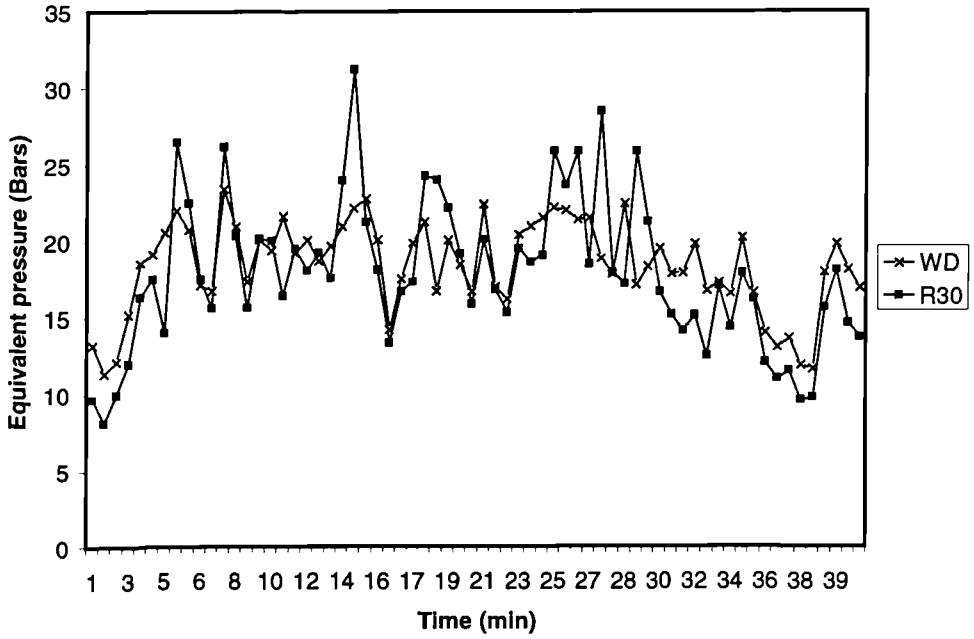

Figure 5.12. The equivalent pressure from machining test at speed 150 m/min, depth of cut 1.0 mm and feed rate 0.3 mm/rev.

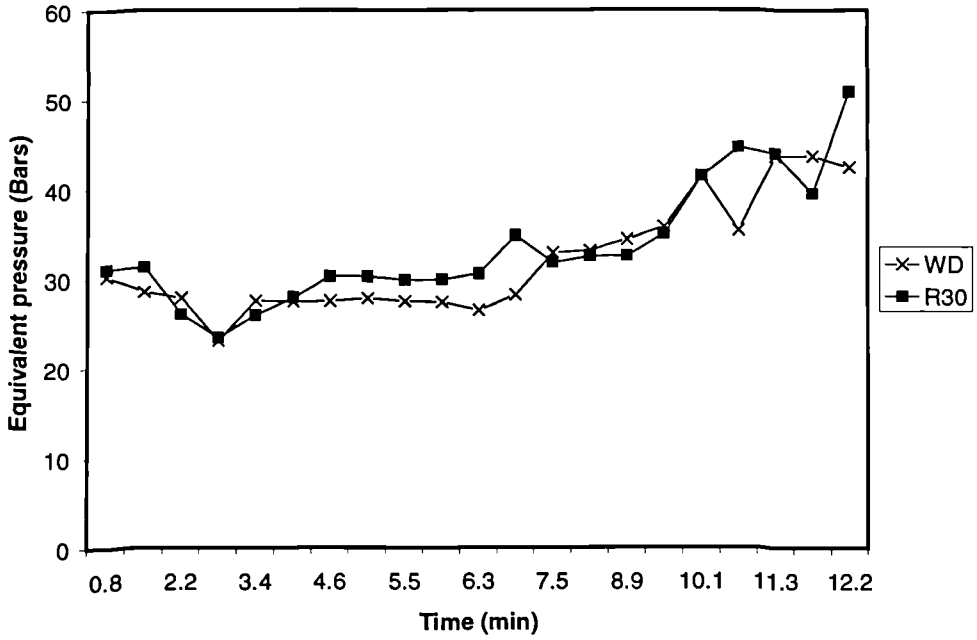

Figure 5.13. The equivalent pressure from machining test at speed 250 m/min, depth of cut 0.75 mm and feed rate 0.25 mm/rev.

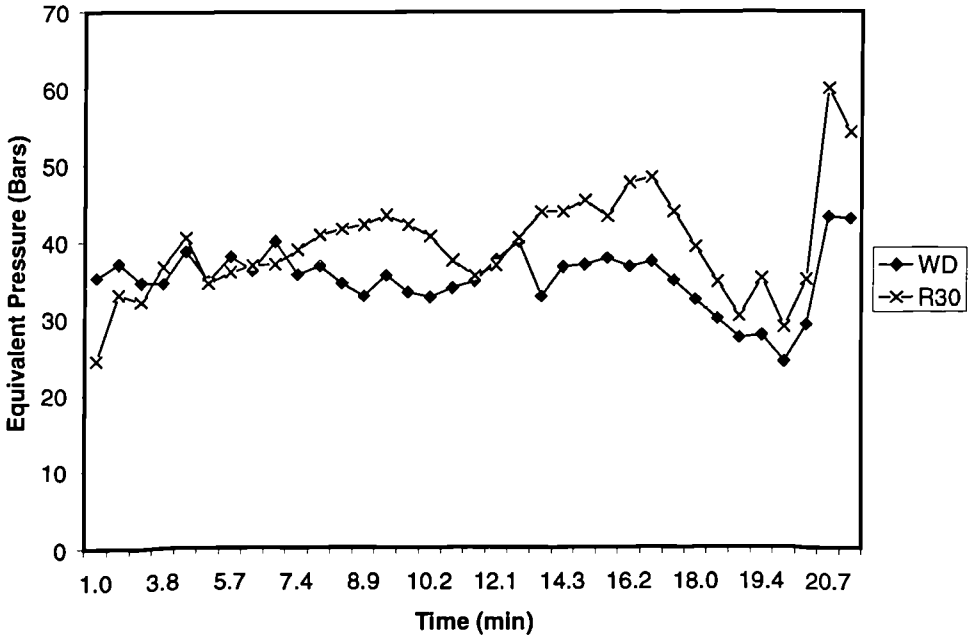

Figure 5.14. The equivalent pressure from machining test at speed 300 m/min, depth of cut 0.5 mm and feed rate 0.2 mm/rev.

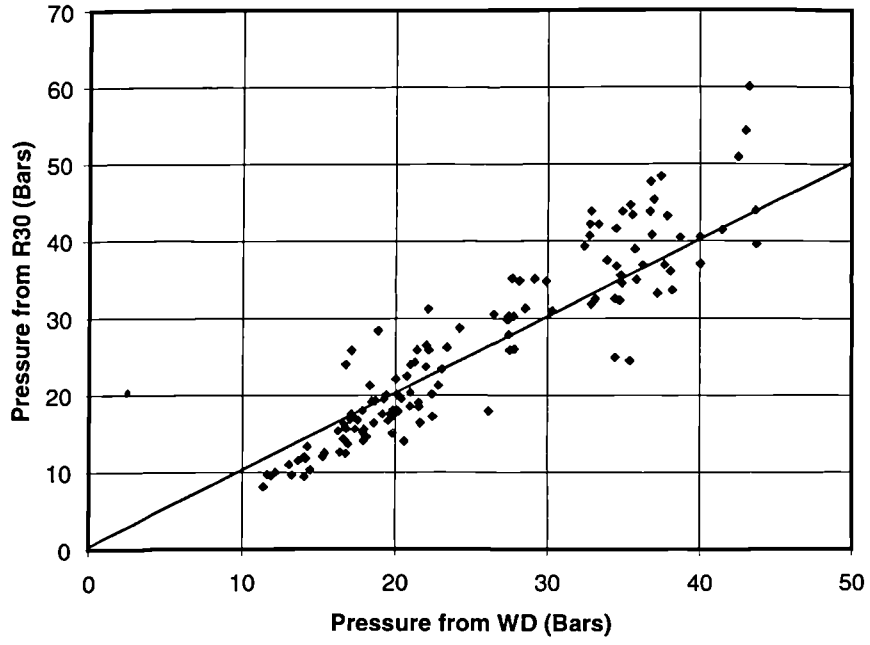

Figure 5.15. The scatter plot of pressure values from the two sensors for all three cutting conditions.

However the use of variability of ratio is fraud with problem. This is because it is very sensitive to the value of the denominator in taking a ratio and taking the mean of ratios is not as reliable as the method, which is described below.

One can plot the AErms scores of one sensor against those of the other for various stages of tool wear. Thus, Figure 5.15 of can be represented by a graph with the pairs of AErms equivalent pressure scores plotted as points, one for each of sensors, namely R30 versus WD. A straight line can then be fitted to the set of paired-scores. The gradient of the straight line in the above-mentioned graph provides a better estimate of the mean ratio between the AErms from the pair of sensors. The gradient is in theory the same as the AErms ratio between the pair of sensors if the straight line passes through the origin of the graph. That the line should pass through the origin is to be expected since both sensors will give zero AErms output when no air jet is directed at the tool tip. Then the relationship between AErms for each sensor can be established using the Pearson correlation coefficient.

The Pearson correlation coefficient describes the degree of relationship between the two variables and can be defined as [Haris (1975)]

$$r = \frac{\sum_i Z_X Z_Y}{(N-1)} = \frac{\sum_i (X-\bar{X})(Y-\bar{Y})}{\sqrt{\sum_i (X-\bar{X})^2 \sum_i (Y-\bar{Y})^2}} \qquad (5.8)$$

where

Z = standard score

$\bar{X}$ and $\bar{Y}$ are means of X and Y respectively

In other words, the Pearson correlation coefficient is the relation between X and Y by finding how closely $Z_X = \frac{(X-\bar{X})}{\sigma_X}$ matches $Z_Y = \frac{(Y-\bar{Y})}{\sigma_Y}$, on the average.

When X_i and Y_i lie on the same side of the mean, contribute positive cross-product (Z_x Z_y) terms to the summation; when they lie on the opposite sides of their respective means, negative terms result. The maximum possible value of Pearson correlation coefficient of +1 occurs when $Z_x = Z_y$ for all data and its minimum possible value of –1 occurs when $Z_x = -Z_y$ for all data.

It must be noted that the Pearson correlation coefficient calculated by Equation 5.8 could be considered the same value as the similarity coefficient computed by Equation 5.2.

One cause of the variability is the varying distance from the AE source to the sensor. The AE propagates from the edge of the tool insert through the medium (coupling interface between the insert/the tool holder, the tool holder and coupling interface between the tool holder/sensor) and arrives at the sensors at different time. This is especially the case for a burst type AE signal produced from the breakage of chips and their ensuing impact on the tool or workpiece; the burst waveform is oscillatory in shape, with a rapid increase in amplitude from an initial reference level, then followed by a drop back to the initial revel. This variability can be reduced by increasing the time length of measurement or increasing the number of averages of the AErms spectrum.

5.10 Correlation of AErms and cutting condition

The relationship between the AE signal and cutting conditions was shown in Figures 5.16, 5.17 and 5.18. Compared to the experimental results obtained by other research workers using different AE systems and techniques, it can be said that the AErms increasing with speed agrees with the result reported by Heiple et al (1991), Chaung and Asibu (1985), Inasaki and Yunetsu (1981), Asibu and Dornfeld (1981), Asibu and Dornfeld (1981), Teti and Dornfeld (1981), Capitany and Citi (1984)]. The observation that AE signal is hardly affected by the feed rate and the depth of cut agrees with the finding of Inasaki and Yunetsu (1981).

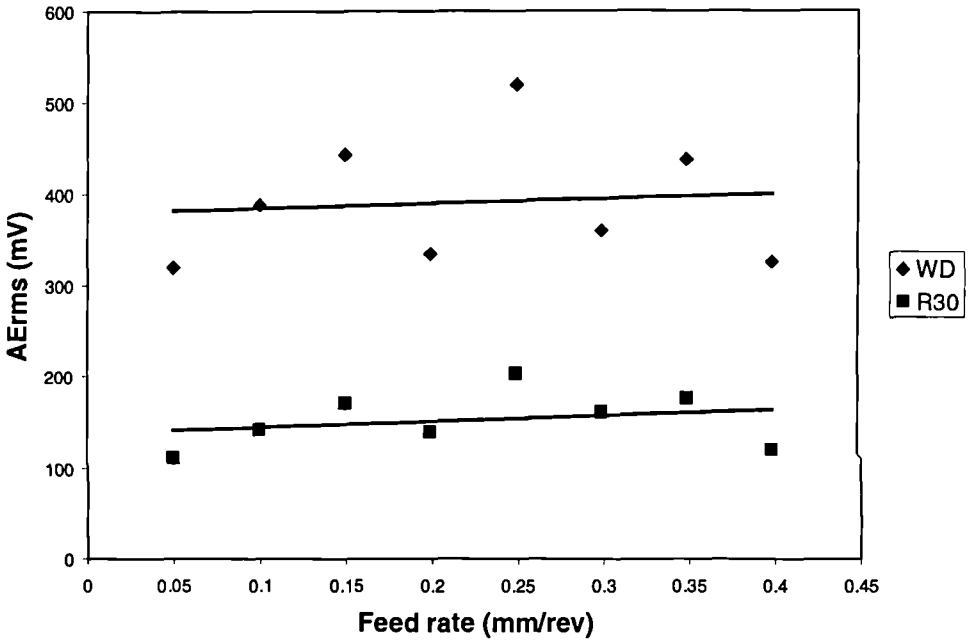

Figure 5.16. AErms and variable feed rates at constant cutting speed 120m/min and constant depth of cut 0.75 mm.

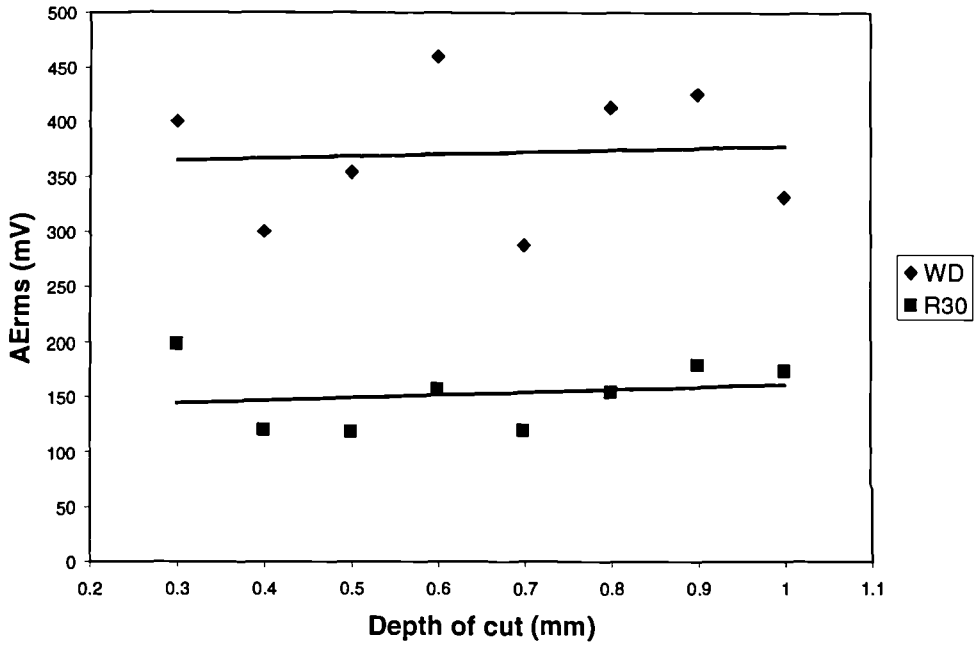

Figure 5.17. AErms and variable depths at constant feed rate 0.2 mm/rev and constant depth of cut 0.75 mm.

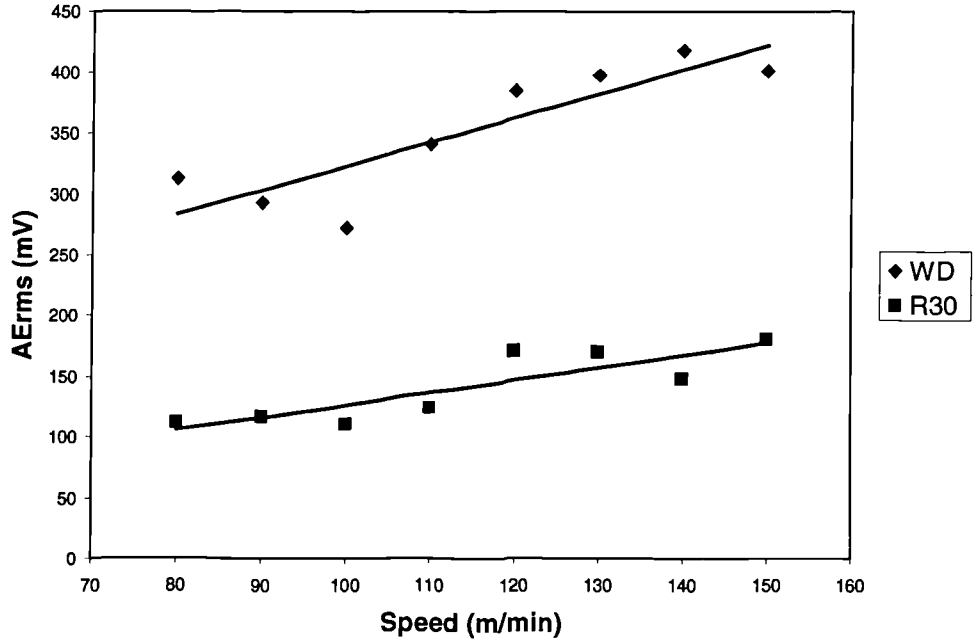

Figure 5.18. AErms and variable speeds of cut at constant feed rate 0.2 mm/rev and constant cutting speed 120 m/min.

5.11 Effects of number of AErms spectra used in calculating the average on variability

The number of AErms spectra used in computing their averages for the machining tests and air jet tests were quite different, being 250 and 70 respectively. A larger number was required for the machining tests because such tests tended to produce AE signals that were quite variable. Evidently by increasing the number even further the variability will be made smaller.

In order to investigate the effect on variability of the number spectra involved in forming an average, a cutting experiment was conducted with the cutting condition chosen as: cutting speed 120 m/min, feed rate 0.2 mm/rev and depth of cut 0.75 mm. Unlike the situation for air-jet tests and tool wear tests, the sensors used in this case were both of type WD, one mounted at the end and the other at the side of the tool holder, Figure 5.3. This difference would only affect the shape of the AErms spectrum.

Two sample sizes, 70 and 1000, were used for calculating their averaged AErms spectra and the results, in the form of scatter diagrams, were as shown in Figures 5.19 and 5.20. The set of 1000 samples, Figure 5.20, had scatter much smaller than had the set of 70 samples, Figure 5.19. Their corresponding Pearson correlation coefficients were 0.57 and 0.96 respectively.

Although a larger number of samples is desirable for reduced variability, there is a problem with its implementation because of the non-instantaneous processing time for the averaged spectra to be computed. This time is proportional to the number of spectra involved in forming the average. If monitoring is to be of any practical value, it should be timely in providing information. The compromise of 250 samples was therefore adopted for the tool wear tests.

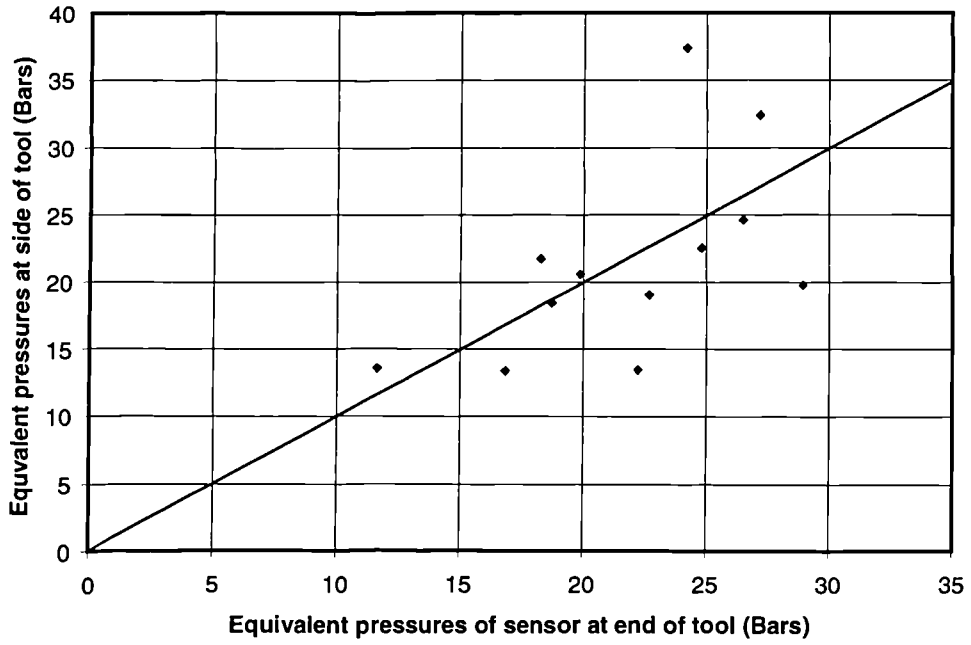

Figure 5.19. Scatter diagram of the equivalent pressure with number for average of 70.

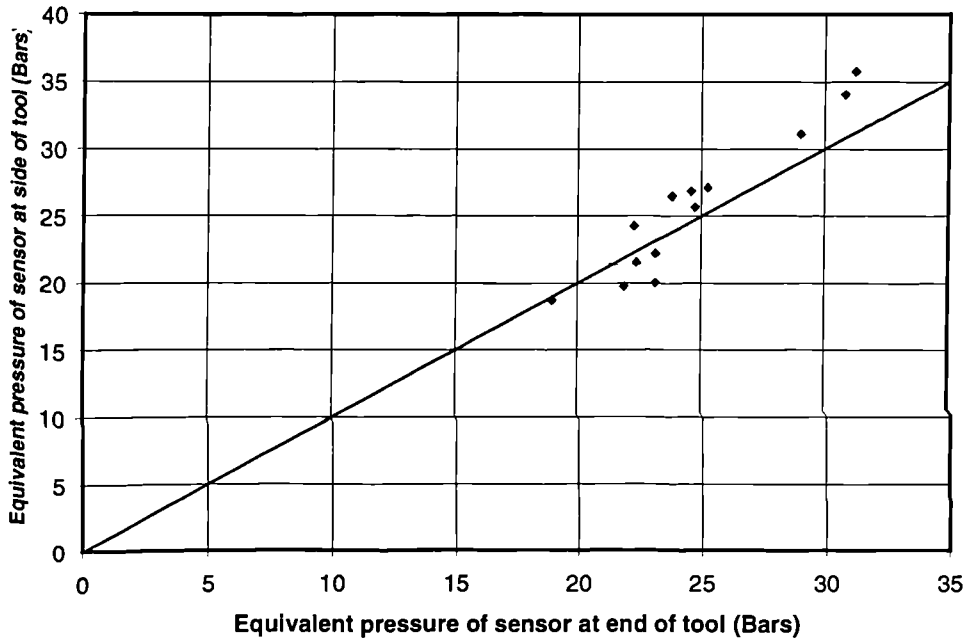

Figure 5.20. Scatter diagram of the equivalent pressure with number for average of 1000.

5.12 Conclusions

The frequency spectra of the AE produced by the air jet and machining were very similar to each other. The similarity of air jet at different pressures is great with similarity coefficients close to 1.

The frequency response function of the tool/sensor system was purely a function of the frequency and was independent of the input states or input mechanisms such as produced by air pressure or machining. Using the calibration as prescribed, it is possible to convert an AErms value into an equivalent air-jet pressure value. With the proposed calibration, it will be possible to make comparison between results obtained from different set-ups.

Pearson correlation coefficient from the equivalent pressure for all three cutting conditions and for rough, semi-rough and finishing are 0.93, 0.75, 0.87 and 0.60 respectively. The set of 1000 samples had scatter much smaller than had the set of 70

samples, Their corresponding Pearson correlation coefficients were 0.96 and 0.57 respectively.

AErms was sensitive to flank wear and cutting conditions: AErms increased with speed and was hardly affected by the feed rate and the depth of cut.

Chapter 6

Vibration and Coherence Function

6.1 Introduction

The main difficulty of monitoring tool wear and failure using data features is that these features are often sensitive to cutting conditions such as the feed, speed and depth of cut. In this chapter is presented a theory of tool wear monitoring based on the coherence function of the tool acceleration signals in the tangential and feed directions. The coherence function is believed to be relatively insensitive to the process variables except tool wear. The benefit of the coherence function is that its value is always between 0 to1, hence providing some degree of normalisation, which is particularly beneficial in the situation of turning where the number of combinations of process variables is large.

6.2 Model of cutting forces and tool

A cutting tool in turning is typically mounted as a cantilever. The dynamic forces that occur during cutting can be resolved into three mutually perpendicular components along the radial, tangential and feed directions referred to respectively as the x-, y- and z-directions. Since the radial force acting in the x- direction is relatively low compared to the other two forces, the tools tip mainly moves in the yz-plane. The dynamic shear force component along the shear plane is resolvable into a y-component and a z-component, and hence they are correlated. On the other hand, the dynamic friction force components that occur at the chip-tool and the tool-workpiece interfaces are mainly forces confined in the respective z- and y- directions because of the geometry of the tool and hence largely uncorrelated.

6.3 Acceleration frequency response of tool

Figure 6.1 shows a block diagram for single point turning in which the transfer relation between force input and acceleration output is depicted. The diagram uses the following notations:

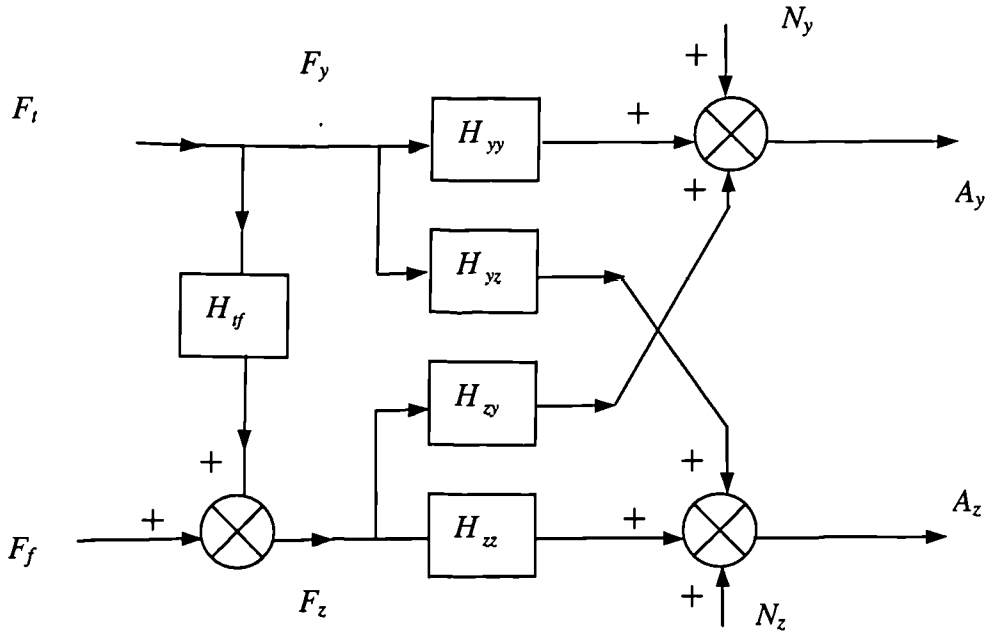

Figure 6.1 Block diagram of the tool wear model demonstrating the transfer relation between force input and acceleration output.

F_t = Fourier transform of the cutting force or tangential force = F_y

F_f = Fourier transform of the uncorrelated part of the feed force F_z

F_y = Fourier transform of the tangential force

F_z = Fourier transform of the feed force

A_y = Fourier transform of the acceleration in y direction (main cutting force direction)

A_z = Fourier transform of the acceleration in z direction (feed force direction)

N_y and N_z = Fourier transform of the noise inputs due to instrumentation and mechanical effects.

H_{tf}, H_{yy}, H_{yz}, H_{zy} and H_{zz} = the frequency response functions representing the transfer characteristics at the tool tip from the cutting force to the acceleration.

It is noted that the variables defined above are functions of frequency.

As mentioned in Section 6.2, the tangential force F_y and feed force F_z are partially correlated; the extent of correlation depends on the cutting condition and on the state of wear on the cutting tool. To model this correlation, two dynamic forces F_t and F_f as shown in Figure 6.1, are used. Using the frequency response function H_{tf}, the correlation between F_y and F_z is produced. Thus

$$F_y = F_t \tag{6.1}$$

and $$F_z = H_{tf} F_t + F_f . \tag{6.2}$$

When F_y acts on the tool tip, it causes vibration in both y- and z- directions. The transfer relationship in these directions is represented by the frequency response functions H_{yy} and H_{yz} respectively. Similarly, F_z produces vibration through the frequency response functions H_{zz} and H_{zy}. The system is assumed to be linear, and the principle of reciprocity applies, leading to $H_{yz} = H_{zy}$. Finally noise sources arising from the electronic instrumentation and the mechanical motion of the machine tool are represented by N_y and N_z.

From the block diagram in Figure 6.1, the acceleration in the y-direction (main cutting force direction) can be defined as

$$A_y = H_{yy} F_y + H_{zy} F_z + N_y .$$

Substituting Equations (6.1) and (6.2) for F_y and F_z yields

$$A_y = H_{yy} F_t + H_{zy} (H_{tf} F_t + F_f) + N_y$$

Collecting terms gives

$$A_y = (H_{yy} + H_{zy} H_{tf}) F_t + H_{zy} F_f + N_y . \tag{6.3}$$

Similarly, the acceleration in the z-direction (feed force direction) can be expressed as

$$A_z = H_{zz} F_z + H_{yz} F_y + N_z$$

$$A_z = H_{zz} (H_{tf} F_t + F_f) + H_{yz} F_t + N_z$$

and

$$A_z = (H_{zz} H_{tf} + H_{yz}) F_t + H_{zz} F_f + N_z . \tag{6.4}$$

Multiplying A_y by its complex conjugate, A_y^*, one obtains

$$\begin{aligned} A_y\, A_y^* &= [(H_{yy}+H_{zy}H_{tf})F_t+H_{zy}F_f+N_y][(H_{yy}+H_{zy}H_{tf})^*F_t^*+H_{zy}^*F_f^*+N_y^*] \\ &= \left|H_{yy}+H_{zy}H_{tf}\right|^2(F_tF_t^*)+\left|H_{zy}\right|^2(F_fF_f^*)+(N_yN_y^*) \\ &+H_{zy}^*(H_{yy}+H_{zy}.H_{tf})(F_tF_f^*)+(H_{yy}+H_{zy}H_{tf})(F_tN_y^*) \\ &+H_{zy}(H_{yy}+H_{zy}H_{tf})(F_fF_t^*)+H_{zy}(F_fN_y^*) \\ &+(H_{yy}+H_{zy}H_{tf})^*(F_t^*N_y)+H_{zy}^*(F_f^*N_y). \end{aligned}$$

In the Equation, $|x|$ means the absolute value of x.

The corresponding autospectrum is by definition,

$$G_y=\lim_{T\to\infty}\frac{2}{T}E[A_yA_y^*] \tag{6.5}$$

Since F_t and F_f and N_y are uncorrelated

$E[F_t.F_f^*] = E[F_tN_y^*] = E[F_fF_t^*] = E[F_fN_y^*] = E[F_t^*N_y] = E[F_f^*N_y] = 0$

resulting in

$$G_Y=2[\left|H_{YY}+H_{ZY}H_{tf}\right|^2S_t+\left|H_{ZY}\right|^2S_f+S_{ny}] \tag{6.6}$$

where S_t, S_f and S_{ny} are the auto spectra of F_t, F_f and N_Y, defined in an analogous fashion to Equation (6.5)

Similarly G_z can be shown to be:

$$G_Z=2[\left|H_{YZ}+H_{ZZ}H_{tf}\right|^2S_t+\left|H_{ZZ}\right|^2S_f+S_{nz}] \tag{6.7}$$

where S_{nz} are the auto spectra of N_z, with a definition analogous to Equation (6.5)

The cross spectrum between A_y and A_z can be found by calculating $A_y.A_z^*$, where A_z^* is the complex conjugate of A_z. Following a similar procedure of derivation to that for G_y, we obtain

$$G_{YZ}=2[(H_{ZY}H_{tf}+H_{YY})(H_{ZZ}H_{tf}+H_{YZ})^*S_t+H_{ZY}H_{ZZ}{}^*S_f] \tag{6.8}$$

6.4 Coherence Function of the tool acceleration (γ^2)

The coherence function between the two acceleration outputs A_y and A_z signals is defined as

$$\gamma^2 = |Gyz|^2 / GyGz \tag{6.9}$$

or, on substitution,

$$\gamma^2 = \frac{\left|H_{yy} + H_{zy}H_{tf}\right|^2 \left|H_{yz} + H_{zz}H_{tf}\right|^2 S_t^2 + \left|H_{zy}H_{zz}\right|^2 S_f^2}{[\left|H_{yy} + H_{yz}H_{tf}\right|^2 S_t + \left|H_{zy}\right|^2 S_f + S_{ny}\ ][\left|H_{yz} + H_{zz}H_{tf}\right|^2 S_t + \left|H_{zz}\right|^2 S_f + S_{nz}\ ]} \tag{6.10}$$

It can be seen from Equation (6.10) that the presence of noise reduces the coherence function. The reason is that the noise terms S_{ny} and S_{nz} being associated with G_y and G_z both appear in the denominator of the Equation 6.10. To make the analysis simple, we shall now ignore the effects of noise; that is the noise terms are removed from Equation (6.10).

Since $|H_{yz}|$ is much smaller than either $|H_{yy}|$ or $|H_{zz}|$ in the vicinity of the resonance frequencies of the tool in the y- and z-directions, we shall assume $|H_{yz}|$=0. Thus Equation 6.10 simplifies to

$$\gamma^2 = \frac{\left|H_{yy}\right|^2 S_t^2 \left|H_{zz}H_{tf}\right|^2}{\left|H_{yy}\right|^2 S_t [\left|H_{zz}H_{tf}\right|^2 S_t + \left|H_{zz}\right|^2 S_f\ ]}$$

H_{yy} and H_{zz} being the frequency response functions of the cutting tool are not a function of wear. Furthermore defining

$$\alpha = \frac{S_f}{S_t} \tag{6.11}$$

the coherence function can be simply written as

$$\gamma^2 = \frac{\left|H_{tf}\right|^2}{\left|H_{tf}\right|^2 + \alpha} \tag{6.12}$$

To find out how γ^2 changes with $|H_{tf}|$ and α, it is observed that the total differential $d\gamma^2$, from Equation (6.12) is

$$d\gamma^2 = \frac{\partial \gamma^2}{\partial(|H_{tf}|^2)} d(|H_{tf}|^2) + \frac{\partial \gamma^2}{\partial \alpha} d\alpha \tag{6.13}$$

where

$$\frac{\partial \gamma^2}{\partial(|H_{tf}|^2)} = \frac{\alpha}{(|H_{tf}|^2 + \alpha)^2} > 0 \tag{6.14}$$

and

$$\frac{\partial \gamma^2}{\partial \alpha} = -\frac{|H_{tf}|^2}{(|H_{tf}|^2 + \alpha)^2} < 0 \tag{6.15}$$

From Equation (6.14) and (6.15), It can be concluded that increasing the value of (H_{tf}) and decreasing the value of $\propto$, both cause the coherence function γ^2 to rise in value.

As a tool begins to wear, the extent of correlation between F_y and F_z varies. It is reasonable to postulate that the correlation, as represented by H_{tf} in Figure 6.1, is inversely related to the wear rate on the cutting edge of the tool. The second postulate is that the ratio $\alpha = \frac{S_f}{S_t}$ remains approximately constant with the progression of wear in the frequency band around the resonance of the cutting tool.

The first postulate suggests that when the cutting edge is wearing quickly, the correlation between F_y and F_z is small, meaning H_{tf} is also small, and vice versa. A graph of flank wear against machining time has the characteristic shape as shown in Figure 6.2.

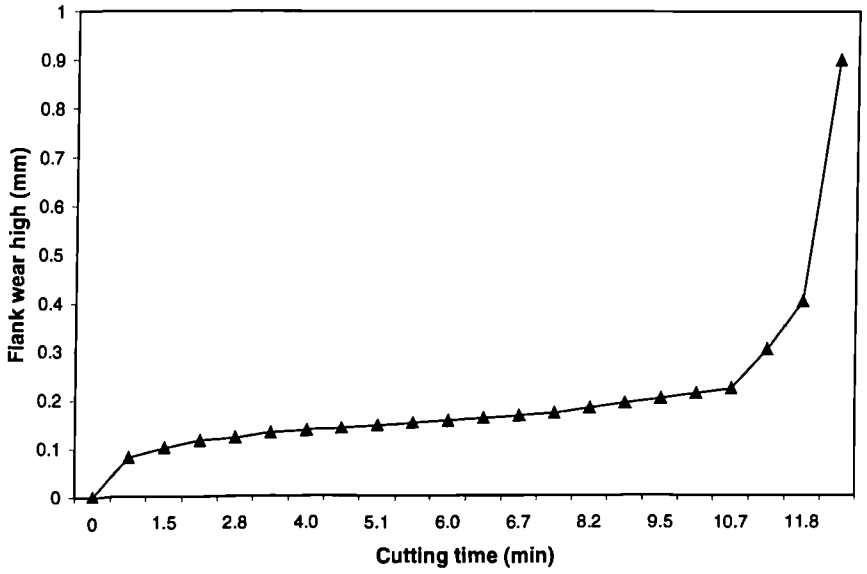

Figure 6.2 Characteristic shape of flank wear against machining time (from machining test at speed 250 m/min depth of cut 0.75 mm and feed rate 0.25 mm/rev).

The gradient of this curve is the wear rate and the graph of wear rate versus time looks like Figure 6.3.

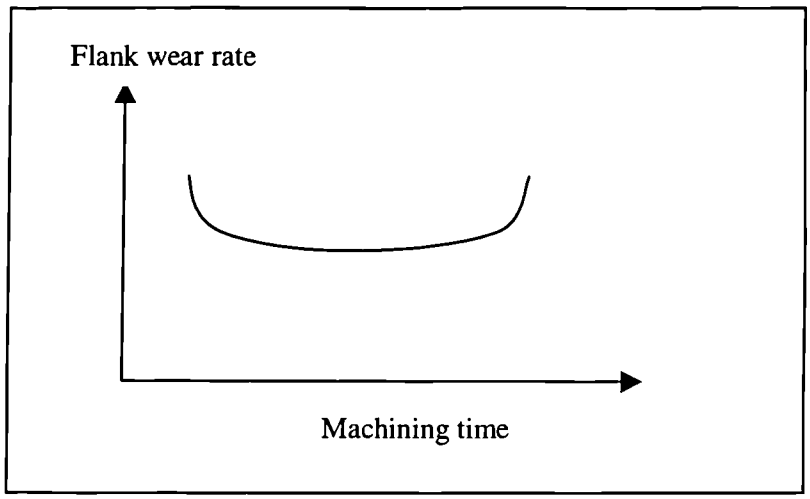

Figure 6.3 Typical wear rate versus time.

H_{tf} is just the opposite of flank wear rate and so it looks like Figure 6.4.

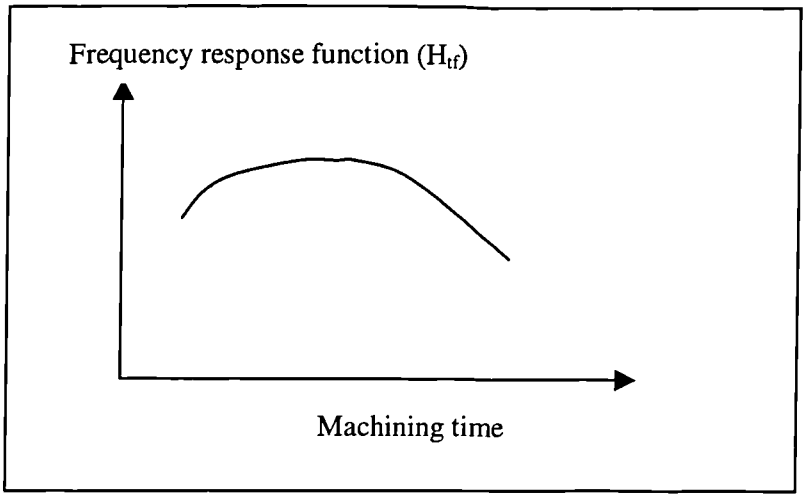

Figure 6.4 Typical of frequency response function (H_{tf}) versus time.

The second postulate of constant α appears to be acceptable. The reason is that the auto-spectra, S_f and S_t, correspond to the uncorrelated friction forces on the two interfaces and that tool wear is likely to affect equally both S_f and S_t.

Since, by Equation (6.12), both H_{tf} and the γ^2 have the same trend, it can be concluded that the value of the coherence function γ^2 is low when the tool is sharp, rises to a higher level during the secondary stage of tool wear when the wear rate is constant, and then falls in the tertiary stage when the cutting edge crumples rapidly leading to eventual failure.

6.5 Tool wear, acceleration and coherence function

To validate the theory of coherence function, cutting experiments were performed. These were identical to those for AE tests and their conditions are repeated bellow.

Machine Test Set Number	cutting speed (m/min)	feed (mm/rev)	depth of cut (mm)
1) Roughing	150	0.3	1
2) Semi- Roughing	250	0.25	0.75
3) Finishing	300	0.2	0.5

Table 6.1. Cutting conditions of three machining test sets.

Two compact accelerometers model (PCB303A03) were mounted at the insert end of tool shank: one in the direction of tangential force and the other in the direction of feed force. They have the frequency ranges of 1 - 10,000 Hz (±5%) and 0.7 - 20,000 Hz (±10%). They are designed for adhesive mounting. Due to the high temperature, glass-ceramic-discs measured 10x1 mm^2, were used as heat insulators between the tool shank and the accelerometers. A silicone rubber compound which can be withstand temperature up to 250°C was used as a couplant between the accelerometers and glass-ceramic insulators. The accelerometer outputs of the accelerometers were fed into the SI 1220 multi-channel spectrum analyser, set to display an average spectrum over 8 successive spectra in the frequency range 0Hz-25kHz with the resolution of 500 points.

For each set of machining tests, a fresh insert (GC 4035) was used and cuts were performed until the insert was considered to be worn. Acceleration signals in the feed and tangential directions were recorded for every other cut.

The tangential and feed acceleration amplitude were displayed as a waterfall plot using the MATLAB software. In this waterfall plot the three axes are the frequency, the acceleration amplitude and the cutting time respectively. The results for the three machining test sets were shown in Figure 6.5 to Figure 6.10. It can be seen from these diagrams that the cutting tool has resonant frequencies between 2.5 kHz and 5.5 kHz in both the tangential and feed directions. As the cutting speed increases and the depth of cut and feed rate decrease, the acceleration spectra in the feed direction also reveal additional tool resonant frequencies at around 15 kHz. In the lower frequency range of 2.5 to 5.5 kHz, the variation in peak heights in the tangential direction is somewhat random with the progression of tool wear for all three machining test sets, Figures 6.5, 6.7 and 6.9; but in the feed direction, for the machining test sets 1 and 2 (known as roughing and semi-roughing respectively), the peaks are highest both at the initial and final stages of tool wear, Figures 6.6 and 6.8.

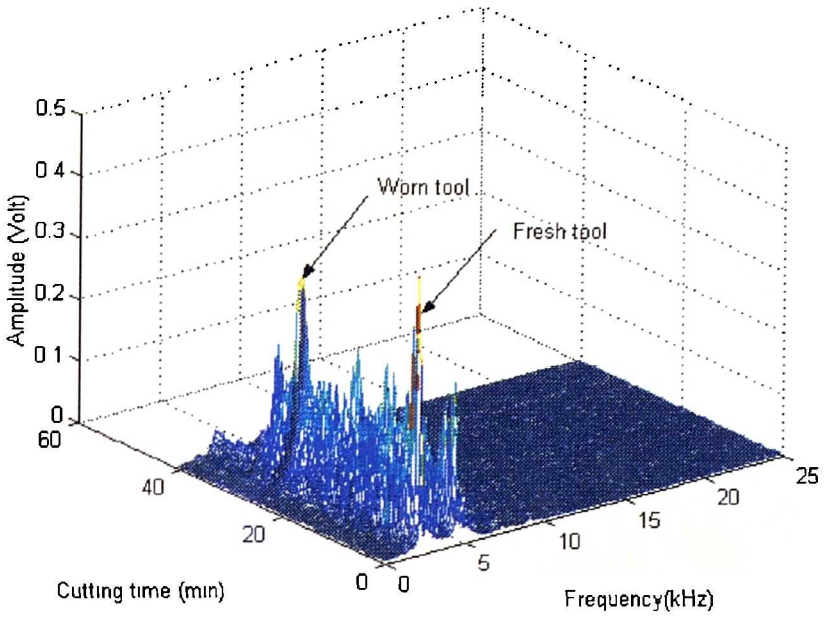

Figure 6.5. Acceleration spectra in tangential direction of cutting speed 150 m/min, depth of cut 1 mm and feed rate 0.3 mm/rev.

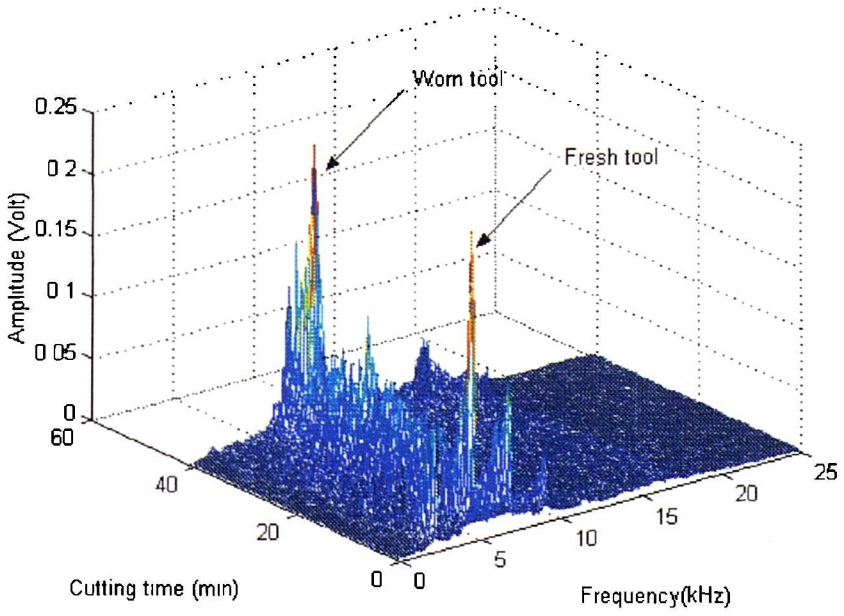

Figure 6.6. Acceleration spectra in feed direction of cutting speed 150 m/min, depth of cut 1 mm and feed rate 0.3 mm/rev.

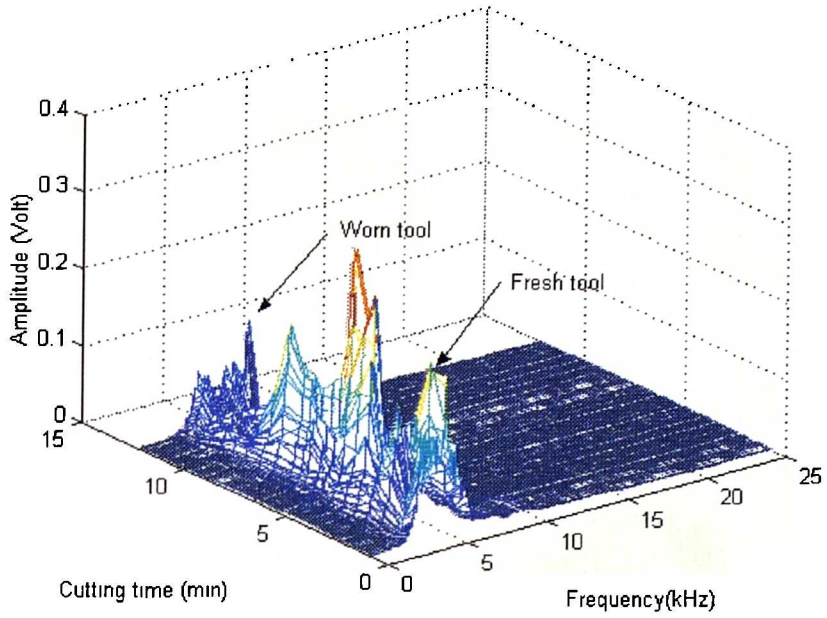

Figure 6.7. Acceleration spectra in tangential direction of cutting speed 250 m/min, depth of cut 0.75 mm and feed rate 0.25 mm/rev.

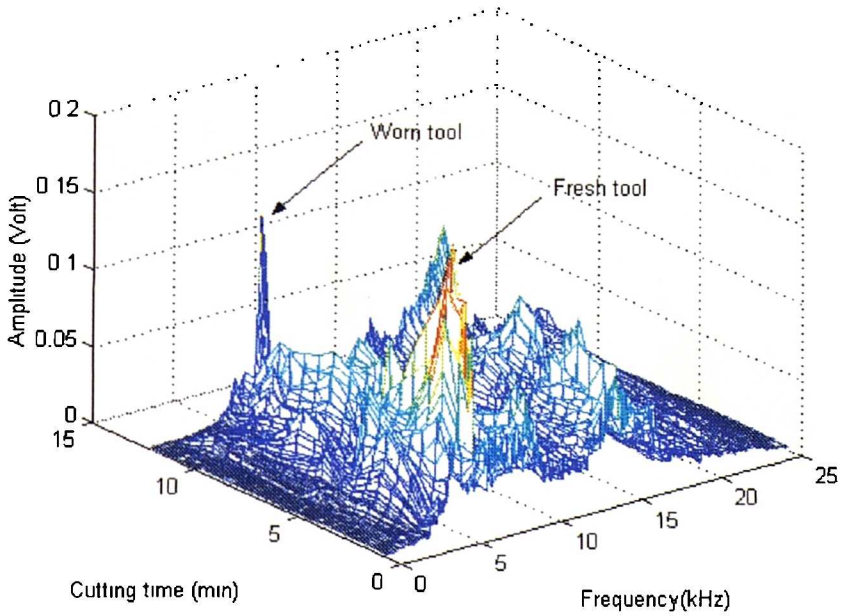

Figure 6.8. Acceleration spectra in feed direction of cutting speed 250 m/min, depth of cut 0.75 mm and feed rate 0.25 mm/rev.

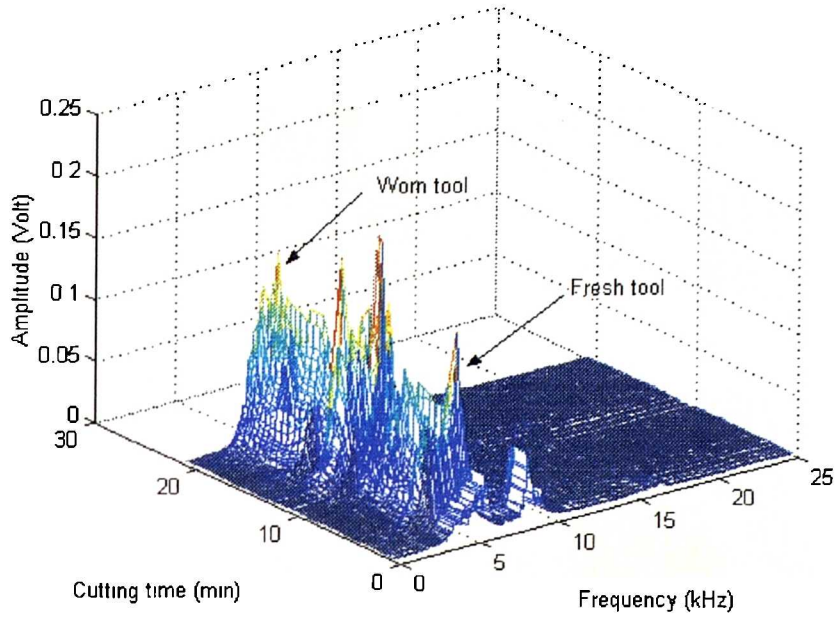

Figure 6.9. *Acceleration spectra in tangential direction of cutting speed 300* m/min, depth of cut 0.5 mm and feed rate 0.2 mm/rev.

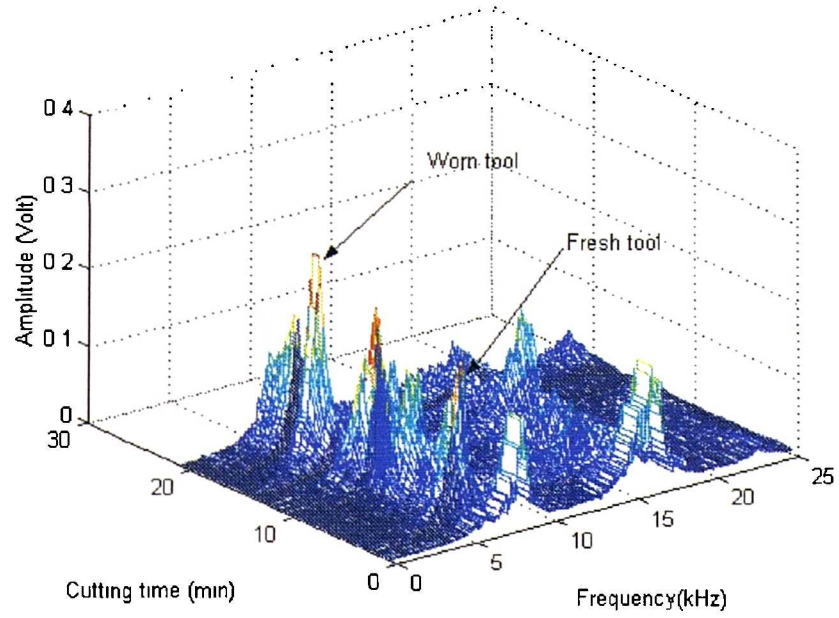

Figure 6.10. Acceleration spectra in feed direction of cutting speed 300 m/min, depth of cut 0.5 mm and feed rate 0.2 mm/rev.

The coherence spectra of the acceleration signals for each of the three machining conditions are shown in Figures 6.11, 6.13 and 6.15 as waterfall plots. The three axes in these diagrams represent the frequency, the cutting time and the coherence. An alternative, maybe better, perspective to the waterfall plot is to take a plan view of the waterfall plot using colours to code the values of the coherence function. These corresponding plan views are shown in Figures 6.12, 6.14 and 6.16.

For roughing cuts, it can be seen from Figure 6.12 that in the frequency range of 2.5 to 5.5 kHz, the coherence values rise rapidly in the initial stage of tool wear, stay at a high plateau value in the secondary stage and then fall in the tertiary stage. This pattern is repeated, Figure 6.14, for semi-roughing cuts; and, to a lesser extent, for the finishing cuts, Figure 6.16. As expected, the curves corresponding to coherence in the 2.5-5.5 kHz frequency range in Figures 6.20, 6.21 and 6.22 bear out the same fact. The pattern of coherence values agrees with the theory proposed in Sections 6.3 and 6.4.

At the high frequency end, between 18 and 25 kHz, the coherence values for roughing, semi-roughing and finishing cuts rise in the tertiary stage of tool wear, Figures 6.12, 6.14 and 6.16 or Figures 6.20, 6.21 and 6.22. The reason for this trend is not known as the theory of coherence developed in Sections 6.3 and 6.4 applies only for the 2.5-5.5 kHz, the resonant frequency region of the cutting tool.

To better detect the possible trends of coherence with tool wear in the various frequency bands, a set of scatter plots were produced using Axium 6. Figures 6.17 6.18 and 6.19 are such scatter plots for the roughing cuts, semi-roughing cuts and finishing cuts respectively. A scatter plot matrix is an array of pairwise scatter plots showing the relationship between any pair of variables in a multivariate data set. The description "0 to 25k" shown at the top left corner of the scatter plot matrix in the Figures 6.17 to 6.19 refer to the frequency band 0-25 kHz. This frequency band is the value of the y-axis for all plots along the top row and it is the value of the x-axis for all plots down the first column. Similarly, "1 to 5 k" refers to the frequency band 1-5 kHz and applies to the second row and column of scatter plots in the matrix. Thus, for example, the scatter plot situated in the first row and the second column is the scatter plot of the coherence function spectra with frequency band 0-25 kHz on

the y-axis and the frequency band 1 to 25 kHz on the x-axis. In these plots, where a linear trend is shown, it suggests that the two parameters involved are linearly proportional to each other. For example, in Figure 6.17, the coherence values in the two frequency bands 1-5 kHz and 3-5 kHz are linearly related, not surprising as the first is a subset of the second.

The more interesting set of scatter plots appear in the column before last column of Figures 6.17, 6.18 and 6.19 as they relate to coherence against tool wear. For roughing cuts, the single-hump pattern is seen for the coherence in the low frequency range (2.5-5.5 kHz) with tool wear, Figure 6.17. This pattern is not that obvious for semi-roughing and finishing cuts, Figures 6.18 and 6.19. At the high frequency end (18-25 kHz), the coherence values increase with wear for the three cutting conditions.

The relationship between coherence values in the low- and high-frequency bands and cutting time is shown in Figures 6.20, 6.21 and 6.22 for the three cutting conditions. Also shown in these diagrams are the tool wear, expressed in terms of the flank wear height, measured at the end of each cut.

6.6Cutting condition and coherence function

The effects of cutting conditions on the coherence function was investigated. The cutting conditions, identical to those in Section 5.4, is repeated below for reference:

- Cutting condition 1: Variable feed rates from 0.05 mm/rev to 0.4 mm/rev in increments of 0.05 mm/rev. Cutting speed and depth of cut were constant at 120 m/min and 0.75 mm respectively.
- Cutting condition 2: Variable speeds from 80 m/min to 150 m/min in increments of 10 m/min. Feed rate and depth of cut were constant at 0.2 mm/rev and 0.75 mm respectively.
- Cutting condition 3: Variable depths of cut from 0.3 mm to 1.0 mm in increments of 0.1 mm. Cutting speed and feed rate were constant at 120 mm/min and 0.2 mm/rev respectively.

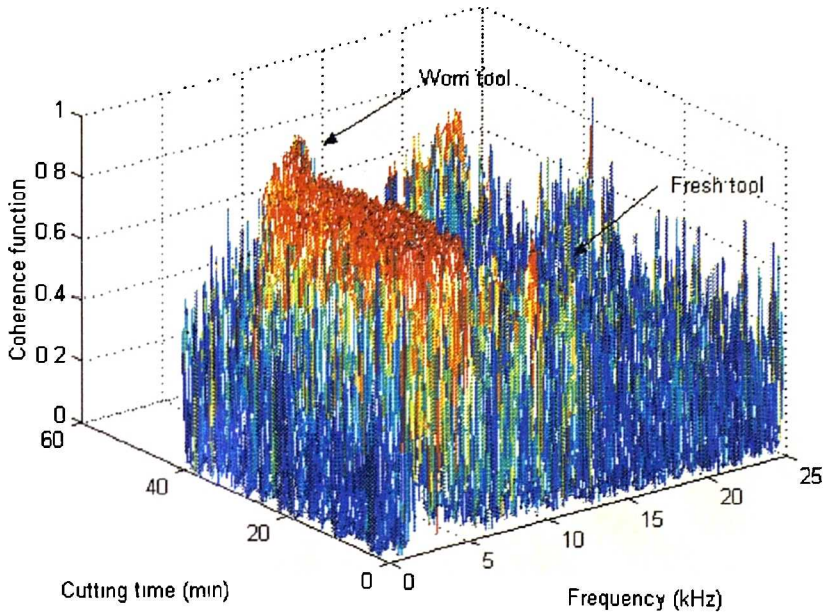

Figure 6.11. Three-dimension plot of the coherence spectra of the accelerations in the tangential and feed directions of cutting speed 150 m/min, depth of cut 1 mm and feed rate 0.3 mm/rev.

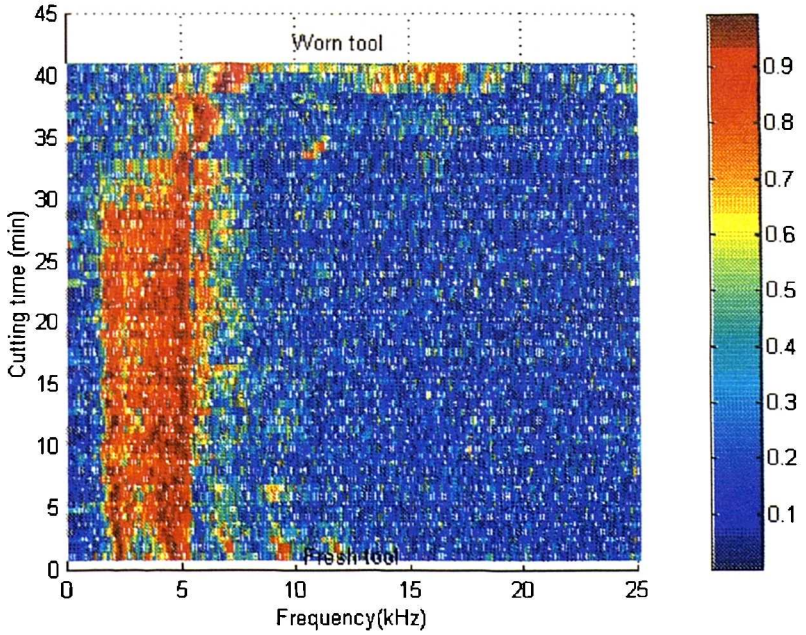

Figure 6.12. Plane view plot of the coherence spectra of the accelerations in the tangential and feed directions of cutting speed 150 m/min, depth of cut 1 mm and feed rate 0.3 mm/rev.

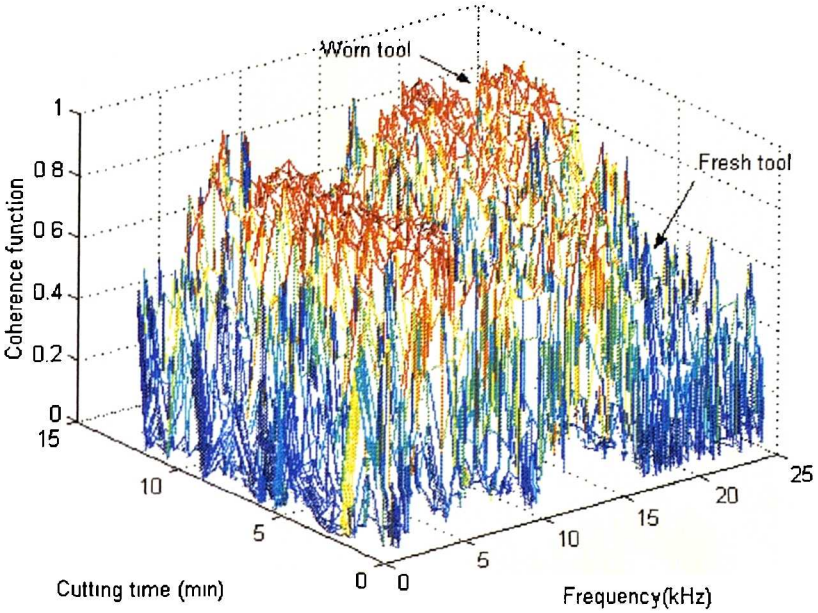

Figure 6.13. Three-dimension plot of the coherence spectra of the accelerations in the tangential and feed directions of cutting speed 250 m/min, depth of cut 0.75 mm and feed rate 0.25 mm/rev.

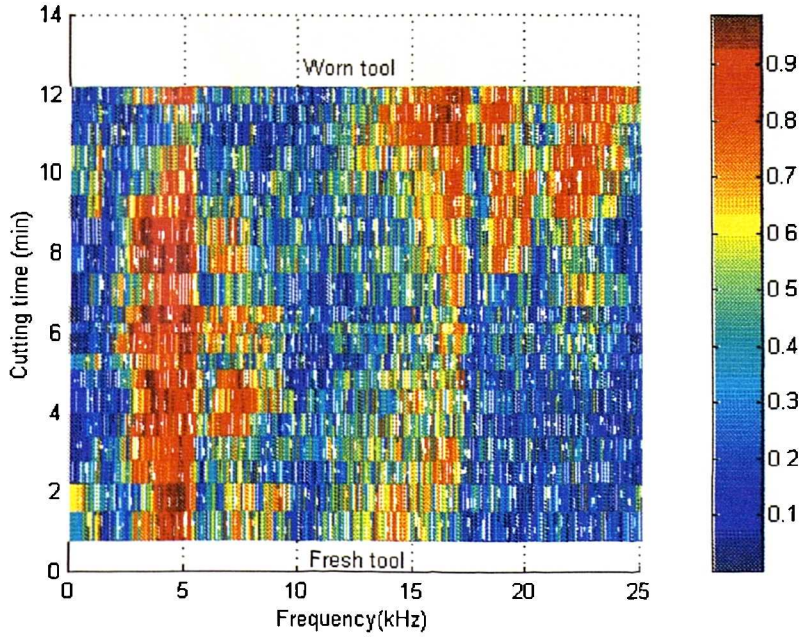

Figure 6.14. Plane view plot of the coherence spectra of the accelerations in the tangential and feed directions of cutting speed 250 m/min, depth of cut 0.75 mm and feed rate 0.25 mm/rev.

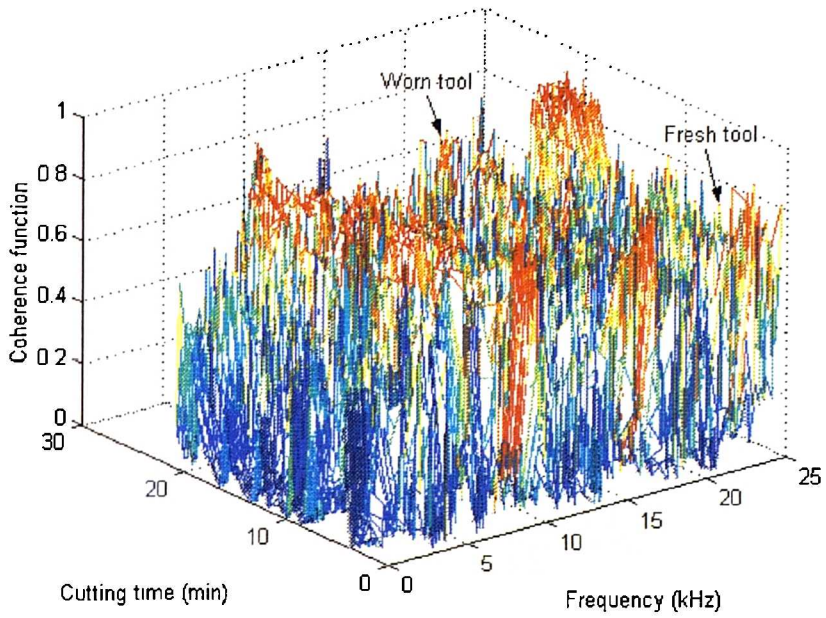

Figure 6.15. Three-dimension plot of the coherence spectra of the accelerations in the tangential and feed directions of cutting speed 300 m/min, depth of cut 0.5 mm and feed rate 0.2 mm/rev.

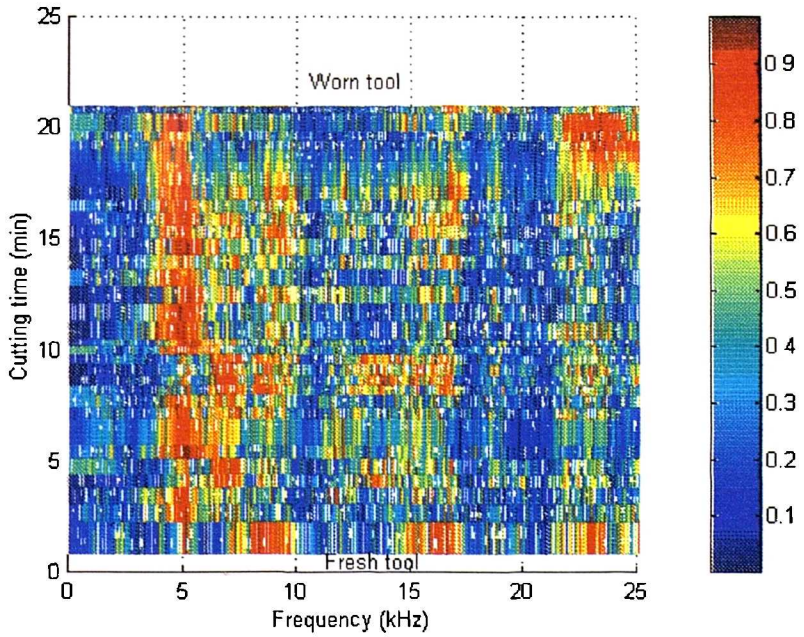

Figure 6.16. Plane view plot of the coherence spectra of the accelerations in the tangential and feed directions of cutting speed 300 m/min, depth of cut 0.5 mm and feed rate 0.2 mm/rev.

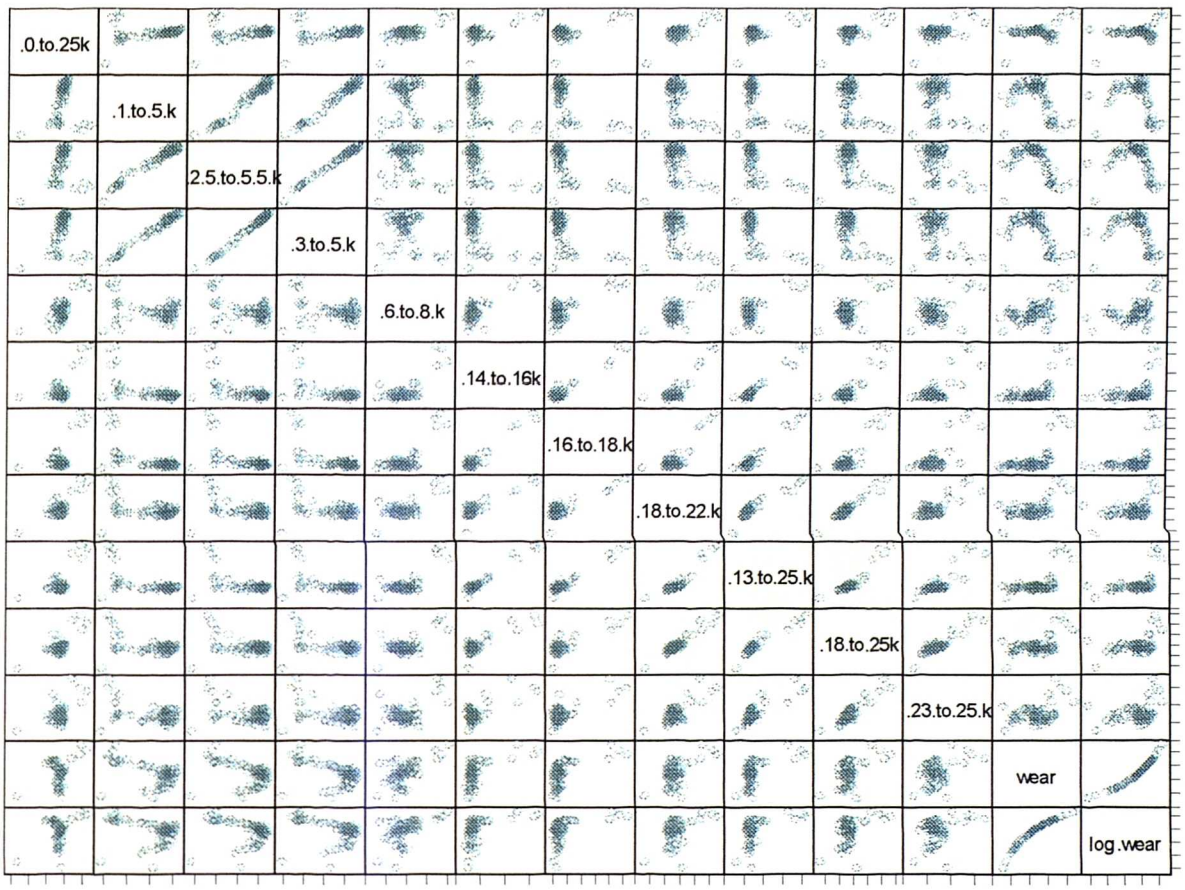

Figure 6.17. Scatter plot of each frequency range of the coherence spectra of cutting speed 150 m/min, depth of cut 1 mm and feed rate 0.3 mm/rev.

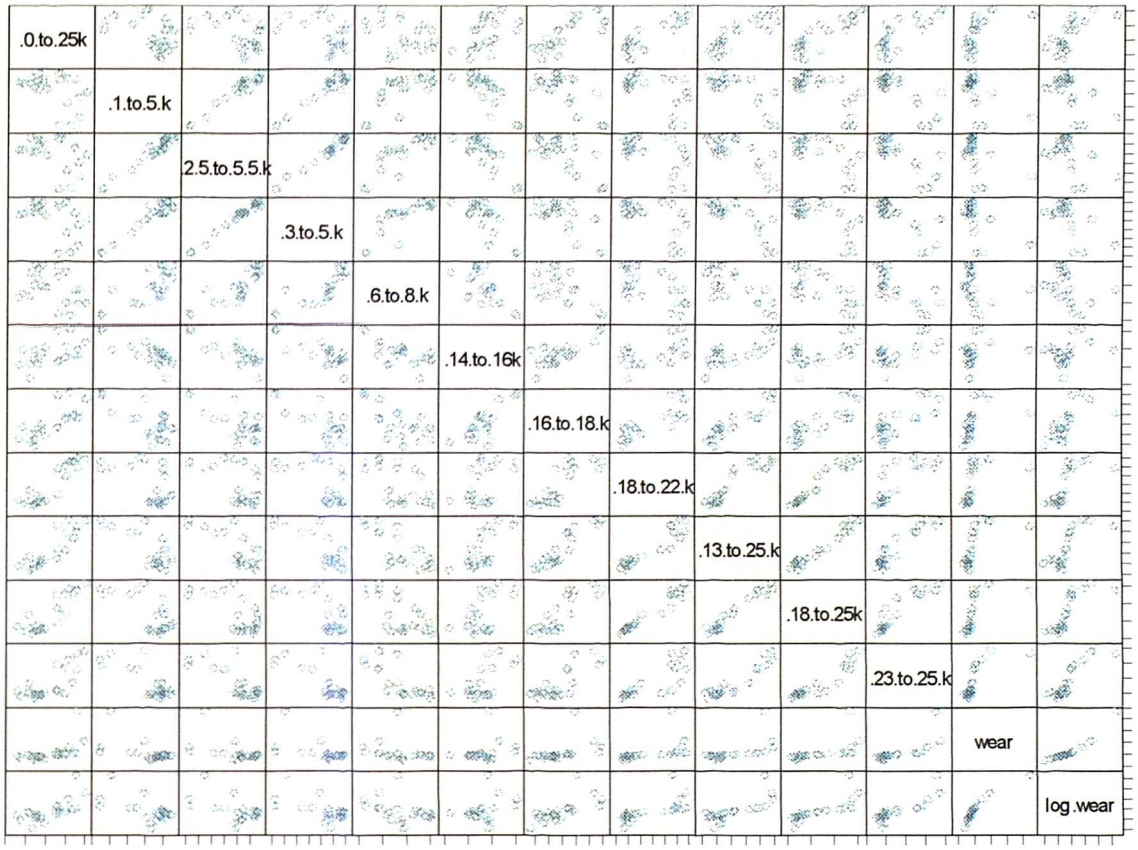

Figure 6.18. Scatter plot of each frequency range of the coherence spectra of cutting speed 250 m/min, depth of cut 0.75 mm and feed rate 0.25 mm/rev.

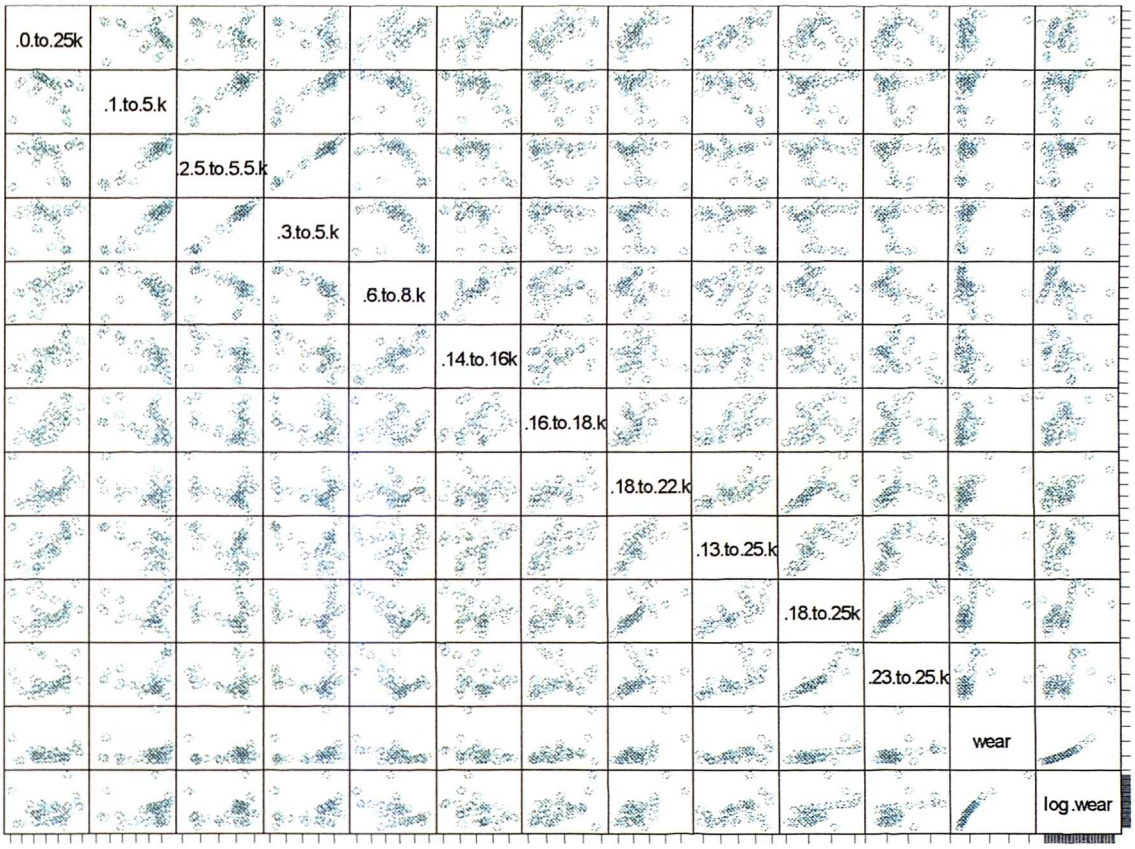

Figure 6.19. Scatter plot of each frequency range of the coherence spectra of cutting speed 300 m/min, depth of cut 0.5 mm and feed rate 0.2 mm/rev.

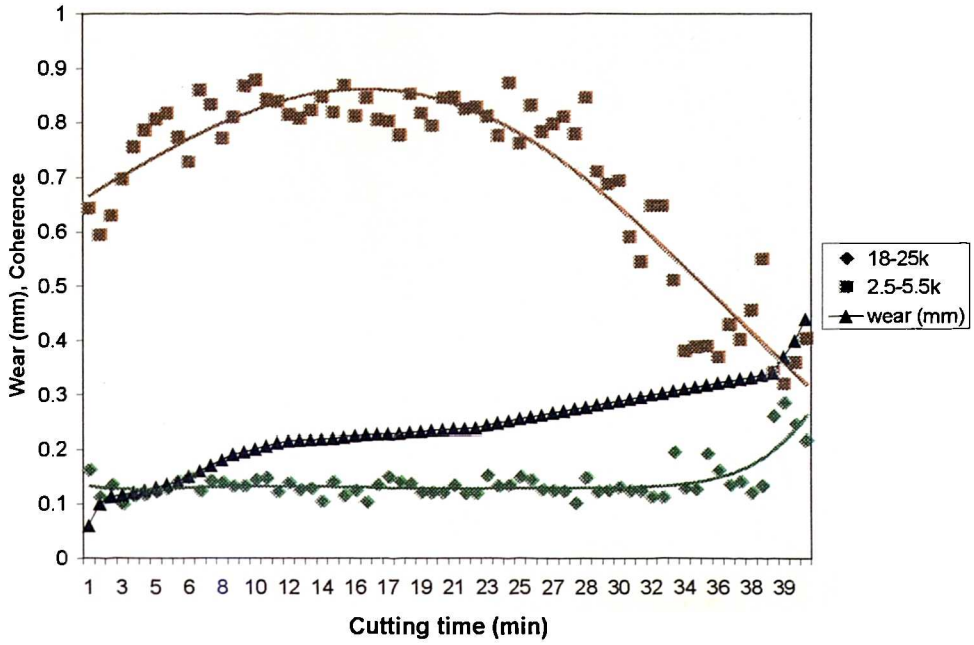

Figure 6.20 Coherence at frequency range 2.5-5.5 kHz and 18-25 kHz and flank wear with cutting time of cutting speed 150 m/min depth of cut 1.0 mm and feed rate 0.3 mm/rev.

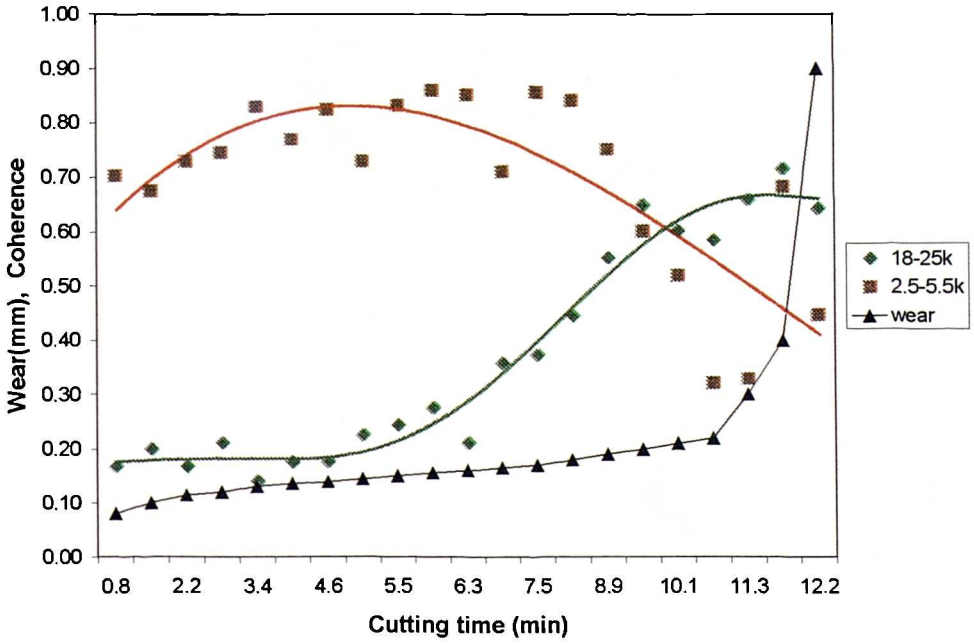

Figure 6.21 Coherence at frequency range 2.5-5.5 kHz and 18-25 kHz and flank wear with cutting time of cutting speed 250 m/min depth of cut 0.75 mm and feed rate 0.25 mm/rev.

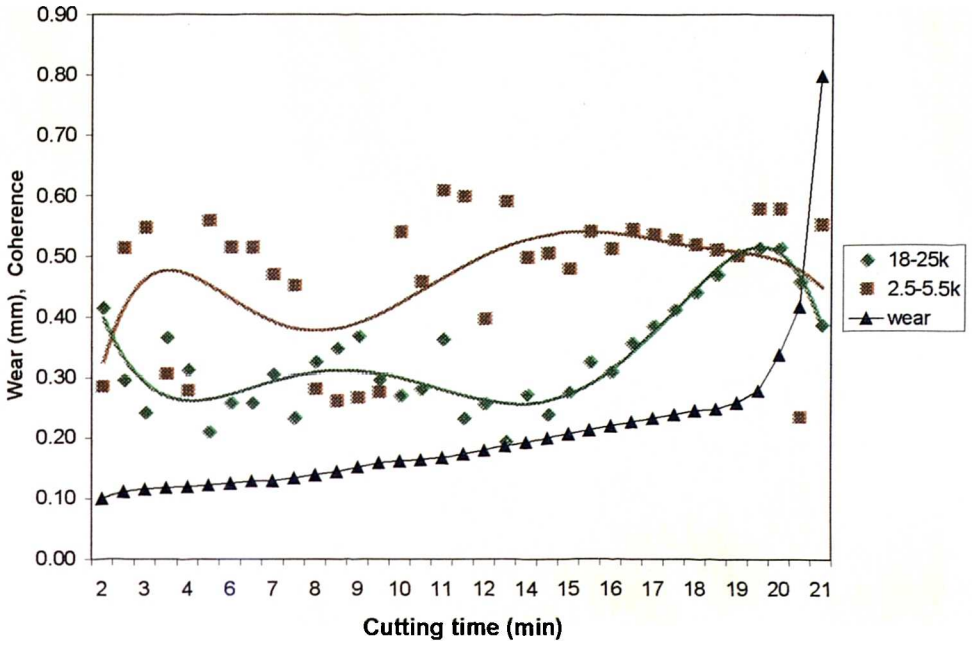

Figure 6.22. Coherence at frequency range 2.5-5.5 kHz and 18-25 kHz and flank wear with cutting time of cutting speed 300 m/min depth of cut 0.5 mm and feed rate 0.2 mm/rev.

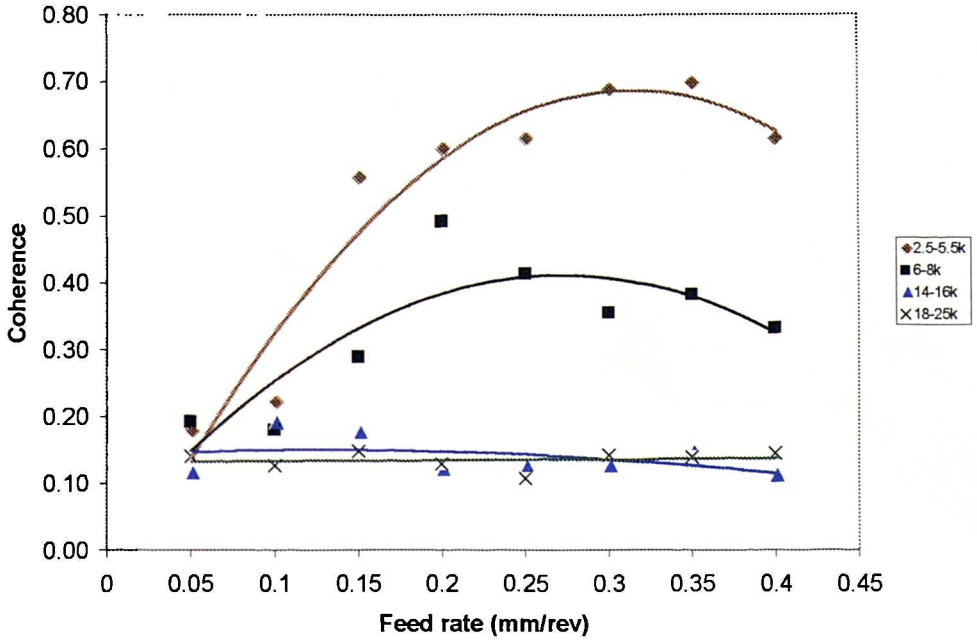

Figure 6.23. Coherence at various frequency ranges with variable feed rates from 0.05 mm/rev to 0.4 mm/rev at constant speed 120 m/min and 0.75 mm depth of cut.

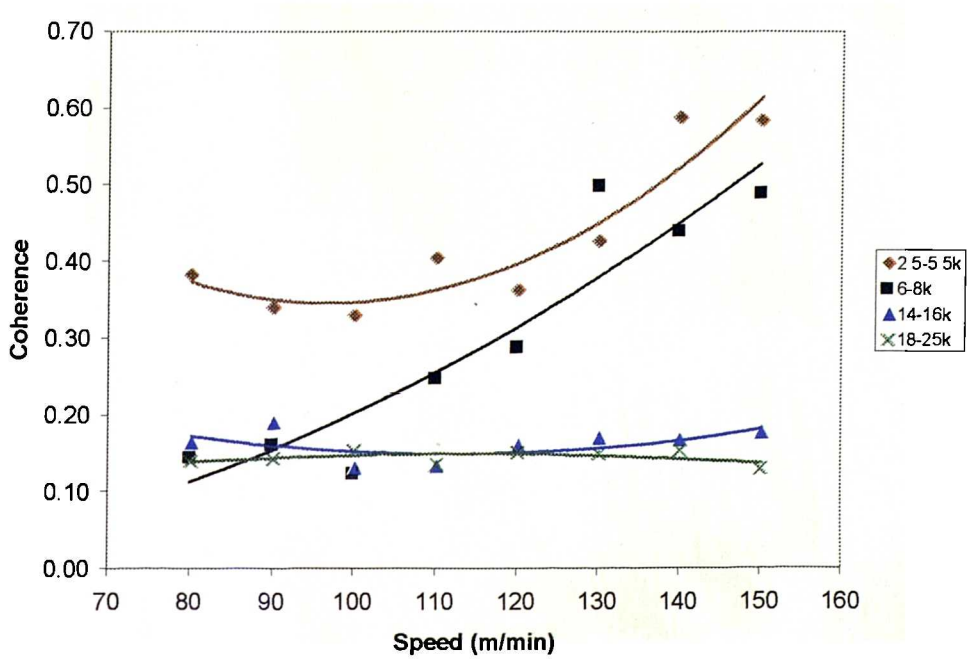

Figure 6.24. Coherence at various frequency ranges with variable speeds from 80 m/min to 150 m/min at constant feed rate 0.2 mm/rev and depth of cut 0.75 mm.

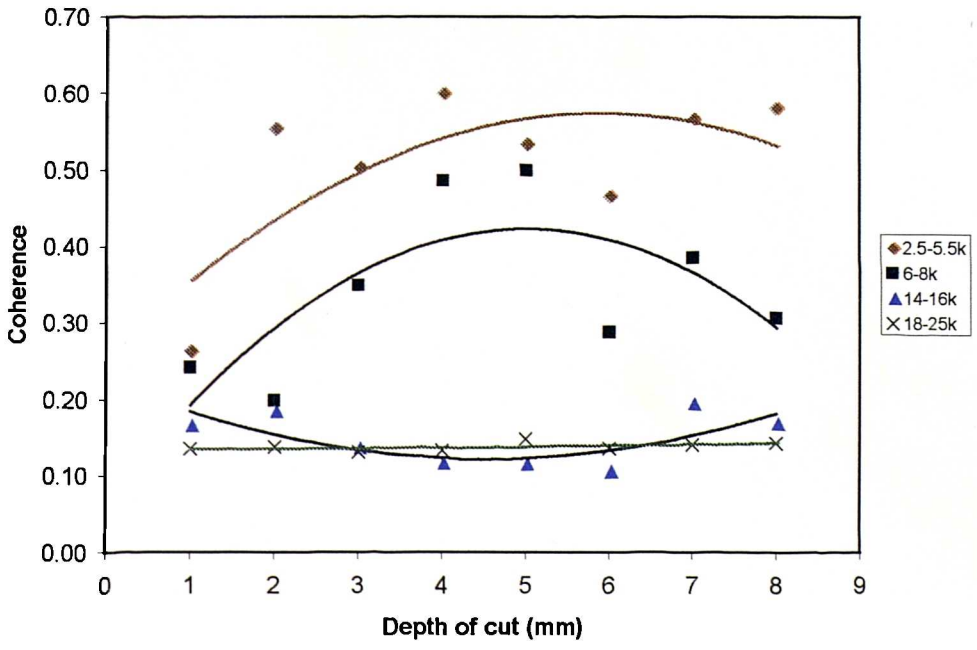

Figure 6.25. Coherence at various frequency ranges with variable depths of cut from 0.3 mm to 1.0 mm at constant speed 120 mm/min feed rate 0.2 mm/rev.

The relation between coherence function, on the one hand, and variable feeds, speeds and depths of cut, on the other, were as shown in Figures 6.23, Figure 6.24 and Figure 6.25. Results show that the coherence function in the frequency range of 14 kHz -16 kHz and 18 kHz -25 kHz is fairy constant with the feed rate, the speed and the depth of cut. At around natural frequency, 2.5 kHz -5.5 kHz and 6 kHz -8 kHz, the coherence increases with the feed rate, the speed and the depth of cut. The coherence at the high frequency end therefore provides the benefit that it is not sensitive to cutting conditions.

6.7 Conclusions

1. A coherence function model was developed to describe the behaviour of coherence with tool wear. It was predicted that in the resonant frequency region of the cutting tool, the coherence values would rise in the initial stage of tool wear, would stay in a higher plateau value in the secondary stage and would fall in the tertiary stage. Both the initial and tertiary stages of tool wear were observed to be very short in comparison to the secondary stage.

2. The theory postulated that the degree of correlation between the dynamic tangential and feed vibration components, measured as acceleration, was inversely related to the rate of tool wear. When the wear rate was high, as would be the case in the initial and tertiary stages of tool wear, the correlation was low; that, in turn, according to the theory, would give a low coherence. When the wear rate was low during the secondary stage of wear, the correlation and its corresponding coherence would then be high.

3. Three sets of machining tests were conducted corresponding to the roughing, semi-roughing and finishing conditions. It was observed that for roughing and semi-roughing conditions, in the frequency range of 2.5-5.5 kHz, the above-mentioned prediction of coherence turned out to be valid; for the finishing condition, there was a greater discrepancy. At the high frequency end, 18 - 25 kHz, the coherence value was low in the initial and secondary stages of wear but rose in the tertiary stage for all three cutting conditions.

4. The effects of cutting conditions on coherence was also investigated. It was observed that the coherence values in the 14-16 kHz and 18-25 kHz bands were approximately constant for a range of feed rates, cutting speeds and depths of cut. By contrast, the coherence values in the 2.5-5.5 kHz and 6-8 kHz bands increase with the feed rates, cutting speeds and depths of cut. The insensitivity of coherence in the high frequency bands to cutting conditions was considered a useful attribute for it to be suitable in tool wear monitoring.

Chapter 7

Data Fusion and Analysis

7.1 Introduction

From the machining tests reported in Chapter 5 and Chapter 6, it was observed that the values of AErms and coherence function in the low frequency band (2.5 kHz – 5.5 kHz) and the high frequency band (18 kHz – 25 kHz) were sensitive to tool wear. In summary for roughing cuts, the AErms increased within the primary stage of wear and then settled down to a constant level with much local fluctuation; for semi-roughing cuts during the latter half of the secondary stage of tool wear the AErms increased with the progression of flank wear; and for finishing cuts the AErms was roughly constant with the progression of tool wear until the tertiary stage of wear when the AErms dropped before it rose again corresponding to the point when the tool was so worn that it could not be used. Calibrated values of AErms, by expressing them in terms of the air jet pressure in the units of bars was implemented. This was to permit comparability of results obtained from different sensors (WD and R30) placed at different locations. For the vibration results, the machining tests showed that the coherence function in the vicinity of the natural frequency of the tool decreased with tool wear whilst that in high frequency band increased.

In order to detect tool wear more reliably, an expert system was designed using a software package named NETICA. This expert system is also known as a belief network. The knowledge of AErms and coherence function as related to the different stages of tool wear was used in this belief network. Error rates of the belief network are computed for the cases of AErms equivalent pressure from the WD sensor and R30 sensor expressed as equivalent pressure readings.

7.2 Bayesian Theorem

Data fusion and classification techniques have been used by many researchers. Most of them implemented neural networks to estimate the relationship between the input data and the types of tool wear. However the performance of a neural network is

dependent on the quality of the input data, the training sequence, the number of iterations, the number of hidden layers, the learning rate and the type of transfer function. The best configuration of a neural network is often achieved through trial and error.

Alternatives to neural network are rule-based systems. In this project, Netica software package was used. The advantages of Netica are its ease of use due to a user-friendly, graphical interface and its low cost. Netica provides probabilistic reasoning using Bayes' rule and the law of total probability. Bayes' rule is derived from Bayes' theorem, which was defined in Section 2.2.4.2 of Chapter 2 as

$$P(S_i \mid A) = \frac{P(A \mid S_i)P(S_i)}{\sum_{j=1}^{k} P(A \mid S_j)P(S_j)} \tag{7.1}$$

for $i = 1,2,...,k$

where A and S_i refer to events and

$P(S_i \mid A)$ = Conditional (a posteriori) probability of S_i given A

$P(A \mid S_i)$ = Conditional probability of A given S_i, and

$P(S_i)$ = a priori probability of S_i

The law of total probability can be expressed by

$$P(A) = P(S_1)P(A \mid S_1) + P(S_2)P(A \mid S_2) + P(S_3)P(A \mid S_3) + ... + P(S_k)P(A \mid S_K) \tag{7.2}$$

where S_i $(i = 1,...,k)$ and A have the same meaning as before.

The function of classification is to assign an observation on the basis of a set of quantifiable features to one of a number of possible groups. In Equation 7.1, the events S_i $(i=1,2,...,k)$ are events corresponding to possible groups, for example, "tool not worn" and "tool worn"; The event A refers to a set of features, for example, values of AErms equivalent pressure and coherence function.

Bayes' rule is a classification rule which assigns an observation to the groups (worn and not worn) with the highest conditional probability. In other words, if $P(S_1|A) > P(S_2|A)$, then assign the observation to group 1.

The inequality can be rewritten using Equation 7.1 and noting that the denominators are identical, as

$$P(A|S_1)\,P(S_1) > P(A|S_2)\,P(S_2)$$

The reason why this form is preferred is that $P(A|S_1)$ is much easier to obtain from experiments that $P(S_1|A)$

To use a belief network both a priori probabilities and conditional probabilities of the different events need to be specified. In many applications, these probabilities are educated guesses from experts. In this research the probabilities were learnt by NETICA from what is called a file of cases. This file contains information on the coherence function in the frequency values 2.5 kHz -5.5 kHz and 18 kHz -25 kHz, AErms equivalent pressure, cutting condition and the two stages of tool wear (worn and not worn) as obtained from machining tests reported in Chapters 5 and 6.

7.3 Learning Bayesian belief network from a case file

The conditional probability relations can be learnt from a file of cases. A case is a set of findings that can be entered into the nodes of a belief network and it represents an example of a particular situation. In this application, the set of findings consists of:

1) AE pressure,ie, AErms converted to pressure units in bars
2) Coherence function in the high-frequency band (18-25 kHz)
3) Coherence function in the low-frequency band (2.5-5.5 kHz)
4) Cutting condition: roughing, semi-roughing and finishing
5) Status of tool: either worn or not worn

These findings were divided into 2 equal subsets and were held in separate cases files. Because of the limitation number of worn tool cases, all worn tool cases were used to train the network. The first cases file contains findings with odd Idnumbers

(Appendix H1) whereas the second cases file stores findings with even Idnumbers (Appendix H2). The first cases file was used for training the network; the second cases file was then use to test the network.

The demarcation between 'worn' and 'not worn' tool was defined by on the onset of the tertiary stage of tool wear. It was found from the machining tests reported in Chapter 6 that for roughing cuts, the flank wear at the onset of this tertiary stage was 0.34 mm occurring after 38.9 min of machining. Corresponding value for semi-roughing and finishing cuts were 0.22 mm at 10.7 min and 0.28 mm at 19.9 min respectively.

7.3.1 Create the belief network from a file of cases

A file of cases was created in an Excel program and then saved in the format of a text file (.txt). The text file was opened in Netica and then the command "File -> Save case" was issued to change the text file to a case file (.cas). The file must contain "// ~->[CASE-1] ->~" somewhere in the first three lines, followed by a line consisting of headings for the columns. Each heading corresponds to one variable of the case and is the name of the node used to represent the variable. The headings are separated by spaces and/or tabs.

The belief network can be established by the steps as shown below.

7.3.1.1 Create nodes for the variables of interest

The words "node" and "variable" are used interchangeably, but "variable" usually refers to the real world or the original problem, while "node" usually refers to its representation within the belief network.

The nodes or variables consist of Cutting condition, AEpressure, Coherence function of the vibration signal at the high frequency end (High_end), Coherence function of vibration at the low frequency end (Low_end) and Stage of tool wear (not worn and worn). Parameters of AEpressure and the coherence function at high and low frequency ends were divided into categories based on tool states, worn and not worn, for each cutting condition. Values of each parameter are divided as follows:

1) **Cutting condition**

   Three cutting conditions are used. They are rough (roughing-cuts), semi (semi-roughing cuts) and finishing (finishing-cuts).

2) **AErms**

   Four values of AErms equivalent pressure are, 0-13, 13-24, 24-41 and 41-65 bars respectively.

3) **Coherence function of vibration signal in frequency band 18-25 kHz (High_end)**

   Four values of high_end are 0-0.2, 0.2–0.38, 0.38-0.5 and 0.5-1 respectively.

4) **Coherence function of vibration in frequency band 2.5-5.5 kHz (Low_end)**

   Two values of low end are 0-0.45 and 0.45-1.

5) **Stages of tool wear (not worn and worn)**

   The stages of tool were chosen from each cutting condition using the on set of the tertiary wear stage as the boundary.

When the belief network is constructed, one node is used for each variable, which may be discrete, continuous, or propositional (true/false). It can be seen that the AEpressure, High_end and Low_end nodes are continuous, and the Tool_wear and the cutting condition nodes are discrete.

7.3.1.2 Connect the nodes with links

The nodes in the network are linked in order to capture the dependencies between them. If there is a link from node A to node B, then node A is sometimes called the parent and node B the child. Thus, in Figure 7.1, the "cutting condition" node is the parent of the "tool wear" node. The "tool wear" node is the parent of "AEpressure", "High_end" and "Low_end" nodes. In the other words, "AEpressure", "High_end" and "Low_end" nodes are child nodes.

7.3.1.3 Learn prior probability for parent nodes

After constructing the network and creating the case file, the conditional probability or probability of each node can be learnt by use menu command "Relation->

Incorporate Case". The query for a "degree" is then asked. The degree is normally 1. By making it 2, the network in effect learns the same case twice.

The calculation of the probability of a parent node is performed in the following manner:

From the cases file used for learning in Netica

The number of cases for	rough	=	35 cases
	semi	=	13 cases
	finish	=	19 cases
with the total		=	67 cases

The probability of Cutting_codition node(which is a parent node) is then calculated as follows:

P(Cutting_condition = rough)	= 35/67	=	52.2 %
P(Cutting_condition = semi)	= 13/67	=	19.4 %
P(Cutting_condition = finish)	= 19/67	=	28.4 %

However Netica uses a correction based on a form of Bayesian learning and calculate the probability as:

P(Cutting_condition = rough)	= (35+1)/(67+3)	=	51.4 %
P(Cutting_condition = semi)	= (13+1)/(67+3)	=	20.0 %
P(Cutting_condition = finish)	= (19+1)/(67+3)	=	28.6 %

The correction is needed because of the small number of cases in the case file. If the number is large, the correction will not make much difference. However, if there is only one case in a file, the difference between the two methods is substantial. For example, if the case file contained only "Cutting_condition = rough". Then the frequency calculation would become

P(Cutting_condition = rough)	= 1/1	=	100 %
P(Cutting_condition = semi)	= 0/1	=	0 %
P(Cutting_condition = finish)	= 0/1	=	0 %

This suggests that the cutting condition is certainly a roughing cut. But it is hard to be absolutely certain based on just one single case.

On the other hand, using the Bayesian method of correction gives

P(Cutting_condition = rough)	= (1+1)/(1+3)	=	50 %
P(Cutting_condition = semi)	= (0+1)/(1+3)	=	25 %
P(Cutting_condition = finish)	= (0+1)/(1+3)	=	25 %

which means that the roughing cutting condition is the more likely conduction but it does not rule out completely the other two conditions.

Figure 7.1 shows the diagram of belief network learnt from the case file. The five nodes of the belief network are referred to as 1) High_end, 2) Low_end, 3) AEpressure, 4) Cutting_condition and 5) Tool_wear nodes. In the "cutting condition" node, the first column shows the three values of cutting conditions: rough, semi and finishing. The second column indicates the probability values learnt from the case file.

7.3.1.4 Learn the conditional probability tables (CPTs) for child nodes

CPTs are the contingency tables of conditional probabilities stored at each node given each configuration of parent values. The CPTs learnt from the case file, must provide a probability for each state of the child, for each possible configuration of parent values. For example, the node High_end (which takes 4 values), the node Low_end (which takes 2 values) and the node AEpressure (which takes 4 values) are the three child nodes of the node Tool_wear (which can take 2 stages: worn and not worn).

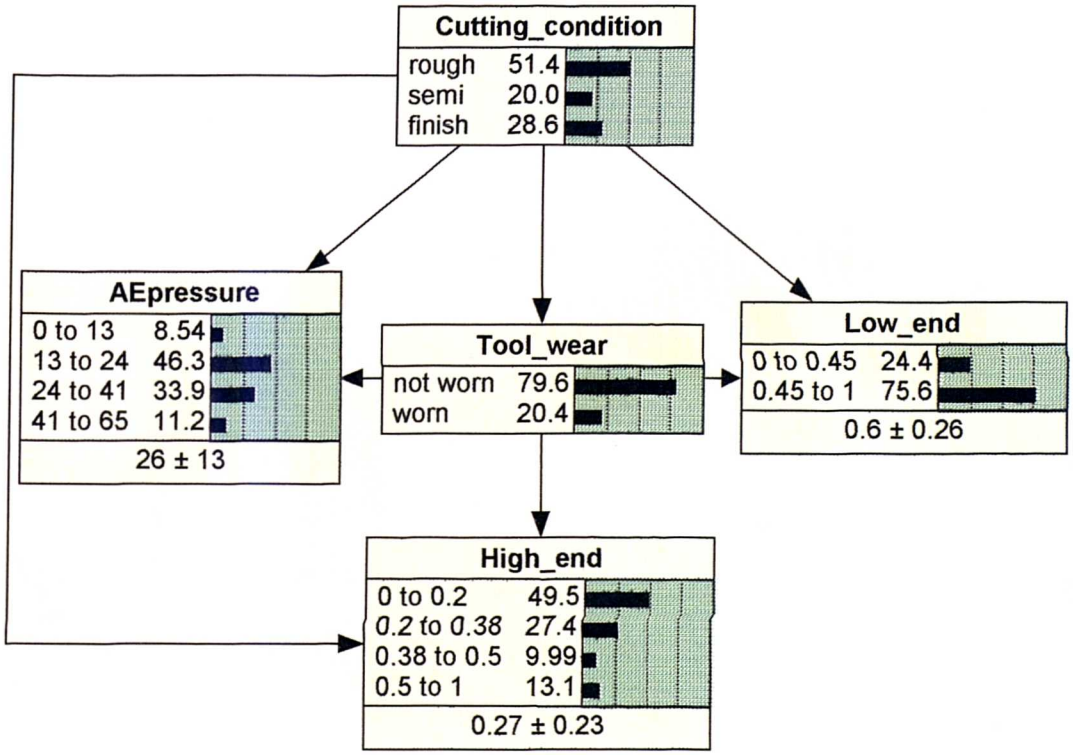

Figure 7.1. The belief network to predict the stages of tool wear.

The node cutting condition is the parent of the node tool wear. The conditional probability of the tool wear node can be computed as follows:

For the rough cut, the number of cases in worn tool		=	4	cases
	in not_worn	=	31	cases
P(not_worn | rough)	= (4+1)/(35+2)	=	13.5 %	
P(worn | rough)	= (31+1)/(35+2)	=	86.5 %	

The conditional probability expressed as a percentage of the tool wear node is shown in Table 1 below:

Cutting_codition	Not_worn	worn
rough	86.5	13.5
semi	66.7	33.3
finish	76.2	23.8

Table 7.1. Conditional probability of the tool wear node.

The first column in Table 7.1 shows the three cutting conditions. The second and third columns show the corresponding conditional probabilities for the two stages of tool condition, Not worn and worn. For example, the 86.5 % in the table is the value of P(Tool_wear = not_worn | Cutting condition = rough).

The CPTs of the node High_end, the node Low_end and the node AEpressure are calculated in a similar fashion. The corresponding conditional probabilities are shown in Table 7.2 to Table 7.4.

Cutting_condition	tool wear	0 to 0.2	0.2 to 0.38	0.38 to 0.5	0.5 to1
rough	not_worn	91.4	2.9	2.9	2.8
rough	worn	12.5	62.5	12.5	12.5
semi	not_worn	38.5	30.8	7.7	23.0
semi	worn	12.5	12.5	12.5	62.5
finish	not_worn	5.3	73.7	15.8	5.2
finish	worn	12.5	12.5	37.5	37.5

Table 7.2. Conditional probability of the High_end node.

Tool_wear	Cutting_condition	0 to 0.45	0.45 to 1
not_worn	rough	12.1	87.9
not_worn	semi	9.1	90.9
not_worn	finish	29.4	70.6
worn	rough	83.3	16.7
worn	semi	50.0	50.0
worn	finish	33.3	66.7

Table 7.3. Conditional probability of the Low_end node.

Cutting_conditon	Tool_wear	0 to 13	13 to 24	24 to 41	41 to 65
rough	not_worn	8.6	85.7	2.9	2.8
semi	worn	12.5	62.5	12.5	12.5
finish	not_worn	7.7	7.7	69.2	15.4
rough	worn	12.5	12.5	25	50
semi	not_worn	5.3	5.3	84.2	5.2
finish	worn	12.5	12.5	37.5	37.5

Table 7.4. Conditional probability of the AEpressure node.

The probability of the stages of tool wear (not_worn 79.6 % and worn 20.4 %) were calculated by Equation (7.2) as shown below:

From the Law of total probability of Bayes' Rule:

$$P(not\_worn) = P(S_1)P(not\_worn|S_1) + P(S_2)P(not\_worn|S_2) + P(S_3)P(not\_worn|S_3)$$

and

$$P(worn) = P(S_1)P(worn|S_1) + P(S_2)P(worn|S_2) + P(S_3)P(worn|S_3)$$

where

S_1, S_2, S_3 = a set of possible configurations of parent values: rough, semi and finishing respectively.

The probabilities of tool_wear, High_end, Low_end and AEpressure nodes were also calculated as described above and the probabilities of each node is as follows

- Tool_wear node

P(not_worn) = 79.6%

P(worn) = 20.4%

- High_end node (Coherence function at frequency band 18-25 kHz)

P(High_end = 0-0.2) = 49.5 %

P(High_end = 0.2-0.38) = 27.4 %

P(High_end = 0.38-0.5) = 9.99 %

P(High_end = 0.5-1) = 13.1 %

- Low_end node (Coherence function at frequency band 2.5-5.5 kHz)

P(Low_end = 0-0.45) = 24.4 %

P(Low_end = 0.45-1) = 75.6 %

- AEpressure

P(AEpressure = 0-13 bars) = 8.5 %

P(AEpressure = 13-24 bars) = 46.3 %

P(AEpressure = 24-41 bars) = 33.9 %

P(AEpressure = 41-65 bars) = 11.2 %

7.3.2 Test network using cases

The objective of this command is to grade a belief network using a set of real cases to see how well the predictions of diagnosis of the network match the actual case.

New cases in the case file can be tested manually case by case by mouse clicking all cases or by using a menu command.

To test manually case by case, an interval of each node must be selected. Each combination of an interval of all 4 nodes is a configuration of the parent. An example is shown in Figure 7.2, the value of the probability obtained from Tool_wear node, P(Tool_wear=not_worn | AEpressue=0-13, Low_end =0.45-1, Cutting condition = rough, High_end = 0-0.2) = 82.4 %. The value of the probability obtained (82.4) is the probability computed from the Equation 7.1. The calculation is shown in Appendix H3.

Netica will pass through the case file, processing the cases one-by-one. Netica first reads in the case, except for any findings for the unobserved nodes. It goes back and checks the true value for that node as supplied by the case file, and compares them with the beliefs it generates, It accumulates all the comparisons into summary statistics as shown in Section 7.4.

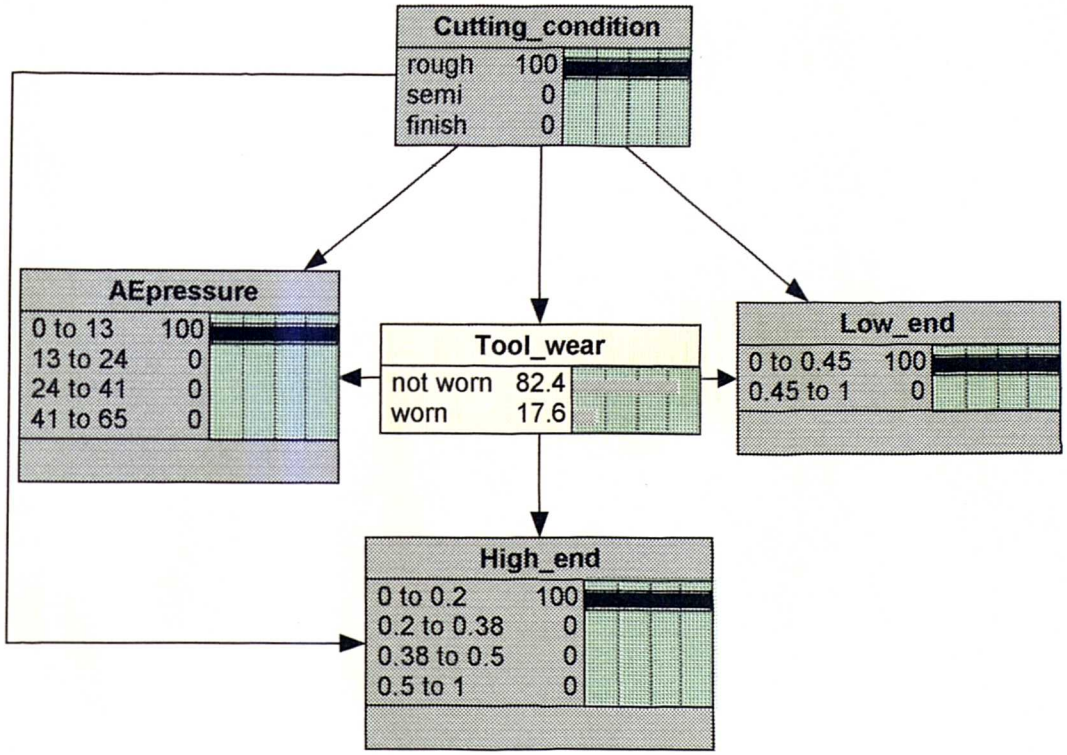

Figure 7.2. The belief network to predict the stage of tool wear for a case.

7.4 Results of Learning and testing Bayesian belief network from the case file

7.4.1 Train by calibrated AE obtained from WD sensor and test by calibrated AE obtained from WD sensor

All four features (AErms equivalent pressure of WD sensor, coherence function at the low end (2.5 kHz –5.5 kHz), coherence function at the high end (18 kHz –25 kHz) and cutting condition were used. The numbers of cases used to train and test the network were 67 and 61 respectively. The predicted results, called the confusion matrix of prediction, of 61 cases for WD sensor, were shown in Table 7.5 below:

Predicted		Actual	Error (%)
not_worn	worn		
55	0	not_worn (55 cases)	0
1	5	worn (6 cases)	16.7

The total error rate 1.6 %

Table 7.5. The predicted result of the belief network trained and tested using calibrated AE obtained from WD sensor.

A confusion matrix titled "Confusion" shows that the possible states of tool wear are "not worn" and "worn". For each case processed, Netica generates beliefs for each of these states. The most likely state, which has the highest belief, is chosen as its prediction.

The error rate means that in 1.6 % of the cases supplied by the case file, the network made the wrong prediction.

7.4.2 Train by calibrated AE obtained from WD sensor and test by calibrated AE obtained from R30 sensor

The calibrated AE expressed in the pressure unit of bars from R30 sensor was used to test the belief network instead of WD. The confusion matrix of prediction is shown in Table 7.6. The data used for testing in Table 7.7 are also from R30 sensor, being the same set as that used for training the network in Table 7.5. The difference is that the set used for training in Table 7.5 is the WD sensor.

Predicted		Actual	Error (%)
not_worn	worn		
54	1	not_worn (55 cases)	1.8
2	4	worn (6 cases)	33.3

the total error rate = 4.9 %

Table 7.6. The predicted result of the belief network trained with calibrated AE from WD sensor and tested using calibrated AE from R30 sensor.

Predicted		Actual	Error (%)
not_worn	worn		
54	1	not_worn (55 cases)	1.8
3	9	worn (12 cases)	25.0

the total error rate = 5.9 %

Table 7.7. The predicted result of the belief network trained with calibrated AE from WD sensor and tested using calibrated AE from R30 sensor for all worn-tool cases.

From Table 7.5, it can be seen that the misclassification error for the "not worn" status is 0/55 = 0 % and the error for the "worn" status is 1/6 = 16.7 %. Taking the two statuses together, the total error rate of misclassification is (0+1)/(55+6) = 1.6 %.

The error rates presented in Tables 7.6 and 7.7 based on the calibrated AE results from R30 sensor are higher. The higher error rates from testing by R30 sensor instead of WD sensor, due to the variability of converting AErms obtained from different sensors and locations to be AE equivalent pressure.

Although the missed detection of worn tool is relatively high, monitoring can be made more robust with immediate sequential assessments. If the subsequent assessments return the same verdict, then the initial belief is reinforced. For example, set the number of worn tool detection (such as 3 or 4 times) as a threshold.

In general, the accuracy of prediction is affected by the number of data used to train. A larger data set makes the prediction more accurate. In the case that new cases are available to add to the knowledge base, the belief network can facilitate this using the command "Relation-> Incorporate Case".

7.5 Conclusions

The belief network based on Bayes' rule was used to fuse information from AE and vibration in order to improve the correct recognition rate of the "worn" tool status. The three features and cutting condition obtained from the three machining tests were used to train and test the network. The overall error rate of the network in detecting a worn tool using calibrated AE from the WD sensor is 1.6 %, whilst the error rate of using the results from R30 sensor for testing the network is 4.9 % for the 6 worn_tool cases and 5.9 % for the 12 worn_tool cases.

Chapter 8

Conclusions

8.1 Summary of findings

The main findings in this research are summarised as follows:

8.1.1 Air jet chosen as artificial AE calibration source

Compared to the pulsed laser source, the variability of the AErms obtained from the air jet source, defined as the ±1 standard deviation divided by the mean, was ± 2.26 %, which is slightly bigger than the ±1.92 % for the laser source. Comparison has been also made between a reference AE source and a machining AE source based on the degree of likeness between the two frequency spectra of the respective AE signals using a measure called similarity coefficient. In this case, the air jet source was found to have a more similar RMS AE-spectrum to that obtained from machining than the pulsed laser source; the similarity coefficient of RMS AE spectrum compare to the air-jet source and the pulsed laser source are 0.86 and 0.56 respectively. Furthermore, the air-jet source has the advantages that it is relatively safe compared to a laser source and that air is readily available in a machine shop. Consequently the air jet source was chosen to be the artificial calibration source for studying machining process.

8.1.2 Calibration procedure with the air-jet as an artificial AE source for tool wear monitoring defined

A calibration procedure using an air-jet as the artificial AE source has been established for single-point tool wear monitoring. The calibration procedure involves setting up an air-jet at a fixed stand-off distance from the top rake of the tool tip, applying in sequence a set of increasing pressures and measuring the corresponding AE. The AErms obtained is linearly proportional to the pressure applied. The set-up data for the air jet is specified below:

- Diameter of nozzle 1.0 mm
- Stand-off distance 5 mm
- Pressure 5 – 8 bars in increment of 0.5 bars

8.1.3 Optimum insert clamping torque established

The AErms obtained in the air jet calibration test is found to be sensitive to the torque used to tighten the insert onto the tool holder. The AErms decreases as the torque increase from 0.4 to 1.2 Nm. When the applied torque was greater than 1.2 Nm, the AErms remains constant. Thus, once the tightening torque is above this threshold, the AErms value obtained from a sensor can be converted into an air pressure value. A safe clamping torque for the tool holder used in this research is 2 Nm. Above 2 Nm there is the risk of damaging the hexagonal head of the tightening screw. The optimum insert clamping torque is therefore recommended to be 2 Nm.

8.1.4 Linearity of AE propagation tool system proven

The AE obtained from machining is much stronger that produced from the air jet. But it has been proved from the theory and empirical evidence that the AE frequency response functions of the tool system are insensitive to the input regardless of whether it is AE produced from an air-jet or from machining.

8.1.5 Effects of cutting conditions on AErms studied

Three machining test sets were performed to relate the effects of cutting conditions to AErms. For the cutting conditions tested, AErms has been found to be sensitive to cutting conditions: AE increases with speed but is hardly affected by the feed rate and depth of cut.

8.1.6 AErms obtained from the two different AE sensors related

Experiments were conducted under three different cutting conditions. The AErms for each cutting condition was recorded by two different sensors which were placed at different locations. The AErms signals detected by the two sensors were converted to an equivalent pressure and then compared using Pearson correlation coefficient. The Pearson correlation coefficient for the cutting conditions of roughing, semi-roughing and finishing, are 0.75, 0.87 and 0.60 respectively.

8.1.7 Number of samples needed for computing the average AErms spectrum established

Two sample sizes of 1000 and 70 AErms spectra were used for calculating the averages. The results were shown in the form of scatter diagrams. The set of 1000 samples has a smaller scatter than has the set of 70 samples. Their corresponding Pearson correlation coefficients were 0.96 and 0.57 respectively.

8.1.8 Coherence function model developed to explain the behaviour of coherence with tool wear

It was predicted that in the resonant frequency region of the cutting tool, the coherence value would rise in the initial stage of tool wear, would stay in a higher plateau value in the secondary stage and would fall in the tertiary stage. The theory postulated that the degree of correlation between the dynamic tangential and feed vibration components, measured as acceleration, was inversely related to the rate of tool wear. When the wear rate was high, as would be the case in the initial and tertiary stages of tool wear, the correlation was low; and vice versa.

8.1.9 Coherence function model validated by cutting tests

Three sets of machining tests, roughing, semi-roughing and finishing conditions were performed to validate the coherence function model. For roughing and semi-roughing conditions, in the frequency range of 2.5-5.5 kHz containing the resonance frequency of the tool, the coherence function model was in agreement with observation; for the finishing condition, there was a greater discrepancy. At the higher frequency end, 18 - 25 kHz, the coherence value was low in the initial and secondary stages of wear but rose in the tertiary stage for all three cutting conditions.

8.1.10 Relationship of coherence function and cutting condition established

Machining tests under cutting conditions identical to those in Section 8.1.5 were conduced. The coherence values in the 14-16 kHz and 18-25 kHz bands are approximately constant for a range of feed rates, cutting speeds and depths of cut. By contrast, the coherence values in the 2.5-5.5 kHz and 6-8 kHz bands increase

with the feed rates, cutting speeds and depths of cut. The insensitivity of coherence in the high frequency bands to cutting conditions was considered a useful attribute for it to be suitable in tool wear monitoring.

8.1.11 Belief network trained and tested with machining tests results producing low misclassification error

Three features were identified to be sensitive to tool wear and they are AErms, coherence function at natural frequency (2.5-5.5 kHz) and at high frequency end (18-25 kHz) respectively. A belief network based on Bayes' rule was implemented to fuse information for tool wear classification. The conditional probabilities were learnt by the network using data from a file of cases. The three cutting conditions were used as features. Data was divided into two equal groups for training and testing purposes. The overall error rate of the network in detecting a worn tool using calibrated AE from the WD sensor is 1.6 %, whilst the error rate of using R30 sensor to test the network is 4.9 %.

8.2 Contribution to knowledge

The author considers the following to be a contribution to knowledge:

8.2.1 Using an air jet artificial AE source for calibrating a tool system in tool wear monitoring

An air jet source was used as an artificial AE source for calibrating the AE propagation in a tool system from the tool insert to the AE sensor. Air is cheap, safe and readily available in a machine shop. A new calibration procedure was established. The optimal insert clamping torque was determined which would reduce AE variability caused by the coupling interface between sensor and the tool holder. AE signals can be converted to a common representation independent of the tool system, coupling condition and sensor location, thus facilitating knowledge transfer. This is, hopefully, a first step towards the building up of a meaningful knowledge base on tool wear monitoring using AE.

8.2.2 Using coherence function in a broad frequency range up to 25 kHz for monitoring tool wear

A novel approach using coherence function in the 18-25 kHz frequency range to monitor tool wear was validated. The coherence function in this frequency range was found to be relatively insensitive to cutting conditions but tool wear.

8.2.3 Fusing AE and vibration data sets in a belief network to provide a more robust tool wear monitoring system

A simple classification technique was used based on the belief network instead of commonly used techniques (for example, neural network). The advantage of belief networks is that the knowledge base can be updated very quickly and efficiently.

8.3 Suggestion for further work

In the course of doing this research, the following ideas have occurred which may be worth further research and development:

8.3.1 Drier air may reduce calibration uncertainty

The main AE source of an air jet arises from the impact of the air stream on the top rake of a tool tip. The consistency of impact depends on the consistency of the mass flow rate of air. The moisture content in the air can affect the mass density and hence the mass flow rate. By connecting a moisture remover in the air supply circuit, drier air can be produced at the prescribed pressure and so the variability in the AE signal can be reduced.

8.3.2 Study the effects of the geometry of the tool post, tool holder and machine on AE propagation

In this research, a comparative study was made on the AErms obtained from two different sensors and locations but on the same tool post, the tool holder and machine. In order to address more thoroughly the issue of transferability, work needs to be done on different tool posts, tool holders and machines.

8.3.3 Investigate a more thorough measure of tool wear rather than just flank wear height

In this research, the measure of wear is chosen to be the flank wear height. However crater wear can sometimes occur and as has been found by other researchers, crater wear can influence AErms especially when the cutting condition is severe (for example, high speed and feed rate). When crater wear is as significant as flank wear, not mention account for crater wear can lead to substantial errors in tool wear classification. It will be useful to have a meaningful measure that can quantify not just the existence of flank wear but also crater wear. The size and /or the contour of both types of wear can be integrated and used to determine the end of tool life.

8.4 Conclusions

1. The methodology for calibrating the acoustic emission signal for the whole tool system was established using the air jet as the calibration source. The AE obtained from different set-ups can be compared in terms of the equivalent pressure.
2. The reliable inferences on the various stages of tool wear were investigated. AErms and the coherence function were extracted from the raw AE and vibration signal and related to the flank wear on a carbide tool tip.
3. The belief network was designed and tested using fused data from AE and acceleration and inferences on tool wear were made.

Acoustic emission measurements can be made transferable using the air jet calibration source. However, recalibration is needed whenever a new insert is used. The system provides real-time condition monitoring at a reasonably low cost, and it does not rely on the experience of the operator.

References

Aindow A.M. , Dewhurst R.J., Hutchins D. A. and Palmer S.B., "Laser-generated ultrasonic pulses at free metal surfaces", J. Acoust.Soc.Am, 69 (2) (1981) 449-455.

Asibu E.K. and Dornfeld D.A. , "Quantitative relationships for acoustic emission from orthogonal metal cutting", Trans.ASME, Journal of Engineering for Industry, 103 (3) (1981) 330-340.

ASTM: Standard method for primary calibration of acoustic emission sensors, E1106-86 (reapproved 1992), 485-494.

Au Y.H.J. and Owen C., "Coherence analysis for tool wear monitoring, Part1-Therory", Proc. Of Int. Conf. COMADEM92, 15-17 July (1992).

Bendat J.S. and Piersol A.G., (1986) "Random data analysis and measurement procedures 2nd edition" A Wiley-Interscience Publisher" New York.

Berlinsky Y., Rosen M., Simmons J. and Wadley H.N.G., "A calibration approach to acoustic emission energy measurement", Journal of Nondestructive Evaluation, 10 (1) (1991) 1-5.

Blum T. and Inasaki I., "A study of acoustic emission from the orthogonal cutting process", Trans. ASME, J. Engineering for Industry, 112 (1990) 203-211.

Blum T., Suzuki I, Inasaki I,"AE monitoring system for the detection of single point and multipoint cutting tool failures", The Japanese Society for NDI, (1988).

Boothroyd G. (1983), "Fundamentals of Metal Machining and Machine Tools", McGRAW-HILL KOGAKUSHA,LTD.

Bueno R., Etxeberria J., "Tool wear monitoring by acoustic emission in turning. Influence of Machined Material on AE signal" Internal report for BRITE programme CECDG XII (1989-1993).

Capitani R. and Citi P.,"Using acoustic emission to assess cutting tool condition" (1984).

Carolan T.A. , Kidd S.R., Hand D.P., Wilcox S.J., Wilkinson P., Barton J.S. , Jones J.D.C. and Reuben R.L. , "Acoustic emission monitoring of tool wear during the face milling of steels and aluminium alloys using a fibre optic sensor", Part1: energy analysis, Proc Instn Mech Engrs, 211(1997) 299-309.

Colwell L. V., "Cutting temperature versus tool wear", Ann.CIRP 24, (1975) 73-76.

Constantinides N., Bennett S., "An investigation of methods for on-line estimation of tool wear", International Journal of Machine Tools and Manufacture 27 (2) (1987) 225-237.

Cook N.H., "Tool wear sensors", Wear 62 (1980) 49-57.

Course Handbook for SNT-TC-1A Qualification (1991), Physical Acoustic Corporation.
Dalpiaz G., Remondi M., "Use of Acoustic emission for Cutting Process Monitoring in Turning", Condition Monitoring, 1 (4) (1988).

Dan L. and Mathew J., "Tool wear and failure monitoring techniques for turning-a review", 1st J.Mach. Tools Manufact, 30 (4) (1990) 579-598.

Diei E.N., Dornfeld D.A., "A model of tool fracture generated acoustic emission during machining", Trans.ASME, Journal of Engineering for Industry, 109 (3) (1987) 229-237.

Dimila D.E., Lister P. M. and Leighton N.J., "Neural network solution to the tool condition monitoring problem in metal cutting - A Critical Review of Methods" Journal of Mechanical Tools Manufacturing, 37 (9) (1997) 1219-1241.

Dimla D.E. and Lister P.M. , "On-line metal cutting tool condition monitoring-1: Force and vibration analyses", International Journal of Machine Tools and Manufacture 40 (5) (2000) 739- 768.

Diniz A.E., Liu J.J. and Dornfeld D.A., "Correlating tool life, tool wear and surface roughness by monitoring acoustic emission in finish turning", Wear, 152 (1992) 395-407.

E.O., Doebelin, (1990), "Measurement Systems, Application and Design", 4th Edition, McGraw-Hill International Editions, P56.

Emel E. And Asibu E.K. "Tool Failure monitoring in turning by pattern recognition analysis of AE signal", Journal of Engineering for Industry, May Vol.110/137 (1988).

Evans M. J. , "The use of diffuse field measurements for acoustic emission", PhD. Thesis, Imperial College of Science, Technology and Medicine, (1997) 196 P.

Gammerman A. (1995), "Probabilistic Reasoning and Bayesian Belief Networks", Alfred Waller Limtied, Oxon RG9 6JF.

Gomayel J.L.E. and Bregger K.D. , "On-line tool wear sensing for turning operations", J. Engng Ind. 108 (1986) 44-47.

Harris R.J. (1975) "A Primer of Multivariate Statistics", University of New Mexico, Academic Press, Inc, New York, P17.

Hatano H. and Watanabe T., "Reciprocity calibration of acoustic emission transducers in Rayleigh-wave and longitudinal-wave sound fields", The Journal of Acoustical society of America, 101 (3) (1997) 1450-1455.

Hatano H., Mori H and E., "Acoustic emission transducer and its absolute calibration", J. Acoustic,Soc. Amer. 59 (2) (1976) 344-349.

Heiple C.R, Carpenter S.H. and Armentrout D.L., "Origin acoustic emission product during single point machining" Proceedings of the 4th World Meeting on Acoustic Emission and 1st International Conference on Acoustic Emission in Manufaturing, ed. S.J. Vahavislos, ASNT, Columbus, OH, (1991) 463-470.

Hewlett packard standard data format utilities user's guide, Hewlett-Packard company, Washington, USA.

Hopko S. N. and Ume I. C, "Laser generated ultrasound by material ablation using fiber optic delivery", Ultrasonics, 37 (1999) 1-7.

HP 89410A Operator's, Hewlett-Packard company, Washington, USA.

Hsu N.N. and Breckenridge F.R., "Characterisation and calibration of acoustic emission sensors", Materials Evaluation, 39 (1981) 60-68.

Inasaki I. and Yunetsu S., "In process of cutting tool damage by acoustic emission measurement" Proceedings of the 22nd MTDR (Machine Tool Design and Research Conference), (1981) 261-268.

Iwata K. and Moriwaki T., "An application of acoustic emission measurement to in-process sensing of tool wear", C.I.R.P. Annals, 26 (1977) 21-26.

Jeon J.U.and Kim W., "Optical flank wear monitoring of cutting tools by image processing", Wear 127 (1988) 207-217.

Juneja B.L. and Sekhon G.S., "Fundamentals of metal cutting and machine tools", New age international (P) limited, publishers.

Lan M.S. and Dornfeld D.A., "In-process tool fracture detection", Journal of Engineering Materials and Technology, 106 (2) (1984) 111-118.

Lee K.S., Lee L.C. and Teo S.C., "On-Line Tool Wear Monitoring using a PC", Journal of Materials Processing Technology, 29(1992).

Leem C.S., Dornfeld D.A. and Dreyfus S.E. " A Customized neural network for sensor fusion in on-line monitoring of cutting Tool Wear", Transaction of the ASME, (117) May (1995) 152-159.

Levi R.,Villa A., Quaglia G., Ghiara R. and Rutelli G., "An expert control system for tool life management in flexible manufacturing cells", Ann. CIRP 34 (1985) 87-90.

Li X.Q. ,Wong Y.S. and Nee A.Y.C., "Tool wear and chatter detection using the coherence function of two crossed acceleration" Int.J.Manufact. 37 (4) (1997) 425-435.

Liao Y. S., Development of a monitoring technique for tool change purpose in turning operations, Proc. 15th Int. Machine Tool Design and Research Conf. (1974) 251-257.

Liebig V., Pridohl E., Koch S.L., Dresden F. E., Hoppe N., "Absolute calibration of acoustic emission (AE) sensors with laser induced surface waves", EWGAE 1998, 23th European Conference on Acoustic Emission Testing, Vienna, May (1998).

Lin J., "Inverse estimation of the tool-work interface temperature in end milling", International journal of Machine tool and Manufacture 35 (5) (1995) 751-760.

Lin S.C., Ting C.J., "Drill wear monitoring using neural networks" Journal of Mechanical Tools Manufacturing, 36 (4) (1996) 465-475.

Liu J.J. and Dornfeld D.A., "Modelling and analysis of acoustic emission in diamond turning", Journal of Manufacturing Science and Engineering, 118 (1996) 199-206.

LOCAN 320 User's Manual (1990), Physical Acoustic Corporation, Princeton, New Jersey.

McBride S. L and Hutchison T.S., "Helium gas jet spectral calibration of acoustic emission transducers and system" Canadian journal of Physics, 56 (1978) 504-507.

McIntire P. (1987), "Nondestructive Testing Handbook Second Edition" Volume 5 Acoustic Emission Testing, American Society for Nondestructive Testing.

Mendenhall W., Beaver R.J. (1999), B.M. Beaver, "Introduction to Probability and Statistics", Tenth edition, Brooks/Cole Publishing Company, USA.

Microset manual, Replica System for Microscopic Surface Inspection, Applied metallurgical services LTD, England.

Milton C.Shaw (1984), "Metal Cutting Principles", Clarendon Press: Oxford.

Model Metal Cutting - A Practical Handbook, (1994), Sandvik Coromant, Sweden.

Moriwaki T., "Detection for cutting tool fracture by acoustic emission measurement", Annals of CIRP Vol.29(1) (1980)35-39.

Netica Manual, Norsys software Corp.

Owen C. and Au Y.H.J., "Coherence analysis for tool wear monitoring, Part2-Results and wear state classification", Proc. Of Int. Conf. COMADEM92, 15-17 July (1992).

Radulescu R., Kapoor S.G. , "An analytical model for prediction of tool temperature fields during continuous and interrupted cutting", ASME Trans, Journal of Engineering for Industry 116 (2) (1994) 135-143.

Rangwala S. and Dornfeld D., "A study of acoustic emission generated during orthogonal metal cutting-1: Energy Analysis, J. Mech.Sci. 33 (6) (1991) 471-487.

Sadat A. B. and Raman S., "Detection of tool flank wear using acoustic signature analysis", Wear 115 (1987) 265-272.

Sata T., Matsushima K. and Kawabata T., "Recognition and control of the morphology of tool failures", Ann. CIRP 28 (1979) 43-47.

Scruby C.B. , Dewhurst R.J., Hutchins D.A. and Palmer S.B., "Qualitative studies of thermally generated elastic waves in laser-irradiated metals", J.Appl.Phys., 51(12) (1980) 6210-6216.

Scruby C.B., Wadley H.N.G., Dewhurst R.J., Hutchins D.A., and Palmer S.B., "A laser-generated standard acoustic emission source". Meterial Evaluation, 39 (1981) 1250-1254.

Suzuki H. and Weinamann K.J., "An on-line tool wear sensor for straight turning operations", J. Engng Ind. 107 (1985) 397-399.

Taglia A.D., Portunato S. and Toni P., "An approach to on-line measurement of tool wear by spectrum analysis", Proc. 17 th Int. Machine Tool Des. And Res. Conf., (1976) 141-148.

Takeyama, H. Sekiguchi H., Murata R. and Matsuzaki , H. "In-process detection of surface roughness in machining", Ann. CIRP 25 (1976) 467-471.

Teti R. and Dornfeld D.A., "Modelling and experimental analysis of acoustic emission from metal cutting", Trans. ASME, Journal of Engineering for Industry, 111(3) (1989) 229-237.

The American Society for Testing and Materials (ASTM): Standard guide for determining the reproducibility of acoustic emission sensor response, E976-94, (1994) 374-379.

Tlusty J. and Andrews G.C., "A critical review of sensors for unmanned machining", Ann. CIRP 32 (1983) 536-572.

Trent E.M.(1991), "Metal Cutting Third Edition", Butterworth Heinemann.

Turkovich B.F. and Kramer B.M., "A comprehensive tool wear model", Ann. CIRP 35 (1986) 67- 70.

Turning Tools-Metalworking Products, (1998), Sandvik Coromant.

Uehara K., "New attempts for short time tool-life testing", Ann. CIRP 22 (1973) 23-34.
Uehara K., "On the mechanism of crater wear of carbide cutting tool", Ann. CIRP 21 (1972) 31-32.

Waschkies E., Skoarczyk C., Hepp K., "Tool wear monitoring at turning", Journal of Engineering for Industry, (116) November (1994) 521-524.

Weller E.J., Schrier H.M. and Weichbrodt B., "What sound can be expected from worn tool?", J. Engng Ind. (104) (1982), 217-223.

Bibliography

Asher R.C., "Ultrasonic Sensors For Chemical and Process Plant" (1997), Institute of Physics Publishing Bristol and Philadelphia, London.

Bendat J.S.and Piersol A.G., (1986), "Random Data Analysis and Measurement Procedures 2nd Edition", John wiley & Sons, Inc. Canada.

Biran and Breiner M., "MATLAB for Engineers" (1995), Addison-Wesley Publishing Company.

Bolton W. (1995), "Complex numbers", Longman Scientific & technical, Enland.
Butler C., Au J. and Griffiths B. (1996), "Manufacturing Measurement Part 2 " Brunel University.

Caudill M. and Butler C.(1992), " Understanding Neural Network", A Bradford Book The MIT Press.

Conor F.R. (1982), " Introductory topics in electronics and telecommunication Signals second editor", Edward Arnold (Publishers) Ltd, London.

Demuth H. and Beale M.(1992), " Neural Nerwork Toolbox For Use with MATLAB", The Math Works,Inc.

Ehrlich C.D. and Rasberry S.D., "Metrological timelines in traceability" Journal of research if the National Institute of Standards and Technology, 103 (1998) 93-105.

Gorman M.R., "Wave propagation and signal analysis", Short course, 38 th U.S. AEWG meeting, Nasa Langley Research Center, 1 May 1995.

Howard Anton (1994), Elementary Linear Algebra, John Wiley & sons, INC., USA.

Jang J.-S. R. and Gulley N. (1995), " Fuzzy Logic Toolbox for Use with MATLAB", The Math Works, Inc. Bart Kosko (1993), "Fuzzy Thinking", Flamingo.

Judith E. Dayhoff (1990), "Neural Network Architectures and Introduction" Van Nostrand Reinhold, New York.

Karu Z. Z. (1995), Signals and Systems Made Ridiculously Simple, ZiZi Press Cambridge, USA.

Matsuda, Y et al, "Calibration of acoustic emission sensors with laser-generate ultrasonic wave", J. Acoustic. Soc.Jpn (E), 13(2) (1992).

Newland D.E. (1993) " Introduction to Random Vibrations, Spectral & Wavelet Analysis", Longman Scientific & Technical.

Ripley R.D. (1996), " Pattern Recognition and Neural Networks", The press syndicate of Cambridge University, UK.

Sweeney G. (1971), "Vibration of Machine tools", The Machinery Publishing CO.LTD.

Tescione D., and Maddalena P., "A new technique for calibration in frequency of piezoelectric transducers" NDT&E International, 32(1999) 71-77.

Tobias S.A (1965), "Machine-Tool Vibration", Blackie & Son LTD, Glasgow.

Appendix A. CNC Program for Machine Workpiece on Traubs Lathe

```
10 G59 X0 Z132;
20 G26;
30 N3 (ROUGHING)
40 G96 V150 T0909 M4;
50 G0 X61.5 Z2 M9;
60 G1 Z-122 F0.3;
70 G1 X64 Z-120;
80 G0 X64 Z2;
90 G0 X30.5 Z2;
100 G1 Z-121.9;
110 G1 X64 Z-120;
120 G26;
130 T0808;
140 M30;
150 %
```

Remark (the meaning of CNC code)

G59: Additive zero point shift
G26: Approach to tool change point
G96: Constant cutting sped
T0909: Tool number 9
M4: Main spindle CCW
G0: Straight line at rapid traverse
G1: Straight line at feed rate
M9: Coolant off
M30: End of program with skip back.

Appendix B. AE 5500 Setting

Command for access program

c:\5500> AET

Local and Alt key commands

Shift + / (To show list of acceptable command options for your current command)

Alt + Q (View the list of Alt key functions available)

Alt + F (Show DOS directory command)

Atl + F4 (Exit program and return to DOS command prompt)

[Ctrl + J] (cancel)

Set up display for sensor 2

[Ctrl + S] U S 2 <space>	(Set up display for sensor 2..)
EN T	(Energy vs. Time)
P T	(Peak amplitude vs. Time)
R C T <space>	(Ring down count vs. Time)

Data recording

[Ctrl + Q] D TEST <space>	(Queue data recording disk file name = TEST.D01)
<space> (yes)	
[Ctrl + B] E <space>	(Even data recording on file TEST.D01)
<space> S 2	(For Sensor 2)
<space>	(Recording reject ratio (between 0-30000))
[Ctrl + B] R	(Begin to run data)
[Ctrl + E] R S 2	(End run for sensor 2)
[Ctrl + E] D	(End data recording on file TEST.D01

Appendix C. Spectrum Analyser Setting

Input - Channels

Setup Channels	1,2
Active Channels	1,2
Input source	FRONT
Range	AUTO
Scale Factor	1.0000
Auto Calibration	OFF

Analysis - FFT

FFT Mode	BASEBAND
Baseband	25KHZ
Lines	500

Average - Type

Average Type	RMS		
Completion	COUNT	Completion Action	STOP
Completion Count	8		

Results Function

Result A

Function	POWER SPECTRUM	Format	MAGNITUDE
Source	CHANNEL 1		
Data Type	AVERAGE		
Voltage Type	PEAK	Voltage Scale	dB
dB Reference	1.000 V		

Result B

Function	POWER SPECTRUM	Format	MAGNITUDE
Source	CHANNEL 2		
Data Type	AVERAGE		
Voltage Type	PEAK	Voltage Scale	dB
dB Reference	1.000 V		

Result C

Function	COHERENCE		
Source	CHANNEL 1	2ND Source	CHANNEL2

Appendix D. Resolution and Record Length Calculation for AE Signals

D1. Maximum time record length

The maximum time record length can be defined as

$$T_{max} = \frac{(FP-1)}{span}$$

Where:

FP = number of frequency points = 401

Span = 1 MHz (0Hz-1MHz)

Then the maximum time record length for the number of frequency point = 400 is

$$T_{max} = \frac{(401-1)}{1\times10^{6}} = 400 \text{ x } 10^{-6} \text{ second}$$

(The number of frequency points was set at 401 (and 3201 points). The span was set to cover 0Hz to 1MHz)

The actual time record length (T) can be calculated form:

$$T = \frac{WBW}{RBW}$$

where:

RBW = resolution bandwidth = 10 kHz

WBW = window bandwidth = 3.8193596

Then

$$T = \frac{WBW}{RWB} = \frac{3.8193596}{10\times10^{3}} = 381.93 \text{ x } 10^{-6} \text{ second}$$

(The resolution bandwidth (RBW) is adjusted automatically by HP, in order to optimise the measurement resolution and measurement speed. The window bandwidth (WBW) is based on a Flattop window.

D2. Time record size

The time record size (TP) can be defined as:

$$TP = SR\times T$$

Where:

SR is sample frequency rate = $2.56 \text{ x } 10^{6}$

Then

$TP = SR \times T$ $= 2.56 \times 10^{6} \times 381.93 \times 10^{-6}$ $= 978$ (977.74)points

(The sample frequency rate was automatically determined by HP 89410A. It is 2.56 times of the span (in baseband mode))

D3. Display resolution

Display resolution = Frequency span/ (Number of frequency points-1)

Then

$$\text{Display resolution} = \frac{1 \times 10^{6}}{401 - 1} = 2.5 \times 10^{3} \text{ Hz}$$

In a similar fashion, the number of frequency points set at 3201 points can be calculated and the parameter were shown below:

RBW = 3×10^{3} Hz

T = 1.27×10^{-3} second

TP = 3260 (3259.19) points

Display resolution = 312.5 Hz

Appendix E. Tool Maker's Microscope Program

Program for measuring the distance between points

```
startp;
loop2;
pick1;
pt1;
endl;
dis1=pt1,pt2
ver
endp;
```

Program for measuring the diameter of a circle

```
startp;
pick4;
cil;
ver;
endp;
```

Appendix F. HP49410A Vector Signal Analyser Setting

Measurement mode:	Vector mode
Frequency span:	Start 0 stop 1Mhz
Data format:	Linear
Window type:	Flat top window
Number of frequency point:	401

Average

Average:	On
Number of average:	70
Average type:	Rms (video)
Repeat average:	off

System utility

Auto zero calibration:	Off (must use single auto zero at least once every 30 minutes)
Auto calibration:	Off
Trigger type :	Off

Appendix G. AErms, Air-Jet Pressure and Variability for Different Stand-off Distances of 1.4-mm Nozzle

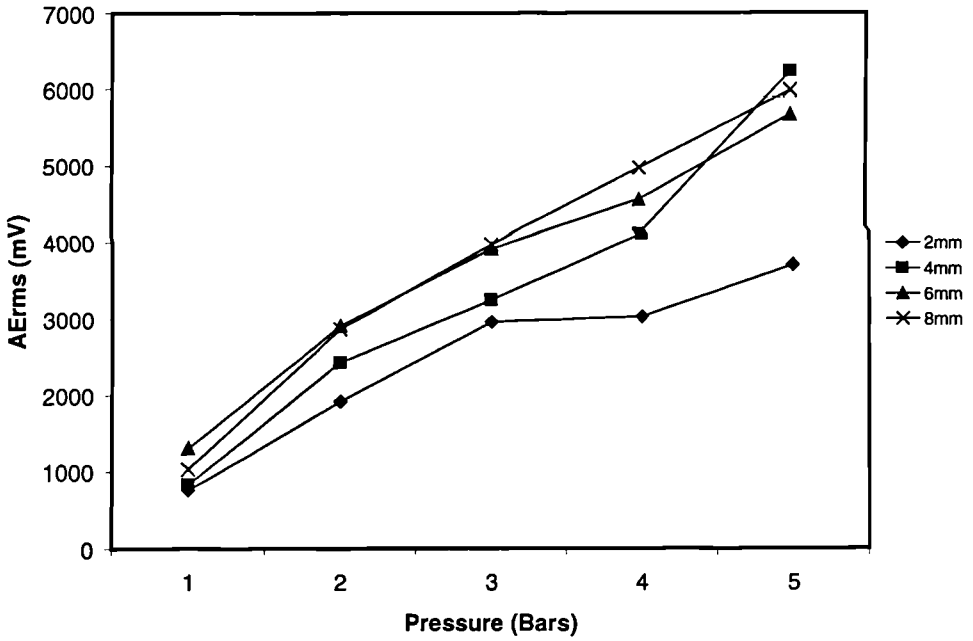

Figure G1. AErms of the air-jet at pressure, 1-5bars and stand-off distances 2-8 mm of 1.4 mm nozzle.

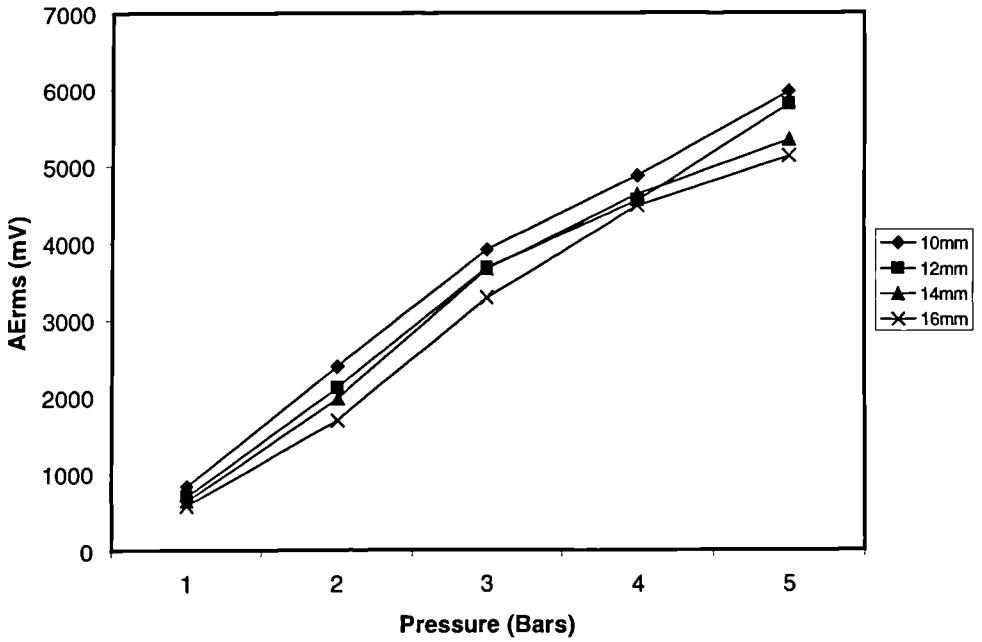

Figure G2. AErms of the air-jet at pressure, 1-5bars and stand-off distances 10-16 mm of 1.4 mm nozzle.

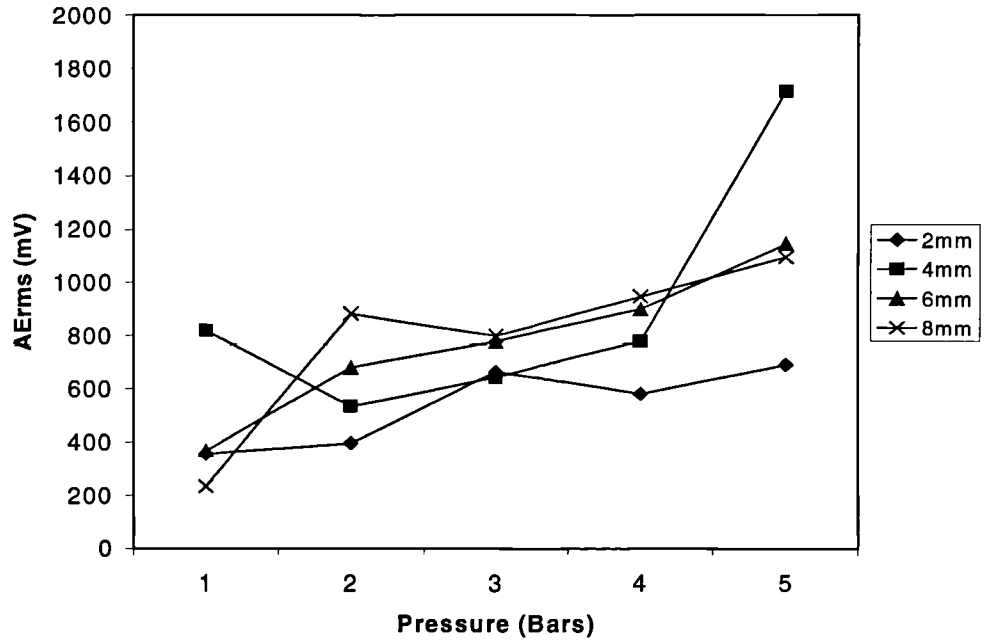

Figure G3. Peak AErms of the air-jet at pressure, 1-5bars and stand-off distances 2-8 mm of 1.4 mm nozzle.

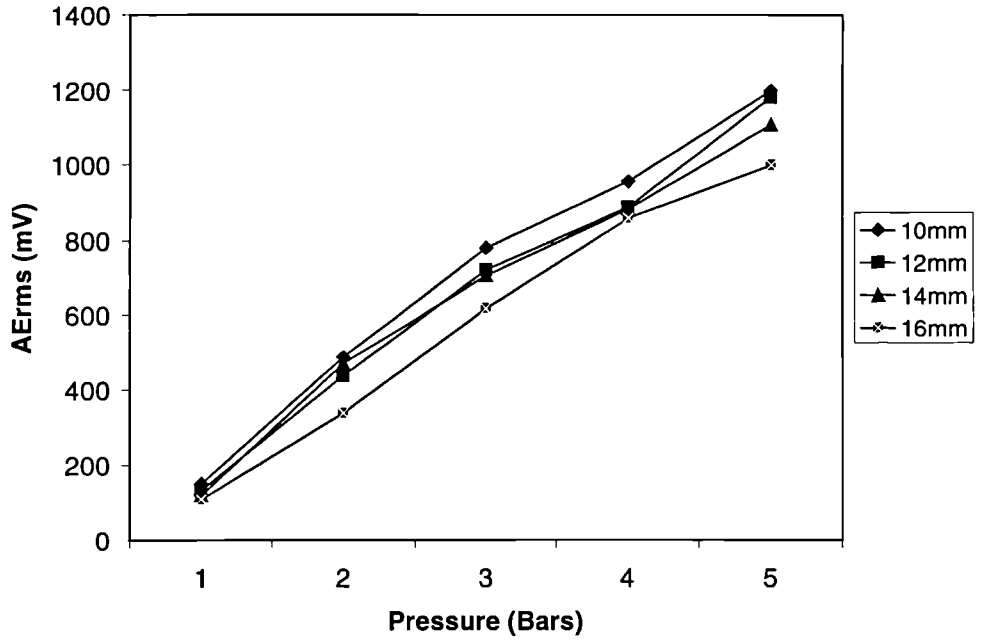

Figure G4. Peak AErms of the air-jet at pressure, 1-5bars and stand-off distances 10-16 mm of 1.4 mm nozzle.

Pressure	Variability of AErms at the stand-off distance (%)							
(bar)	2mm	4mm	6mm	8mm	10mm	12mm	14mm	16mm
1	4.61	6.99	3.27	3.69	3.08	2.04	4.69	3.51
2	1.89	1.52	1.73	3.78	1.50	1.98	2.13	1.83
3	3.03	1.27	1.64	1.26	1.98	1.77	1.62	2.28
4	1.83	1.24	1.42	3.00	3.24	1.41	2.26	2.09
5	2.66	2.53	2.26	1.71	2.00	1.20	3.28	2.30
	2.84	2.76	2.01	2.93	2.45	1.80	2.68	2.43

Table 4.1. Variability of AErms with the 1.4-mm diameter nozzle at different stand-off distances.

Appendix H1. The Case File Used to Train the Belief Network

// ~->[CASE-1]->~

Idnumber	AEpressure	High_end	Low_end	Tool_wear	Cutting_condition
1	13.21	0.16	0.64	not_worn	rough
3	12.13	0.13	0.63	not_worn	rough
5	18.59	0.11	0.75	not_worn	rough
7	20.59	0.12	0.80	not_worn	rough
9	20.75	0.14	0.77	not_worn	rough
11	16.78	0.12	0.86	not_worn	rough
13	20.98	0.14	0.77	not_worn	rough
15	20.11	0.13	0.87	not_worn	rough
17	21.63	0.15	0.84	not_worn	rough
19	20.07	0.14	0.81	not_worn	rough
21	19.66	0.13	0.82	not_worn	rough
23	22.15	0.14	0.82	not_worn	rough
25	20.09	0.12	0.81	not_worn	rough
27	17.53	0.13	0.80	not_worn	rough
29	21.25	0.14	0.78	not_worn	rough
31	20.03	0.12	0.82	not_worn	rough
33	16.71	0.12	0.84	not_worn	rough
35	17.04	0.12	0.82	not_worn	rough
37	20.43	0.15	0.81	not_worn	rough
39	21.50	0.13	0.87	not_worn	rough
41	22.01	0.14	0.83	not_worn	rough
43	21.54	0.12	0.79	not_worn	rough
45	17.82	0.10	0.78	not_worn	rough
47	17.12	0.12	0.71	not_worn	rough
49	19.52	0.13	0.69	not_worn	rough
51	17.90	0.12	0.54	not_worn	rough
53	16.74	0.11	0.65	not_worn	rough
55	16.58	0.13	0.38	not_worn	rough
57	16.63	0.19	0.39	not_worn	rough
59	13.04	0.13	0.43	not_worn	rough
61	11.85	0.12	0.45	not_worn	rough
63	17.95	0.26	0.34	worn	rough
64	19.81	0.29	0.32	worn	rough
65	18.11	0.25	0.36	worn	rough
66	16.90	0.22	0.40	worn	rough
67	30.26	0.17	0.70	not_worn	semi
69	27.80	0.17	0.73	not_worn	semi
71	27.50	0.14	0.83	not_worn	semi
73	27.46	0.18	0.82	not_worn	semi
75	27.41	0.24	0.83	not_worn	semi
77	26.46	0.21	0.85	not_worn	semi
79	32.87	0.37	0.86	not_worn	semi

81	34.41	0.55	0.75	not_worn	semi
83	41.44	0.60	0.52	not_worn	semi
84	35.40	0.59	0.32	worn	semi
85	43.67	0.66	0.33	worn	semi
86	43.72	0.72	0.68	worn	semi
87	42.51	0.64	0.45	worn	semi
89	37.19	0.30	0.51	not_worn	finish
91	34.52	0.28	0.41	not_worn	finish
93	34.87	0.21	0.56	not_worn	finish
95	36.21	0.27	0.50	not_worn	finish
97	35.71	0.32	0.40	not_worn	finish
99	34.51	0.35	0.26	not_worn	finish
101	35.55	0.30	0.28	not_worn	finish
103	32.74	0.28	0.46	not_worn	finish
105	34.81	0.34	0.58	not_worn	finish
107	40.00	0.30	0.53	not_worn	finish
109	36.70	0.24	0.51	not_worn	finish
111	37.85	0.33	0.54	not_worn	finish
113	37.39	0.36	0.54	not_worn	finish
115	32.40	0.41	0.53	not_worn	finish
117	27.41	0.47	0.51	not_worn	finish
119	24.22	0.52	0.58	worn	finish
120	29.14	0.52	0.58	worn	finish
121	43.23	0.46	0.24	worn	finish
122	43.01	0.39	0.55	worn	finish

Appendix H2. The Case File Used to Test the Belief Network

// ~->[CASE-1]->~

Idnumber	AEpressure	High_end	Low_end	Tool_wear	Cutting_condition
2	11.38	0.11	0.59	not_worn	rough
4	15.23	0.10	0.69	not_worn	rough
6	19.16	0.12	0.78	not_worn	rough
8	22.01	0.13	0.81	not_worn	rough
10	17.13	0.15	0.72	not_worn	rough
12	23.39	0.14	0.83	not_worn	rough
14	17.34	0.13	0.81	not_worn	rough
16	19.41	0.14	0.88	not_worn	rough
18	19.23	0.12	0.84	not_worn	rough
20	18.69	0.13	0.81	not_worn	rough
22	20.98	0.10	0.85	not_worn	rough
24	22.80	0.11	0.87	not_worn	rough
26	14.21	0.10	0.84	not_worn	rough
28	19.86	0.15	0.80	not_worn	rough
30	16.73	0.14	0.85	not_worn	rough
32	18.46	0.12	0.79	not_worn	rough
34	22.39	0.13	0.85	not_worn	rough
36	16.23	0.12	0.83	not_worn	rough
38	20.97	0.13	0.77	not_worn	rough
40	22.18	0.15	0.76	not_worn	rough
42	21.42	0.12	0.78	not_worn	rough
44	18.84	0.12	0.81	not_worn	rough
46	22.45	0.15	0.84	not_worn	rough
48	18.32	0.12	0.69	not_worn	rough
50	17.86	0.12	0.59	not_worn	rough
52	19.81	0.11	0.65	not_worn	rough
54	17.29	0.19	0.51	not_worn	rough
56	20.22	0.13	0.39	not_worn	rough
58	14.00	0.16	0.37	not_worn	rough
60	13.61	0.14	0.40	not_worn	rough
62	11.63	0.13	0.55	not_worn	rough
64	19.81	0.29	0.32	worn	rough
66	16.90	0.22	0.40	worn	rough
68	28.51	0.20	0.67	not_worn	semi
70	23.03	0.21	0.74	not_worn	semi
72	27.44	0.18	0.77	not_worn	semi
74	27.76	0.23	0.73	not_worn	semi
76	27.33	0.27	0.86	not_worn	semi
78	28.15	0.36	0.71	not_worn	semi
80	33.13	0.44	0.84	not_worn	semi
82	35.82	0.65	0.60	not_worn	semi

84	35.40	0.59	0.32	worn	semi
86	43.72	0.72	0.68	worn	semi
88	35.39	0.41	0.29	not_worn	finish
90	34.73	0.24	0.55	not_worn	finish
92	38.68	0.31	0.28	not_worn	finish
94	38.07	0.24	0.53	not_worn	finish
96	40.02	0.31	0.47	not_worn	finish
98	36.83	0.33	0.33	not_worn	finish
100	32.80	0.37	0.27	not_worn	finish
102	33.35	0.27	0.54	not_worn	finish
104	33.90	0.36	0.61	not_worn	finish
106	37.66	0.32	0.55	not_worn	finish
108	32.85	0.27	0.50	not_worn	finish
110	36.96	0.28	0.48	not_worn	finish
112	36.74	0.31	0.51	not_worn	finish
114	34.90	0.39	0.54	not_worn	finish
116	29.91	0.44	0.52	not_worn	finish
118	27.68	0.50	0.50	not_worn	finish
120	29.14	0.52	0.58	worn	finish
122	43.01	0.39	0.55	worn	finish

Appendix H3. Calculation of Posterior Probability of the Tool Wear Node.

From Bayes' theorem

$$P(S_i \mid A) = \frac{P(A \mid S_i)P(S_i)}{\sum_{j=1}^{k} P(A \mid S_j)P(S_j)}$$

where

$P(S_i|A)$ = P (not_worn tool | Cutting_condition = rough,
AEpressure = 13bars, High_end = 0-0.2, Low_end = 0-0.45)

$P(S_i)$ = P (not_worn_tool/ Cutting condition = rough)
$P(S_j)$ = P (worn_tool/ Cutting condition = rough)
$P(A)$ = P(AEpressure =13bars, High_end = 0-0.2, Low_end = 0-0.45)

From table
$P(S_i)$ = P (not_worn_tool/ Cutting condition = rough) = 0.86
$P(S_j)$ = P(worn_tool/ Cutting condition = rough) = 0.14

P(AEpressure =13bars | not_worn tool , rough) = 0.86
P(AEpressure =13bars | worn tool , rough) = 0.13

P(High_end = 0-0.2 | not_worn tool , rough) = 0.91
P(High_end = 0-0.2 | worn tool , rough) = 0.13

P(Low_end = 0-0.45 | not_worn tool , rough) = 0.12
P(Low_end = 0-0.45 | worn tool , rough) = 0.83

Substituting Bayes' theorem

$$P(S_i \mid A) = \frac{(0.86\times0.91\times0.12)\times0.86}{(0.86\times0.91\times0.12)\times0.86+(0.13\times0.13\times0.83)\times0.14}$$

$$= 0.82$$

Appendix I: Papers Published

A. Prateepasen, Y. H. J. Au and B.E. Jones, Comparison of Artificial Acoustic Emission Sources as Calibration Sources for Tool Wear Monitoring in Single-Point Machining, "Proceedings of the 24th European Conference on Acoustic Emission Testing" (Senlis, 24-26. May 2000), CETIM, France, 2000. P.253-260
(Published in Journal of Acoustic Emission Vol 18, 2000. P 196-204)

A. Prateepasen, Y. H. J. Au, Acoustic Emission and Vibration for Tool Wear Monitoring in Single-Point Machining Using Belief network, "Doctoral Research Conference 2000", (Brunel, 14-15 September 2000), UK, 2000
(Accepted by "IMTC 2001 Instrumentation and Measurement Technology Conference" (Budapest 21-24 May 2001), Hungary, 2001.

A. Prateepasen, Y. H. J. Au and B.E. Jones, Calibration of Acoustic Emission for Tool Wear Monitoring, "XVI IMEKO World Congress" (Vienna 25-28. September 2000), Austria, 2000, Volume VI, P. 255-260.

Comparison of Artificial Acoustic Emission Sources as Calibration Sources for Tool Wear Monitoring in Single-Point Machining

A. Prateepasen, Y. H. J. Au and B. E. Jones
The Brunel Centre for Manufacturing Metrology,
Brunel University, Uxbridge, Middlesex UB8 3PH

Abstract: *Two artificial acoustic emission (AE) sources, an air jet and a pulsed laser, were evaluated in reference to their suitability as a calibration source for single-point machining and tool wear monitoring. The air jet source was found to have a more similar RMS AE-spectrum to that obtained from machining than the pulsed laser source. The RMS value of the AE signal (AErms) produced by the air jet source was observed to be linearly proportional to the air pressure applied and sensitive to the torque used to tighten the insert onto the tool holder. When the applied torque was greater than 1.2 Nm, the AErms remained constant. Thus, once the tightening torque is above this threshold, the AErms value obtained from a sensor can be converted into an air pressure value. In this way, providing a set-up is calibrated using the air jet source under a defined condition, results obtained from different set-ups, having been identically calibrated, can be compared, thus facilitating a transfer and sharing of knowledge.*

1. INTRODUCTION

Research into the use of acoustic emission (AE) for tool wear monitoring [1-10] has established that there exists a definite relation between AE and tool wear. Attempts were made to model the AE process in machining, but despite the fact that general trends could be predicted satisfactorily, the absolute values of AE produced in apparently identical machining processes could still differ markedly from one set-up to another.

The root cause of the problem is that the components that make up the AE transmission and measurement system as well as the interfaces between the components are highly variable. For single-point machining, typically, the components comprise an insert, a tool-holder and a sensor whereas the interfaces refer to those that occur between the tool insert and the tool-holder; and between the tool-holder and the sensor. Changes in either the components or the interfaces can produce a very different AE response. A striking example is the coupling between the insert and the tool-holder where, as will be reported in this paper, an increase in the clamping torque on the insert results in a significant drop in the root-mean-square value of the AE signal (AErms). Consequently, AE results obtained from different research centres are not easy to compare making knowledge transfer at best difficult, if not impossible.

To achieve transferability of results and hence knowledge, some form of AE calibration is necessary. The process of calibration involves a measurement procedure carried out under specified conditions. Its objective is to establish the relationship between the value of a quantity as indicated by a measuring instrument and the corresponding value from a reference standard. When the result of the measurement can be ultimately related to a stated reference, such as a national or international standard, through an unbroken chain of comparisons all having stated uncertainties, then the measurement is said to be traceable to the standard.

It is important to note that the calibration of a sensor, as is conventionally done, in order to determine the AE at the sensing element of the sensor is not of much practical value. This is because one is often only interested in the character of AE at its source, for example, at the cutting edge in machining. What is immensely more useful is the calibration of the whole AE system with the location of the AE source known and the point of the sensor attachment decided. Understandably, once the layout of the source and sensor is changed, the system has to be calibrated again.

In this paper, two artificial AE sources, an air jet source and a pulsed laser source, were studied to assess their suitability as an AE calibration source for the single-point machining process. The effects on the AE were investigated of the clamping torque applied to the tool insert and a calibration procedure was suggested.

2. ARTIFICIAL AE SOURCES

Based on the wave shapes, artificial AE sources can be classified into three different categories [11] as:

1. Noise – produced from, for example, helium gas jet impact, fracture of silicon carbine particles, stress corrosion cracking and phase transformation in AU-47.5% Cd;
2. Continuous waves - generated by exciting piezoelectric, electro-magnetic and electro-static devices;
3. Impulses – arising from sparks, breakage of glass capillary, breakage of pencil lead, dropping of a steel ball on a hard surface to produce an impact, point-contact resistive heating and laser pulse heating.

Berlinskey [12] used two artificial sources, a dropping ball and a pulsed laser, in the study of martensitic transformation in Fe-30. McBride [13] used a helium gas jet to calibrate the AE system for measuring crack propagation in the vicinity of a notch. Evans [14] tested the diffuse field theory with a conical piezoelectric AE transmitter and sensor.

The American Society for Testing Materials (ASTM) issued a standard guide E976-94 for determining the reproducibility and checking for degradation of AE sensors [15]. It recommended three artificial AE sources: an electrically driven ultrasonic sensor, a gas jet and an impulsive source produced by breaking pencil lead. The standard guideline E1106-86 [16] used a step point-force by breaking a glass capillary against a very large steel block.

To qualify as an AE calibration source in tool wear monitoring, the source should possess similar characteristics to the AE sources produced in machining, in addition to the also important characteristic of reproducibility. Here, similarity suggests that the comparing sources have RMS AE-spectra that closely resemble each other in appearance.

The pulsed laser has been frequently used as an artificial AE source in the past two decades [17-20] for a number of reasons. Firstly, the laser source is broad-band and highly reproducible because the pulse parameters can be clearly defined and tightly controlled. Secondly, the energy of a laser pulse is readily quantifiable once the electrical parameters that drive the laser are known. Thirdly, laser can be delivered to remote locations via optical fibres. However, a pulsed laser is not without its drawbacks: it is expensive, requires stringent safety consideration and produces low power, hence weak AE, when, by necessity, operated within the thermo-elastic range so as not to cause damage to the impinged surface.

In many respects, an air jet source is similar to the helium jet source. The advantages of the air jet source are that it is non-contact, inexpensive, relatively safe, portable and readily available in a machine shop. The disadvantage is that the behaviour of an air jet in respect of the AE produced is affected by a host of environmental factors such as temperature and humidity.

3. Similarity Coefficient

An n-point RMS discrete AE-spectrum can be thought of as a vector u defining a point in the n-dimensional vector space. By analogy with vectors in the three-dimensional space, the length squared of u is the inner product of u with itself. Thus, the length of u can be computed from

$$|u| = \sqrt{u.u} = \sqrt{\sum_{k=1}^{n} u_k^2} \,. \qquad (1)$$

This length is the same as the AErms of the signal from which the n-point discrete spectrum is derived. The vector u can be normalised by dividing its elements by the length of the vector. A normalised vector, denoted by $\overline{u}$, has a unit length.

Given two normalised vectors, $\overline{u}$ and $\overline{v}$, in the n-dimensional space, the included angle θ between them is related to the inner product of $\overline{u}$ and $\overline{v}$ as

$$\cos\theta = \overline{u}.\overline{v} \,. \qquad (2)$$

If the two vectors are identical, then $cos\theta = 1$, whereas if they are orthogonal to each other, meaning that the projection of one vector on the other is zero, then $cos\theta = 0$. Since the value of $cos\theta$ suggests the degree of similarity between the two vectors, it is named the *similarity coefficient.*

4. AE COMPARISON OF AIR JET, LASER AND MACHINING

Three sets of tests were conducted to compare the shapes of the RMS AE-spectra obtained from single-point machining, the air jet and the pulsed laser. The repeatability of RMS AE-spectra from the air jet and pulsed laser sources was also assessed.

4.1 Machining tests

Machining tests were performed with the cutting process variables changing as follows:

- Surface cutting speeds from 80 to 150 m/min;
- Feed rates from 0.1 to 0.4 mm/rev; and
- Depths of cut from 0.3 to 1.0 mm.

The work-piece was made from EN24T (0.35-0.45 % carbon) and measured 63.5-mm diameter by 150 mm length. Tool inserts of type GC 4035 DCMT 11 T3 04 UF and a tool shank of type SDJCL 1616H 11 (Sandvik Coromant) were used. Details of the insert geometry are: cutting edge length 11mm, insert thickness 3.97mm, insert shape 55°, rake angle 0°, clearance angle 7° and nose radius 0.4 mm.

A broad band AE sensor (125 kHz – 2 MHz) was mounted at the end of the tool holder with silicone rubber compound. A Hewlett Packard HP 89410A Vector Signal Analyser was used to produce a 401-line RMS AE-spectrum with frequency from 0 to 1 MHz averaged over 70 consecutive spectra.

4.2 Air Jet Tests

As shown in the block diagram of Figure 1, air from an air supply passed through an air filter, a precision regulator, a precision pressure gauge, an on/off valve and a nozzle sequentially, emerging as an air jet.

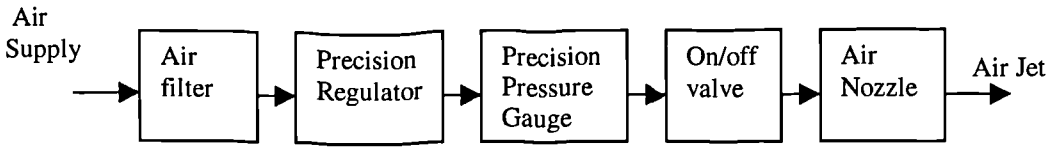

Figure 1. Block diagram of the air jet equipment.

The air jet was directed normally at the top rake surface of the insert, 3 mm from the nose tip and equally distant from the leading and trailing edges of the insert. The insert was clamped to the tool-holder with a clamping torque of 2 Nm and the tool holder was, in turn, held in a fixture. Both the stand-off distance from, and the location of the point of impact on, the rake face were controlled by micrometers. The measuring instruments and their settings were the same as those for the machining tests. Two resolutions of the frequency spectrum were used, namely 401 and 3201 lines. The schematic diagram of the AE signal propagation path is shown in Figure 2.

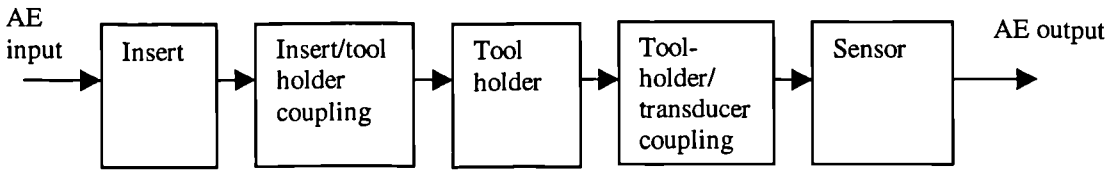

Figure 2. Schematic diagram showing the signal propagation path of AE in tool wear monitoring.

The tests were performed with two different sizes of nozzle diameters: 1.0 mm and 1.4 mm. The stand-off distance was varied from 2 to 16 mm, in increments of 2mm. The air jet pressure was varied between 1 and 5 bars, in increments of 1 bar.

4.3 Pulsed Laser Test

A pulsed Nd: YAG laser system was used as the laser source. The energy of the laser was such chosen that it was insufficient to cause damage to the insert. The energy level of the laser was measured with a laser power meter which registered a value of 3 mJ when the tip of the optical fibre was 2 mm away from the measuring matt black surface. The procedure and the set up of the measuring system were the same as those for the air jet tests excepting the spectrum resolution which was 3201 lines.

5. SIMILARITY OF ARTIFICIAL AND MACHINING AE SOURCES

All RMS AE-spectra from the machining tests have similar appearance with the average spectrum as shown in Figure 3.

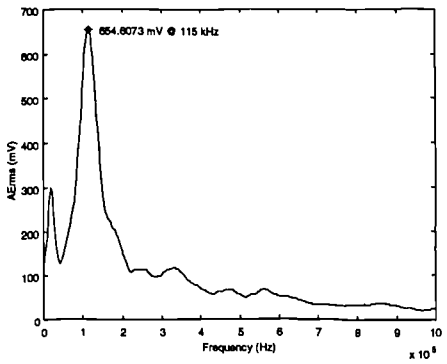

Figure 3. RMS AE-spectrum from machining EN24T with a GC 4035 insert.

Figures 4 and 5 show the typical AE time signals of the air jet and the pulsed laser. The air jet waveform is continuous whereas the pulsed laser is of burst type.

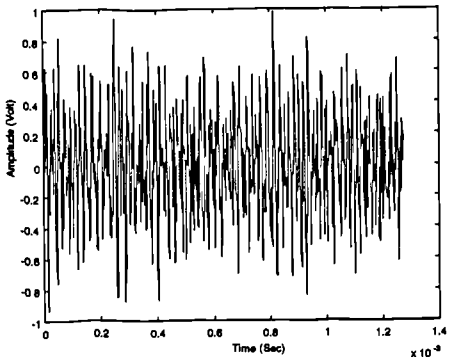

Figure 4. Time domain of the air jet.

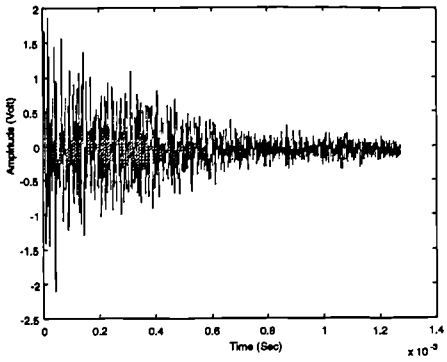

Figure 5. Time domain of the laser.

Figures 6 and 7 show the RMS AE-spectra for the two different artificial sources. It is evident that both the air jet and pulsed laser sources produced sufficient frequency bandwidth, 100 kHz –500 kHz, for tool wear monitoring purposes but the energy level of the pulsed-laser source is much lower.

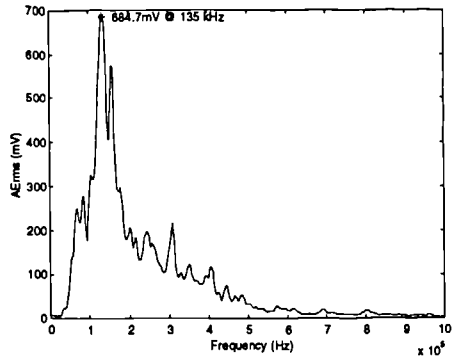

Figure 6. Power spectrum of the air jet.

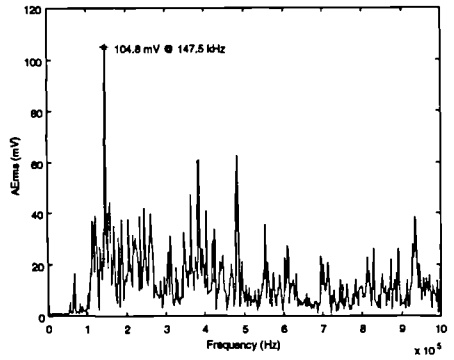

Figure 7. Power spectrum of the laser pulsed.

Using the machining RMS AE-spectrum as the reference, its extent of similarity compared to the air-jet source and the pulsed-laser source, expressed in terms of the similarity coefficients as defined in Equation (2), are 0.8653 and 0.5604 respectively. This result is to be expected as is apparent from the RMS AE-spectra of Figures 3, 6 and 7.

6. AE AND AIR-JET PRESSURE AT DIFFERENT STAND-OFF DISTANCES

Using Equation (1), the AErms value of the AE signal was calculated. For the air jet tests, the relationship was established between the AErms and the air-jet pressure at a stand-off distance from 2 to 16 mm, with bore diameters at the nozzle of 1 mm and 1.4 mm. The shapes of the RMS AE-spectra at the two bore diameters were similar but the peak magnitude was higher for the bore diameter of 1.4 mm. On the other hand, the 1-mm diameter nozzle produced spectra that had lower variability. Using the 1-mm diameter nozzle, the relation between AErms and the air-jet pressure for different stand-off distances is as shown in Figure 8. The variability of the AErms, defined as the ±1 standard deviation divided by the mean, was ± 2.62 %.

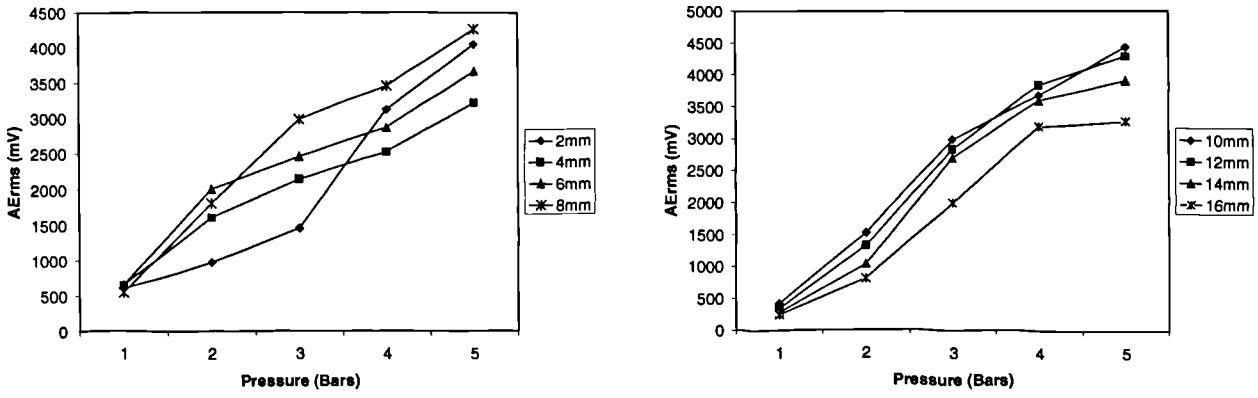

Figure 8. AErms of the air-jet at pressure, 1-5bars, at stand-off distances (a) 2-8 mm, and (b) 10-16mm.

The condition at the stand-off distance of 2 mm and pressure of 2 bars was chosen to show the variability of the measurements. These were the lowest values amongst the set of stand-off distances and pressures tested.

Peak amplitude on the RMS AE-spectrum with 401-point resolution = ± 5.05 %
Peak amplitude on the RMS AE-spectrum with 3201-point resolution = ± 5.84 %
AErms from the RMS AE-spectrum with 401-point resolution = ± 1.14 %
AErms from the RMS AE-spectrum with 3201-point resolution = ± 1.27 %

For the pulsed laser tests, the variability of the measurements at the stand-off distance of 2mm and laser energy of 3 mJ are:

Peak amplitude on the RMS AE-spectrum with 3201-point resolution = ±2.02%
AErms from the RMS AE-spectrum with 3201-point resolution = ± 1.92 %

It is observed from these results that both artificial sources have similar variability.

7. AE, AIR JET PRESSURE AND INSERT CLAMPING TORQUE

Air jet tests were conducted to study the effects of different sensor location and of different insert clamping torque on the AErms. Similar to the air-jet tests in Section 4.2, the air jet was positioned vertically above the top rake face of the insert 2 mm inwards from both the leading and trailing edges of the insert, at a stand-off distance of 5 mm. Three pairs of AE sensors were mounted with the first of each pair on the tool holder and the second on the tool post, all held in position using a silicone rubber compound. These were all PAC sensors and the pairs were: WD and WD with response bandwidth of 100kHz-1MHz, UT1000 and UT1000 with response bandwidth of 60 kHz-1MHz, R30 (100 kHz-400 kHz) and R15 (50kHz-200kHz). The outputs of these sensors were amplified by 60dB and band-pass filtered from 20kHz to 1MHz. The Hewlett Packard HP89410A Vector Signal Analyser was used to produce an RMS AE-spectrum with 401-point resolution averaged over 70 successive spectra. The insert was tightened to three levels of torque, namely 0.4 Nm, 1.2 Nm and 2.0 Nm. The air-jet pressure was varied between 3 and 8 bars in 1-bar increments.

Results showed that the AErms were linearly proportional to the air-jet pressure applied for all levels of clamping torque. It was also observed that the AErms was the highest at the torque value of 0.4 Nm, therefore suggesting that the AErms was sensitive to the torque applied. The graph for the clamping torque of 2.0 Nm is as shown in Figure 9.

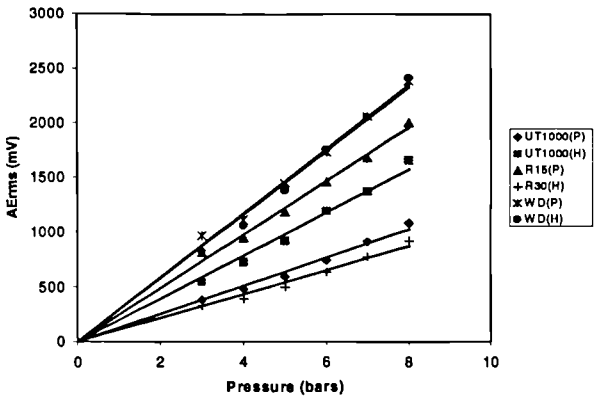

Figure 9. AErms related to air jet pressure for different sensors.

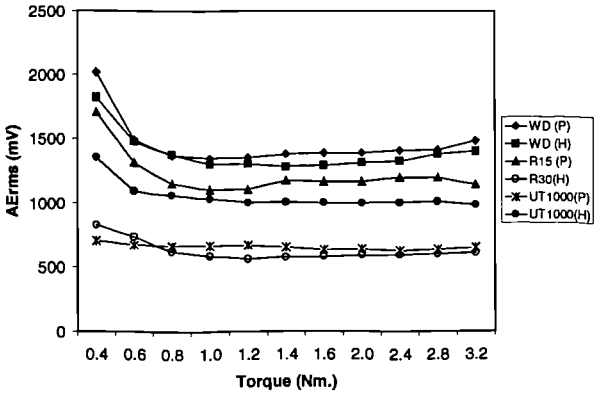

Figure 10. AErms related to clamping torque at constant pressure of 5 bars.

To study the relation between clamping torque and AErms, the air-jet pressure was fixed at 5 bars whilst the clamping torque was changed from 0.4 Nm to 3.2 Nm using an adjustable torque wrench. The results, as in Figure 10, show that the AErms decreases as the torque increases from 0.4 to1.2 Nm and then remains constant from 1.2 Nm to 3.2 Nm. The ratios of AErms between the different pairs of sensors, one on the tool holder and the other on the tool post, were calculated for each value of clamping torque and they are as shown in the table below:

Sensor pair	Mean of ratios	Standard Deviation of ratios	Variability (%)
WD/WD	1.049	0.031	2.984
UT1000/UT1000	0.630	0.038	6.093
R30/R15	2.223	0.076	3.411

8. CONCLUSION

Compared to the pulsed laser, the air jet is more suitable as an artificial calibration source for measuring systems used for machining study and tool wear monitoring. This is because the air jet source has an RMS AE-spectrum more similar to that observed in machining than the pulsed laser, is relative safe to use, is less expensive and is more readily available in a workshop.

For a fixed stand-off distance, the AErms of the air-jet increases linearly with the air-jet pressure. The clamping torque applied to the insert can affect the AErms if the torque value is low; but when the clamping torque exceeds 1.2 Nm, the AErms remains constant. A safe clamping torque for the tool holder used in this research is around 2 Nm beyond which there is the risk of damaging the hexagonal head of the tightening screw.

In summary, a calibration procedure may be suggested as follows. With the insert clamping torque above 1.2 Nm, the AErms value obtained from a sensor can be converted into an air pressure value using the calibration graphs such as Figures 8 and 9. In this way, providing a set-up is calibrated using the air jet source under a prescribed condition, results obtained from different set-ups that have been calibrated in the same manner, can be compared.

ACKNOWLEDGEMENTS

The authors wish to acknowledge support from the INTErSECT Faraday Partnership, the Engineering and Physical Sciences Research Council and the Royal Thai Government.

REFERENCES

(1) E.N.Diei and D.A.Dornfeld, "A model of tool fracture generated acoustic emission during machining", *Trans.ASME, Journal of Engineering for Industry*, 109 (3) (1989) 229-237.

(2) E. Kannatey-Asibu, Jr. and D.A.Dornfeld, "Quantitative relationships for acoustic emission from orthogonal metal cutting", *Trans.ASM, Journal of Engineering for Industry*, 103 (3) (1981) 330-340.

(3) L. Dan and J.Mathew, "Tool wear and failure monitoring techniques for turning-a review", *1st J.Mach. Toos Manufact*, 30 (4) (1990) 579-598.

(4) R.Teti and D.A. Dornfeld, "Modelling and experimental analysis of acoustic emission from metal cutting", *Trans. ASME, Journal of Engineering for Industry*, 111(3) (1989) 229-237.

(5) M.S. Lan and D.A Dornfeld, "In-process tool fracture detection", *Journal of Engineering Materials and Technology*, 106 (2) (1984) 111-118.

(6) T. Blum and I. Inasaki, "A study of acoustic emission from the orthogonal cutting process", *Trans. ASME, J. Engineering for industry*, 112 (1990) 203-211.

(7) A.E. Diniz, J.J. Liu and D.A. Dornfeld, "Correlating tool life, tool wear and surface roughness by monitoring acoustic emission in finish turning", *Wear*, 152 (1992) 395-407.

(8) J.J. Liu and D.A. Dornfeld, "Modelling and analysis of acoustic emission in diamond turning", *Journal of Manufacturing Science and Engineering*, 118 (1996) 199-206.

(9) T. A Carolan, S.R. Kidd, D. P. Hand, S. J. Wilcox, P. Wilkinson, J. S. Barton, J. D. C. Jones and R.L. Reuben, "Acoustic emission monitoring of tool wear during the face milling of steels and aluminium alloys using a fibre optic sensor", Part1: energy analysis, *Proc Instn Mech Engrs*, 211(1997) 299-309.

(10) K. Iwata and T. Moriwaki, "An application of acoustic emission measurement to in-process sensing of tool wear", *C.I.R.P. Annals*, 26 (1977) 21-26.

(11) N.N. Hsu and F.R. Breckenridge, "Characterisation and calibration of acoustic emission sensors", *Materials Evaluation*, 39 (1981) 60-68.

(12) Y. Berlinsky, M. Rosen, J. Simmons and H.N.G. Wadley, "A calibration approach to acoustic emission energy measurement", *Journal of Nondestructive Evaluation*, 10 (1) (1991).

(13) S. L.McBride and T.S. Hutchison, "Helium gas jet spectral calibration of acoustic emission transducers and system" *Canadian journal of Physics*, 56 (1978) 504-507.

(14) M. J. Evans, "The use of diffuse field measurements for acoustic emission", PhD. Thesis, Imperial College of Science, Technology and Medicine, (1997) 196 P.

(15) The American Society for Testing and Materials (ASTM): Standard guide for determining the reproducibility of acoustic emission sensor response, E976-94, (1994) 374-379.

(16) ASTM: Standard method for primary calibration of acoustic emission sensors, E1106-86 (reapproved 1992), 485-494.

(17) Y. Berlinsky, M.Rosen, J. Simmons and H.N.G. Wadley, "A calibration approach to acoustic emission energy measurement", *Journal of Nondestructive Evaluation*, 10 (1) (1991) 1-5.

(18) A.M. Aindow, R.J. Dewhurst, D. A. Hutchins and S.B. Palmer, "Laser-generated ultrasonic pulses at free metal surfaces", *J. Acoust.Soc.Am.*69 (2) (1981) 449-455.

(19) C.B. Scruby, R.J. Dewhurst, D.A. Hutchins and S.B. Palmer, "Qualitative studies of thermally generated elastic waves in laser-irradiated metals", *J.Appl.Phys.*, 51(12) (1980) 6210-6216.

(20) S. N. Hopko and I. C Ume, "Laser generated ultrasound by material ablation using fiber optic delivery", *Ultrasonics*, 37 (1999) 1-7.

Comparison of Artificial Acoustic Emission Sources as Calibration Sources for Tool Wear Monitoring in Single-Point Machining

A. Prateepasen, Y. H. J. Au and B. E. Jones
The Brunel Centre for Manufacturing Metrology,
Brunel University, Uxbridge, Middlesex UB8 3PH

Abstract: *Two artificial acoustic emission (AE) sources, an air jet and a pulsed laser, were evaluated in reference to their suitability as a calibration source for single-point machining and tool wear monitoring. The air jet source was found to have a more similar RMS AE-spectrum to that obtained from machining than the pulsed laser source. The RMS value of the AE signal (AErms) produced by the air jet source was observed to be linearly proportional to the air pressure applied and sensitive to the torque used to tighten the insert onto the tool holder. When the applied torque was greater than 1.2 Nm, the AErms remained constant. Thus, once the tightening torque is above this threshold, the AErms value obtained from a sensor can be converted into an air pressure value. In this way, providing a set-up is calibrated using the air jet source under a defined condition, results obtained from different set-ups, having been identically calibrated, can be compared, thus facilitating a transfer and sharing of knowledge.*

1. INTRODUCTION

Research into the use of acoustic emission (AE) for tool wear monitoring [1-10] has established that there exists a definite relation between AE and tool wear. Attempts were made to model the AE process in machining, but despite the fact that general trends could be predicted satisfactorily, the absolute values of AE produced in apparently identical machining processes could still differ markedly from one set-up to another.

The root cause of the problem is that the components that make up the AE transmission and measurement system as well as the interfaces between the components are highly variable. For single-point machining, typically, the components comprise an insert, a tool-holder and a sensor whereas the interfaces refer to those that occur between the tool insert and the tool-holder; and between the tool-holder and the sensor. Changes in either the components or the interfaces can produce a very different AE response. A striking example is the coupling between the insert and the tool-holder where, as will be reported in this paper, an increase in the clamping torque on the insert results in a significant drop in the root-mean-square value of the AE signal (AErms). Consequently, AE results obtained from different research centres are not easy to compare making knowledge transfer at best difficult, if not impossible.

To achieve transferability of results and hence knowledge, some form of AE calibration is necessary. The process of calibration involves a measurement procedure carried out under specified conditions. Its objective is to establish the relationship between the value of a quantity as indicated by a measuring instrument and the corresponding value from a reference standard. When the result of the measurement can be ultimately related to a stated reference, such as a national or international standard, through an unbroken chain of comparisons all having stated uncertainties, then the measurement is said to be traceable to the standard.

It is important to note that the calibration of a sensor, as is conventionally done, in order to determine the AE at the sensing element of the sensor is not of much practical value. This is because one is often only interested in the character of AE at its source, for example, at the cutting edge in machining. What is immensely more useful is the calibration of the whole AE system with the location of the AE source known and the point of the sensor attachment decided. Understandably, once the layout of the source and sensor is changed, the system has to be calibrated again.

In this paper, two artificial AE sources, an air jet source and a pulsed laser source, were studied to assess their suitability as an AE calibration source for the single-point machining process. The effects on the AE were investigated of the clamping torque applied to the tool insert and a calibration procedure was suggested.

2. ARTIFICIAL AE SOURCES

Based on the wave shapes, artificial AE sources can be classified into three different categories [11] as:

1. Noise – produced from, for example, helium gas jet impact, fracture of silicon carbine particles, stress corrosion cracking and phase transformation in AU-47.5% Cd;
2. Continuous waves - generated by exciting piezoelectric, electro-magnetic and electro-static devices;
3. Impulses – arising from sparks, breakage of glass capillary, breakage of pencil lead, dropping of a steel ball on a hard surface to produce an impact, point-contact resistive heating and laser pulse heating.

Berlinskey [12] used two artificial sources, a dropping ball and a pulsed laser, in the study of martensitic transformation in Fe-30. McBride [13] used a helium gas jet to calibrate the AE system for measuring crack propagation in the vicinity of a notch. Evans [14] tested the diffuse field theory with a conical piezoelectric AE transmitter and sensor.

The American Society for Testing Materials (ASTM) issued a standard guide E976-94 for determining the reproducibility and checking for degradation of AE sensors [15]. It recommended three artificial AE sources: an electrically driven ultrasonic sensor, a gas jet and an impulsive source produced by breaking pencil lead. The standard guideline E1106-86 [16] used a step point-force by breaking a glass capillary against a very large steel block.

To qualify as an AE calibration source in tool wear monitoring, the source should possess similar characteristics to the AE sources produced in machining, in addition to the also important characteristic of reproducibility. Here, similarity suggests that the comparing sources have RMS AE-spectra that closely resemble each other in appearance.

The pulsed laser has been frequently used as an artificial AE source in the past two decades [17-20] for a number of reasons. Firstly, the laser source is broad-band and highly reproducible because the pulse parameters can be clearly defined and tightly controlled. Secondly, the energy of a laser pulse is readily quantifiable once the electrical parameters that drive the laser are known. Thirdly, laser can be delivered to remote locations via optical fibres. However, a pulsed laser is not without its drawbacks: it is expensive, requires stringent safety consideration and produces low power, hence weak AE, when, by necessity, operated within the thermo-elastic range so as not to cause damage to the impinged surface.

In many respects, an air jet source is similar to the helium jet source. The advantages of the air jet source are that it is non-contact, inexpensive, relatively safe, portable and readily available in a machine shop. The disadvantage is that the behaviour of an air jet in respect of the AE produced is affected by a host of environmental factors such as temperature and humidity.

3. Similarity Coefficient

An n-point RMS discrete AE-spectrum can be thought of as a vector u defining a point in the n-dimensional vector space. By analogy with vectors in the three-dimensional space, the length squared of u is the inner product of u with itself. Thus, the length of u can be computed from

$$|u| = \sqrt{u.u} = \sqrt{\sum_{k=1}^{n} u_k^2} \,. \qquad (1)$$

This length is the same as the AErms of the signal from which the n-point discrete spectrum is derived. The vector $\boldsymbol{u}$ can be normalised by dividing its elements by the length of the vector. A normalised vector, denoted by $\overline{u}$, has a unit length.

Given two normalised vectors, $\overline{u}$ and $\overline{v}$, in the n-dimensional space, the included angle θ between them is related to the inner product of $\overline{u}$ and $\overline{v}$ as

$$\cos\theta = \overline{u}.\overline{v} \,. \qquad (2)$$

If the two vectors are identical, then $cos\theta = 1$, whereas if they are orthogonal to each other, meaning that the projection of one vector on the other is zero, then $cos\theta = 0$. Since the value of $cos\theta$ suggests the degree of similarity between the two vectors, it is named the *similarity coefficient*.

4. AE COMPARISON OF AIR JET, LASER AND MACHINING

Three sets of tests were conducted to compare the shapes of the RMS AE-spectra obtained from single-point machining, the air jet and the pulsed laser. The repeatability of RMS AE-spectra from the air jet and pulsed laser sources was also assessed.

4.1 Machining tests

Machining tests were performed with the cutting process variables changing as follows:

- Surface cutting speeds from 80 to 150 m/min;
- Feed rates from 0.1 to 0.4 mm/rev; and
- Depths of cut from 0.3 to 1.0 mm.

The work-piece was made from EN24T (0.35-0.45 % carbon) and measured 63.5-mm diameter by 150 mm length. Tool inserts of type GC 4035 DCMT 11 T3 04 UF and a tool shank of type SDJCL 1616H 11 (Sandvik Coromant) were used. Details of the insert geometry are: cutting edge length 11mm, insert thickness 3.97mm, insert shape 55°, rake angle 0°, clearance angle 7° and nose radius 0.4 mm.

A broad band AE sensor (125 kHz – 2 MHz) was mounted at the end of the tool holder with silicone rubber compound. A Hewlett Packard HP 89410A Vector Signal Analyser was used to produce a 401-line RMS AE-spectrum with frequency from 0 to 1 MHz averaged over 70 consecutive spectra.

4.2 Air Jet Tests

As shown in the block diagram of Figure 1, air from an air supply passed through an air filter, a precision regulator, a precision pressure gauge, an on/off valve and a nozzle sequentially, emerging as an air jet.

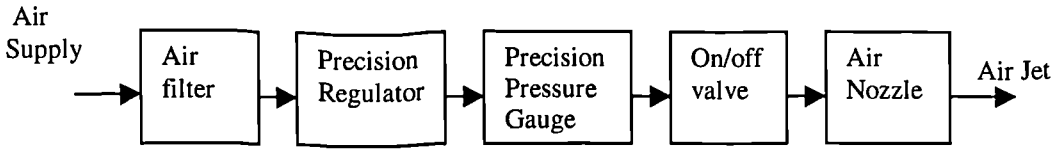

Figure 1. Block diagram of the air jet equipment.

The air jet was directed normally at the top rake surface of the insert, 3 mm from the nose tip and equally distant from the leading and trailing edges of the insert. The insert was clamped to the tool-holder with a clamping torque of 2 Nm and the tool holder was, in turn, held in a fixture. Both the stand-off distance from, and the location of the point of impact on, the rake face were controlled by micrometers. The measuring instruments and their settings were the same as those for the machining tests. Two resolutions of the frequency spectrum were used, namely 401 and 3201 lines. The schematic diagram of the AE signal propagation path is shown in Figure 2.

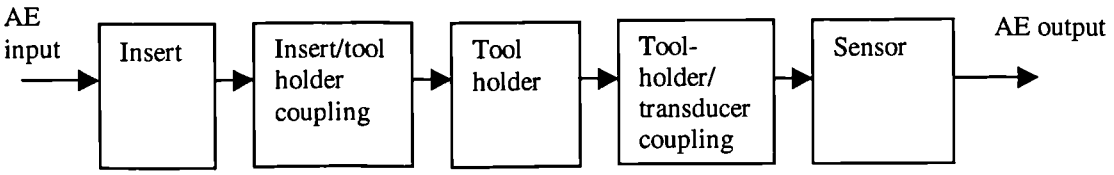

Figure 2. Schematic diagram showing the signal propagation path of AE in tool wear monitoring.

The tests were performed with two different sizes of nozzle diameters: 1.0 mm and 1.4 mm. The stand-off distance was varied from 2 to 16 mm, in increments of 2mm. The air jet pressure was varied between 1 and 5 bars, in increments of 1 bar.

4.3 Pulsed Laser Test

A pulsed Nd: YAG laser system was used as the laser source. The energy of the laser was such chosen that it was insufficient to cause damage to the insert. The energy level of the laser was measured with a laser power meter which registered a value of 3 mJ when the tip of the optical fibre was 2 mm away from the measuring matt black surface. The procedure and the set up of the measuring system were the same as those for the air jet tests excepting the spectrum resolution which was 3201 lines.

5. SIMILARITY OF ARTIFICIAL AND MACHINING AE SOURCES

All RMS AE-spectra from the machining tests have similar appearance with the average spectrum as shown in Figure 3.

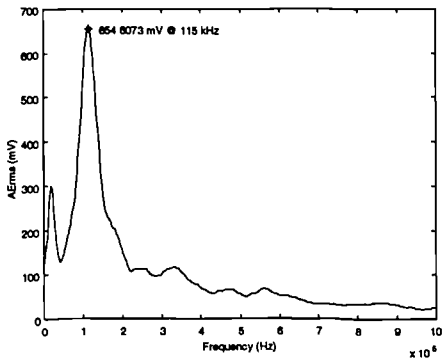

Figure 3. RMS AE-spectrum from machining EN24T with a GC 4035 insert.

Figures 4 and 5 show the typical AE time signals of the air jet and the pulsed laser. The air jet waveform is continuous whereas the pulsed laser is of burst type.

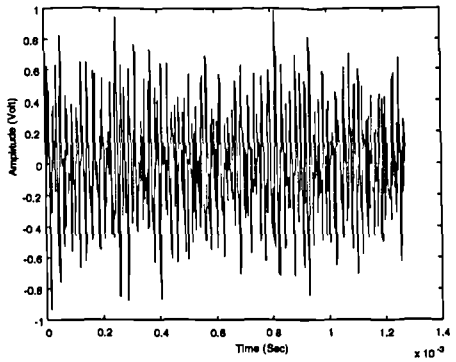

Figure 4. Time domain of the air jet.

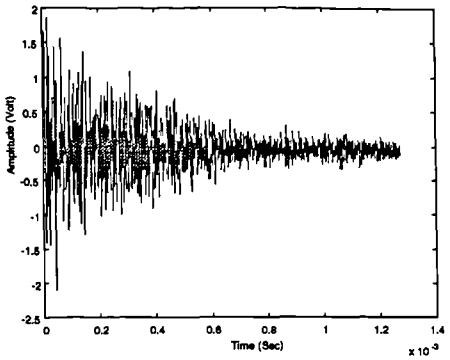

Figure 5. Time domain of the laser.

Figures 6 and 7 show the RMS AE-spectra for the two different artificial sources. It is evident that both the air jet and pulsed laser sources produced sufficient frequency bandwidth, 100 kHz –500 kHz, for tool wear monitoring purposes but the energy level of the pulsed-laser source is much lower.

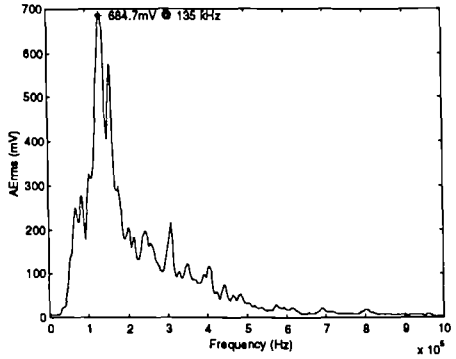

Figure 6. Power spectrum of the air jet.

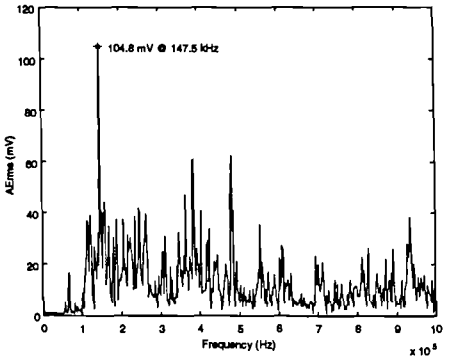

Figure 7. Power spectrum of the laser pulsed.

Using the machining RMS AE-spectrum as the reference, its extent of similarity compared to the air-jet source and the pulsed-laser source, expressed in terms of the similarity coefficients as defined in Equation (2), are 0.8653 and 0.5604 respectively. This result is to be expected as is apparent from the RMS AE-spectra of Figures 3, 6 and 7.

6. AE AND AIR-JET PRESSURE AT DIFFERENT STAND-OFF DISTANCES

Using Equation (1), the AErms value of the AE signal was calculated. For the air jet tests, the relationship was established between the AErms and the air-jet pressure at a stand-off distance from 2 to 16 mm, with bore diameters at the nozzle of 1 mm and 1.4 mm. The shapes of the RMS AE-spectra at the two bore diameters were similar but the peak magnitude was higher for the bore diameter of 1.4 mm. On the other hand, the 1-mm diameter nozzle produced spectra that had lower variability. Using the 1-mm diameter nozzle, the relation between AErms and the air-jet pressure for different stand-off distances is as shown in Figure 8. The variability of the AErms, defined as the ±1 standard deviation divided by the mean, was ± 2.62 %.

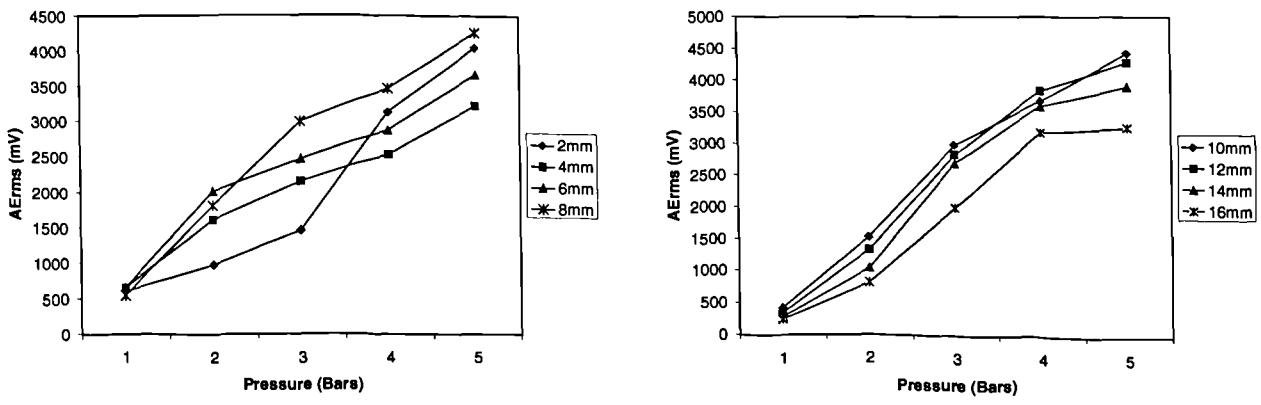

Figure 8. AErms of the air-jet at pressure, 1-5bars, at stand-off distances (a) 2-8 mm, and (b) 10-16mm.

The condition at the stand-off distance of 2 mm and pressure of 2 bars was chosen to show the variability of the measurements. These were the lowest values amongst the set of stand-off distances and pressures tested.

Peak amplitude on the RMS AE-spectrum with 401-point resolution = ± 5.05 %
Peak amplitude on the RMS AE-spectrum with 3201-point resolution = ± 5.84 %
AErms from the RMS AE-spectrum with 401-point resolution = ± 1.14 %
AErms from the RMS AE-spectrum with 3201-point resolution = ± 1.27 %

For the pulsed laser tests, the variability of the measurements at the stand-off distance of 2mm and laser energy of 3 mJ are:

Peak amplitude on the RMS AE-spectrum with 3201-point resolution = ±2.02%
AErms from the RMS AE-spectrum with 3201-point resolution = ± 1.92 %

It is observed from these results that both artificial sources have similar variability.

7. AE, AIR JET PRESSURE AND INSERT CLAMPING TORQUE

Air jet tests were conducted to study the effects of different sensor location and of different insert clamping torque on the AErms. Similar to the air-jet tests in Section 4.2, the air jet was positioned vertically above the top rake face of the insert 2 mm inwards from both the leading and trailing edges of the insert, at a stand-off distance of 5 mm. Three pairs of AE sensors were mounted with the first of each pair on the tool holder and the second on the tool post, all held in position using a silicone rubber compound. These were all PAC sensors and the pairs were: WD and WD with response bandwidth of 100kHz-1MHz, UT1000 and UT1000 with response bandwidth of 60 kHz-1MHz, R30 (100 kHz-400 kHz) and R15 (50kHz-200kHz). The outputs of these sensors were amplified by 60dB and band-pass filtered from 20kHz to 1MHz. The Hewlett Packard HP89410A Vector Signal Analyser was used to produce an RMS AE-spectrum with 401-point resolution averaged over 70 successive spectra. The insert was tightened to three levels of torque, namely 0.4 Nm, 1.2 Nm and 2.0 Nm. The air-jet pressure was varied between 3 and 8 bars in 1-bar increments.

Results showed that the AErms were linearly proportional to the air-jet pressure applied for all levels of clamping torque. It was also observed that the AErms was the highest at the torque value of 0.4 Nm, therefore suggesting that the AErms was sensitive to the torque applied. The graph for the clamping torque of 2.0 Nm is as shown in Figure 9.

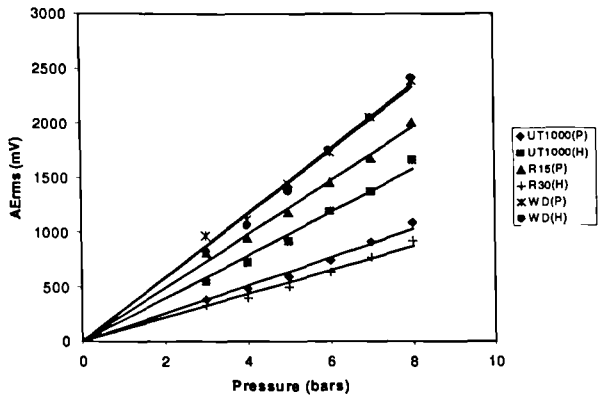

Figure 9. AErms related to air jet pressure for different sensors.

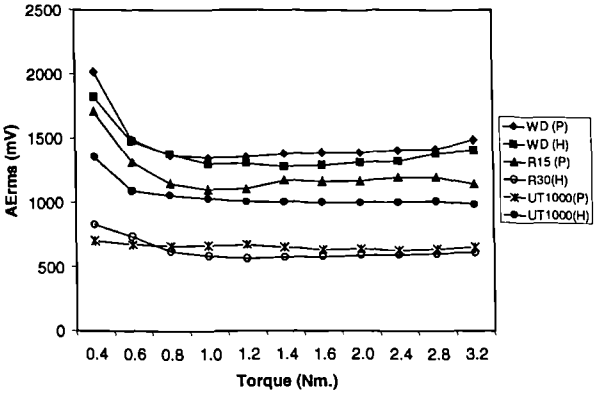

Figure 10. AErms related to clamping torque at constant pressure of 5 bars.

To study the relation between clamping torque and AErms, the air-jet pressure was fixed at 5 bars whilst the clamping torque was changed from 0.4 Nm to 3.2 Nm using an adjustable torque wrench. The results, as in Figure 10, show that the AErms decreases as the torque increases from 0.4 tol.2 Nm and then remains constant from 1.2 Nm to 3.2 Nm. The ratios of AErms between the different pairs of sensors, one on the tool holder and the other on the tool post, were calculated for each value of clamping torque and they are as shown in the table below:

Sensor pair	Mean of ratios	Standard Deviation of ratios	Variability (%)
WD/WD	1.049	0.031	2.984
UT1000/UT1000	0.630	0.038	6.093
R30/R15	2.223	0.076	3.411

8. CONCLUSION

Compared to the pulsed laser, the air jet is more suitable as an artificial calibration source for measuring systems used for machining study and tool wear monitoring. This is because the air jet source has an RMS AE-spectrum more similar to that observed in machining than the pulsed laser, is relative safe to use, is less expensive and is more readily available in a workshop.

For a fixed stand-off distance, the AErms of the air-jet increases linearly with the air-jet pressure. The clamping torque applied to the insert can affect the AErms if the torque value is low; but when the clamping torque exceeds 1.2 Nm, the AErms remains constant. A safe clamping torque for the tool holder used in this research is around 2 Nm beyond which there is the risk of damaging the hexagonal head of the tightening screw.

In summary, a calibration procedure may be suggested as follows. With the insert clamping torque above 1.2 Nm, the AErms value obtained from a sensor can be converted into an air pressure value using the calibration graphs such as Figures 8 and 9. In this way, providing a set-up is calibrated using the air jet source under a prescribed condition, results obtained from different set-ups that have been calibrated in the same manner, can be compared.

ACKNOWLEDGEMENTS

The authors wish to acknowledge support from the INTErSECT Faraday Partnership, the Engineering and Physical Sciences Research Council and the Royal Thai Government.

REFERENCES

(1) E.N.Diei and D.A.Dornfeld, "A model of tool fracture generated acoustic emission during machining", *Trans.ASME, Journal of Engineering for Industry*, 109 (3) (1989) 229-237.

(2) E. Kannatey-Asibu, Jr. and D.A.Dornfeld, "Quantitative relationships for acoustic emission from orthogonal metal cutting", *Trans.ASM, Journal of Engineering for Industry*, 103 (3) (1981) 330-340.

(3) L. Dan and J.Mathew, "Tool wear and failure monitoring techniques for turning-a review", *1st J.Mach. Toos Manufact*, 30 (4) (1990) 579-598.

(4) R.Teti and D.A. Dornfeld, "Modelling and experimental analysis of acoustic emission from metal cutting", *Trans. ASME, Journal of Engineering for Industry*, 111(3) (1989) 229-237.

(5) M.S. Lan and D.A Dornfeld, "In-process tool fracture detection", *Journal of Engineering Materials and Technology*, 106 (2) (1984) 111-118.

(6) T. Blum and I. Inasaki, "A study of acoustic emission from the orthogonal cutting process", *Trans. ASME, J. Engineering for industry*, 112 (1990) 203-211.

(7) A.E. Diniz, J.J. Liu and D.A. Dornfeld, "Correlating tool life, tool wear and surface roughness by monitoring acoustic emission in finish turning", *Wear*, 152 (1992) 395-407.

(8) J.J. Liu and D.A. Dornfeld, "Modelling and analysis of acoustic emission in diamond turning", *Journal of Manufacturing Science and Engineering*, 118 (1996) 199-206.

(9) T. A Carolan, S.R. Kidd, D. P. Hand, S. J. Wilcox, P. Wilkinson, J. S. Barton, J. D. C. Jones and R.L. Reuben, "Acoustic emission monitoring of tool wear during the face milling of steels and aluminium alloys using a fibre optic sensor", Part1: energy analysis, *Proc Instn Mech Engrs*, 211(1997) 299-309.

(10) K. Iwata and T. Moriwaki, "An application of acoustic emission measurement to in-process sensing of tool wear", *C.I.R.P. Annals*, 26 (1977) 21-26.

(11) N.N. Hsu and F.R. Breckenridge, "Characterisation and calibration of acoustic emission sensors", *Materials Evaluation*, 39 (1981) 60-68.

(12) Y. Berlinsky, M. Rosen, J. Simmons and H.N.G. Wadley, "A calibration approach to acoustic emission energy measurement", *Journal of Nondestructive Evaluation*, 10 (1) (1991).

(13) S. L.McBride and T.S. Hutchison, "Helium gas jet spectral calibration of acoustic emission transducers and system" *Canadian journal of Physics*, 56 (1978) 504-507.

(14) M. J. Evans, "The use of diffuse field measurements for acoustic emission", PhD. Thesis, Imperial College of Science, Technology and Medicine, (1997) 196 P.

(15) The American Society for Testing and Materials (ASTM): Standard guide for determining the reproducibility of acoustic emission sensor response, E976-94, (1994) 374-379.

(16) ASTM: Standard method for primary calibration of acoustic emission sensors, E1106-86 (reapproved 1992), 485-494.

(17) Y. Berlinsky, M.Rosen, J. Simmons and H.N.G. Wadley, "A calibration approach to acoustic emission energy measurement", *Journal of Nondestructive Evaluation*, 10 (1) (1991) 1-5.

(18) A.M. Aindow, R.J. Dewhurst, D. A. Hutchins and S.B. Palmer, "Laser-generated ultrasonic pulses at free metal surfaces", *J. Acoust.Soc.Am.*69 (2) (1981) 449-455.

(19) C.B. Scruby, R.J. Dewhurst, D.A. Hutchins and S.B. Palmer, "Qualitative studies of thermally generated elastic waves in laser-irradiated metals", *J.Appl.Phys.*, 51(12) (1980) 6210-6216.

(20) S. N. Hopko and I. C Ume, "Laser generated ultrasound by material ablation using fiber optic delivery", *Ultrasonics*, 37 (1999) 1-7.

IEEE Instrumentation and Measurement
Technology Conference
Budapest, Hungary,
May 21-23, 2001

Acoustic Emission and Vibration for Tool Wear Monitoring in Single-Point Machining Using Belief network

A.Prateepasen*,**, Y.H.J.Au**, B.E. Jones**
* King Mongkut's University of Technology Thonburi, Bangmod,
Toong-kru, Bangkok, Thailand
Phone (662) 4709678
Email: iasaasen@kmutt.ac.th
** The Brunel Centre for Manufacturing Metrology,
Brunel University, Uxbride, Middlesex UB8 3PH
Phone (044-1895) 274000
Email: joe.au@brunel.ac.uk

Abstract-This paper proposes an implementation of calibrated acoustic emission (AE) and vibration techniques to monitor progressive stages of flank wear on carbide tool tips. Three cutting conditions were used on workpiece material, type EN24T, in turning operation. The root-mean-square value of AE (AErms) and the coherence function between the acceleration signals at the tool tip in the tangential and feed directions was studied. Three features were identified to be sensitive to tool wear: AErms, coherence function in the frequency ranges 2.5-5.5 kHz and 18-25 kHz. Belief network based on Bayes' rule was used to integrate information in order to recognise the occurrence of worn tool. The three features obtained from the three cutting conditions and machine time were used to train the network. The set of feature vectors for worn tools was divided into two equal sub-sets: one to train the network and the other to test it. The AErms in term of AE pressure equivalent was used to train and test the net work to validate the calibrated acoustic. The overall success rate of the network in detecting a worn tool was high with low an error rate.

Keywords- Acoustic emission, Vibration, Tool wear monitoring, Belief network.

I. INTRODUCTION

In machining, whether a tool needs to be changed is decided either by a machine operator or by the life expectancy of the tool. The judgement of the machine operator is often based on the visual inspection of the tool and the surface finish produced on the work piece, both requiring a certain degree of skill.
The decision based on tool-life expectancy suggests the idea of an average life for a class of tools calculated from previous data. For a particular machining condition, the tool manufacturer gives a recommended tool life for a given insert. This practice of tool replacement based on fixed tool life may not be the most economical since a tool can be replaced prematurely or only after damage has been done. Consequently, besides the unnecessary wastage of some tools, the frequent tool changes cause higher machine downtime, decreasing thereby the system productivity and increasing production costs.

In manufacturing, cutting cost and improving product quality are the necessary measures to adopt in an increasingly competitive world. In addition to the developments within manufacturing technology leading to the machining of larger or complicated workpieces and the use of expensive materials, the need for condition monitoring of cutting tools becomes increasingly evident. For these reasons, quality and productivity requirements through international competition have forced many manufacturers to use automated monitoring systems.

A variety of tool wear and failure sensing techniques have established the effectiveness of tool failure detection in the last few decades. Optical techniques have been used to measure the progress of tool wear by using a CCD camera [1] or a TV camera [2]. Uehara [3] detected tool wear by scanning chips with an electron microprobe analyser for wear debris removed from the cutting edge. Cook [4] used abraded radioactive wear particles; a small amount of radioactive material was implanted in the flank of the tool. The spot was checked at the end of every cutting cycle. If the spot disappeared, the spot would be considered to be worn. Gomayel [5] used an electromagnetic sensor to measure the change in diameter of a work piece and converted it to the size of wear on the tool. The voltage output obtained from the electromagnetic sensor was directly related to the gap between the sensor and the workpiece. Cutting forces have been used to relate to tool wear and tool breakage [6,7]. Sadat [8] detected flank wear by using the noise spectra resulting from the rubbing action of the tool with the workpiece. It was found that the noise in the frequency range 2.75 – 3.5 kHz significantly increased from 9 to 24 dB as the tool became worn. Motor current [9] and motor power [10] of the spindle were investigated to sense the tool wear and tool breakage. Turkovich and Kramer [11], and Lin [12] attempted to

measure the temperature in the cutting zone and relate it to tool wear. The temperature around the cutting tool edges was found to be related to wear, and the friction between the chip and the cutting tool. Takeyama [13] proposed that the slightest change of the cutting edge due to chipping or wear be detected by using a pair of optical reflection systems. However, these techniques are not widely adopted in industry.

This paper described the development of a novel on-line tool wear condition monitoring intelligent system for single point machining operations. This system used acoustic emission and vibration techniques for monitoring the different stages of tool wear. The root-mean-square value of the AE (AErms) and the coherence function between the acceleration signals at the tool tip in the tangential and feed directions are used to detect the progress of flank wear in carbide tool tips. An expert system, called the "Belief network" based on bayes' rule, was utilised to integrate the information of AE and vibration parameters for classifying the tool condition.

II. THEORIES OF ACOUSTIC EMISSION AND COHERENCE FUNCTION FOR TOOL WEAR DETECTION

A. Acoustic emission and tool wear

Acoustic emissions, by definition, are transient elastic waves generated by the rapid release of energy from localised sources within a material [14]. These elastic waves can be detected by transducers attached to the surface of the specimen. Research into the use of acoustic emission (AE) for tool wear monitoring [15-19] has established that there exists a definite relation between AErms and tool wear.

AErms is the root mean square value of the AE signal. Since acoustic emission activity is attributed to the rapid release of energy in a material, the energy content of the acoustic emission signal can be related to this energy release. AErms can be defined as

$$V_{rms} = \left(\frac{1}{T}\int_0^T V^2(t)dt\right)^{\frac{1}{2}} \qquad (1)$$

where
$V(t)$ = the voltage signal from an AE transducer, and
T = the duration of the signal.

B. Coherence function and tool wear

A cutting tool in turning is a typically mounted as a cantilever. The cutting force can be represented by the three mutually perpendicular components known as the radial, tangential and feed force components respectively along to as the x-, y- and z-axes. The radial force is relatively low compared to the others and so the tool tip can be assumed to move mainly in the yz-plane. The shear force associated with the shear plane is resolvable into both the y- and z-directions, and thus the two component forces are correlated. On the other hand, the frictional forces that occur at the chip-tool and tool-workpiece interfaces are mainly forces confined in the respective z- and y-directions because of the geometry of the tool; these frictional forces are therefore largely uncorrelated.

The coherence function between the two acceleration signals is defined as

$$\gamma^2 = |Gyz|^2 / GyGz \qquad (2)$$

where Gyz is the cross spectrum between the acceleration signals in the tangential and feed directions;
and Gy and Gz are the auto spectrum of the acceleration signals in the tangential and feed directions.

The value of the coherence function can be divided in to three cases:

- If the tangential force and feed force are completely uncorrelated so that $G_{yz} = 0$, then $\gamma^2 = 0$
- If the tangential force and feed force are completely correlated, then $\gamma^2 = 1$
- In actual practice, since the two forces are never completely correlated, $0 \le \gamma^2 \le 1$

III. EXPERIMENTAL SET-UP AND RESULTS

A tool shank (SDJCL 1616H 11) and carbide tool inserts (CG 4035 DCMT 11 T3 04-UF), both from Sandvick Coromant, were used. Details of the insert geometry was: insert shape angle 55°, clearance angle 7°, rake angle 0°, cutting edge length 11 mm, thickness 3.97 mm and nose radius 0.4 mm.

An AE sensor (type WD from PAC) was mounted at the end of the tool-holder. Signals were amplified with a total gain of 34 dB band-passed filtered from 100 kHz to 1 MHz. The AE signal detected at the sensor was analysed in real time using a Hewlett Packard HP 89410A Vector Signal Analyser to produce a 401-line AErms spectrum spanning 0 to 1 MHz averaged over 250 consecutive spectra. The over-all root mean square was calculated from the AErms spectrum.

Two accelerometers (model 303A03 from PCB) powered by a PCB power supply were mounted close to the tool tip: one in the direction of tangential force and the other in the direction of feed force. The measuring frequency ranges of the accelerometers are 1 - 10,000 Hz at ±5% and 0.7 - 20,000 Hz at ±10%. This model of accelerometer is designed for adhesive mounting. Because of the high temperature in cutting, glass-ceramic-disk insulators, measured 10 mm diameter by 1 mm thick, were attached between the tool shank and the accelerometers. Silicone Rubber Compound which can withstand up to 250°C was used to mount both the accelerometers and glass-ceramic

insulators. The outputs of the accelerometers were fed to the SI 1220 multi-channel spectrum analyser. 500 spectral points were recorded and analysed in the frequency range of 0 Hz -25 kHz over 8 consecutive spectra.

Three sets of machining tests were conducted and their conditions are detailed in the following:

- Machining condition 1: Cutting speed, depth of cut and feed rate were constant at 150 m/min, 1mm and 0.3 mm/rev respectively.
- Machining condition 2: Cutting speed, depth of cut and feed rate were constant at 250 m/min, 0.75mm and 0.25 mm/rev respectively.
- Machining condition 3: Cutting speed, depth of cut and feed rate were constant at 300 m/min, 0.5mm and 0.2 mm/rev respectively.

For all three machining conditions the wear curves show that flank wear increases approximately linearly with the cutting time as in Fig. 1, 2 and 3. The rapid flank wear is apparent at the final stage. The final flank wear length of the three cutting conditions before the onset of rapid wear rate are 0.44 mm at 40.9 min, 0.22 mm at 10.7 min and 0.28 mm at 19.9 min respectively.

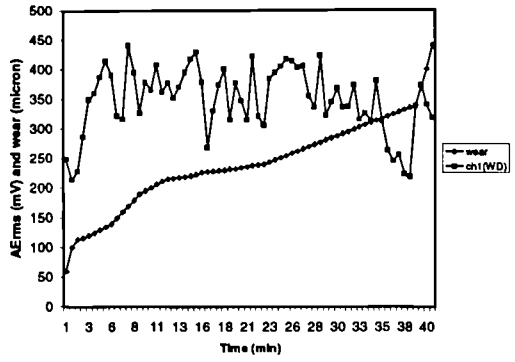

Fig 1. The AErms obtained from machining test at speed 150 m/min, depth of cut 1.0 mm and feed rate 0.3 mm/rev.

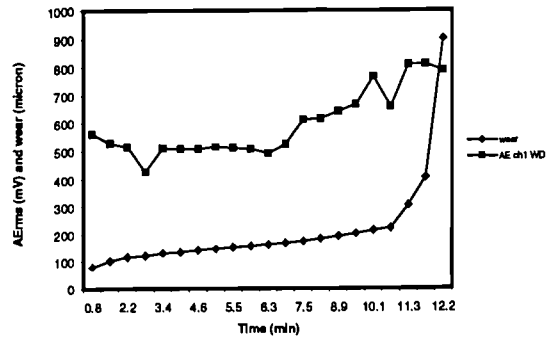

Fig 2. The AErms obtained from machining test at speed 250 m/min, depth of cut 0.75 mm and feed rate 0.25 mm/rev.

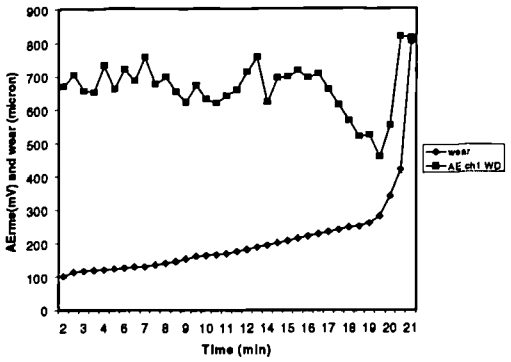

Fig 3. The AErms obtained from machining test at speed 300 m/min, depth of cut 0.5 mm and feed rate 0.2 mm/rev.

For machining condition 1, AErms increased within the initial stage of wear and then settled down to a constant level with much local fluctuation. Machining condition 2 shows that during the second half stage the AErms increased with the progression of flank wear. Machining condition 3 shows that AErms was rougly constant with the progression of tool wear until the final stage when the AErms dropped before it rose again to the point when the tool was so worn that it could not be used.

Results of the coherence with tool wear show that the values of the coherence function at the vicinity of the natural frequency (2.5 kHz –5.5 kHz) decreased with tool wear whilst at the high frequency end (18 kHz – 25 kHz) the coherence value increased. The relation of coherence function in the two frequency ranges, 2.5 kHz –5.5 kHz and 18 kHz – 25 kHz, with tool wear are demonstrated as in Fig 4, 5 and 6 for the three machining conditions.

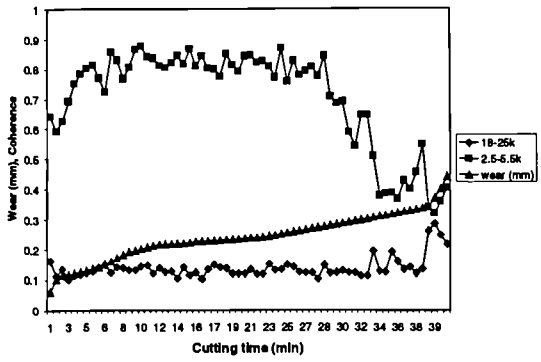

Fig 4. Coherence at frequency range 2.5-5.5 kHz and 18-25 kHz and flank wear with cutting time of cutting speed 150 m/min depth of cut 1.0 mm and feed rate 0.3 mm/rev.

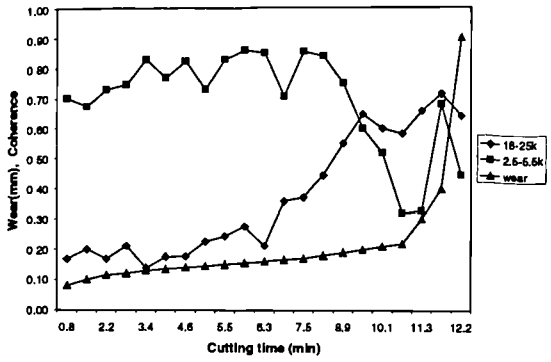

Fig 5. Coherence at frequency range 2.5-5.5 kHz and 18-25 kHz and flank wear with cutting time of cutting speed 250 m/min depth of cut 0.75 mm and feed rate 0.25 mm/rev.

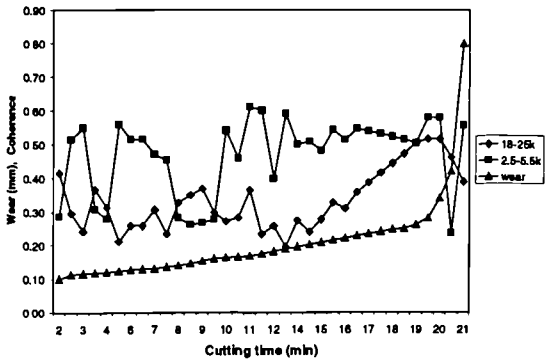

Fig 6. Coherence at frequency range 2.5-5.5 kHz and 18-25 kHz and flank wear with cutting time of cutting speed 300 m/min depth of cut 0.5 mm and feed rate 0.2 mm/rev.

Forces acting on the tool tip can be considered to be made up of two parts: that which is correlated due to the common shear force and that which is uncorrelated due to friction at the two interfaces as explained in Section 2.2. The tangential and feed forces in the respective y- and z-directions are partially correlated through the shear force. The friction forces at the chip/tool and tool/workpiece interface are uncorrelated forces appearing in the feed (z-) direction and tangential (y-) direction. These friction forces vary with the severing of contacting asperities. At the advanced stage of wear the correlation represented by the coherence function at the natural frequency is much reduced because the frictional effect becomes more dominant than that due to shear. Consequently, at around the resonance frequency of the tool, the coherence function falls with the progression of tool wear.

IV. BELIEF NETWORK

In order to improve the robustness of the tool wear monitoring system, information from both the coherence function and AErms must be fully exploited. An expert system, named Netica, was used. The advantages of Netica are its ease of use, user-friendly graphical interface and low cost. Netica operates on the principle of "Bayes rule" which can be defined as

$$P(S_i \setminus A) = \frac{P(A \setminus S_i)P(S_i)}{\sum_{j=1}^{k} P(A \setminus S_j)P(S_j)} \quad (3)$$

for i = 1,2,....k

where $P(S_i \setminus A)$ = posterior probability of *Si* given *A*.

$P(A \setminus S_i)$ = conditional probability of *A* given *Si*

$P(S_i)$ = prior probability

$S_2, S_3.....S_k$ = a set of events.

In order to use belief networks, the distribution of conditional probability for each variable needs to be specified. In many applications, these probabilities are allocated by experts. In this paper the conditional probability was obtained from the case data contained in a file. This case file holds information of the coherence function in frequency ranges 2.5 kHz -5.5 kHz and 18 kHz -25 kHz, AErms, machine time and the stages of tool wear (worn and not worn).

The three features and machine time obtained form the three cutting conditions were used to train the network. The set of feature vectors for worn tools was divided into two equal sub-sets: one to train the network and the other to test it. It must be noted that the boundary between a worn and not-worn tool expressed in terms of the flank wear height was slightly different in the three machining conditions. The final flank wear height measured for the machining conditions 1, 2 and 3 before the onset of rapid wear rate which were 0.44 mm at 40.9 min, 0.22 mm at 10.7 min and 0.28 mm at 19.9 min respectively. Since the number of "worn" cases is small, they were used as a group to train the believe network.

Fig 7. shows the five nodes of the belief network referred to as 1) High_end, 2) Low_end, 3) AErms, 4) Machine_time and 5) Tool_wear nodes. The time range of the Machine_time node was divided into four sub-intervals taking into consideration the tool life of each cutting condition. The intervals, as shown in the first column in the Machine_time node in Figure 7, are 0-8 min, 8-16 min, 8-16 min, 16-32 min, and 32-45 min respectively. The second column of the Machine_time node indicates the probability values learnt from the case file. Similar to the Machine_time node, the ranges of AErms, High_end and Low_end nodes were divided into sub-ranges also based on the stages of tool wear, worn or not worn, for each machining condition. In the Tool_wear node, there are two stages: not_worn and worn. The probability of each stage was calculated using Equation 4.

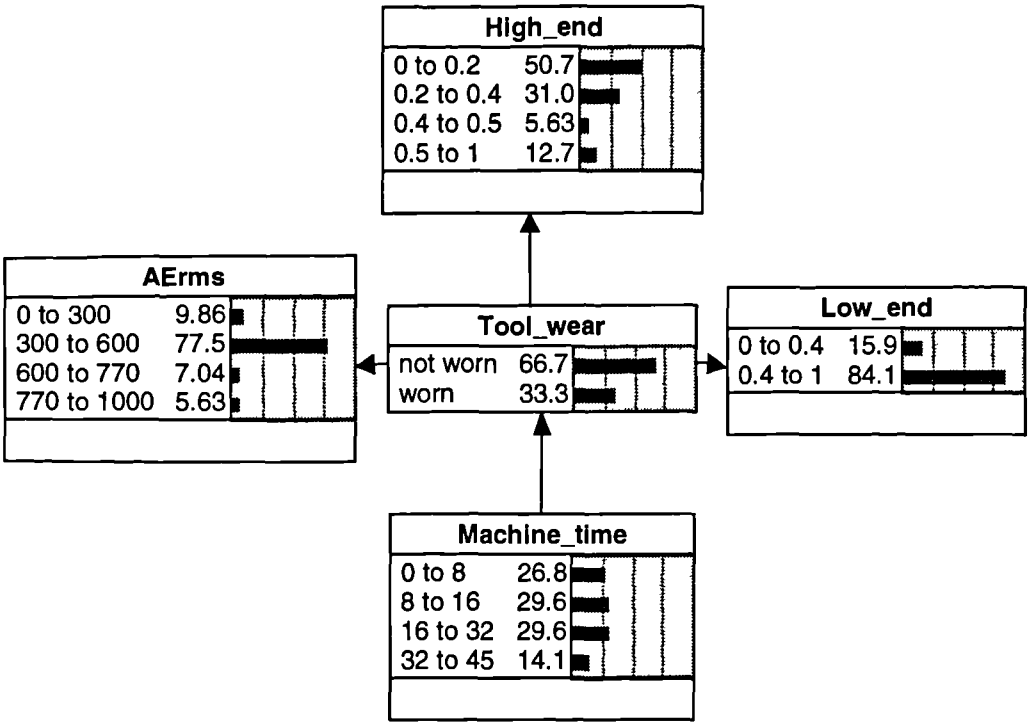

Fig 7. The belief network to predict the two stages of tool wear.

The numbers of cases used to train and test the network were 67 and 61 respectively. The predicted results of 61 cases were as shown in Table1 below.

Predicted		Actual
not_worn	worn	
54	1	not_worn (55 cases)
1	5	Worn (6 cases)

Table 1. The predicted result of the belief network.

From Table 1, it can be seen that the misclassification error for the "not worn" status is 1/55 = 1.8% and the error for the "worn" status is 1/6 = 16.7%. Taking the two statuses together, the total error rate of misclassification is (1+1)/(55+6) = 3.3%. Although the missed detection of worn tool is relatively high, the monitoring can be made more robust by immediate sequential assessments. If the subsequent assessments return the same verdict, then the initial belief is reinforced.

V. CONCLUSIONS

Three cutting conditions were conducted on workpiece material, type EN24T, in a turning operation. The root-mean-square values of the AE (AErms) appear to be sensitive to tool wear and cutting condition.

At the advanced stage of tool wear, the values of the coherence function in the vicinity of the natural frequency (2.5 kHz –5.5 kHz) of the cutting tool decreased with tool wear because the frictional effects were more dominant than shear effects. Whilst in the high frequency range (18 kHz – 25 kHz) the coherence function increased.

The belief network based on Bayes' rule was used to integrate information from AE and vibration in order to improve the correct recognition rate of the "worn" tool status. The three features and machine time obtained from the three cutting conditions were used to train and test the network. The overall success rate of the network in detecting a worn tool was high with an error rate of 3.3 %.

ACKNOWLEDGMENTS

The authors wish to acknowledge support from the Royal Thai Government and the INTErSECT Faraday Partnership, the Engineering and Physical Sciences Research Council.

REFERENCES

[1] R. Levi, A. Villa, G. Quaglia, R. Ghiara and G. Rutelli, An expert control system for tool life management in flexible manufacturing cells, Ann. CIRP 34, 87-90 (1985).

[2] T. Sata, K. Matsushima and T. Kawabata, Recognition and control of the morphology of tool failures, Ann. CIRP 28, 43-47 (1979).
[3] K. Uehara, On the mechanism of crater wear of carbide cutting tool, Ann. CIRP 21, 31-32 (1972).
[4] N.H. Cook, Tool wear sensors, Wear 62, 49-57 (1980).
[5] J.L.E. Gomayel and K.D. Bregger, On-line tool wear sensing for turning operations, J. Engng Ind. 108, 44-47 (1986).
[6] J. Tlusty and G.C. Andrews, A critical review of sensors for unmanned machining, Ann. CIRP 32, 536-572 (1983).
[7] M.S. Lan and D.A. Dornfeld, In-process tool fracture detection, J. Engng Mater. Technol. 106, 111-118 (1984).
[8] A. B. Sadat and S. Raman, Detection of tool flank wear using acoustic signature analysis, Wear 115, 265-272 (1987).
[9] Y. S. Liao, Development of a monitoring technique for tool change purpose in turning operations, Proc. 15th Int. Machine Tool Design and Research Conf. 251-257 (1974).
[10] N. Constantinides, S. Bennett, An investigation of methods for on-line estimation of tool wear, International Journal of Machine Tools and Manufacture 27 (2) (1987) 225-237.
[11] B.F. Turkovich and B.M. Kramer, A comprehensive tool wear model, Ann. CIRP 35, 67- 70 (1986).
[12] J. Lin, Inverse estimation of the tool-work interface temperature in end milling, International journal of Machine tool and Manufacture 35 (5) (1995) 751-760.
[13] H. Takeyama, H. Sekiguchi, R. Murata and H. Matsuzaki, In-process detection of surface roughness in machining, Ann. CIRP 25, 467-471 (1976).
[14] P. McIntire (1987), "Nondestructive Testing Handbook Second Edition" Volume 5 Acoustic Emission Testing, American Society for Nondestructive Testing.
[15] E.N.Diei and D.A.Dornfeld, "A model of tool fracture generated acoustic emission during machining", Trans.ASME, Journal of Engineering for Industry, 109 (3) (1989) 229-237.
[16] E. Kannatey-Asibu, Jr. and D.A.Dornfeld, "Quantitative relationships for acoustic emission from orthogonal metal cutting", Trans.ASME, Journal of Engineering for Industry, 103 (3) (1981) 330-340.
[17] L. Dan and J.Mathew, "Tool wear and failure monitoring techniques for turning-a review", 1st J.Mach. Toos Manufact, 30 (4) (1990) 579-598.
[18] R.Teti and D.A. Dornfeld, "Modelling and experimental analysis of acoustic emission from metal cutting", Trans. ASME, Journal of Engineering for Industry, 111(3) (1989) 229-237.
[19] M.S. Lan and D.A Dornfeld, "In-process tool fracture detection", Journal of Engineering Materials and Technology, 106 (2) (1984) 111-118.

CALIBRATION OF AE FOR TOOL WEAR MONITORING

A. Prateepasen, Y.H.J. Au and B.E. Jones
The Brunel Centre for Manufacturing Metrology
Brunel University, Uxbridge, Middlesex UB8 3PH, UK

Abstract: A calibration procedure using an air-jet as the artificial AE source was applied to single-point tool wear monitoring. The calibration procedure involves setting up an air-jet at a fixed stand-off distance from the top rake of the tool tip, applying in sequence a set of increasing pressures and measuring the corresponding AE. The root-mean-square value of the AE (AErms) obtained is linearly proportional to the pressure applied. This paper presents the results of machining tests and air-jet pressure test, both of which confirm that the tool system is linear with respect to AE propagation. Thus, irrespective of the layout of the sensor and AE source in a tool structure, AE can be expressed in terms of the common currency of 'pressure' using the calibration curve produced for that layout. Tool wear stages can then be defined in terms of 'pressure' levels.

Keywords: Calibration, Acoustic Emission, Single-point machining.

1 INTRODUCTION

Acoustic emission (AE) is the generation of stress waves created by the release of strain energy as a result of the material yielding under stress. In single-point metal machining, four different sources of AE, as shown in Figure 1, can be identified [1]:

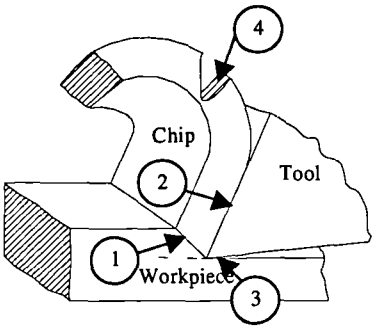

Figure 1. Four different sources of AE.

1. plastic deformation on the shear plane;
2. sliding friction and plastic deformation at the chip/tool interface;
3. sliding friction at the tool flank/workpiece interface; and
4. breakage of chips and their impact on the tool or workpiece.

Previous tool wear monitoring research has shown a direct correspondence between the energy or the root mean square value of the AE signal (AErms) and the different stages of tool wear [1-10]. The energy and AErms refer to the respective energy and root-mean-square value of the voltage output from the AE sensor. Models were proposed [1] that described the influence on the AErms of process variables in machining such as the feed rate, depth of cut and cutting velocity in single-point machining.

Modern machining uses indexable insert tools. An insert, clamped onto a tool-holder, is used to remove metal and when all its cutting edges are worn, a new insert is substituted. When monitoring tool wear using AE, the transmission characteristics of the tool between the tool tip and the sensor are exceedingly changeable. Not only is the sensed AE signal dependent on the geometry of the tool structure and the response characteristic of the sensor, it is also influenced by the subtle changes in the sensor and insert couplings with the tool holder, not to mention the effect of tool wear as observed by different researchers. As a result, AE data are hardly comparable between set-ups, making knowledge transfer very difficult, if not impossible.

To overcome the problem stated above, some form of calibration needs to be performed in order to establish the relationship between the AE measured by the sensor and the AE produced from a known reference source located on the tool tip. Two artificial AE sources, an air-jet and a pulsed laser, have been studied [11] and it is concluded that the air jet source had much in common with the AE produced during single-point machining. The comparison has been made between a reference AE source and a machining AE source based on the degree of likeness between the two frequency spectra of the respective AE signals using a measure called *similarity coefficient*. In addition, the air-jet source has the advantages that it is relatively safe compared to a laser source and that air is readily available in a machine shop.

In this paper, a calibration procedure using an air jet as the artificial AE source is described. The procedure establishes the relationship between the AErms and air pressure. The paper then presents evidence that the tool system (including the tool insert, tool holder, insert/tool holder coupling, sensor/tool holder coupling, and sensor) can be considered linear with respect to AE propagation so that an AErms value can be converted into a common equivalent value based on the pressure of the air jet.

2 COMPARISON OF SHAPES AND SIZES OF AE SPECTRA

An n-point RMS discrete spectrum can be thought of as a vector u defining a point in the n-dimensional vector space. By analogy with vectors in the three-dimensional space, the length squared of u is the inner product of u with itself. Thus, the length of u can be computed from

$$|u| = \sqrt{u.u} = \sqrt{\sum_{k=1}^{n} u_k^2} \tag{1}$$

This length is the same as the AErms of the signal from which the n-point discrete spectrum is derived. The vector $\boldsymbol{u}$ can be normalised by dividing its elements by the length of the vector. A normalised vector, denoted by $\overline{u}$, has a unit length.

Given two normalised vectors, $\overline{u}$ and $\overline{v}$, in the n-dimensional space, the included angle θ between them is related to the inner product of $\overline{u}$ and $\overline{v}$ as

$$\cos\theta = \overline{u}.\overline{v}. \tag{2}$$

If the two vectors are identical, then $\cos\theta = 1$, whereas if they are orthogonal to each other, meaning that the projection of one vector on the other is zero, then $\cos\theta = 0$. Since the value of $\cos\theta$ suggests the degree of similarity between the two vectors, it is named the *similarity coefficient*.

Suppose there are m number of spectrum-vectors, u_1, u_2,..., u_m, to be compared, the individual lengths of these vectors can be computed by means of equation (1) and the corresponding normalised vectors obtained, namely, $\overline{u}_1$, $\overline{u}_2$, ..., $\overline{u}_3$. These normalised vectors, treated as column vectors, are then assembled into an n-by-m matrix A such that

$$A = (\overline{u}_1, \overline{u}_2, ..., \overline{u}_m). \tag{3}$$

The similarity coefficient matrix C, by virtue of equation (2), is given by

$$C = A^T \cdot A \tag{4}$$

where the element c_{ij} in C is the similarity coefficient between the spectrum-vectors u_i and u_j. It is noted that the matrix C is a symmetric matrix.

3 ARTIFICIAL AE AIR-JET SOURCE AND AIR PRESSURE

Calibration involves comparison between a reference source and a given source. Whereas comparison in one dimension is relatively straightforward, comparison in n-dimensions is not so easily defined. The method suggested is to consider an AE signal from the perspective of its RMS spectrum and then proceed to make comparison with the reference RMS spectrum in respect of its size and shape. The size relates to the strength of the signal whilst the shape corresponds to the distribution of the energy in the relevant frequency range. The size of a signal can be represented by the overall AErms of its spectrum. When comparing two signals to decide if they are similar in shape, the similarity coefficient can be used.

The air supply system that drove the air jet calibration rig is shown in the block diagram of Figure 2. A nozzle with a 1.0-mm diameter bore was placed normal to the rake face of the tool insert at a fixed distance of 5 mm. The centre of the air stream was positioned 2 mm from both the leading and trailing edges of the insert. The insert was clamped to the tool holder with a tightening torque of 2 Nm. The air pressure was varied from 5 to 8 bars in increments of 0.5 bar.

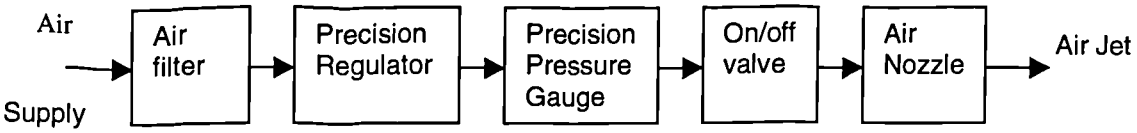

Figure 2. Block diagram of the air jet equipment.

A tool shank of type SDJCL 1616H 11 and carbide tool inserts of type CG 4035 DCMT 11 T3 04-UF (Sandvik Coromant) were used. The detail of the insert geometry was as follows: insert shape 55°, clearance angle 7°, rake angle 0°, cutting edge length 11 mm, thickness 3.97 mm and nose radius 0.4 mm.

Two AE sensors were mounted on the tool-holder: a WD sensor (PAC) at the end of the tool-holder and an R30 sensor (PAC) on the side as shown in Figure 3. Both signals were amplified by 40 dB at the pre-amplifiers fitted with a 100 kHz – 1 MHz band-pass filter. The AE signals detected at the two sensors were analysed in real-time using a Hewlett Packard HP 89410A Vector Signal Analyser to produce a 401-line AErms spectrum spanning 0 to 1 MHz averaged over 70 consecutive spectra.

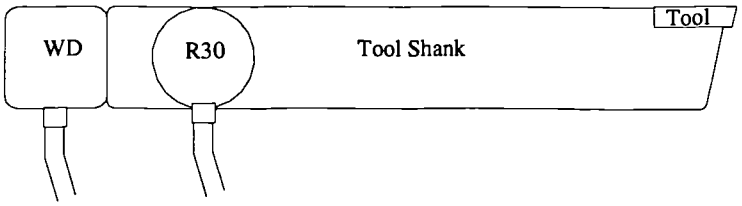

Figure 3. Two AE sensors (WD and R30) on the tool holder.

Typical AErms spectra of the air jet at the pressure of 5 bars obtained from the two sensors are shown in Figure 4. Their difference in shape is significantly due to the different frequency responses of the two sensors.

The AErms values of the air jet spectra obtained from pressures of 5 to 8 bars were computed using equation (1). The results from both the WD and R30 sensors are plotted in Figure 5. It can be seen that the AErms and air pressure are linearly related and the gradients for the WD and R30 sensors are 19.658 and 7.552 mV/bar respectively. These values represent the sensitivity of the two sensing systems.

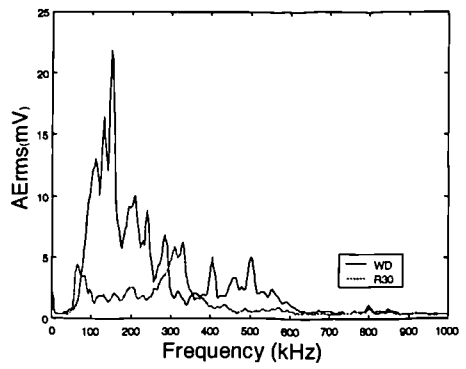

Figure 4. AErms spectra of the air-jet at the pressure of 5 bars.

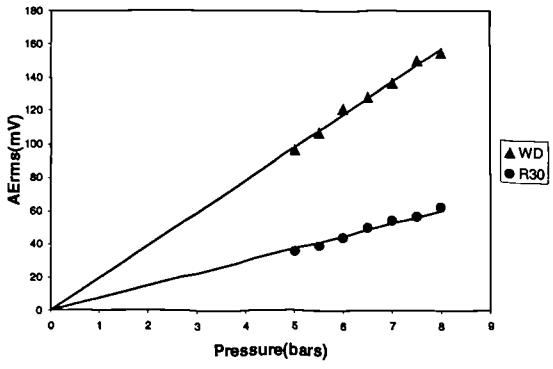

Figure 5. Relation between air-jet pressure and AErms.

The degree of likeness is computed using equation (4), returning the similarity coefficient matrix C for the WD sensor as

1	0.997	0.995	0.992	0.991	0.987	0.984
0.997	1	0.996	0.993	0.994	0.992	0.988
0.995	0.996	1	0.996	0.997	0.993	0.993
0.992	0.993	0.996	1	0.994	0.992	0.994
0.991	0.994	0.997	0.994	1	0.995	0.996
0.987	0.992	0.993	0.992	0.995	1	0.996
0.984	0.988	0.993	0.994	0.996	0.996	1

For the R30 sensor, the corresponding similarity coefficient matrix is given by

1	0.992	0.986	0.961	0.989	0.992	0.991
0.992	1	0.997	0.985	0.99	0.99	0.985
0.986	0.997	1	0.991	0.987	0.987	0.981
0.961	0.985	0.991	1	0.97	0.968	0.957
0.989	0.99	0.987	0.97	1	0.991	0.991
0.992	0.99	0.987	0.968	0.991	1	0.997
0.991	0.985	0.981	0.957	0.991	0.997	1

In these matrices, the rows and the columns represented the progressive pressure values of 5.0, 5.5, 6.0, 6.5, 7.0, 7.5 and 8.0 bars. It is evident from these matrices that the RMS spectra of a sensor are very similar to each other within this range of pressure as the coefficients are all very close to 1.

An RMS spectrum is simply the square root of the energy spectrum, also known as the spectral density function. In terms of the spectral density functions, the transfer characteristics from the air-jet input source to the output of the sensing instrument is governed by

$$G_y(f) = |H(f)|^2 \cdot G_x(f)$$

where the respective spectral density functions of the input and output are $G_x(f)$ and $G_y(f)$, and $H(f)$ is the frequency response function describing the dynamics of the signal transmission process which includes that of the tool and of the sensor. It should be noted that $G_x(f)$ denotes the AE produced at the tool tip as a result of the action of the air jet and not the air pressure itself.

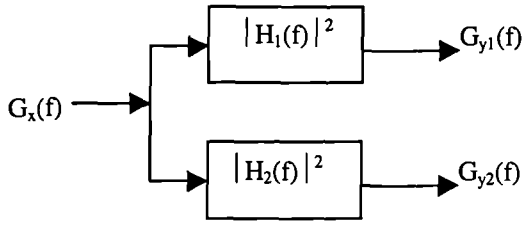

Figure 6. Different signal propagation paths with common input.

Figure 6 shows the different signal propagation paths with common input for the two different layouts of the WD and R30 sensors denoted by the respective subscripts of 1 and 2. Since the same input Gx(f) is used, their transfer equations can be written as

$$G_{y1}(f) = |H_1(f)|^2 \cdot G_x(f) \quad (5)$$

and

$$G_{y2}(f) = |H_2(f)|^2 \cdot G_x(f) \quad (6)$$

Dividing equation (5) by equation (6), we obtain

$$G_{y1}/G_{y2} = |H_1|^2 / |H_2|^2 \quad (7)$$

Figure 7 shows the ratio G_{y1}/G_{y2} for the range of air pressures from 5 to 8 bars with the curve of the mean ratio shown in bold solid line. The curves have been smoothed using the kernel smoothing technique. It is evident that all the curves are close to each other. According to equation (7), this suggest that the ratio of the frequency response functions, corresponding to the different sensors layouts, remain the same at any pressure within 5 to 8 bars. There are only two possible inferences from this: 1) that $H_1(f)$ and $H_2(f)$ are not affected by the input states of the air pressure, or 2) that both $H_1(f)$ and $H_2(f)$ are affected equally by the input states such that the resulting ratio remain constant. The second possibility is highly improbable, as it means that the condition must be maintained at all frequencies, 0 to 1 MHz, across the spectrum.

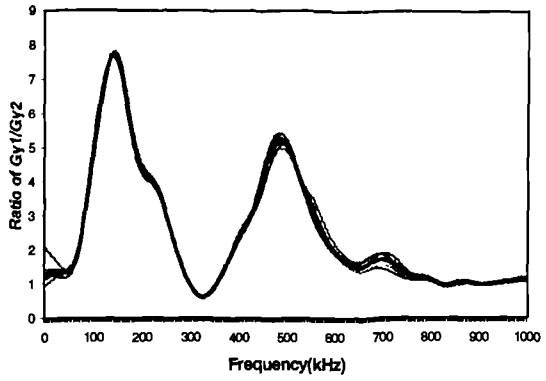

Figure 7. The ratio of G_{y1}/G_{y2} of air pressure from 5 to 8 bars.

Referring to either of equation (5) or (6), since neither $G_{yi}(f)$ nor $H_i(f)$ $(i=1,2)$ changes its shape with pressure, so will $G_x(f)$ retain its own shape. Thus, the sensitivity values of 19.658 and 7.552 mV/bar for the respective WD and R30 sensors apply not just to the overall AErms of the total signal, but also to the individual spectral components too.

Whilst the theory presented proves adequate for AE signals produced by the air jet with 5- to 8-bars of pressure, the AE produced from machining is much stronger and so the question of whether the calibration as described can be applied to the machining process needs to be answered.

4 AE FROM SINGLE-POINT MACHINING

The instrumentation used for the machining tests was identical to that for the air-jet calibration except that the total gain of the sensor output was 34 dB instead of 40 dB. It was necessary to use a lower gain in order to avoid saturation of the signal.

Three sets of machining tests were conducted and their conditions are detailed in the following:

- Machining Test Set 1: Variable feed rates from 0.05 mm/rev to 0.4 mm/rev in increments of 0.05 mm/rev. Cutting speed and depth of cut were constant at 120 m/min and 0.75 mm respectively.
- Machining Test Set 2: Variable speeds from 80 m/min to 150 m/min in increments of 10 m/min. Feed rate and depth of cut were constant at 0.2 mm/rev and 0.75 mm respectively.
- Machining Test Set 3: Variable depths of cut from 0.3 mm to 1.0 mm in increments of 0.1 mm. Cutting speed and feed rate were constant at 120 mm/min and 0.2 mm/rev respectively.

The material of the workpiece, measured 63.5 mm in diameter and 150 mm in length, was EN24T with 0.35-0.45 %carbon. All tests were conducted on a Traub lathe.

The ratios of G_{y1}/G_{y2} for the three sets of machining tests were first obtained and then the mean ratios for each set were calculated. The mean ratios for the three different machining conditions and for the air jet calibration are shown in Figure 8.

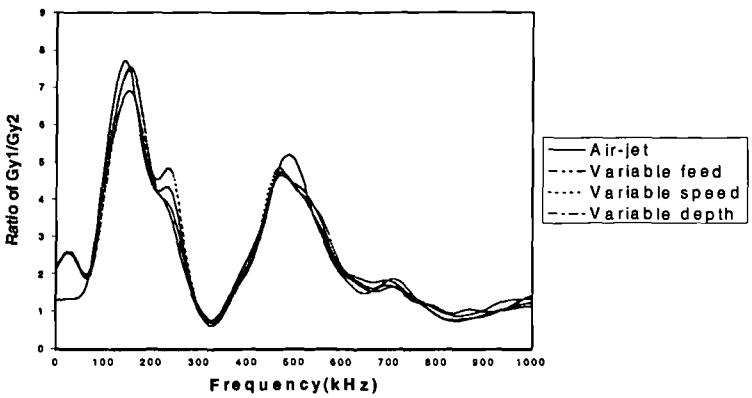

Figure 8. The ratios of G_{y1}/G_{y2} for the three sets of machining tests.

It can be observed that these curves match each other very closely. The implication is that the frequency response functions $H_1(f)$ and $H_2(f)$ in equations (5) and (6) are insensitive to the input states, whether they be caused by air-jet pressure or by machining.

5 CALIBRATION PROCEDURE

Based on the results presented, a simple calibration procedure for AE in machining studies is proposed. Using the air-jet artificial AE source set up under the conditions as stipulated in this paper, the AErms output of a sensor is measured over the range of air pressures from 5 to 8 bars. The sensitivity is then calculated from the gradient of the straight line fitted to the data points similar to Figure 5. With the sensitivity value known for a given layout of the AE sensor, the sensor output can then be converted into the pressure unit in bars. This unit is the common currency which forms the basis for comparison between results obtained with different sensor layouts or coupling conditions.

6 CONCLUSIONS

A number of conclusions can be made from the work. First, the frequency spectra of the AE produced by the air jet and machining were very similar to each other. Secondly, the frequency response function of the tool/sensor system was purely a function of the frequency and was independent of the input states or input mechanisms such as produced by air pressure or machining. Thirdly, using the calibration as prescribed, it is possible to convert an AErms value into an equivalent air-jet pressure value.

With the proposed calibration, it will be possible to make comparison between results obtained from different set-ups. This is, hopefully, a first step towards the building up of a meaning knowledge base on tool wear monitoring using AE.

ACKNOWLEDGEMENTS

The authors wish to acknowledge support from the INTErSECT Faraday Partnership, the Engineering and Physical Sciences Research Council and the Royal Thai Government.

REFERENCES

[1] R.Teti, D.A. Dornfeld, Modelling and experimental analysis of acoustic emission from metal cutting, *Trans. ASME, Journal of Engineering for Industry*, **111** (3) (1989) 229-237.

[2] E.N.Diei, D.A.Dornfeld, A model of tool fracture generated acoustic emission during machining, *Trans. ASME, Journal of Engineering for Industry*, **109** (3) (1987) 227-234.

[3] E. Kannatey-Asibu, Jr. and D.A. Dornfeld, Quantitative relationships for acoustic emission from orthogonal metal cutting, *Journal of Engineering for Industry*, **103** (3) (1981) 330-340.

[4] L. Dan, J.Mathew, Tool wear and failure monitoring techniques for turning-a review, *Int J.Mach.Tools Manufact*, **30** (4) (1990) 579-598.

[5] M.S .Lan, D.A. Dornfeld, In-process tool fracture detection, *Journal of Engineering Materials and Technology*, **106** (2) (1984) 111-118.

[6] T.Blum, I. Inasaki, A study of acoustic emission from the orthogonal cutting process, *Trans. ASME, J. Engineering for industry*, **112** (1990), 203-211.

[7] A.E. Diniz, J.J. Liu and D.A. Dornfeld, Correlating tool life, tool wear, and surface roughness by monitoring acoustic emission in finish turning, *Wear*, **153** (1) (1992) 396-407.

[8] J.J. Liu, D.A. Dornfeld, Modelling and analysis of acoustic emission in diamond turning, *Journal of Manufacturing Science and Engineering*, **118** (1996) 199-206.

[9] T.A. Carolan, S.R. Kidd, D.P. Hand, S. J. Wilcox, P. Wilkinson, J.S.Barton, J.D.C. Jones and R.L. Reuben, Acoustic emission monitoring of tool wear during the face milling of steels and aluminium alloys using a fibre optic sensor, part1: energy analysis, *Proc Instn Mech Engrs*, **211** (1997) 299-309.

[10] K.Iwata, T. Moriwaki, An application of acoustic emission measurement to in-process sensing of tool wear, *Annals of the CIRP*, **26** (1)(1977) 21-26.

[11] A. Prateepasen, Y. H. J. Au and B.E. Jones, Comparison of artificial acoustic emission sources as calibration sources for tool wear monitoring in single-point machining, *"Proceedings of the 24th European Conference on Acoustic Emission Testing"* (Senlis, 24-26. May 2000), CETIM, France, 2000.